FAULTING IN RIGID PAVEMENT SYSTEM OF HIGHWAYS

Von der Fakultät für Bauingenieurwesen und Geodäsie

der Gottfried Wilhelm Leibniz Universität Hannover

zur Erlangung des Grades eines

DOKTORS DER INGENIEURWISSENSCHAFTEN

Dr.-Ing.

genehmigte Dissertation
von

M.Sc. Mohamed El-Nakib

geboren am 21.12.1967 in Ägypten

2007

Referent : apl. Prof. Dr.-Ing. habil. Jürgen Hothan

Korreferent : Prof. Dr.-Ing. Martin Achmus

Tag der Promotion: 20.12.2006

Preface and Acknowledgements

This PhD research was carried out at the Institute of Transport Engineering and Planning of Hannover University in Germany. The research was supervised by the Head of Pavement Engineering Section, Prof. Dr.-Ing. Jürgen Hothan.

First of all, I wish to express my deepest gratitude and best thanks for my advisor, guide and principle referee, Prof. Dr.-Ing. Jürgen Hothan for his positive support to the completion of this doctoral thesis, for his generous efforts, valuable advice and comments. I would especially like to thank and acknowledge Prof. Dr.-Ing. Martin Achmus, the Head of the Institute of Soil Mechanics, Foundation Engineering and Water Power Engineering, who was the second referee for my research, for his valuable advice in the field of mechanical behavior of soils under cyclic loads and for his feedback and suggestions. I would like also to acknowledge the chairman of the Examination Committee, Prof. Dr.-Ing. Ludger Lohaus.

Also I am very grateful to Dr.-Ing. Khalid Abdel-Rahman for his continuous help and support in many matters during my research.

I appreciate the help given by all my colleagues and friends at the Pavement Engineering Section in the Institute of Transport Engineering and Planning. They were always helpful and friendly.

Last but not least, I am deeply indebted to my parents and my wife for their continuous support and encouragement.

Finally, I would like to dedicate this thesis to my Parents.

Hannover, January 2007

Mohamed El-Nakib

Vorwort des Herausgebers

Die Dimensionierung von Betonstraßen findet in Deutschland nach einem festen Regelwerk statt, das auf der Erfahrung von Jahrzehnten wie auch auf der rechentechnischen Untermauerung aufbaut. Betonfahrbahnen gelten als langlebig, vor allem bleiben sie während der gesamten Betriebsdauer frei von merklichen Spurrinnen. Die Hauptversagensform von Betonfahrbahnen ist die Stufenbildung zwischen den Fahrbahnplatten in Fahrrichtung. (Rissbildung ist als struktureller Schaden von Bedeutung; für Erhaltungsmaßnahmen nur durch damit ein-hergehende Stufenbildung relevant). Dabei wird, wenn eine gewisse Beweglichkeit in der Dübellage erreicht ist, bei Überrollung eine relative Bewegung der aufeinander folgenden Platten erzeugt, die mit einem Feinteiltransport von der nachfolgenden unter die vorhergehende Platte verbunden ist. Dieser Vorgang wird durch Feuchtigkeitsanreicherung verstärkt. Deshalb wird versucht, den Wasserhaushalt in der Befestigung durch Abdichten der Fugen und schnelles Ableiten von eindringendem Wasser auf möglichst niedrigem Niveau zu halten. Somit scheint der Schadensmechanismus hinreichend gedeutet zu sein. Eine numerische Behandlung dieser Vorgänge stand bisher aus und erschöpfte sich bisher in verbaler Beschreibung.

Hier setzen die Untersuchungen von Herrn El-Nakib ein, der von einer Betonbefestigung auf ungebundener Unterlage ausgeht und unter Einbeziehung aller erreichbaren Fakten zum mechanischen Verhalten ungebundener Schichten ein FE-Modell entwickelt, das für eine Simulation der Stufenbildung geeignet ist. Mit Hilfe von Fluidelementen wird die Feinteilbewegung nachempfunden und deutlich der Einfluss von Lastwechselzahlen und Feuchtigkeitsgehalt aufgezeigt. Herrn El-Nakib ist es gelungen, durch sehr aufwändige Berechnungen den numerischen Zugang zur Stufenbildung von Betonplatten zu öffnen.

Hannover im Januar 2007

Prof. Dr.- Ing. habil. Jürgen Hothan

Abstract

The modeling of pavement structures has been based for many years on a lot of simplifications, which are being refined continuously during the time. The use of linear behavior for building materials is regarded as history. Progress was made, particularly, in the mechanical behavior of unbound granular materials, whose non-linearity is actually known for long time ago. But because of complex computations, it is not widely considered in the pavement analysis. In order to obtain progress with the simulation of rigid pavements, the inclusion of real behavior of unbound materials of base layers is inevitable. Therefore, in the current research, this behavior will be included in failure analysis of rigid pavement due to faulting problem under cyclic loads of traffic. The analysis will be conducted using the commercial finite element program ABAQUS available at the University of Hannover.

After the investigation into the mechanical behavior of unbound granular materials, the non-linearity in both elastic and plastic phases will be implemented through a user material subroutine (UMAT) to define the constitutive law for these materials in the finite element code. Validation of UMAT will be done through comparing results of FEM analysis and experimental results to approve the correctness of implementing constitutive laws in the user subroutine. The accumulation of permanent strains under cyclic loads of traffic resulted in a formation of an elevation difference between concrete slabs, defined as faulting. With the help of the UMAT, modeling of rigid pavement with a simple 3-D model under two cases of loading shall be conducted and an equivalent traffic load for a 2-D model shall be estimated. For the computation of faulting, a 2-D model is chosen, consisting of three concrete slabs each 5.00 m long, 0.26 m thickness, which are supported over an unbound granular base layer of 0.60 m thickness and a subgrade soil of 6.00 m depth. A reasonable model for the rigid pavement analysis is built this way to take into account the following: the interface between concrete slabs and the underlying base layer through friction, to minimize the computing time and reduce the computing cost because of the big number of loading cycles of moving traffic (considered as static loads). The faulting is computed depending on the load amplitude and the number of cycles as well as the moisture content of the unbound granular material of base layer.

Recommendations for future research regarding the optimization of riding quality and suggestions for the minimization of the maintenance cost during the life period of rigid pavement structures are given.

Key words: cyclic loads, faulting, Finite Element, unbound granular materials, UMAT, non-linear behavior.

Kurzfassung

Die Modellierung von Fahrbahnbefestigungen geht von einer Vielzahl von Vereinfachungen aus, die im Laufe der Zeit von Verfeinerungen abgelöst wurden. Der Ansatz der Linearität für die Baustoffe ist als historisch anzusehen. Fortschritte wurden vor allem in der Ansprache des Verhaltens ungebundener Stoffe erzielt, deren Nichtlinearität schon lange bekannt ist, aber wegen der aufwändigen Berechnung nur zögernd Verbreitung gefunden hat. Um Fortschritte bei der Simulation von Betonstraßen erzielen zu können, ist die Einbeziehung des realen Verhaltens ungebundenen Schichten unumgänglich. Deshalb wird in dieser Arbeit dieses Verhalten in die Analyse des Versagens von Betonstraßen durch Stufenbildung unter zyklischer Verkehrsbelastung einbezogen. Für die Analyse mittels finiter Elemente (FEM) wird das kommerzielle Programm ABAQUS benutzt.

Nach der Ermittlung des ‚State of the Art' von ungebundenen Schichten wird das nichtlinear- elastische und plastische Verhalten ungebundener Schichten mittels einer lokalen Benutzerroutine (UMAT) in dem finite Elemente System implementiert und eine Einbettung in eine Routine zur Simulation wiederholter Belastungen, die in eine akkumulierte dauerhafte Stufenbildung von Betonstraßen münden, gestaltet. Die Validierung der UMAT wird durch einen Vergleich der FEM Berechnungen mit experimentellen Ergebnissen belegt. Mittels UMAT wird ein einfaches 3-D-Modell der Betonstraße für zwei Belastungsfällen analysiert und eine vergleichbare Verkehrsbelastung für ein 2-D-Modell abgeschätzt, um den Rechenaufwand in handhabbaren Grenzen zu halten.

Für die Stufenbildungsberechnungen wird ein 2-D-Modell generiert, das aus drei Betonplatten von 5,00 m Länge und 0,26 m Dicke besteht und auf einer 0,60 m dicken ungebundenen Tragschicht aufliegt, die wiederum auf einem 6,00 m mächtigen Untergrund lagert. Dieses Modell wird mit folgenden Eigenschaften ausgestattet: Die Interaktion zwischen den Betonplatten und der ungebundenen Tragschicht wird durch Reibungselemente geschaffen; die Verkehrslasten werden als schrittweise versetzte statische Lasten betrachtet vor dem Ziel die Berechnungszeiten wegen der großen Zahl von Lastzyklen gering zu halten. Die Stufenbildung wird in Abhängigkeit von Lastgröße und –zahl sowie dem Feuchtigkeitsgehalt der ungebundenen Schicht simuliert und Empfehlungen für zukünftige Forschungen hinsichtlich der Optimierung der Fahrbahnqualität und Ansätze zur Minimierung der Instandhaltungskosten während der Betriebsdauer von Betonstraßen gegeben.

Schlagwörter: zyklische Belastung, Stufenbildung, finite Elemente, Tragschicht ohne Bindemittel, UMAT, nichtlineares Stoffverhalten

Table of Contents

Notations and Abbreviations

Greek Lower Case Letters

σ_1 : absolute value of maximum principal stress

σ_2 : absolute value of middle principal stress

σ_3 : absolute value of minimum principal stress

σ_3 : confining pressure (in triaxial test)

$\sigma_{3,0}$: regression constant

$\sigma_{3,s}$: static primary stress state

σ_c : maximum stress at the corner loading position, Westergaard theory

σ_d : deviator stress

σ_{hr} : residual lateral stress

σ_i : maximum stress at the interior loading position, Westergaard theory

σ_v : vertical overburden stress

σ_z : vertical stress

$\overline{\sigma}$: effective stress

Δ_c : maximum deflection at the corner loading position, Westergaard theory

Δ_i : maximum deflection at the interior loading position, Westergaard theory

α : empirical regression parameter

β : empirical regression parameter

ε_1^r : resilient axial strain

$\varepsilon_{1,p}$: total permanent axial strain

$\varepsilon_{1,p}^*$: axial permanent strain with removal of first 100 cycles

$\varepsilon_{2,cp}^N$: cyclic strain in σ_2 direction

$\varepsilon_{3,cp}^N$: cyclic strain in σ_3 direction

ε_a : axial strain

ε_{cp1}^1 : cyclic plastic strain for the 1st load cycle (N=1)

ε_q : deviator strain

ε_{cp}^{N} : cyclic deformation portions

ε_p : permanent strain

$\varepsilon_{p,\,wa}$: permanent strain at actual water content

$\varepsilon_{p,\,wr}$: permanent strain at reference water content

ε_v : volumetric strain

$\varepsilon_{vp}^{N,t}$: visco-plastic strain at time t

$\dot{\varepsilon}$: total strain rate

$\dot{\varepsilon}_n^p$: vertical strain rate

$\dot{\gamma}^p$: horizontal strain rate

ζ : empirical regression parameter

η : viscosity

θ : sum of principal stresses (bulk stress)

θ : Lode angle - deviator polar angle

λ_1 : ratio of cyclic strain in 2nd direction to the axial cyclic strain

λ_2 : ratio of cyclic strain in 3rd direction to the axial cyclic strain

μ : coefficient of friction

ν : Poisson ratio

ν_r : resilient Poisson ratio

ρ : density

τ : shear stress

φ : angle of internal friction (static)

φ_c' : angle of internal friction (cyclic)

χ : empirical regression parameter

Ψ : dilatation angle (static)

Ψ_c' : dilatation angle (cyclic)

ω_o : empirical regression parameter

Latin Upper Case Letters

A : material constant

A_1 : strain rate – type parameter

B : material constant

C : material constant

D : material constant

D_0^{el} : initial (undamaged) elastic stiffness

E : modulus of elasticity

F_c : reduced cyclic Mohr Coulomb failure criterion

G : shear modulus

G_f : flow potential

G_a : material constant

K : bulk modulus

K : deviatoric failure stress parameter

K : spring constant

K_a : material constant

M_r : resilient modulus of elasticity

P_a : arbitrary pressure equal to atmospheric pressure (100 kPa)

Q : material constant

Q_1 : material constant

Q_2 : material constant

R : material constant

S_{cf} : cyclic deviator failure stress

S_{sf} : static deviator failure stress

U1 : displacement in X direction

U2 : displacement in Y direction

U3 : displacement in Z direction

X : parameter (cyclic)

Latin Lower Case Letters

a : radius of the tire print

a : material constant

a_1 - a_4 : material constant

b : material constant

b_1 - b_4 : material constant

c : material constant

c : cohesion (static)

c_c' : cohesion (cyclic)

d : scalar stiffness degradation variable

e : pore number

h : thickness of concrete layer

k : subgrade reaction modulus

k_o : coefficient of lateral earth pressure for lateral stress

k_1 to k_3 : material constants

k_p : passive coefficient of lateral earth pressure

l : radius of relative stiffness

m_{mob} : mobilized fraction of static failure stress

n : material constant

p : mean normal stress

p^* : stress parameter

q : contact pressure of tire

q : deviator stress

q_r : cyclic deviator stress

w_a : actual water content

w_r : reference water content

Indices

a : Index for axial direction

c : cyclic

c,f : cyclic failure

cp : cyclic plastic

o : primary state

pl : plastic

r : Index for radial coordinate

s : static

s,f : static failure

vp : visco-plastic

z : Index for vertical coordinate

Abbreviations

‘2-D’ : two Dimensional

‘3-D’ : three Dimensional

AASHTO : American Association of State Highway and Transportation Officials

AC : Asphalt Concrete

CCP : Constant Confining Pressure

COST 337 : Project for Review of Models and Modeling Requirements of Unbound Granular Materials for Road Pavements

COURAGE : European Commission ‘COnstruction with Unbound Road AGgregates in Europe’

D : modulus of rigidity

D : Diabase material

DDR : Relative Dry Density

DEM : Distinct Element Method

DFG : Central Public Funding Organization for Academic Research in Germany (In German: Deutsche Forschungsgemeinschaft)

DOC : Degree of Compaction

DOF : Degree of Freedom

E : modulus of Elasticity

Eqn : Equation

FEM : Finite Element Method

FWD : Falling Weight Deflectometer

Gr : Granodiorite

G/S : Gravel Sand

HVS : Heavy Vehicle Simulator

JPCP : Jointed Plain Concrete Pavement

LCPC : French network of Laboratories des Ponts et Chaussées (In French: Laboratoire Central des Ponts et Chaussées)

MS : Multi Stage

N : Number of load cycles

OCR : Over-Consolidation Ratio

OMC : Optimum Moisture Content

PCC : Portland Cement Concrete

RCC&A : Recycled Crushed Concrete & Asphalt

RLT : Repeated Load Triaxial

RMC : Relative Moisture Content

[RStO] : Richtlinie für die Standardisierung des Oberbaues von Verkehrsflächen (In English: Empirical German pavement design guideline), Forschungsgesellschaft für Straßen- und Verkehrswesen, Köln, 2001.

S&G : Sand and Gravel

ST : Static Triaxial

UGL : Unbound Granular Layer

UGMs : Unbound Granular Materials

UMAT : User MATerial subroutine

W/C : water content

VCP : Variable Confining Pressure

List of Figures

List of Tables

1 INTRODUCTION

Research concerning the structural behavior of pavement systems receives great recognition, especially after the growing use of heavy trucks in goods' transportation. The Institute for Roads and Railways Technology of Karlsruhe University stated in its 1992 Report '*Traffic in graphic*' that traffic performance of goods transportation in 1990 was about 169 billion ton-kilometer. The Institute for Economic Research stated that in the year 1995, the traffic performance of goods' transportation was about 284 billion ton-kilometer. With this development of goods' transportation using heavy trucks, and in order to minimize damage to the existing rigid pavement highways, it was necessary to study the behavior of those pavement systems under heavy running loads.

Nevertheless, much of the existing rigid pavement research has been based on the classical two-dimensional (2-D) theories developed by Westergaard and Burmister. These classical methods were adequate analysis and design tools until 1980, but are now outdated. Nowadays, modern computers can provide much better computing ability than those used during the 1980s. Furthermore, the classical theories neglect many important aspects compared to the finite element analysis regarding the behavior of pavement systems.

Recently, Finite Element Method (FEM) has been increasingly viewed as a fundamental tool to investigate the behavior of numerous structural systems. It has been widely applied to various structural analysis problems, from bridges to buildings in civil engineering applications and from automobiles to aircrafts in mechanical engineering. Also it is increasingly being used as an extremely powerful method for solving many geotechnical problems, such as dams, foundations, and pavement structures.

1.1 Definition of the problem

The structural behavior of rigid pavement systems is more complicated than that of flexible pavements because they have more complex structural components (for example, joints and load transfer devices). For rigid pavement systems, stress, strain, and displacement distributions are all different in terms of the loading positions because joints and load transfer devices make a significant impact on the structural behavior.

One of the known problems in rigid pavement systems is stepping (faulting), which is defined as the difference of elevation across joints or cracks, as illustrated in Figure 1.1. Faulting is considered an important distress of Portland Concrete Pavements (PCP) because it affects riding quality. If significant joint faulting occurs, there will be a major impact on the life-cycle costs of the rigid pavement system in terms of rehabilitation and vehicle operating costs.

Faulting is caused in part by a buildup of loose materials under the approach slab near the joint or crack combined with the depression of the leave slab. Lack of load transfer devices contributes greatly to faulting [30].

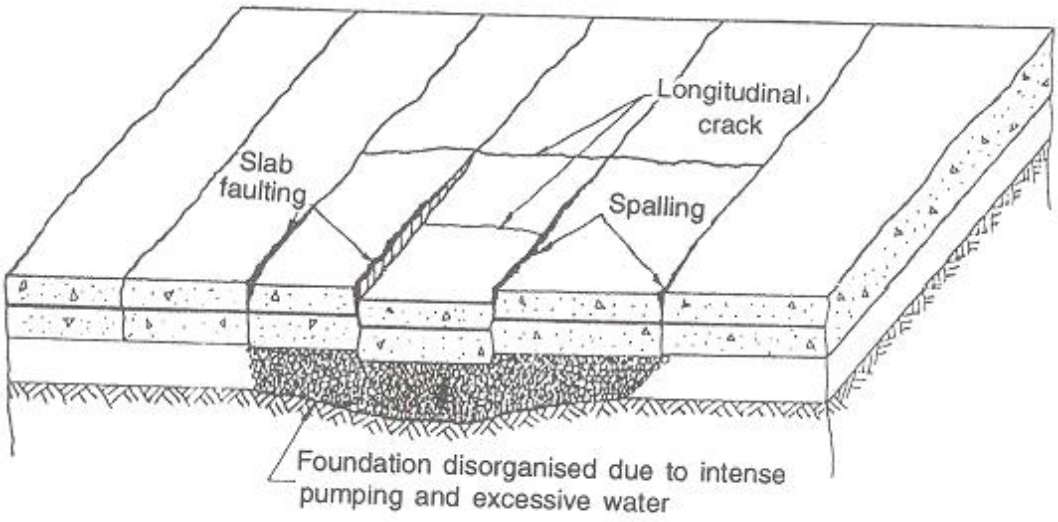

Fig. 1.1: Diagrammatic representation of a punch-out [30]

The pumping and faulting are a continuous process, which occurs due to the presence of water in cracks and transverse joints between concrete slabs. This process takes place during the crossing of traffic loads to joints, which do not have load transfer devices (i.e. dowels) or those with a very low load transfer efficiency factor.

The process can be explained in 5 steps as the following (Figure 1.2):

1- Unsealed joints and cracks allow water to enter the pavement structure and accumulate under the concrete slabs.

2- The joint deflects as a load moves across it. The water under the approach slab (slab no. 1) is ejected gradually, carrying materials with it, and accumulates under the leave slab (slab no. 2). This movement of materials by water pressure is called pumping.

3- As the load moves to the leave slab, water and material from underneath the leave slab are suddenly pumped back underneath the approach slab. Thus, the original materials from underneath the approach slab are returned back, however, with additional fine materials.

4- This process leads to the accumulation of material underneath the approach slab and loss of material from underneath the leave slab. The approach slab bends up to accommodate the extra material, while the leave slab bends down to fill the associated void.

5- These causes an elevation difference between the approach and leave slabs. This elevation difference, called a fault (stepping), is a major contributor to rigid pavement roughness and distress.

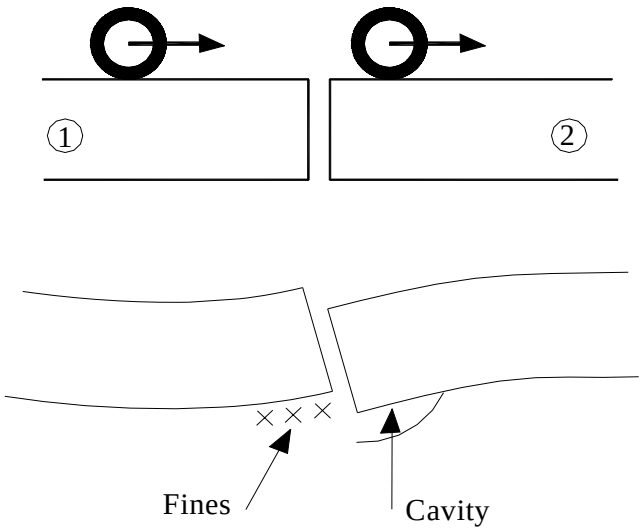

Fig. 1.2: Pumping and faulting

The specific problem of the research is simulating the above-mentioned process with the finite element method. It is clear that, the behavior of unbound granular materials (UGMs) with high moisture content combined with the absence of an effective load transfer device between concrete segments are the main reasons for the faulting problem. Therefore, the modeling of unbound granular materials under cyclic loads with the possibility of using the available material model in the finite element program shall be the main subject of this research to simulate the faulting process.

1.2 Thesis overview

This dissertation introduces a new numerical tool, which simulates the structural behavior of a rigid pavement system under cyclic loads through the modeling of unbound granular materials of base layer in both elastic and plastic ranges of deformation. Following are brief summaries of the main chapters.

Chapter two introduces existing pavement analysis approaches. Two important analytic theories developed by Westergaard and Burmister will be briefly overviewed. Three different numerical analysis approaches will be briefly introduced, namely; numerical computation software for Burmister theory, axisymmetric FEM software, and 2-D FEM programs based on Westergaard theory. Numerical modeling for rigid pavement with commercial FEM programs like ANSYS and ABAQUS may introduce better analysis methods through their available tools. For example, effective mesh construction, interface between different layers, and better modeling for unbound granular layers, etc.

A recent research concerning an empirical method for the calculation of faulting in rigid pavement systems is presented.

Chapter three reviews the different models for modeling unbound granular materials (UGMs) regarding both resilient and permanent deformation behavior under cyclic loading due to traffic. The effect of initial stresses on the resilient modulus will be addressed. Dresden Model for the description of UGMs in both resilient and permanent deformation behavior shall be discussed in detail. The influence of moisture content on the behavior of UGMs and how it should be considered in the modeling shall be discussed.

Chapter four reviews the implementation of constitutive laws used for the modeling of the behavior of unbound granular materials under cyclic loading in a user material subroutine (UMAT). The subroutine shall be used throughout the ABAQUS program to simulate the rigid pavement system subjected to cyclic loading of traffic. Different material parameters required for this subroutine shall be defined. The subroutine is based on the well-known Mohr Coulomb Theory of Plasticity.

Chapter five covers the development of an existing UMAT subroutine to follow the Dresden Model conception for the UGMs. Validation of the new version of the UMAT subroutine shall be proved through a comparison of finite element results with existing analytical and experimental results.

A simple 3-D model was chosen for the simulation of a rigid pavement system. Geometry of the model, generated mesh, elements, boundary conditions, loading history, and material properties (plain concrete, unbound granular base, subgrade soil) shall be discussed. Results of the analysis shall be presented and assessed. Comparison with Westergaard's theory is presented. An equivalent traffic load for a 2-D model shall be determined for the purpose of simulation of the faulting problem.

Chapter six covers the description of the numerical modeling of rigid pavement structure with regard to the problem of faulting. A 2-D model is chosen for the simulation. Geometry of the model, elements, boundary conditions, loading history, and definition of properties for different materials shall be discussed. Results of the analysis and calculation of faulting shall be presented and assessed.

Chapter seven gives in brief conclusions of the current research and recommendations for future research.

The well-known nonlinear finite element package ABAQUS [2] has been used to perform the finite element analysis of rigid pavement system and the program PATRAN has been employed as the pre-processor. The analysis platform is the Unix based workstation belonging to the North Germany Organization for Highest Computation Performance (in German: Norddeutschen Verbundes für Hoch- und Höchstleistungs-rechnen ,,HLRN").

2 LITERATURE REVIEW

Typical rigid pavement structures are composed of a Portland cement concrete slab layer and at least one treated and/or compacted granular base layer on top of natural soil subgrade, as illustrated in Figure 2.1-a. Transverse thermal joints (both expansion and contraction joints) are provided to prevent thermal cracking of the concrete slab. For convenience during construction, longitudinal construction joints are present through the whole length of the highway. In order to prevent joint failure under wheel load, load transfer devices (dowels for transverse joints and tie-bars for construction joints) are included to transfer wheel load from loaded slab segment to adjacent slab segments, as illustrated in Figure 2.1-b.

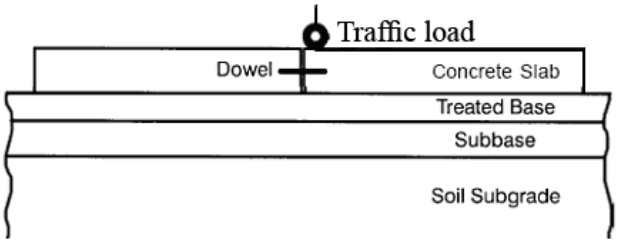

a) Cross section

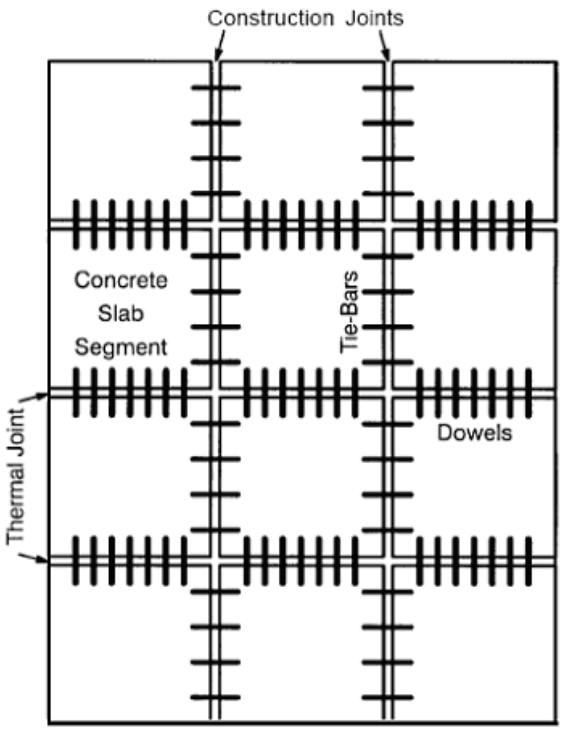

b) Plan view

Fig. 2.1: Rigid pavement system

2.1 Existing pavement analysis methods

Structural analysis of pavement systems has evolved from the two important classical theories developed by Westergaard and Burmister. In the Westergaard theory, the rigid pavement system is idealized as an elastic plate resting on Winkler foundation.

Nearly two decades after the Westergaard theory, Burmister developed a closed-form solution for layered linear elastic half-space problems for pavement systems, including both rigid and flexible pavements. This axisymmetric solution is able to consider pavement layers with different linear elastic material properties.

2.1.1 Classic methods for solution

2.1.1.1 Westergaard theory

The Westergaard theory was the first rational and mechanical approach ever attempted to analyze a pavement system. From existing test data and experience, he identified the three most critical loading positions: the interior (also called center), edge, and corner, as illustrated in Figure 2.2, because the behavior of a rigid pavement is highly dependant on the loading position relation to the joints. In terms of pavement analysis and design, obtaining the maximum bending stress under the given wheel load was the most important concern for early pavement engineers.

The magnitude of displacement is also required to estimate the damage to joints. If the displacement is too large, then the pavement will be damaged when the wheel load moves from one concrete slab segment to another.

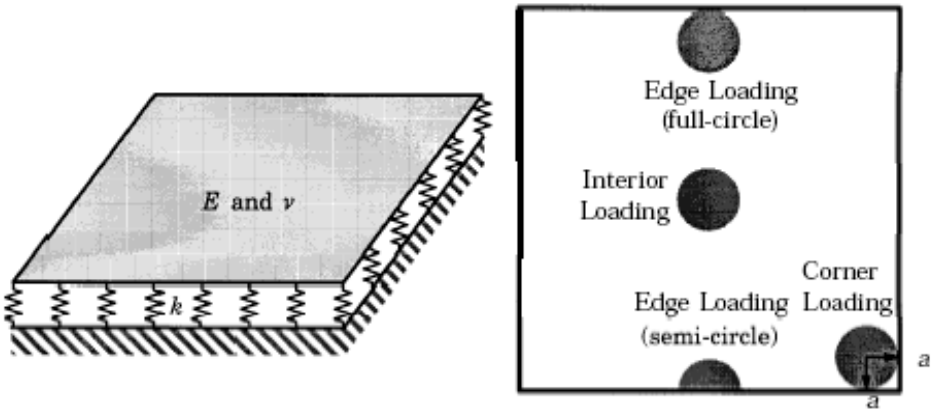

Fig. 2.2: Problem definition by Westergaard, three loading positions

Westergaard [69, 70, 71, 72] idealized a Portland cement concrete pavement to be a two-layered linear elastic system (concrete slab and subgrade layer) to create a linear elastic solution for stress and deflection. He considered the concrete slab to be an infinite (for internal loading) or semi-infinite (edge and corner loading) Kirchhoff plate and the subgrade layer to be a Winkler foundation.

Westergaard developed formulae for stress and deflection of three different loading positions using the method of successive approximation. Some of his formulae are still used in pavement research and design. In order to simplify the solution, Westergaard defined the radius of relative stiffness, denoted by *l.* The radius of relative stiffness is a measurement of the stiffness of the concrete slab relative to that of the subgrade (Winkler foundation) and has a dimension of length:

$$l = \left[\frac{Eh^3}{12(1-v^2)k} \right]^{0.25} \tag{2.1}$$

Where E is the Young's modulus, v is the Poisson's ratio of concrete, h is the thickness of the concrete slab, and k is the modulus of subgrade reaction. He derived an equation for the approximate maximum stress under single circular distributed wheel load acting at the interior (center) loading position as [70]:

$$\sigma_i = \frac{3(1+v)P}{2\pi h^2} \left[\ln\left(\frac{l}{b}\right) + 0.6159 \right] \tag{2.2}$$

Here, definition of b depends on the radius of the tire print a and the thickness of the concrete slab h

$$\begin{aligned} b &= a && \text{when } a \geq 1.724h \\ b &= \sqrt{1.6a^2 + h^2} - 0.675h && \text{when } a < 1.724h \end{aligned} \tag{2.3}$$

The maximum deflection due to an interior center loading is [71]:

$$\Delta_i = \frac{P}{8kl^2} \left\{ 1 + \frac{1}{2\pi} \left[\ln\left(\frac{a}{2l}\right) - 0.673 \right] \left(\frac{a}{l}\right)^2 \right\} \tag{2.4}$$

Corner loading formulae for stress and displacement were derived from a circular pressure load, where the center is located at a radius away from the two edges of the corner, as illustrated in Figure 2.2.

$$\sigma_c = \frac{3P}{h^2} \left[1 - \left(\frac{a\sqrt{2}}{l} \right)^{0.6} \right] \tag{2.5}$$

$$\Delta_c = \frac{P}{kl^2} \left[1.1 - 0.88 \left(\frac{a\sqrt{2}}{l} \right) \right] \tag{2.6}$$

Several different versions of edge loading solutions were created by Westergaard [70, 71, 72]. The solution was initially derived under a semi-circular uniformly distributed load acting on the edge [70], as illustrated in Figure 2.2, then later extended to a full circular loading. Following are the latest equations for both circular (Eqns 2.7 and 2.9) and semi-circular (Eqns 2.8 and 2.10) loads for the edge loading position.

$$\sigma_e = \frac{3(1+v)P}{\pi(3+v)h^2}\left[\ln\left(\frac{Eh^3}{100ka^4}\right)+1.84-\frac{4v}{3}+\frac{1-v}{2}+\frac{1.18(1+2v)a}{l}\right] \quad (2.7)$$

$$\sigma_e = \frac{3(1+v)P}{\pi(3+v)h^2}\left[\ln\left(\frac{Eh^3}{100ka^4}\right)+3.84-\frac{4v}{3}+\frac{(1+2v)a}{2l}\right] \quad (2.8)$$

$$\Delta_e = \frac{P\sqrt{2+1.2v}}{\sqrt{Eh^3k}}\left[1.0-\frac{(0.76+0.4v)a}{l}\right] \quad (2.9)$$

$$\Delta_e = \frac{P\sqrt{2+1.2v}}{\sqrt{Eh^3k}}\left[1.0-\frac{(0.323+0.17v)a}{l}\right] \quad (2.10)$$

2.1.1.2 Burmister theory

Nearly two decades after Westergaard theory, Burmister [9] derived a closed-form solution for the layered linear elastic half-space system, which is the idealization of the multi-layered pavement system. The prime objective of this solution is to compute stress, strain, and displacement based on linear elasticity. In addition, interface behavior between layers was included in the solution.

In order to simplify solution development for the 3-D multi-layered system, Burmister assumed axisymmetric and infinite problem domain, as illustrated in Figure 2.3.

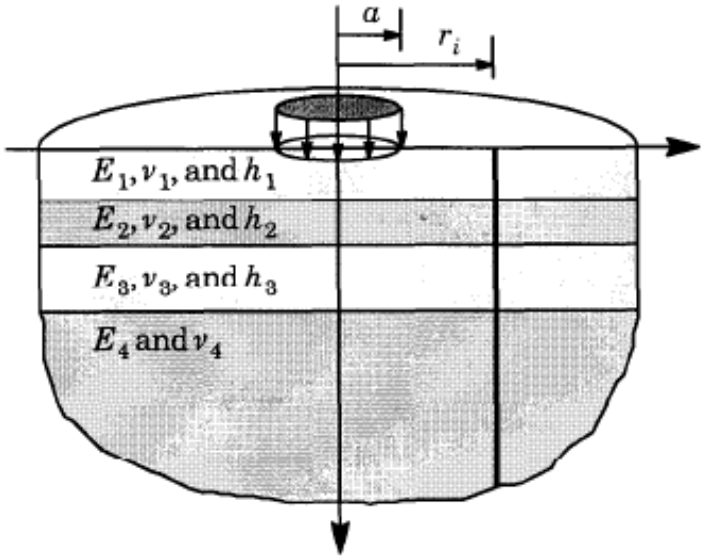

Fig. 2.3: Problem definition by Burmister

Burmister [9] assumed a stress function composed of Bessel and exponential functions, satisfying the bi-harmonic equation, to obtain a linear elastic solution of a multi-layered system:

$$\phi = J_o(mr)[Ae^{mz}+Be^{-mz}+zCe^{mz}+zDe^{-mz}] \quad (2.11)$$

Where r is the radial and z is the vertical coordinate variables, m is a parameter, and A, B, C, D are the four constants. For a multi-layered system, four constants need to be determined for each layer by the boundary and compatibility conditions. After determination of those constants, stress, strain, and displacement can be calculated by the traditional linear elasticity formulation in a radial coordinate system. Since the Burmister solution is derived based on linear elasticity, multiple wheel load analysis became possible under the principle of superposition.

Due to the 2-D axisymmetry assumption, the Burmister theory cannot be applied to the edge and corner of the pavement. Further, only circular shaped uniform pressure loads can be applied, even though in general the wheel load tire print is an ellipse. Besides this, nonlinear behavior of granular material cannot be included because the Burmister theory is derived based on linear elasticity assumption. Nevertheless, this solution is still a core part of many pavement analysis and design programs.

2.1.2 Solution based charts and tables

Due to limited computing abilities up to the 1970s, tables and charts were the two most effective analysis and design methods for pavement engineers. Therefore, numerous charts and tables were created for both classical methods (Westergaard and Burmister). However, those charts and tables were quite complicated because several design variables (for instance, Young's modulus, Poisson's ratio, and thickness of layers) are required to compute output results.

These charts and tables successfully eliminated most of the computing cost from the pavement analysis and design process and were an efficient tool for many pavement engineers. However, they inherited the shortcomings of both the Westergaard and Burmister theories.

2.1.3 Existing analysis programs for rigid pavement

This section briefly overviews existing pavement analysis and design programs and their algorithms. Every program has its own detailed features and each one's applicability to rigid pavement analysis shall be investigated. For convenience, existing pavement programs are classified by three major categories:

1- Burmister solution-based programs

2- 2-D axisymmetry finite element programs

3- 2-D plates on elastic foundation based programs

2.1.3.1 Burmister solution-based programs

Many numerical programs have been developed for the numerical evaluation of the Burmister solution since the emergence of the computer in the late 1950s. The prime objective of these programs was to eliminate the complex computations involved in obtaining stress, strain, and displacement from the Burmister solution.

The first generation of software in this category is ILLI-AC written by Mehta and Veletsos [36] and CHEVRON written by Michelow [37], but they were not widely used among pavement engineers. In 1978, the Shell laboratory in Amsterdam [53] developed BISAR. This became the first widely used pavement analysis software because it was written in FORTRAN language and was portable to many existing computers using different operating systems. Through these initial attempts, evaluation of the Burmister theory became more convenient and therefore, these programs gradually replaced existing charts and tables for the pavement analysis and design process.

Nearly ten years later, Van Cauwelaert [65] developed another version of Burmister solution computing software: WESLEA. Unlike other developers, he paid more attention to the fast integration algorithm of exponential and Bessel functions in the solution. He separated Burmister solution into two parts: one for closed-form integrable terms and the other for numerically integrable terms. As a result, WESLEA was able to compute the answers much faster than previous programs.

In addition to known facts from the Burmister solution, pavement engineers also found that these programs overestimate tensile bending stress in the supporting layer. Such an overestimation is caused by the linear elastic constitutive model, which has the same stress and strain relationship for both the tensile and the compressive sides. However, all supporting layers are composed of granular materials, which is a group of discrete particles. The Burmister solution considered the multi-layered pavement system as a continuous linear elastic body. As a result, any point above the neutral plane is subjected to compression and any point below is under tension. Hence, the stress state of the whole base and subgrade layers often stays in tension because the composite neutral plane of the multi-layered system is frequently located between the center and bottom of a pavement layer. Due to their tensile strength, such a tensile stress state is not admissible for the granular materials, although it is not a problem for a pavement layer composed of asphalt or Portland cement concrete. The predicted stress state in a pavement layer is often underestimated due to this overestimation of the tensile stress in the granular layer. Such an approximation error became a motivation for future use of nonlinear material models.

2.1.3.2 2-D axisymmetry finite element programs

After the introduction of finite element methods, numerous axisymmetry 2-D finite element codes were developed for pavement analysis and design. Their prime objective was to include nonlinear elastic constitutive models into the existing 2-D axisymmetry pavement analysis framework initially derived by Burmister. In addition to linear elasticity, a visco-elastic constitutive model was implemented for asphalt concrete, and resilient behavior based non-linear elasticity models were included to capture the complex behavior of granular materials. Further, the Mohr Coulomb failure criterion was included to simulate the failure of granular materials. However, the codes still preserved the axisymmetry assumption in order to reduce the problem size, as illustrated in Figure 2.4-a.

Raad and Figueroa [46] developed the ILLI-PAVE program, which was the first software available to the public in this category. Thompson et al [61, 62] applied ILLI-PAVE into numerous practical pavement problems. Other important programs in this category are MICH-PAVE developed by Harichandran et al [21] and KENLAYER developed by Huang [26].

These programs no longer assume infinite domains, so an artificial roller boundary condition was imposed at both the horizontal and vertical boundaries (Figure 2.4-a).

Stress dependent non-linear elastic material models (so-called resilient behavior models) were included in these programs in addition to the linear elasticity models. Here, the resilient behavior means an almost elastic behavior of granular materials shown after enough axial load repetitions in the triaxial test (Figure 2.4-b). Hicks and Monismith [23], and Uzan [64] developed non-linear elastic K-θ and Uzan models respectively from such nearly elastic behavior. Detailed description for these material models is discussed in Chapter 3. These non-linear material models could provide better solutions, but a costly nonlinear solution procedure was inevitable.

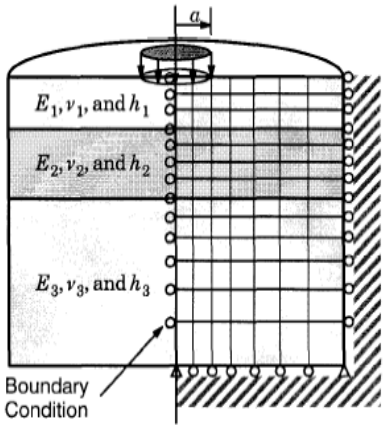

a) *Problem definition*

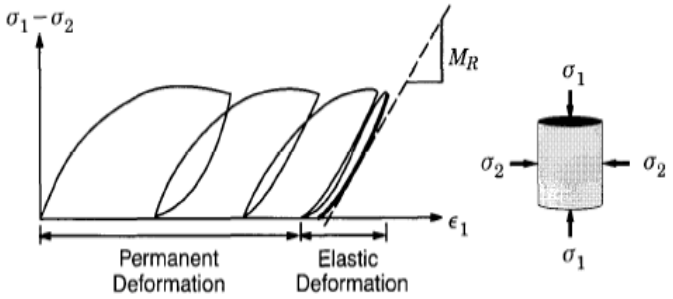

b) *Resilient behavior of granular materials*

Fig. 2.4: 2-D axisymmetry FEM programs

Taciroglu [58] used the method of fixed-point iteration for the non-linear solution algorithm. It has the following procedures:

1- Assume initial resilient modulus

2- Compute displacement by linear analysis

3- Compute strain and stress using displacement results

4- Compute new (or updated) resilient modulus

5- Compute the difference between former and updated resilient modulus

6- If the difference is within a given tolerance, then stop iteration, otherwise return to procedure 2 until the solution converges

This algorithm is very easy to implement but it has critical drawbacks, not least that the convergence of the solution is slow and not guaranteed (depending on the initial guess).

In spite of using non-linear material models, a large magnitude of tensile stress was still predicted from the bottom of the granular base layer, discussed in detail in the previous section. Such an unrealistic tensile stress remained in this approach because resilient behavior based material models, although non-linear, are still elastic models. In fact, the behavior of the tensile and compressive sides is symmetric in the space of deviator stress versus axial strain, which defines the resilient modulus.

In order to attenuate this unrealistic tensile stress prediction, Huang [26] developed an ad-hoc method that divides granular base layers into multiple sub-layers and updates any computed tensile stress from a sub-layer to zero. According to stress results, it eliminates tensile stress but, at the same time, is a time consuming process due to the corresponding non-linear iteration procedures.

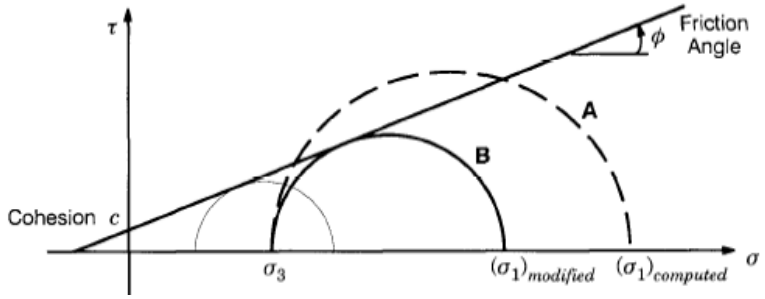

Fig. 2.5: Mohr Coulomb failure criterion [46]

The well-known Mohr Coulomb failure criterion was implemented in the ILLI-PAVE program. This criterion identifies element level failure in granular supporting layers and then limits the stress state of the failed elements. For example, if a computed stress state of a given element exceeds the failure criterion (circle A), that stress state is modified by reducing the major principal stress until the new circle touches the failure surface (circle B), as illustrated in Figure 2.5 [46].

Software in this category could simulate rigid pavement behavior better than those based on the Burmister theory. Nevertheless, fixed point iteration and the ad-hoc methods could create solution convergence problems. Analysis at the edge and corner of pavement is still restrained due to the axisymmetry assumption.

2.1.3.3 2-D plates on elastic foundation based programs

Soon after the introduction of finite element methods, many structural analysis programs were developed, with structural elements (for example, beam, spring, plate, and shell elements), including FINITE, SAP, and others. Pavement engineers also developed their own finite element software by employing such structural elements. ILLI-SLAB by Tabatabaie [57] was the first software in this category, and it provided a major breakthrough in rigid pavement research.

Furthermore, several other programs were developed during the 1980s with the objective of analyzing two-layered dowel-jointed rigid pavement systems. Ioannides [28, 29] made ILLI-SLAB more user-friendly and implemented more features. KEN-SLAB developed by Huang [25] and JSLAB developed by Tayabji and Colley [59] used the same 2-D plates on elastic foundation approach.

Tabatabaie [57] employed plates on a Winkler foundation into computer code ILLI-SLAB, but he no longer assumed infinite plates, as Westergaard had fifty years earlier. Instead, he used finite size Kirchhoff plate bending elements for simulating the concrete slab (Figure 2.6-a). Also, he included joint modeling capability by using beam elements, which simulated the dowel load transfer system. For the supporting layer's modeling, he employed an elastic foundation in his program, in addition to the Winkler foundation. The elastic foundation element like the Kirchhoff plate element has three DOFs (one vertical displacement and two transverse rotations) per node (Figure 2.6-a, -d) while the Winkler foundation element has only one DOF (vertical displacement).

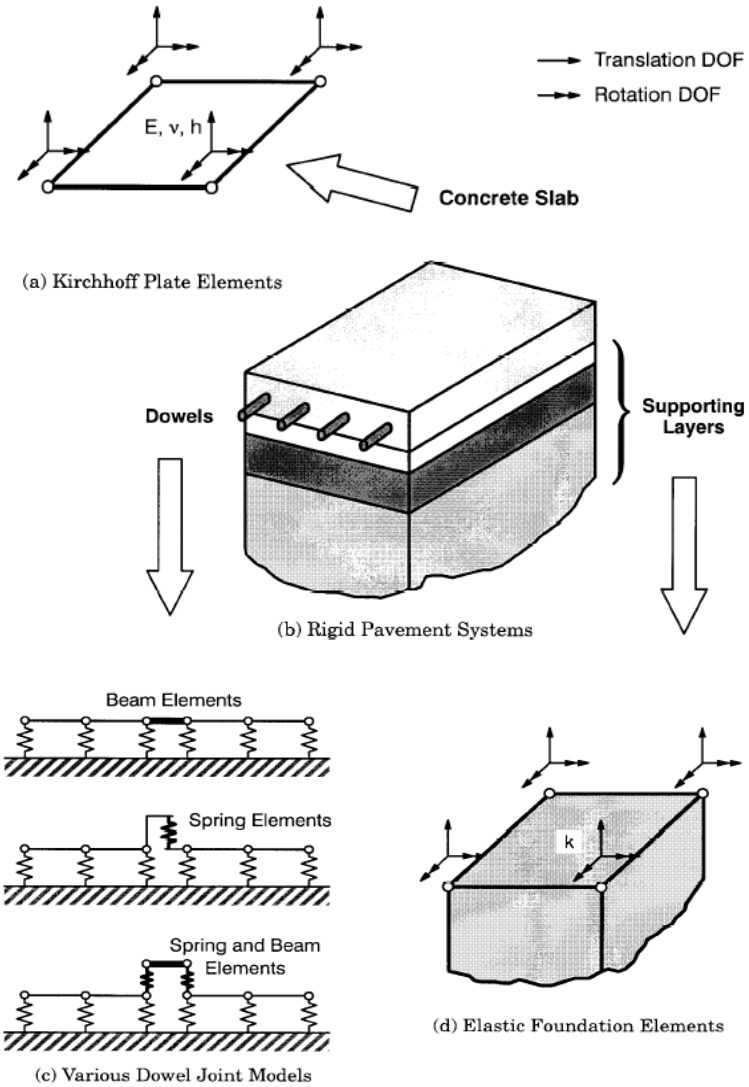

Fig. 2.6: Problem definition for 2-D plates on elastic foundation based programs

In providing support to the concrete slab, both elastic and Winkler foundation showed similar behavior (Figure 2.7) but the elastic foundation is closer to real subgrade behavior. The deformed shape of the supporting layer predicted from the elastic foundation is more reasonable than that from the Winkler foundation. However, both foundation models cannot account for the horizontal displacement of the supporting layer.

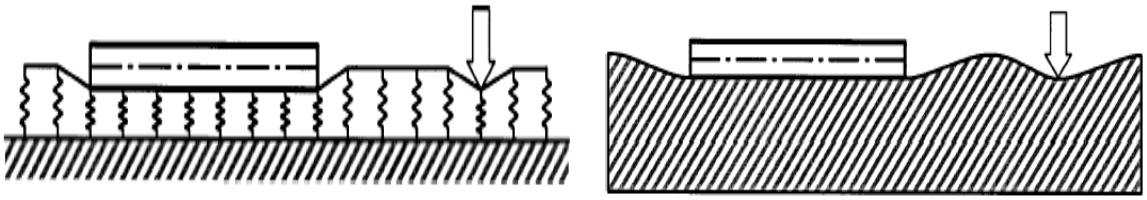

a) Behavior of Winkler foundation *b) Behavior of elastic foundation*

Fig. 2.7: Behavior of Winkler and elastic foundations

Ever since Westergaard, modeling of the dowel joints has been one of the most important issues in rigid pavement analysis. Tabatabaie [57] first simulated dowels using Tirnoshenko beam element in ILLI-SLAB, as demonstrated in Figure 2.6-c. After that, numerous modeling attempts were made in order to better simulate the behavior of dowel joints.

All aforementioned programs have shown good performance for ordinary pavement analysis and design through a series of numerical calibrations with field test measurements. As a result, they are widely used by numerous pavement engineers. Yet, important behavior of pavement systems was neglected by the 2-D assumptions behind this approach, including the kinematics' hypothesis, no shear deformation for Kirchhoff plate theory, and the subgrade reaction modulus for elastic foundation.

Recent pavement systems are often subjected to a much higher load magnitude in comparison to those 50 years ago. As a result, pavement systems are composed of a thick concrete slab and multiple supporting layers. Therefore, the above approach may produce a significant error in analysis of rigid pavement systems for the following reasons:

1- Multiple supporting layers cannot be replaced by the subgrade reaction modulus (denoted by k).

2- Rigid pavements are thick enough to produce nonlinear and shear deformation, which are not allowed in Kirchhoff plate theory.

3- Interface behavior, often caused by a bond-breaking interlayer between concrete slab and supporting layer, is ignored because plates are perfectly bonded with elastic foundation.

2.2 Numerical modeling of rigid pavement system

The numerical modeling of rigid pavement system is a very challenging problem because of its inherent complexity. The problem contains both geometric and material non-linearity and shows heterogeneous behavior originating from the multi-layered pavement structure. Also, applied loads and problem geometry are not symmetric. Hence, a suitable finite element approach is required to accurately investigate the behavior of rigid pavement systems. This section introduces some numerical difficulties associated with rigid pavement system.

1- Rigid pavement is a multi-layered system with different material properties in each layer. In order to capture the unique behavior of each pavement layer, a finite element approach with continuum solid elements is absolutely required because Kirchhoff plates on elastic foundation approach cannot represent multi-layered system with different material properties. A refined finite element mesh is needed to capture accurately the stress and strain variation across the thickness. A coarse mesh is required in remote regions to reduce the problem size. Meanwhile, such a combination of refined and coarse meshes could cause a bad aspect ratio problem in the remote region due to relatively thin pavement layers. This may increase the level of approximation error. Hence, attention to both mesh refinement and mesh ill-conditioning is needed.

2- Problem domain is unbounded while applied loading is highly localized. Approximately eighty cm thick rigid pavement sits on natural soil subgrade, an essentially unbounded domain. In contrast, applied loading can be enclosed within a 0.25 m by 0.25 m surface. Hence, there is a strong demand for an efficient transition mesh, which connects between refined elements at the vicinity of load and coarse elements in the remote domain. Furthermore, the unbounded domain also needs special treatment.

3- Non-linear material modeling is required to capture the behavior of granular material in supporting layers. Granular materials demonstrate a unique behavior, including limited tension carrying capacity, pressure dependent hardening, friction-governed behavior between grains, and volumetric dilatation. Hence, non-linear material modeling is absolutely necessary to capture the above characteristics.

4- Interface behavior exists between all layers of a pavement system. Of particular importance is the interface between the concrete slab and base layer. A thin bond-breaking interlayer, which prevents crack propagation from supporting layers to the concrete slab, is often installed on that interface. It allows discontinuous deformation and vertical opening across the interface under wheel load and temperature variation.

To overcome the above-mentioned difficulties, the next section introduces some important issues in finite element modeling for rigid pavement system.

2.3 Issues in finite element modeling

The Finite Element Method (FEM) has been increasingly viewed as the best approach to analyze the fundamental behavior of pavement structures. Despite many advantages of this powerful tool, it has not been adapted extensively to pavement analysis because of the difficulties associated with the mesh construction, the large amount of memory space required, and the long computational time required to reach a solution. Thus, developing tools to eliminate these difficulties are as important as the pavement analysis itself. Several general finite element programs were applied to rigid pavements, such as ADINA (1981), ANSYS, and ABAQUS (1989). Many researchers have verified the accuracy and reliability of these models. The finite element analysis possesses several advantages over plate theory calculations, as mentioned below:

1- A slab of any arbitrary dimension (uniform and non-uniform) can be analyzed.

2- Voids or loss of support beneath a slab can be considered.

3- Single and multiple wheel loads can be placed at any location on the pavement.

4- Temperature and traffic conditions can be applied simultaneously.

5- Multi-layer pavement systems can be modeled as either bonded or un-bonded.

6- Multiple slabs and cracks can be modeled with various load transfer conditions.

7- Both linear and non-linear stress-strain behavior of materials is permitted.

However, the finite element analysis should be applied with proper modeling for the mesh and element members. In addition, special consideration should be taken regarding the load and support conditions, slab geometry and configuration, and critical stress/deflection locations.

2.3.1 Issues in mesh generation of multi-layered system

The accuracy of finite element analysis depends on the mesh refinement and geometric characteristics of the finite elements, which include smooth transition, element distortion (acute or obtuse element corner angle), and element aspect ratio.

The total number of elements (or total number of degrees of freedom) in the finite element mesh governs the required computing time and data storage space. Three-dimensional meshes require a large number of extra elements in the thickness direction, while 2-D meshes only need a small number of elements in the planar domain.

2.3.1.1 Mesh refinement

The degree of mesh refinement is the most important factor in estimating an accurate stress field in pavement. A fine mesh is required in the vicinity of wheel loads to capture the steep stress and strain gradients. In general, smaller elements can reduce the discrepancy in stress and strain values predicted at the sampling point of each element. In the structural analysis of pavement systems, mesh refinement also determines how

many sampling points are available throughout the thickness of each layer and how close sampling points are to the point of true maximum. Thus, the use of more sampling points helps in capturing smoother variation [32]. Comparison of stress distributions obtained from several different refinement levels determines the optimum degree of mesh refinement.

Figure 2.8 shows the results of an axisymmetric analysis of a layered system with four different degrees of mesh refinement of the region under the load, level (I) being the coarsest and level (IV) the finest. Each subsequent refinement quarters the elements of the previous one. The horizontal stress (σ_{xx}) and the vertical stress (σ_{zz}) are plotted along the axis of symmetry in the figure. Four-node axisymmetric elements are used and stresses are reported at the centroid of each element.

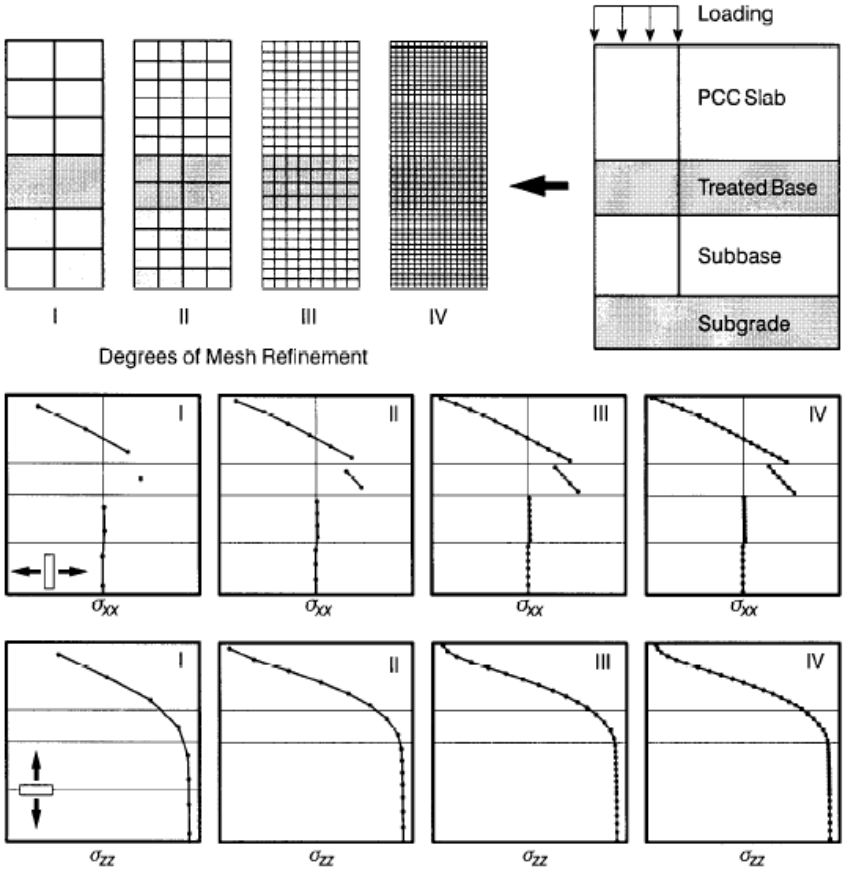

Fig. 2.8: Mesh refinement and stress results [32]

The results clearly show convergence with mesh refinement. Although the element centroids stresses appear to be accurate for the coarse mesh, the extreme values are not well represented, except by extrapolation. For the coarsest mesh, the second layer has only one element, making it impossible to estimate the bending effects in that layer.

Clearly, some of the finer features of the solution do not appear before a certain level of mesh refinement. For this example, one can conclude that refinement level (II) or higher is appropriate.

2.3.1.2 Geometric characteristics of finite elements

The accuracy of finite element analysis also depends on the geometric characteristics of the used finite elements, including element aspect ratio, element distortion, and transition of element size. In the case of continuum solid modeling, using a refined uniform mesh with square elements for 2-D or cubic elements for 3-D (element aspect ratio of 1.0, corner angles of 90^o, and uniform size) are optimal from the standpoint of solution accuracy and equation conditioning [6, 11, 35]. However, since the size of the smallest element is dictated by the stress gradients in the region of the load, a uniform mesh is prohibitively large for any practical application. Hence, a strategy for making a smooth transition to larger elements in the regions of small stress gradients is essential.

Finite boundary truncation was examined by Kim and Hjelmstad [32] with two different artificial boundary conditions, namely, the roller and fixed conditions, which are applied along the truncated domain. Domain size was varied from a 30 to a 250 load radii. This analysis was done for an axisymmetry model under a single wheel load.

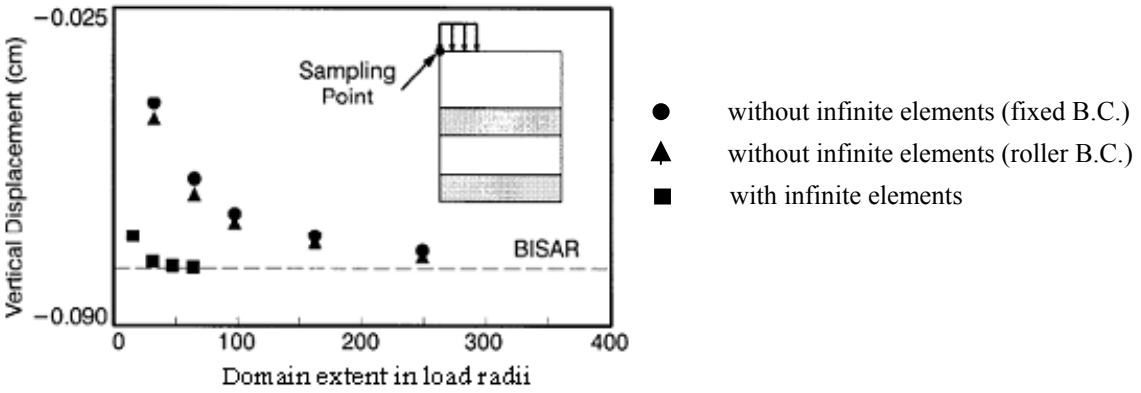

Fig. 2.9: Domain extent analysis with ABAQUS [32]

Figure 2.9 shows that the difference in the displacement under the load from the two different boundary conditions decreases as the domain extent increases. The influence of boundary truncation is negligible (less than 5%) for domains larger than a 150 load radii while exceptional accuracy is achieved for a domain extent of less than a 45 load radii with an infinite element model. The displacements and stresses resulting from an infinite element model with a domain greater than a 45 load radii are identical to the results obtained by BISAR program. The reduction in total elements achieved by using the infinite elements resulted in significantly reduced memory and CPU time requirements.

2.3.2 Frictional contact interface

Rigid pavements are composed of multiple layers, such as concrete slabs, base layer, sub-base, and granular subgrade. Each layer has its own distinct material properties that result in the interface behavior between layers. In rigid pavement analysis, the interface between the Portland cement concrete slab and unbound granular base layer needs more focus due to the following reasons:

1- The material characteristics above and below the interface are very different (strength and material constants).

2- Temperature curling deformation can create openings between layers.

3- The bond-breaking interlayer is often installed to prevent crack propagation from the supporting layer to the concrete slab.

Using a frictional contact interface can be the best treatment for this problem because it allows discontinuous deformation above and beneath the contact surface. Hence, the concrete slab and the supporting layer can behave separately while exchanging contact traction.

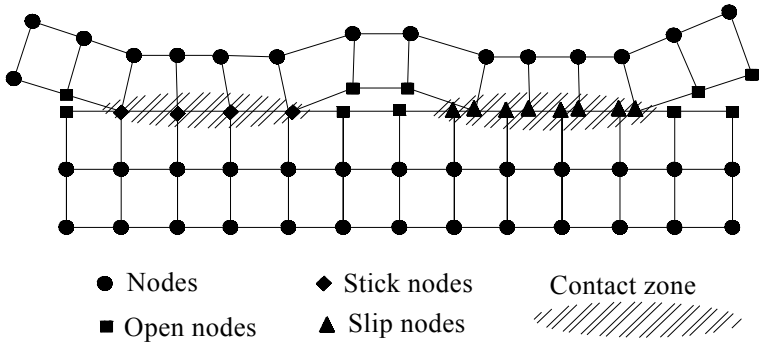

Fig. 2.10: Contact status in contact surface pair

The contact status is determined by non-linear equilibrium and discontinuity iteration procedure and is governed by the transmission of normal and tangential contact pressure and the relative displacement between nodes belonging to the contact surface pair [2].

The classifications of contact nodes are **open, slip,** and **stick,** which have literal meanings, as illustrated in Figure 2.10. The **stick** and **slip** nodes can carry both normal and tangential contact pressure between nodes, while the **open** nodes cannot. The full amount of normal contact pressure can be transmitted through the contact surface pair under **stick** and **slip** status. However, a limited amount of the tangential contact pressure (shear stress) can be carried by the contact surface because Coulomb's law of friction determines the frictional resistance of contact surface.

If the shear stress acting over a certain region of a contact surface pair exceeds its frictional resistance, that region is under **slip** status and a corresponding relative tangential displacement is observed in the direction of applied shear stress. Otherwise, the region is under **stick** and no tangential relative displacement occurs. The normal relative displacement is zero for both **stick** and **slip** and only positive for **open**. Negative normal relative displacement means penetration between two solid bodies and is not allowed. The bending deformation induced by the heavy wheel load causes tangential relative displacement between the concrete slab and the supporting layers. Curling of the concrete slab under temperature gradients causes openings between the concrete slab and the base layer, which can be closed again under heavy wheel loads.

The frictional contact interface eliminates the high tensile bending stress predicted in supporting layers (which was mentioned with the Burmister solution in section 2.1.1 and the 2-D axisymmetric finite element approach in section 2.1.3). Discontinuous deformation above and beneath the contact interface makes the concrete slab and supporting layers behave separately in resisting bending deformation from wheel loads.

The frictional contact algorithm requires a considerable amount of extra computing time for the non-linear equilibrium and discontinuity iterations.

2.3.3 Numerical modeling of granular materials

Neither of the two classical analysis methods of rigid pavement have accounted for the non-linear behavior of granular materials. In these methods, the supporting layers are considered as a Winkler foundation or an elastic layer. Moreover, no consideration for permanent deformation behavior is included.

The supporting layers are the main cause of most problems in both pavement systems, for example rutting in flexible pavement and stepping in rigid pavement. Therefore, growing interest in studying the mechanical behavior of unbound granular materials is involved. In flexible pavements, especially when thinly surfaced, the overall structural performance is largely dependent on the behavior of the unbound granular base layer. Therefore, a proper understanding of the mechanical properties of granular materials is necessary for developing successful analytical design procedures for pavement systems.

Although granular material is one of the most commonly used materials in civil engineering applications, it is one of the most difficult materials to simulate in numerical analysis. Granular material is composed of numerous discontinuous grains and shows a highly non-linear response due to the bonding and friction between grains. Hence, granular material demonstrates very different behavior from continuum solid materials such metals. As a result, it is very difficult to characterize the behavior of granular materials within the context of continuum mechanics. In order to characterize the complex behavior of UGMs, pavement engineers have developed their own non-linear elastic material models for granular materials, for example, K-θ, Boyce, Uzan, Dresden, and other models. These models are based on the resilient behavior of granular materials observed under triaxial test after a high number of load repetitions.

Also a lot of work was done to develop models for permanent deformation behavior of unbound granular materials under cyclic loading. The most famous model is the Paute model. A detailed review of the mechanical behavior of unbound granular materials is discussed in Chapter 3. The problem lies in defining such behavior in finite element programs and learning to make use of them.

2.3.3.1 Material library in ABAQUS

The material library in ABAQUS is intended to provide comprehensive coverage of linear and non-linear, isotropic and an-isotropic material models. Material behavior falls into the following general categories [2]:

1- General properties (material damping, density, thermal expansion)

2- Elastic and inelastic mechanical properties

3- Thermal properties

For the description of the unbound granular materials, the choice between many different material models is available, such as linear elastic model, visco-elastic model, Mohr Coulomb or Drucker Prager plastic models, and many others. In order to characterize the behavior of UGMs differently to those models available in ABAQUS, for example, resilient elastic or permanent deformation behavior under cyclic loading, a user defined material subroutine (UMAT) can be developed and implemented.

2.3.3.2 User defined material subroutine

User defined material subroutine (UMAT) is a powerful option in ABAQUS, which provides an interface to the main solver to allow the definition of any mechanical constitutive model for a material through the user. This is needed when the material behavior does not follow one of the common models available in the material library. The mean features of UMAT subroutine are [2]:

1- It can be used with any procedure that includes mechanical behavior.

2- It can use solution-dependent state variables.

3- It must update the stresses and solution-dependent state variables to their values at the end of the increment for which it is called.

4- It must provide the material Jacobian matrix ($\partial\Delta\sigma/\partial\Delta\varepsilon$) for the mechanical constitutive model.

5- It can be used in conjunction with the user defined field variable subroutine (USDFLD) to redefine any field variables before they are passed in.

UMAT is executed for each integration point of the material at every time increment. The accuracy of the results depends on the size of the chosen time increment. A smaller time increment will yield better results, but at the same time requires longer computing time. User has to find a balance between the accuracy of results and the computing effort.

A complete description of the constitutive laws used for the definition of deformation behavior of UGMs in the UMAT subroutine used in this research is discussed in Chapters 4.

2.4 Computation of faulting

The problem of faulting has not been studied intensively, in spite of its great influence to pavement distress. Khazanovich et al [31] developed an empirical formula to calculate the faulting in rigid pavement system through an accumulative function.

The developed empirical equation has a number of factors which need to be calibrated according to many criteria, for example, the weather conditions, the characteristics of unbound granular base materials, and other related factors as mentioned below:

$$Fault_m = \sum_{i=1}^{m} \Delta Fault_i \quad (2.12)$$

$$\Delta Fault_i = C_{34} \text{ x } (FAULTMAX_{i-1} - Fault_{i-1})^2 \text{ x } DE_i \quad (2.13)$$

$$FAULTMAX_i = FAULTMAX_0 + C_7 \text{ x } \sum_{j=1}^{m} DE_j x \log (1 + C_5 x 5.0^{EROD})^{C_6} \quad (2.14)$$

$$FAULTMAX_0 = C_{12} \text{ x } \delta_{curling} \text{ x } \left[\log(1 + C_5 x 5.0^{EROD}) x \log\left(\frac{P_{200} x WetDays}{P_s} \right) \right]^{C_6} \quad (2.15)$$

Where:

$Fault_m$ = mean joint faulting at the end of month m [inches]

$\Delta Fault_i$ = incremental change (monthly) in mean transverse joint faulting during month i [inches]

$FAULTMAX_i$ = maximum mean transverse joint faulting for month i [inches]

$FAULTMAX_0$ = initial maximum mean transverse joint faulting [inches]

$EROD$ = base/subbase erodibility factor

DE = differential elastic deformation energy

DE = ½ x k x $(W_L + W_{UL})$x$(W_L - W_{UL})$ [kPa.mm]

k = modulus of subgrade reaction [kPa/mm]

W_L = deflection of loaded slab [mm]

W_{UL} = deflection of unloaded slab [mm]

$\delta_{curling}$ = maximum mean monthly slab corner upward deflection due to temperature curling and moisture warping [mm]

P_s = overburden on subgrade [lb]

P_{200} = percent subgrade material passing #200 sieve

Wet Days = average annual number of wet days (greater than 0.1 inch rainfall)

C_1 through C_7 and C_{12}, C_{34} are calibration constants:

C_{12} = $C_1 + C_2$ x $FR^{0.25}$

C_{34} = $C_3 + C_4$ x $FR^{0.25}$

$C_1 = 1.29$, $C_2 = 1.1$, $C_3 = 0.0001725$, $C_4 = 0.0008$, $C_5 = 250$, $C_6 = 0.4$, $C_7 = 1.2$

FR = base freezing index defined as percentage of time the top base temperature is below freezing (32 °F) temperature.

3 MODELING OF UNBOUND GRANULAR MATERIALS

During recent decades, growing interest in the development of so-called analytical or mechanistic road pavement design methods has resulted in substantial research into the mechanical behavior of the materials involved.

In comparison with most concrete and steelwork structures, the layered form of a road pavement is relatively simple. Nevertheless, due to complexities in the behavior of the constituent materials under traffic loads and environmental conditions, pavement design techniques are still far from advanced. A fundamental requirement for an analytical approach to pavement design is a proper understanding of the mechanical properties of the constituent materials. The unbound granular base and sub-base layers in a pavement play an essential role in the overall structural performance of the pavement structure. However, the current knowledge concerning granular materials is limited.

3.1 Resilient behavior of unbound granular materials

Nazarian and Boddspati [39] have shown that non-linear behavior occurs in Falling Weight Deflectometer (FWD) testing. An increase in the load magnitude of the FWD results in an increase in deflection that is less than one to one. Several procedures have been developed to try to handle the non-linearity of unbound layers in pavement structures. Some analyses attempt to model the non-linearity by considering the plastic behavior of subgrade soils. Others approximate non-linear effects through iterative linear elastic procedures. Most recently finite element codes have been utilized in modeling the stress state dependency of granular base layers, and the strain level dependency of subgrade materials.

As stresses and strains are used more and more to determine the relative condition of layers in a pavement structure, the need for consideration of non-linear material behavior becomes increasingly important. Linear elastic approximations of unbound material behavior are no longer acceptable in pavement analysis. Errors from such approximations have been noted and documented. The stress state dependency of granular materials must be considered for an accurate estimation of true pavement response.

Various non-linear elastic models, derived from Repeated Load Triaxial (RLT) tests, have been proposed to describe the response of granular materials under loading. Several widely used models are summarized in Table 3.1.

Table 3.1: Resilient modulus models for granular materials

Model	Model expression	Model constants
K – θ	$M_r = k_1 \theta^{k_2}$	k_1, k_2
Uzan	$M_r = k_1 \theta^{k_2} \sigma_d^{k_3}$	k_1 , k_2 , k_3
UT-Austin	$M_r = k_1 \sigma_d^{k_2} \sigma_3^{k_3}$	k_1 , k_2 , k_3
UT-E1 Paso	$M_r = k_1 \sigma_d^{k_2} \varepsilon_a^{k_3}$	k_1 , k_2 , k_3
Boyce	$M_r = \frac{9KG}{3K+G}$ $K = \frac{K_a.(p/p_a)^{1-n}}{1-\beta(\frac{q}{p})^2}$ $G = G_a.(p/p_a)^{1-n}$ $\beta = \frac{(1-n)K_a}{6G_a}$	K_a, G_a, n
Dresden	$E_r = (Q + C\sigma_3^{Q_1})\sigma_1^{Q_2} + D$ $\nu_r = R\,\sigma_1/\sigma_3 + A\,\sigma_3 + B$	Q, Q_1, Q_2, A, B, C, D, & R

Where:

θ = bulk stress = $\sigma_1 + \sigma_2 + \sigma_3$

σ_d = deviator stress = $\sigma_1 - \sigma_3$

q = deviator stress = $\sigma_1 - \sigma_3$

σ_1 = absolute value of maximum principal stress

σ_3 = absolute value of minimum principal stress

= confining stress = σ_2

P = mean normal stress = $(\sigma_1 + \sigma_2 + \sigma_3)/3$

M_r = resilient modulus

E_r = resilient modulus

ν_r = resilient Poisson's ratio

K = bulk modulus

G = shear modulus

ε_a = axial strain, and

P_a = arbitrary pressure equal to 100 kPa

The experimental models obtained from Constant Confining Pressure (CCP) tests show the influence of stress on the stiffness. The CCP test gives for each stress-level the secant resilient modulus (M_r) determined by the simple expression:

$$M_r = \frac{q_r}{\varepsilon_1^{\,r}} = \frac{\sigma_1^{\,r} - \sigma_3^{\,r}}{\varepsilon_1^{\,r}} \tag{3.1}$$

Where q_r is the cyclic deviator stress and $\varepsilon_1^{\,r}$ being the resilient axial strain. The influence of the stress-level on the resilient modulus (M_r), demonstrating the non-linearity of the elastic behavior, has generally been described by a relationship of the form [23]:

$$M_r = k_1 . \theta^{k_2} \tag{3.2}$$

Where θ is the sum of principle stresses at the maximum deviator stress of a loading cycle and is expressed as:

$$\theta = \sigma_1 + \sigma_2 + \sigma_3 \tag{3.3}$$

k_1 and k_2 are material constants.

The resilient Poisson's ratio is simply determined as: $\nu_r = - \varepsilon_3^{\,r} / \varepsilon_1^{\,r}$, where $\varepsilon_3^{\,r}$ is the resilient radial strain.

The tests carried out with Variable Confining Pressure (VCP) offer more possibilities for resilient modeling. For example, Boyce [7] proposed a non-linear elastic model capable of adequately describing the behavior observed in the VCP tests.

The stress-strain relationships characterizing an isotropic elastic material are:

$$\varepsilon_v = \frac{1}{K} . p \qquad \text{and} \qquad \varepsilon_q = \frac{1}{3G} . q \tag{3.4}$$

Where K is the bulk modulus, G is the shear modulus, p is the mean normal stress, and q is the deviator stress.

The K-θ model was the most popular model in the past due to its simplicity. In this model, the resilient modulus of granular materials is expressed as a function of the bulk stress (θ). Only two material constants (k_1 and k_2) are required, which can be regressed from the experimental data. One drawback of this model is that it neglects the effect of the shear stress on the resilient modulus, which can result in an inaccurate prediction of material behavior.

Uzan's model and the UT-E1 Paso's model overcome this problem by adding either the measured deviator stress (σ_d) or axial strain (ε_a) as the extra parameter to predict the resilient modulus. The UT-Austin's model directly relates two independent variables, the deviator stress (σ_d) and the confining pressure (σ_3) to the resilient modulus. Compared to the K-θ model, Uzan's model, the UT-E1 Paso's model, and the UT-Austin's model all show better agreement with the experimental data.

Boyce's model, widely used in European countries, is one of the advanced models for granular materials. Although better results may be obtained from this model, more

complicated testing and material constants evaluation procedures are required. Thus it is not considered practical in routine use.

The Dresden model has been developed and modified by Wellner in the last ten years at the Dresden University of Technology. The model is expressed in terms of a resilient modulus (E_r) and a resilient Poisson ratio (ν_r) where the values of (E_r) and (ν_r) depend on the applied stresses. The Dresden model will be discussed in detail in section 3.3.

In order to provide models which could be applied in a FEM code for response and performance modeling of pavement structures with unbound granular bases, two non-linear elastic models were used in the COURAGE project [14]: the Boyce's model and the Dresden model.

The two models have been selected in the basis of:

1- The good prediction obtained with the Boyce's model in the preliminary study carried out in the COST 337 project [13]

2- Their ability to describe the results of repeated load triaxial tests with variable confining pressure (i.e. the response of the material to a wide range of different stress paths)

3- The possibility to use these models for pavement structure calculations, using the finite element method

3.1.1 Effect of initial stresses

Most pavement design approaches, including the AASHTO methods, presently use a single value of the resilient modulus of each layer in the thickness selection process. Therefore, to select the design resilient moduli, the representative stress state acting upon each layer must be either known or assumed. The complete stress state consists of the combined effect of the initial residual stresses existing after construction and the dynamic stresses caused by traffic loading. Temperature and moisture induced stresses in stabilized layers are also important, but have received almost no attention.

During construction, heavy compaction equipment is used to densify, in thin lifts, the subgrade, base, and surface layers. The heavy construction equipments then use each completed lift as a temporary working platform. Usually the greatest stresses to which a particular layer is ever subjected are applied during either compaction or else by construction equipment before the pavement is completed. The application of large vertical stresses during the stage of construction causes lateral stresses to develop in granular layers, these stresses are called residual lateral stresses [3, 15, 64].

Uzan [64] has pointed out that residual lateral stresses of 14 kPa have been observed for cohesionless and cohesive soils. Methods of analysis proposed by Uzan [64], Selig [52], and Duncan and Seed [15] are quite encouraging for predicting residual lateral stresses due to compaction of both granular and cohesive soils. Selig [52] concluded that the residual lateral stress is the most important factor limiting permanent deformation in the

bottom of a granular base. Residual lateral stress is also an important factor determining the appropriate confining pressure at which to evaluate the resilient modulus.

The residual lateral stress (σ_{hr}) is relatively large and can be expressed as follows [52]:

$$\sigma_{hr} = k_o \, \sigma_v \qquad (3.5)$$

Where (σ_v) is the vertical overburden stress and (k_o) is the coefficient of lateral earth pressure considering residual stress, which is greater than the unity but less than the passive coefficient of earth pressure (k_p). For a granular material the passive coefficient of lateral earth pressure (k_p) = $tan^2 (45+\varphi/2)$, where (φ) is the angle of internal friction.

Earlier studies have shown that residual stresses develop in granular base due to compaction during construction and subsequent traffic loading. These residual stresses were considered in the GT-PAVE analysis. Residual stresses of 14.0, 21.0, and 34.5 kPa were used for analysis of the pavement cross-section with a 20 cm AC surface, a 108 cm thick granular base layer, and medium strength subgrade. Figure 3.1 shows the effect of residual stresses on surface and subgrade deflections. Including granular base residual stress in the analysis reduces the surface and subgrade deflections, since the residual stress in the horizontal direction reduces the vertical compressive strain and stress in the pavement. Subgrade and surface deflections predicted by the two programs, ILLI-PAV and GT-PAVE are in agreement [17].

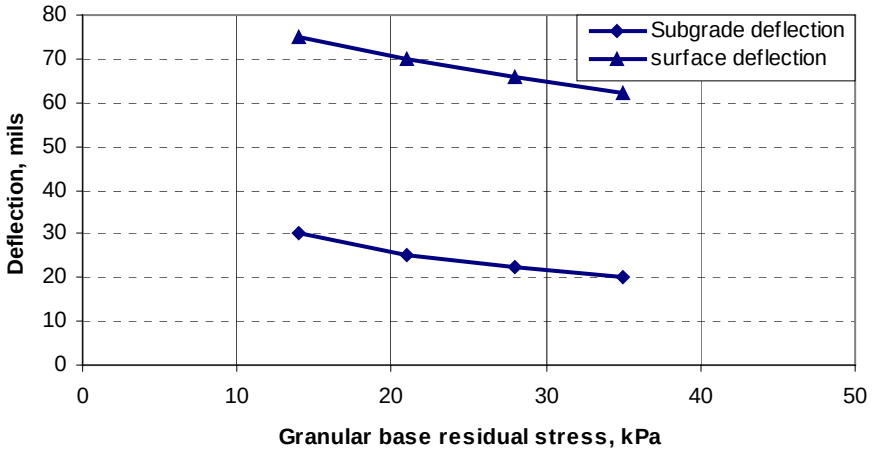

Fig. 3.1: Effect of residual stresses on surface and subgrade deflections [17]

3.2 Permanent deformation of unbound granular materials

Unbound granular materials exhibit both resilient and permanent deformation under traffic loading. The rutting in a flexible pavement system is initiated firstly in the unbound base layer under heavy loads of traffic; this illustrates the permanent deformation behavior of UGMs. To date, no overall framework has been established to satisfactorily explain the response of unbound granular layers to the complex repeated rotational loading, which they undergo due to traffic (Figure 3.2).

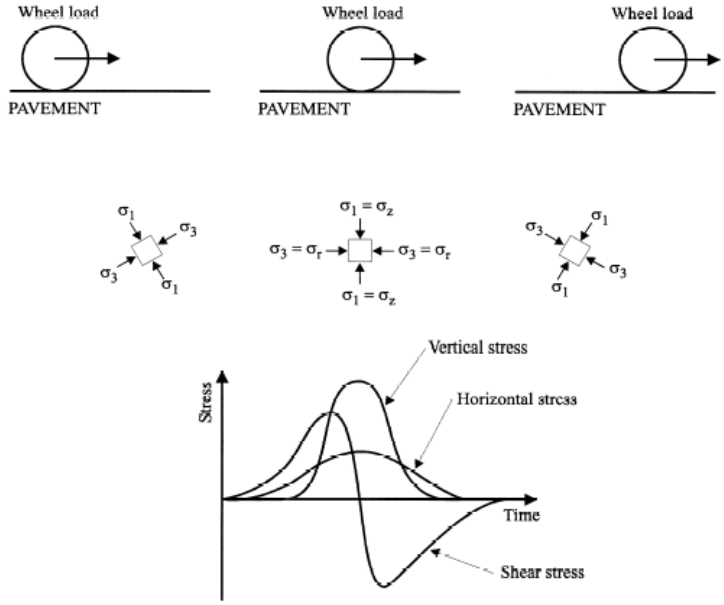

Fig. 3.2: Stresses in a pavement structure due to moving load

Granular materials, when subjected to repeated loading, exhibit permanent deformation in addition to resilient deformation. During each load repetition, the permanent deformation is normally just a fraction of the total deformation produced. However, the gradual accumulation of these small permanent deformation increments with the number of loading cycles could lead to the distress in pavement systems, for example rutting in flexible pavement and faulting in rigid pavement.

For a long time, many researchers have studied the complex behavior of granular materials under repeated loading, using laboratory and in-situ testing techniques. The research has been mainly concentrated on understanding the resilient behavior of these materials and great progress has been made. Compared with the data available on the resilient behavior, the information on the build-up of permanent strain in granular materials is limited. Some current studies concentrate on the understanding of long-term behavior of unbound granular materials regarding the effect of the number of loading cycles and stress-levels on the accumulation of plastic strain. Some of the modeling techniques shall be discussed in the following sections.

3.2.1 Modeling of permanent deformation of UGMs

One of the main objectives of research into the long-term behavior of granular materials is to establish a constitutive model, which allows an accurate prediction of permanent strain. In such a relationship, it is essential to take into account the gradual accumulation of plastic strain as a function of the number of loading cycles as well as the important role played by the stress condition. Over the years several researchers have attempted to outline procedures for predicting permanent strain in unbound granular materials. Barksdale [4] performed a comprehensive study of the behavior of different base course materials using repeated load triaxial tests with 10^5 load

applications. For a given stress condition, the accumulation of permanent axial strain was shown to be proportional to the logarithm of the number of loading cycles and the results could be expressed by a log-normal expression of the form:

$$\varepsilon_{1,p} = a + b \,.\, log\,(N) \qquad (3.6)$$

where :

$\varepsilon_{1,p}$: total permanent axial strain

N : number of loading cycles

a , b : constants for a given level of deviator stress and confining pressure

The long-term behavior of granular materials was also investigated by Sweere [56]. After applying 10^6 loading cycles in repeated load triaxial test, Sweere observed that the log-normal expression did not fit his test results. He then suggested that for large number of cycles, a log-log approach should be employed and expressed the results as follows [56]:

$$\varepsilon_{1,p} = a \,.\, N^{b} \qquad (3.7)$$

In which a and b are regression parameters. The applicability of this log-log model was later questioned by Wolff and Visser [73] who performed full-scale Heavy Vehicle Simulator (HVS) test with several million loading cycles. They suggested a different model given as [73]:

$$\varepsilon_{1,p} = (c \,.\, N + a) \,.\, (1 - e^{-bN}) \qquad (3.8)$$

In which a, b and c are regression parameters.

3.2.2 Modeling with respect to the stress condition

Previous research has shown that the stress-level is one of the most important factors controlling the build-up of permanent strain in granular materials. Several researchers who studied unbound granular materials have found that, with regard to the stress condition, permanent deformation behavior is principally governed by some form of stress ratio. Lashine et al [34] conducted repeated load triaxial tests on crushed stone and noted that the measured permanent axial strain was related to the ratio of q/σ_3, where q and σ_3 are the deviator stress and confining pressure respectively. Pappin [44] described the permanent shear strain as a function of the length of the stress path in the (p-q) space and the applied shear stress ratio (q/p), where p is the mean normal stress.

Other researchers have reported that the amount of permanent strain is determined by how close the applied stresses are to the static failure stress. Barret and Smith [5] suggested that the stress ratio ($q_{max}/q_{failure}$) could be used to estimate the value of permanent strain. Thom [60] stated in his studies that permanent shear strain is related to the stress ratio (($q_{failure} - q_{max}$)/q_{max}). Paute et al [45] employed a new approach to express the influence of both of the number of loading cycles and stress-levels on the build-up of permanent strain in granular materials.

This approach is based on the assumption that permanent strain increases asymptotically towards a limit value, which in turn, is a function of stresses related to the static failure condition of the material. According to the Paute's model, the gradual accumulation of permanent axial strain with the number of loading cycles can be expressed as [45]:

$$\varepsilon_{1,p}^{*}(N) = A_1\left[1-\left(\frac{N}{100}\right)^{-B}\right] \tag{3.9}$$

where:

A_1 : strain rate-type parameter

B : parameter

$\varepsilon_{1,p}^{*}$: axial permanent strain, with removal of first 100 cycles

N : number of loading cycles

This model was developed at the French Network of Laboratories des Ponts et Chaussées (LCPC) and was used in the COURAGE project [14] to model the permanent strain behavior of the unbound granular materials.

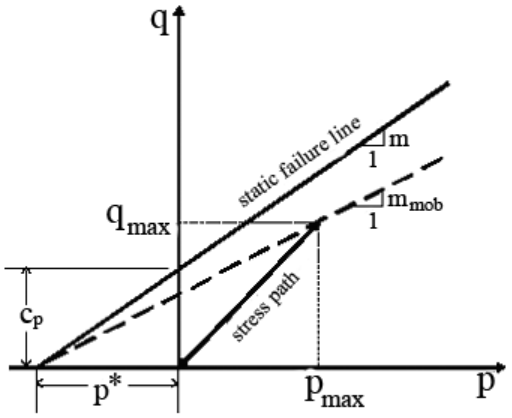

Fig. 3.3: Static failure line and mobilized stress [8]

According to equation 3.9, permanent axial strain ($\varepsilon_{1,p}^{*}$) goes towards a limit value (equal to A_1) as (N) increases towards infinity. The parameter A_1 is, therefore, considered as the limit value for total permanent axial strain. The stress state of the material is compared with the static failure line as shown in Figure 3.3. The maximum shear stress ratio is defined as the value of (q_{max} /(p_{max} + p*)), where p* is the stress parameter obtained by the intersection of the failure line and the p-axis. Thus this maximum shear stress ratio (m_{mob}) is, in soil mechanics terms, a (mobilized) fraction of the static failure condition, which has slope m, as illustrated in Figure 3.3 [8]. It is suggested that the value of total accumulated permanent strain (A_1) increases with the maximum shear stress ratio (m_{mob}) according to equation 3.10, in which b is a regression parameter.

$$A_1 = \frac{m_{mob}}{b.(m - m_{mob})} \tag{3.10}$$

Another model used in the COURAGE [14] is the permanent strain rate (VESYS) model, which defines the permanent deformation of the UGMs and has the following form:

$$\varepsilon_{1,p}^{*}(N) = \varepsilon_1^r \frac{\mu}{\alpha} N^{\alpha} \qquad (3.11)$$

where:

μ and α : parameters

$\varepsilon_{1,p}^{*}$: axial permanent strain, with removal of first 100 cycles

ε_1^r : axial resilient strain

N : number of loading cycles

Taking the derivative of the equation 3.11, with respect to the number of loading cycles, yields the rate of permanent strain parameter at a selected cycle number:

$$\frac{d\varepsilon_{1p}^{*}}{dN}(N) = \varepsilon_1^r \mu N^{\alpha-1} \qquad (3.12)$$

where $\frac{d\varepsilon_{1p}^{*}}{dN}$ is strain rate parameter [% / cycle]

This model, and the LCPC (Paute's model) both neglect the first 100 cycles of measured strains due to the effect of bedding, etc.

3.3 Dresden model for the unbound granular materials

The Dresden model for the unbound granular materials consists of two separate models: the first one is for the elastic resilient behavior, developed by Wellner et al, and the second is for the permanent deformation behavior, developed by Werkmeister.

3.3.1 Non-linear elastic Dresden model for UGMs

Investigations into the resilient strain behavior of UGMs were carried out at the Dresden University of Technology mainly by Wellner [67], Gleitz [18] and Numrich [42]. When conducting modified plate-bearing tests on UGLs by Wellner [67] using cyclic loading, surface heaving was observed at a distances from 0.45 to 1.20 m away from the center of the load (Figure 3.4). At all measured stress-levels, the same behavior was observed. Linear elastic analysis could not predict this heaving behavior. Therefore, RLT tests were conducted on the same UGMs to investigate their non-linear elastic behavior. Detailed analysis of the data from the RLT tests enabled a new material law, the Elastic Dresden Model, to be developed [18, 67]. This non-linear elastic model is expressed in terms of a resilient modulus of elasticity (E_r) and a resilient Poisson's ratio (ν_r):

$$E_r = (Q + C \sigma_3^{\,Q_1}) \sigma_1^{\,Q_2} + D \qquad (3.13)$$

$$\nu_r = R \sigma_1 / \sigma_3 + A \sigma_3 + B; \qquad \text{where } (0.0 < \nu_r < 0.5) \qquad (3.14)$$

where:

D [kPa] : constant term of the resilient modulus of elasticity

B [-] : constant term of the resilient Poisson's ratio

Q_2 [-] : constant

Q, C, Q_1, R, A : model parameters, determined from the RLT tests

σ_1, σ_3 : absolute values of major and minor principal stresses respectively

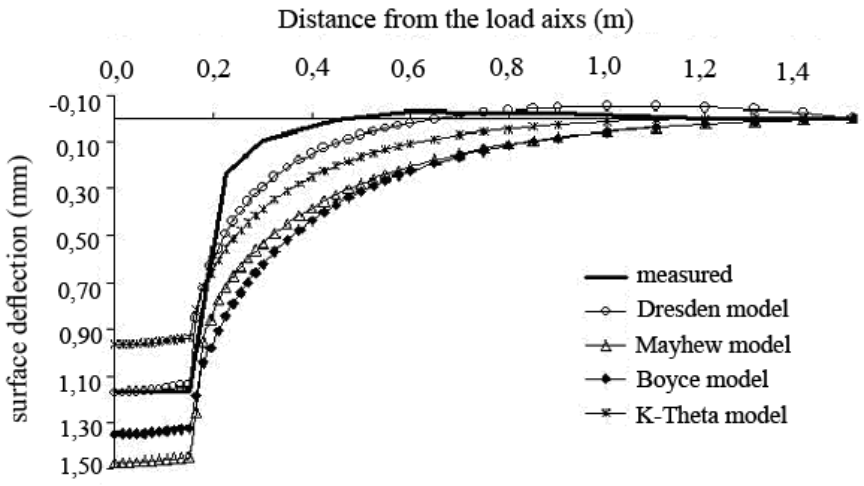

Fig. 3.4: Comparison of measured and FEM results for surface deflections [67]

The Dresden model includes a stress-independent stiffness, parameter D, (as a compensation for the residual confining in-situ stress, discussed in section 3.1.1) of 38.0 MPa for crushed materials and 30.0 MPa for sandy gravel materials. The parameter D is mainly influenced by such macroscopic parameters as the degree of compaction of the UGMs, the content of fines, the shape of the grains, and the water content ratio. The parameter D cannot be determined from the RLT tests because the residual stresses need some time to develop in a real pavement construction. According to the Herzian contact theory, Wellner et al [18, 42, 67] have determined a value of 0.333 for the constant parameter Q_2. To obtain the other model parameters, the RLT apparatus at Nottingham University was used [18].

In Figure 3.4, the surface deflections induced by plate bearing tests were predicted using the FEM program FENLAP. A comparison was carried out to assess the accuracy of other material laws (e.g. Mayhew, Boyce and K-θ models) by comparing the results of calculated deflections from all models against the measured ones. The K-θ model predicted a smaller deflection in the load axis than the measured one, the shape of the deflection basin being similar to that of the measured one (except in the area of heaving). The calculation with Mayhew and Boyce models gives a prediction of the deflections greater than the measured one in the load axis. Gleitz [18] concluded that the resilient elastic Dresden model generated the best solution, because the maximum

deflection under the load agrees with the measured value. In addition heaving away from the loading plate could be observed with the resilient elastic Dresden model.

3.3.2 Dresden model for permanent deformation in UGMs

Various models to describe the permanent deformation behavior of unbound granular materials were discussed in section 3.2, but since none of the previous models obviously fit the experimental results, a conceptual plastic model based on the Huurman's model [27] was developed by Werkmeister [68]. Three different phases of deformation behavior of unbound granular materials have been observed. In general, these can be described mathematically in a separate way (Figure 3.5) [68]:

Phase I : Post-compaction in the ranges A, B and C

Phase II : Stable behavior in the ranges A, B and C

Phase III : Collapse in the ranges B and C

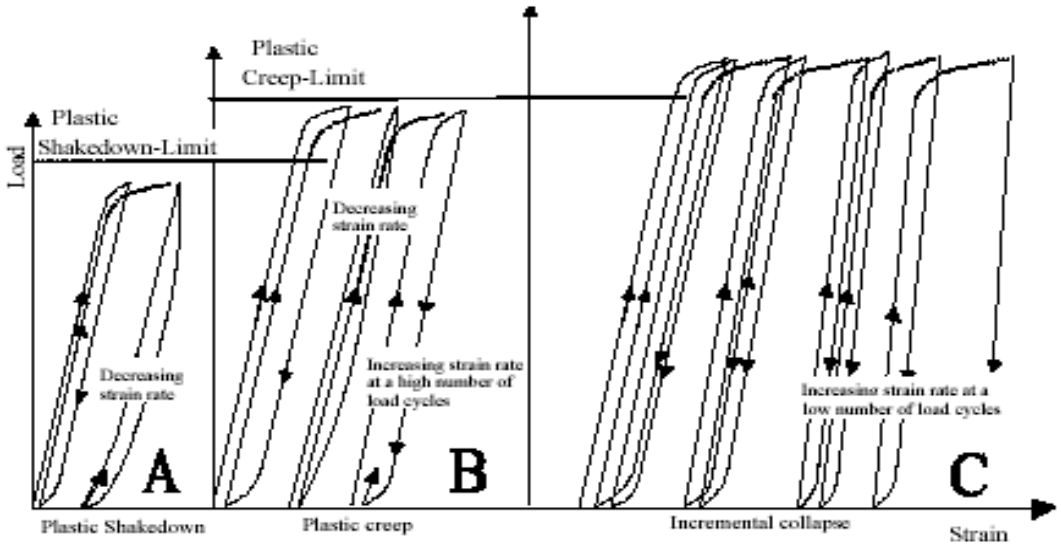

Fig. 3.5: Different phases of deformation behavior of UGMs under cyclic load [68]

The Huurman's model describes phases II and III of the permanent deformation process. However, phase I (the post-compaction) could not be described accurately. This is unimportant because the post-compaction period in pavement structures only occurs once.

As mentioned in section 3.2.1, the permanent deformation behavior can be described through a linear increase of (ε_p) on an (ε_p) versus log (N) scale. Based on the Huurman's model, Werkmeister used the following relationship to describe the permanent deformation behavior in phase II [68]:

$$\varepsilon_p(N) = A.\left(\frac{N}{1000}\right)^B \qquad (3.15)$$

where:

ε_p [‰] : permanent strain

A, B [-] : model parameters

N [-] : number of loading cycles

For the implementation of RLT measured permanent strain in the computation of pavement structures, the permanent strains in the materials have to be determined as a function of the applied stresses and the number of loading cycles.

However, the determination of the parameters *A, B, C* and *D* for the model proposed by Huurman [27] is depending on σ_1 (major principal stress) and $\sigma_{1,f}$ (major principal stress at failure). Investigation for the determination of $\sigma_{1,f}$ from Static Triaxial (ST) tests could not give the required results for the crushed UGMs. A new approach has been proposed by Werkmeister [68] to determine the parameters *A* and *B* as a function of the maximum (σ_1) and minimum (σ_3) principal stresses for the range A (Eqns 3.16 and 3.17) and for the range B (Eqns 3.18 and 3.19) in Phase II, as follows:

$$A = (a_1 . e^{a2.\sigma 3})\sigma_1^2 + (a_3 . \sigma_3^{\ a4})\sigma_1 \tag{3.16}$$

$$B = (b_1 . e^{b2.\sigma 3})\sigma_1 + (b_3 . \sigma_3^{\ b4}) \tag{3.17}$$

$$A = (a_1 . \sigma_3^{a2}).\left(\frac{\sigma_1}{\sigma_3}\right)^2 + (a_3 . \sigma_3^{\ a4})\frac{\sigma_1}{\sigma_3} \tag{3.18}$$

$$B = (b_1 . \sigma_3^{b2}).\left(\frac{\sigma_1}{\sigma_3}\right) + (b_3 . \sigma_3^{\ b4}) \tag{3.19}$$

where:

σ_3 [kPa] : minor principal stress (absolute value)

σ_1 [kPa] : major principal stress (absolute value)

a_1, a_2, a_3, a_4 : model parameters

b_1, b_2 b_3, b_4 : model parameters

To assess the accuracy of the newly developed equations by Werkmeister for the determination of the material parameters *A, B, C,* and *D*, the results of permanent strains obtained from RLT tests for Granodiorite material are compared against those proposed by the Werkmeister model and shown in Figure 3.6. Similar plots for other confining pressures and base course materials have been obtained and can be found in [68].

From Figure 3.6, it can be concluded that, the developed model by Werkmeister is in agreement with the RLT test results, regarding the amount of permanent strain at the first 100 cycles and the rate of increase of vertical permanent strain against (N).

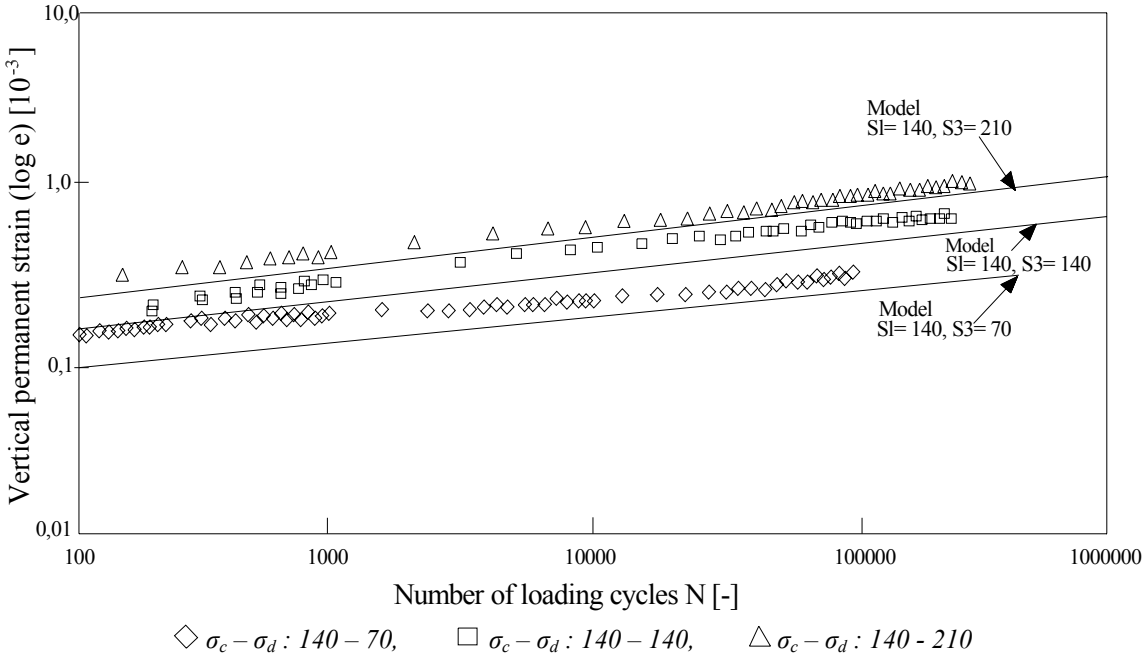

Fig. 3.6: Vertical strains vs. N, data and model for Granodiorite, Grading M, σ_c - σ_d both in kPa

For the higher stress-levels, in Phase III, the observed behavior cannot be described by means of the equation 3.15, therefore a second term was added to the equation. The final equation that was selected is the equation 3.20 as suggested by Huurman [27]. This equation is also commonly used to describe creep curves for asphalt mixes.

$$\varepsilon_p\,(N) = A.\left(\frac{N}{1000}\right)^B + C.\left(e^{D\frac{N}{1000}} - 1\right) \qquad (3.20)$$

where:

ε_p [‰] : permanent strain

e [-] : base of the natural logarithm (= 2.17828….)

N [-] : number of loading cycles

The model parameters C and D are again stress-dependent and unfortunately they cannot be determined for range B because there were not enough test results for recognizing the collapse behavior in the tested material. On the other hand, the parameters A and B were easily determined [68]. Figure 3.7 presents a comparison between the results obtained through the proposed model by Werkmeister [68] and experimental results for Granodiorite materials under high confining stress-levels.

Finally, through the developed models for permanent strains, it was made possible to model the permanent deformation behavior of UGMs in a stress-dependent way. However, it is necessary to model each behavior range separately with related parameters according to RLT test data.

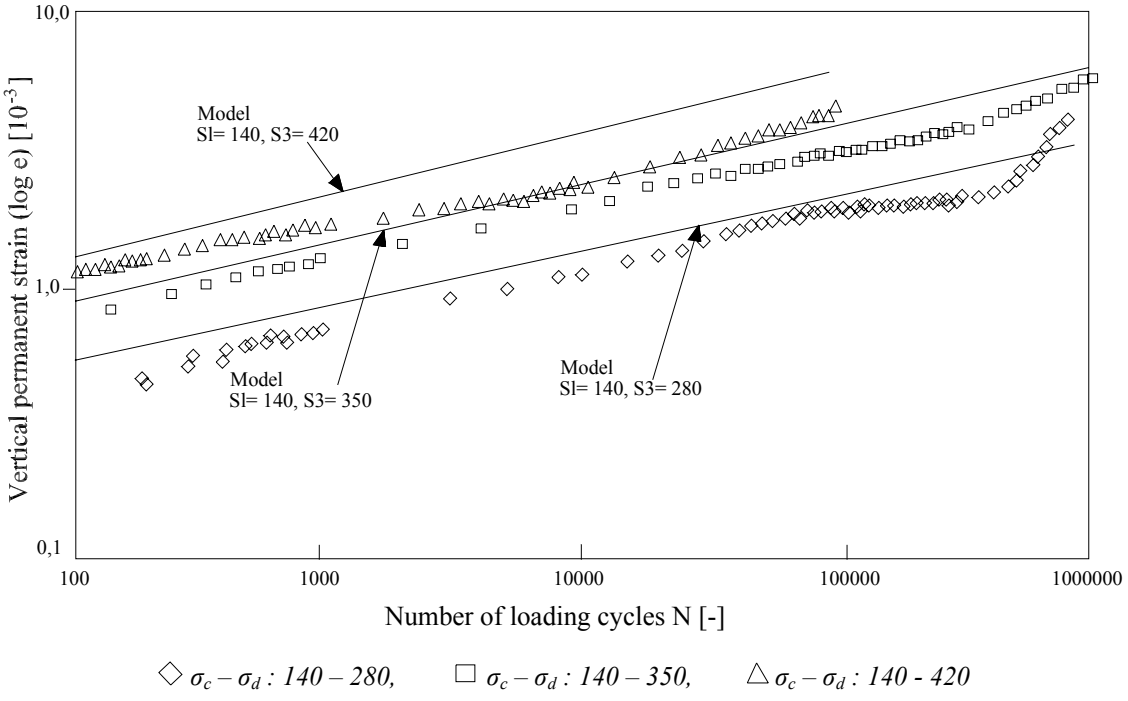

Fig. 3.7: Vertical strains vs. N, data and model, for Granodiorite, Grading M, σ_c - σ_d both in kPa

3.4 Influence of moisture on performance of UGMs

When dry, a granular base course material is quite strong. A pavement structure consisting of concrete slabs and an aggregate base will support traffic in a satisfactory manner as long as water can be kept out of the granular base material. Once the aggregate base becomes saturated, however, the water begins to act as a lubricant. When loaded, the wet granular materials start to move under an applied traffic load.

The in-situ monitoring of the UGMs condition in pavements has revealed that the moisture content of the UGMs changes considerably with the seasons. In the base layers, the variation is between 40 and 90% of optimum moisture content. For the lower sub-bases layer, an even greater variation between 30 and >100% of optimum moisture content was measured [14].

The structural contribution to the pavement of UGMs with varying moisture content was investigated in-situ and in the laboratory. The in-situ monitoring also revealed that the moisture in the pavement structure is very dependent on:

1- Precipitation levels

2- Final preparation for the shoulders of a pavement system (sealed or unsealed, width of the seal, and partial or full)

3- Level of the pavement (raised pavement or pavement in cutting)

4- Ability of the pavement to self drain (the UGMs permeability and the adequacy of the pavement's drainage system)

Pavement performance, as measured in-situ, shows a very serious degradation as the moisture content of the UGMs rises. The RLT test was employed to allow the effects of changing moisture content to be assessed. It was found that significant reductions in the resilient modulus of the UGMs were observed as the moisture content increased. This parameter largely dictates the ability of the UGMs to spread traffic loads safely onto the underlying soil without over-stressing it and the strong influences on the fatigue life of the surfacing layer. In addition, excessive water in joints between concrete slabs leads to the problem of pumping and faulting.

3.4.1 Influence on resilient deformation

The test results in COURAGE were fitted to the Boyce and Dresden models. For comparative purposes, a (characteristic) stress-level (p = 250 kPa and q = 500 kPa) is used with the Hooke's law to define a single value of resilient modulus for each material. All the high-grade aggregates, at their control grading, displayed a marked reduction in their moduli as the moisture content increased relative to the Optimum Moisture Content (OMC). The levels of reduction between the moisture range of Relative Moisture Content (RMC) = 40 to 70% were for Gneiss 10%, Granite 17%, and Limestone 18%.

In the research carried out by Numrich [42], the resilient deformation behavior of a Granodiorite was investigated at moisture content values of 4, 5, 6 and 7 %. During RLT tests at 7 % moisture content (w_{opt}), water was observed draining out of the sample during the test, which indicated the possibility of inhomogeneous conditions. Therefore, it was not possible to determine the material parameters for input into the elastic Dresden model at moisture content values of 6 and 7 %. However, the RLT test results at moisture content values of 4 and 5 % were taken into account for the Dresden model. Figure 3.8 clearly shows a high dependency of the resilient deformation behavior, and hence the model parameters on the moisture content for Granodiorite material. Increasing the water content resulted in a significant reduction in stiffness, thus increasing the resilient strain.

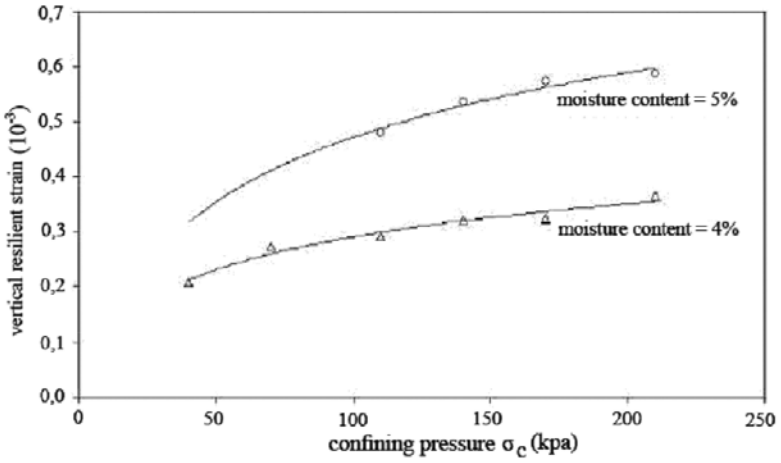

Fig. 3.8: Dependency of resilient strain on water content, Granodiorite material [42]

Table 3.2 gives the obtained parameters of the elastic Dresden model for Granodiorite at two different values of moisture content, with a degree of compaction (DOC) =100%.

Table 3.2: Parameters for Dresden model, Granodiorite, DOC=100 % [42]

Parameters for Elastic Dresden model		Moisture Content	
		4 %	5 %
Q	$[kPa]^{1-Q2}$	5,386.1	10,772.2
C	$[kPa]^{1-Q1-Q2}$	2315.6	599.1
Q1	[-]	0.593	0.690
Q2	[-]	0.333	0.333
R	[-]	0.017	0.037
A	$[kPa]^{-1}$	-0.0024	-0.0012
B	[-]	0.352	0.320

3.4.2 Influence on permanent deformation

Typical results for permanent axial strains during the preconditioning test for granite material at different relative moisture content levels are shown in Figure 3.9. Generally, the plastic strain develops rapidly during the first few loading cycles and the resilient behavior stabilizes as the material approaches a steady state condition.

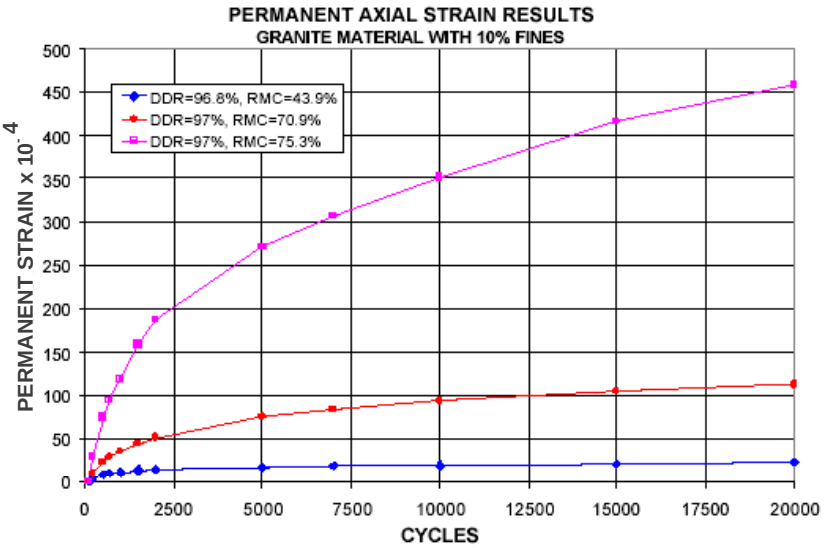

Fig. 3.9: Permanent axial strains vs. load cycles [14]

However, for the granite material with high fines and high moisture content, no steady state condition is observed. As a result of the COURAGE testing [14], it is clear that some materials can support the heavy preconditioning applied load (σ_1= 700 kPa and σ_3 = 100 kPa) and some others cannot. The results for the permanent strain parameter (A_1) of the high-grade aggregates (at their control grading) and RCC&A (at its supply grading) are presented in Figure 3.10.

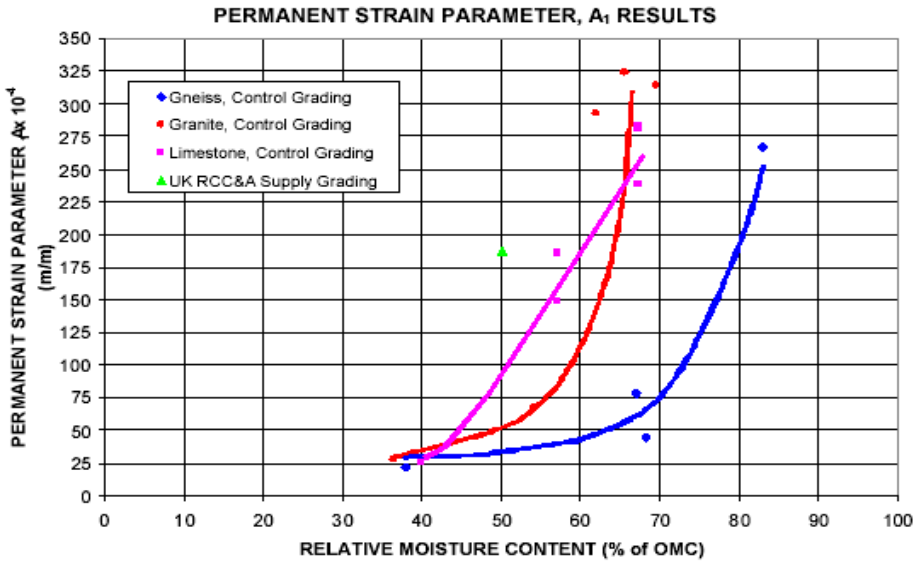

Fig. 3.10: Permanent strain parameter A_1 vs. RMC at DDR=97%, control grading [14]

It can be seen that Figure 3.10 illustrates virtually identical strain susceptibility of the four aggregates. All materials undergo rapid strain increases once a moisture content level of approximately 60% of the optimum is reached.

3.4.3 Modeling of permanent deformation at higher moisture content

The Dresden model for permanent strain behavior, like many other models, does not take into account the influence of moisture content. The tests on UGMs done in the University of Nottingham by Werkmeister [68] were conducted at certain water content ratios, which were measured in samples at the time. Consequently, the parameters of the Dresden model were concluded and only valid at those water content values. No tests were done at higher moisture content levels. Therefore, in this case, the parameters cannot be used to predict the permanent deformation behavior.

From Figure 3.9, it can be concluded that, the permanent deformation of Granite material with 10% fines is going to stabilize at a RMC of 43.9% after a high number of loading cycles (shake down). Moreover, it was rapidly increasing when the RMC was raised to 70.9% and increased too rapidly when the RMC reached 75.3%.

In order to take into account the influence of moisture content on the permanent strain calculation of UGMs, there are two methods:

1- Conducting a new series of RLT tests for different materials at different levels of water content (which is an enormous effort and also time consuming) in order to obtain the material parameters at different RMCs.

2- Conducting tests for each material at some chosen high RMCs, then finding a relation between permanent strain at stabilized conditions (those at low RMCs) and those at high RMCs. This relation can take the following form:

$$\varepsilon_{p,\,wa} = A\,.\,(\varepsilon_{p,wr})^{(w_a / w_r)^2} \qquad (3.21)$$

where:

$\varepsilon_{p,\,wa}$: permanent strain at actual water content (high RMC)

$\varepsilon_{p,\,wr}$: permanent strain at reference water content (low RMC)

w_a : actual water content

w_r : reference water content

A : regression parameter

The parameter A can be determined from comparing the results of permanent strain at reference water content (low RMC) and that at actual water content (high RMC).

According to Figure 3.9, the permanent strain at a low RMC of 43.9% shall be considered as the reference. Applying equation 3.21, the permanent strain at high RMCs (70.9% and 75.3%) can be computed for Granite material. The parameter A is found to be 0.211×10^6 and 6.865×10^6 for actual relative moisture content values of 70.9% and 75.3% respectively. Calculated permanent strains were plotted against the measured values from the RLT tests as shown in Figure 3.11.

The measured values were available only for the first 20000 loading cycles, but the calculated values can be extrapolated to any higher number of loading cycles.

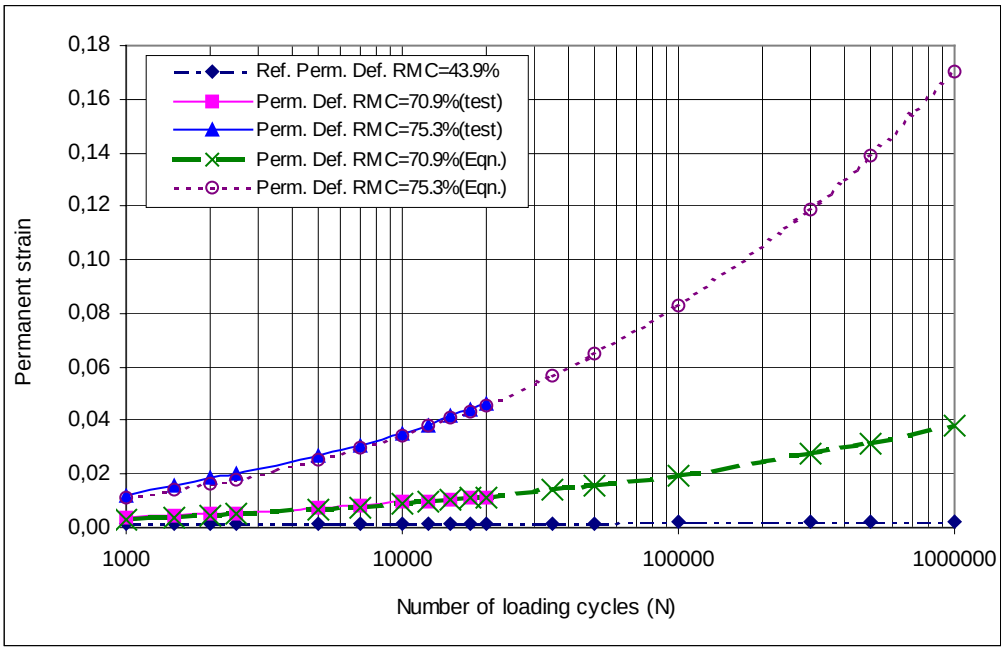

Fig. 3.11: Permanent axial strain vs. number of loading cycles for Granite with 10% fines

4 MATERIAL MODEL AND CONSTITUTIVE LAWS FOR UGMs

Much research [19, 24, 54] has been conducted to model the behavior of UGMs and to develop constitutive laws for these materials in the frame of the European Commission Project (EUROBLAT II) with the cooperation of the Central Public Funding Organization for Academic Research in Germany (in German: Deutsche Forschungs-Geselschaft „DFG") through the research program: System Dynamics and Long Term Behavior of Traffic Structures, Platform and Underground. Stöcker [54] implemented the constitutive equations, which describe the permanent deformation behavior of the unbound granular materials under cyclic loads in a user material subroutine to be used with ABAQUS for solving the problem of cyclic loading in railway structures. The Mohr Coulomb theory of plasticity was used as the basis for the developed material statements taking into consideration the different formulae of permanent deformation models mentioned in section 3.2.

4.1 Permanent deformation calculation

The calculation of permanent deformation behavior under cyclic loading can be done using two procedures:

1- **Implicit procedure**: in which the calculation must exactly follow the loading path, until a relevant permanent deformation adjusts itself. This occurs only after a long time of load application and/or a very high number of loading cycles. It does not place an inherent limitation on the time increment size, as increment size is generally determined from accuracy and convergence considerations. As the computation must be done exactly for all loading cycles, the implicit simulation needs a much higher number of increments than explicit simulations. Beside the high number of loading cycles, which results in a high cost of computation, the risk of error propagation is to be considered because of the non-linear hysteretic material behavior. Thus, errors can accumulate, even if in small magnitudes over the calculation of each load cycle, and the procedure can lead to inaccurate results.

2- **Explicit procedure**: in this procedure, the process of continuously progressing deformations over finite load cycles can be calculated with a quasi-static statement (see Figure 4.1). This statement assumes average load amplitude with the number of loading cycles as reference quantities. Explicit means that a plastic deformation increment is derived depending on the existing state of stresses at the soil element for a finite number of loading cycles. Simulations generally need about 10,000 to 100,000 increments, but the computational cost

per increment is relatively small. Explicit statements are called (quasi-static) due to the reduction of the simulation of the cyclic loading to average monotonous static load amplitude neglecting the mass-inertia effects. In a comparison of both procedures, the decision is in favor of the explicit statement as it suits the requirements of the existing geotechnical problems.

Both terms, **implicit** and **explicit**, refer to the general procedure for the computation of cyclic-plastic deformation and should not be confused with the well-known terms in the numerical integration of strain rates [76, 77].

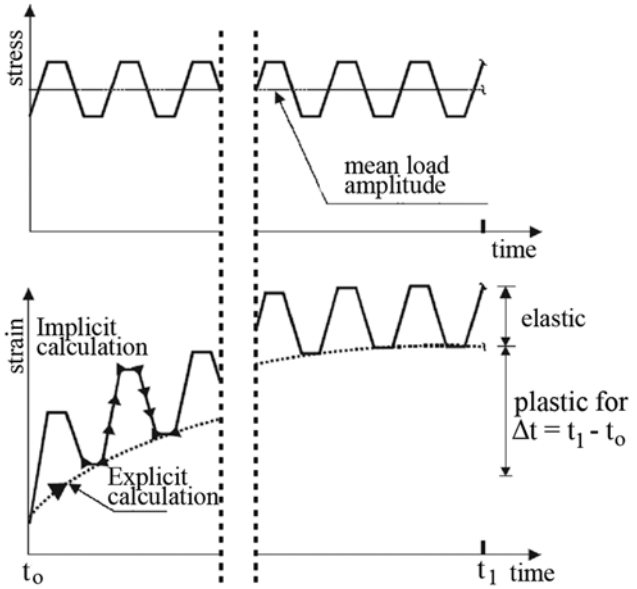

Fig. 4.1: Schematic presentation of stress strain curve for unbound granular materials under cyclic loading, implicit and explicit procedures [54]

4.1.1 Mechanical behavior of granular materials under cyclic load

In relation to the material behavior of soils under dynamic loads, the term cyclic is often used, with the meaning of a temporally variable load effect, which possesses a certain degree of regularity in size, direction and frequency. Cyclic loads can be found in reality. Machines and offshore structures always transfer cyclic stresses in a harmonic way into the foundation bed. The term cyclic load effect does not mean only regular cyclic loads, but also all repeated loads e.g. live loads due to traffic. The behavior of granular materials under cyclic loads is very complex. Each load cycle results in the development of both elastic and plastic strains, which does not return to the starting point with unloading. The plastic strain rates decrease with the growing number of loading cycles. The permanent deformations will be stabilized at a very high number of loading cycles (shake down).

Due to the physical and geometrical structure of the soil, here granular soils, relative motions and sliding between individual grains are observed. Under drained boundary

conditions, the material behavior appears to be elastic (resilient) after a certain number of loading cycles along the stress path (quasi-elastic) (see Figure 4.2-b).

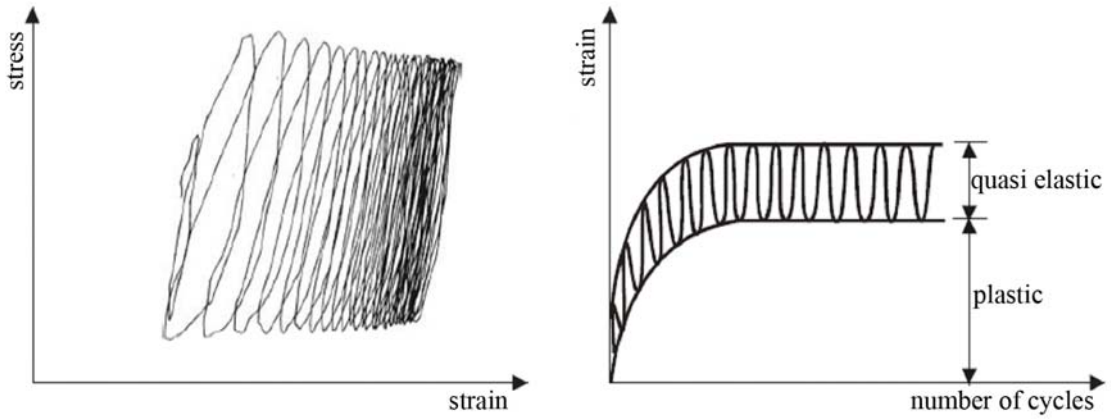

a) Stress strain relationship *b) Strain vs. number of cycles*

Fig. 4.2: General presentation of stress strain behavior of soils under cyclic loads [54]

Some causes of the non-linear material behavior of granular soils under drained conditions and cyclic load effects are:

1- Contraction and dilatation of the material
2- Relocation of individual grains
3- Abrasion at the contact areas
4- Fragmentation of the single grains

Fragmentation and relocation of individual grains are the main causes of the development of permanent deformations [7]. The ratio of plastic strain due to shear stress and grain deformations to the elastic strain within a load cycle is very small. To introduce a realistic material law for the description of the accumulating plastic strains of a soil element under cyclic loading, the following factors are to be considered: hysteretic energy dissipation, and accumulating irreversible strains. The parameters, which describe an accumulation of plastic strains in granular materials, are summarized as follows:

1- Number of loading cycles (N)
2- Static shear parameters φ' and c'
3- Ratio of the cyclic stress amplitude to the static stress state in the triaxial test
4- Hydrostatic pressure (first invariant of the stress tensor (m))
5- Load frequency (f)
6- Degree of saturation (S)
7- Over-consolidation ratio (OCR)
8- Void ratio (e)

4.1.2 Model conceptions for description of plastic strains under cyclic loads

For the development of a material constitutive law for soils under cyclic loading, **implicit** or **explicit** statements described under section 4.1 are crucial.

4.1.2.1 Implicit statements

The implicit statements give the possibility to describe the material behavior of the soil continuously along the load history of each load cycle (Figure 4.1). These statements can also be divided in two categories:

- Dynamic model statements
- Quasi-static model statements

In the case of dynamic models, the inertia forces are considered and sometimes through choice of suitable material constitutive laws, the material non-linearity can be considered. These models can cover the short time dynamics and theoretically the long-term deformation behavior. On the other hand, with implicit (quasi-static) model statements, the mass inertia can be neglected and the load path is illustrated independently of the rate of load application or load frequency. These model conceptions essentially depend on the extensions of the well-known statements for static and monotonic loadings, i.e. the elasto-plastic and visco-plastic model theories or hypo-plasticity. For a comprehensive overview of these theoretical statements, see O'Reilly/Brown [43], Hu [24], and Wang [66]. The majority of these models is in fact founded on the classical material statements and often has a complete theoretical background.

A disadvantage of the implicit formulation of the stress strain history, is the accumulation of error in addition to the very high computing cost. Table 4.1 shows a comparison between the two categories of implicit model statements, with regard to error propagation and computational cost.

Table 4.1: Evaluation of implicit model statements for geotechnical materials [54]

Aspect	Implicit model statements	
	Dynamic	Quasi-static
Physical time dependant quantities i.e. inertia of mass, frequency, loading rate, moving loads, etc.	Yes	No
Non-linear material behavior	Partially	Yes
Error propagation for non-linear material behavior	High	High
Computing cost	High to very high	Extremely high

4.1.2.2 Explicit statements

In the explicit statements, one proceeds from a quasi-static load without consideration of inertia forces, since including the long-term hysteretic deformation behavior stands in the foreground of the interest. Simplification of the quasi-static load effect is divided into two loading steps (Figure 4.3).

The system in the initial condition stands in static equilibrium. The additionally applied cyclic load (considered as quasi-static) does not endanger the stability of the system. Accumulating strain increments are computed with an approximation method. The formulation of explicit statements differs very strongly from the material theories under static and monotonic loading [40, 49, 55].

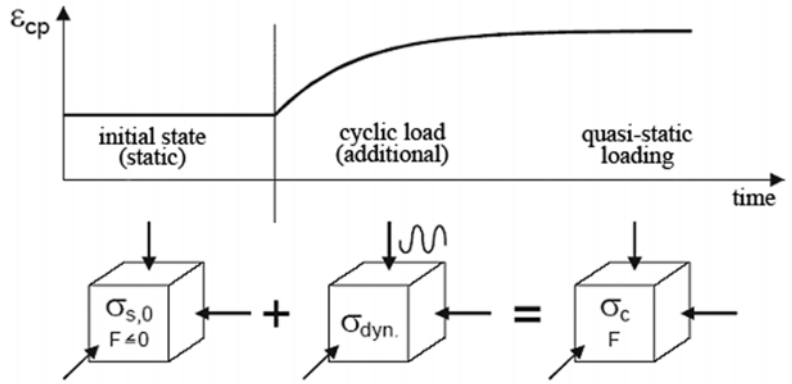

Fig. 4.3: Explicit procedure for permanent strains under cyclic loads [54]

Generally, empirical observations are part of such formulations. These can be expressed through the behavior of volume strains and /or deviator strains against the number of loading cycles, which must be derived from suitable experiments (see Chapter 3). The most suitable experimental test to describe the material behavior under cyclic loading is the cyclic (repeated) load triaxial test (RLT), since the influence of the number of loading cycles on the plastic deformation can be examined under different boundary conditions.

$$\varepsilon_{cp} = \mathrm{f}\,(\sigma_3,\ \sigma_c,\ N,\ f,\ M,\ C) \tag{4.1}$$

with:

ε_{cp} : cyclic axial plastic strain

σ_3 : confining stress

σ_c : cyclic deviator stress

N : number of loading cycles

f : frequency

M : mineralogical characteristics

C : soil-mechanical characteristics

Stress history has direct influence on existing deformations. For constant hydrostatic stress, the size of the permanent deformation after a certain number of loading cycles depends on the difference between the maximum and minimum principle stresses [38]. This means that the stiffness of granular soils is strongly dependent on the hydrostatic stress. An observation of the directions of the three principle stresses for explicit computation statements is therefore of great importance.

Thus, for equation 4.1, the relationship between the permanent deformation and the applied stresses in the space of principle stresses at a defined number of loading cycles can take one form of a log-normal, log-log, or exponential relationship. For example, the axial strain in RLT tests can be described with the following equation:

$$\log \varepsilon_{cp}^{N} = \log A + B \log N \tag{4.2}$$

with:

ε_{cp}^{N} : cyclic plastic strain in the axial direction

N : number of loading cycles

A, B : regression coefficients

The regression coefficients determined from RLT tests, here simplified as A and B, describe the relation between permanent deformations at the element and the load boundary conditions. In this concern, the regression coefficient A stands for the permanent strain due to the first load cycle and coefficient B stands for the magnitude of the following plastic strain increments (please refer to Chapter 3). The aforementioned regression parameters are usually determined by the evaluation of many RLT tests (see Werkmeister [68]).

4.1.3 Applied models and material statements in the field of geotechnique

In the field of geotechnique, a simplified explicit procedure can be selected with a quasi-static load assumption (equivalent to the cyclic load effect) for the description of the permanent deformation behavior against the number of loading cycles [54].

For the description of the plastic strain development, two conditions were observed during the repeated load triaxial tests, depending on the geostatic and cyclic deviator stresses. These are cyclic calming and cyclic failure (Figure 4.4). Here, F_c refers to a reduced Mohr Coulomb cyclic failure criterion and used for distinguishing between these two deformation cases. It is observed that, with the same boundary conditions, a soil element already fails in the cyclic triaxial test under smaller cyclic deviator stress amplitude in comparison to the static triaxial test. This failure process can be characterized as a failure, which happens due to the increasing number of loading cycles (gradual failure).

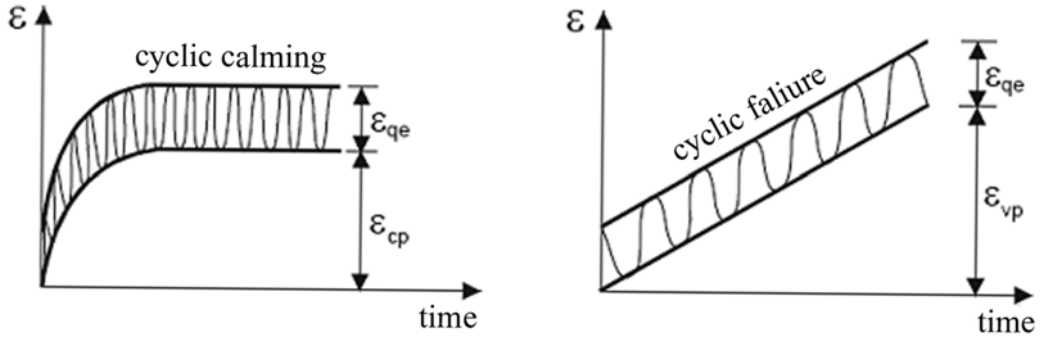

a) Cyclic calming: $F_c \leq 0$ *b) Cyclic failure: $F_c > 0$*

Fig. 4.4: Typical deformation behavior of soil element in RLT tests [54]

In order to correctly describe this phenomenon, a definition for the shear parameters was derived, which seizes the decreased shear strength of granular soils under cyclic loads. The Mohr Coulomb failure criterion used in the developed statements was therefore designated as a reduced cyclic criterion.

In Figure 4.5, the simulation of the plastic strain increments is represented in the space of the three principle stresses. Hexagonal conical Mohr Coulomb is defined as a yield surface. As long as the yield surface is not violated, i.e. the stress state is within the yield surface ($F_c \leq 0$), the cyclic plastic strains (ε_{cp}^{N}) shall be computed. Otherwise stresses shall be relocated through local plastification ($\varepsilon_{vp}^{N,t}$) in other areas.

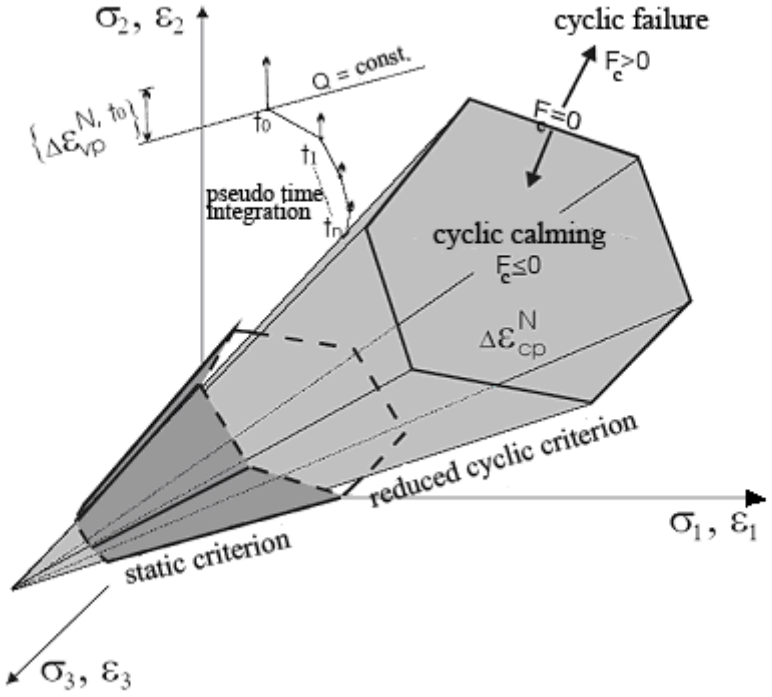

Fig. 4.5: Material statement for deformation cases in space [54]

Here, the yield surface does not have the same function as in the classical elasto-plastic theory of defining the bounding surface between pure elastic and plastic behaviors. The implementation of a yield surface in the material model is to define the empirical cases observed in the repeated load triaxial tests (shake down and failure). This means for numerical computations, that it should be proved in each iteration whether local violation to the yield surface occurs. If this is the case, the stresses should always be relocated within the cyclic failure until the reduced cyclic criterion is fulfilled. The cyclic strain increments will only then continue to be computed.

4.1.4 Mohr Coulomb failure criterion

In order to describe the shear strength of soils, a failure criterion is necessary, within which the results of experimental investigations of the shear strength can be evaluated and represented. Numerous failure criteria were formulated, but in practice the simple criterion of Mohr Coulomb became generally accepted [33].

Figure 4.6 represents the failure criterion for a granular soil, whose stiffness is given only by friction (not by cohesion).

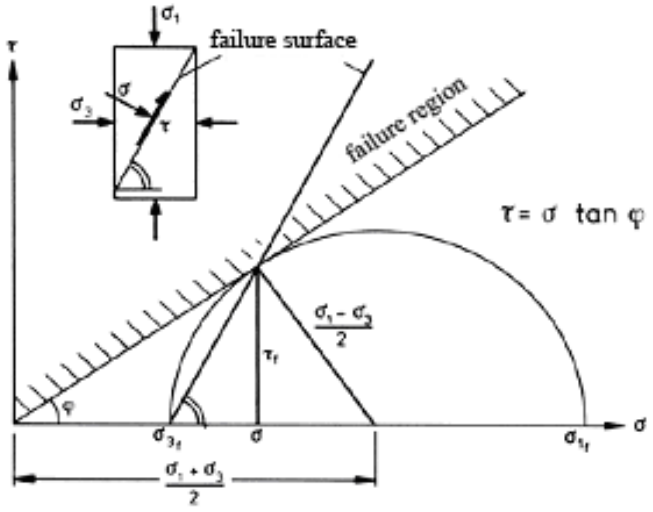

Fig. 4.6: Mohr Coulomb stress circle at failure state of cohesionless soils [33]

The friction angle φ' is expressed in effective stresses as follows:

$$\sin\varphi' = \frac{\sigma_1 - \sigma_3}{\sigma_1 + \sigma_3} \tag{4.3}$$

The criterion means that with a given ratio of the maximum and minimum principle stresses (σ_1) and (σ_3), the stiffness is proportional to the normal stress. According to Figure 4.6, the shear strength of a cohesionless soil can be expressed as:

$$\tau_f = \sigma \tan\varphi' \tag{4.4}$$

Whereby the index *f* stands for failure.

In general form, i.e. for a soil with friction and cohesion (see Figure 4.7), the stiffness can be expressed as:

$$\tau_f = c + \sigma \tan \varphi' \tag{4.5}$$

From equation 4.5, and Figure 4.7, the Mohr Coulomb failure criterion can be expressed as:

$$\sin \varphi' = \frac{\frac{1}{2}(\sigma_1 - \sigma_3)}{\frac{1}{2}(\sigma_1 + \sigma_3) + c \cot \varphi'} \tag{4.6}$$

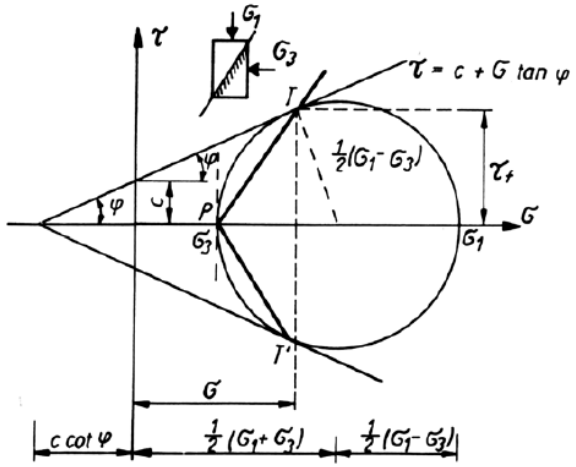

Fig. 4.7: Mohr Coulomb hypothesis in (τ – σ) diagram for cohesive soils [16]

In another form:

$$\frac{1}{2}(\sigma_1 - \sigma_3) = \frac{1}{2}(\sigma_1 + \sigma_3)\sin\varphi' + c'\cos\varphi' \tag{4.7}$$

Or

$$F = \frac{1}{2}\sigma_1(1 - \sin\varphi') - \frac{1}{2}\sigma_3(1 + \sin\varphi') + c'\cos\varphi' = 0. \tag{4.8}$$

with:

σ_1, σ_3 : maximum and minimum principle stresses

φ', c' : internal angle of friction and cohesion

4.1.4.1 Cyclic calming ($F_c \leq 0.$)

With the fulfilled reduced cyclic Mohr Coulomb failure criterion, the plastic strain (ε_{cp}) accumulates to a limit value according to Figure 4.4-a. During continuous load, quasi-elastic strain amplitude (ε_{qe}) would only be developed. The existing condition can also be regarded as hardening of the soil element and is described as cyclic calming.

The explicit formulation for the description of the hysteretic material behavior was derived from repeated load triaxial tests. It was assumed that the empirical relations derived from the triaxial test would also be applied to the three dimensional model. Further, the function X defines the ratio of the cyclic deviator stress (S_c) to the static deviator failure stress (S_{sf}).

$$X = \frac{\sigma_{1,c} - \sigma_{3,c}}{(\sigma_{1,s} - \sigma_{3,s})_f} = \frac{S_c}{S_{sf}} \leq K \leq 1.0, \qquad K = \frac{(\sigma_{1,c} - \sigma_{3,c})_f}{(\sigma_{1,s} - \sigma_{3,s})_f} = \frac{S_{cf}}{S_{sf}} \leq 1.0 \tag{4.9}$$

With (S_{cf}) is the cyclic deviator failure stress.

From equation 4.9, it is assumed that the cyclic deviator stress (S_c) cannot become larger than the static deviator failure stress (S_{sf}). The static deviator failure stress (S_{sf}) is derived from the static primary stress state ($\sigma_{3,s}$) with the assumption of the validity of the Mohr Coulomb failure criterion [54].

$$(\sigma_{1,s} - \sigma_{3,s})_f = \frac{2 \sin \varphi'}{1 - \sin \varphi'} \ \sigma_{3,s} \tag{4.10}$$

Hu [24] derived equations for the axial cyclic strains of ballast and granular soils from triaxial tests. The equations are represented in semi-log and double-log as well as exponential forms.

a) Semi-log form:

$$\varepsilon_{cp1}^{N} = \varepsilon_{cp1}^{1} (1 + \alpha \log N), \tag{4.11}$$

$$\varepsilon_{cp1}^{1} = \beta . \left(\frac{\sigma_{3,s}}{P_a} \right)^{\chi} . X^2 \tag{4.12}$$

with:

ε_{cp1}^{1} : axial cyclic strain for the first load cycle ($N = 1$)

α, β, χ : empirical regression parameters

X : the ratio of cyclic deviator stress to static deviator failure stress

P_a : atmospheric pressure, P_a = 100 kN/m²

The ratio X of the cyclic deviator stress to the static deviator failure stress and in particular the static primary stress state ($\sigma_{3,s}$) is of great importance for ε_{cp1}^{1} and thus serves as a reference quantity for the development of the plastic strains over the following cycles. This applies likewise to the forms **b)** and **c)**.

b) Double-log form:

$$\varepsilon_{cp1}^{N} = \varepsilon_{cp1}^{1} \ N^{\alpha} \tag{4.13}$$

Or in other form

$$\log \varepsilon_{cp1}^{N} = \log \varepsilon_{cp1}^{1} + \alpha \log N \tag{4.14}$$

$$\varepsilon_{cp1}^{1} = \begin{cases} \beta \left(\frac{P_a}{\sigma_{3,s}} \right)^{1/3} X^{\chi}, & \sigma_{3,s} \le 35\, kN/m^2 \\ \beta \left(\frac{\sigma_{3,s}}{P_a} \right)^{\chi} X^{2}, & \sigma_{3,s} > 35\, kN/m^2 \end{cases} \tag{4.15}$$

c) Exponential form:

$$\varepsilon_{cp1}^{N} = a\ e^{b/N} \tag{4.16}$$

with:

$$a = \alpha \left(\frac{\sigma_{1,c}}{\sigma_{3,s}} \right) + \beta \left(\frac{\sigma_{1,c}}{\sigma_{3,s}} \right)^{2} \tag{4.17}$$

$$b = \chi \left(\frac{\sigma_{3,s}}{\sigma_{1,c}} \right) + \zeta \left(\frac{\sigma_{3,0}}{\sigma_{1,c}} \right) \tag{4.18}$$

Where ζ is an empirical regression parameter.

Werkmeister [68] derived an equation based on the Huurman's model [27] for the calculation of the axial cyclic permanent strain in RLT tests for the unbound granular materials in the phase of stable behavior in range A (shake down limit), which corresponds to the case of cyclic calming. This equation has the log-log form as the following:

$$\log \varepsilon_{cp}^{N} = \log A + B \log N \tag{4.19}$$

This equation has the same form of the double-log equation 4.13 of Hu with the difference that A and B are both stress-dependent parameters. To the contrary of equation 4.13 of Hu, only the (ε_{cp1}^{1}) parameter is a function of the applied primary and cyclic stresses. Moreover, for the application of material statement with the UMAT, both (ε_{cp1}^{1}) and (α) are determined as constant parameters through the evaluation of some triaxial tests and are assumed constant from the beginning, remaining unchanged during the analysis of the problem. A new version of UMAT subroutine shall be developed to implement the A and B parameters as stress-dependent parameters (as discussed in Chapter 5).

The cyclic radial permanent strain should also be considered for the developed statements. There is not enough data or experience about the ratio of radial to axial cyclic permanent strain in the conducted researches. Anyhow, the relation between

radial and axial cyclic strain can be concluded from the available researches and implemented in the developed material statements.

In the research done by Raymond and Williams [48], and Gotschol [19], the cyclic permanent strains in the 2nd and 3rd directions of principle stresses are assumed to have the same magnitude and to equal $\varepsilon_{cp,r}^{1}$.

The following relation has been concluded [19]:

$$\varepsilon_{cp,r}^{N} = (\lambda - \omega \log N)\, \varepsilon_{cp,1}^{N} \tag{4.20}$$

With $\varepsilon_{cp,r}^{N}$ is the radial cyclic permanent strain, and $\varepsilon_{cp,1}^{N}$ is the axial cyclic permanent strain. The parameters λ and ω can be determined from the confining stress-level in addition to the actual X (of eqn 4.9) as follows:

$$\lambda = \lambda_1 \left(1 - \frac{\sigma_{3,s}}{\sigma_{3,0}}\right) + \lambda_2 \, X \tag{4.21}$$

$$\omega = \omega_0 \left(\frac{\sigma_{3,s}}{p_a}\right)^{1/2} \tag{4.22}$$

Where $\sigma_{3,s}$ is the confining static stress and $\sigma_{3,0}$ is a regression constant.

λ_1, λ_2, and ω_0 are constants and can be determined from triaxial tests and P_a is atmospheric pressure (P_a = 100 kN/m²).

4.1.4.2 Cyclic failure ($F_c > 0$.)

By violation to the yield surface, as described in section 4.1.3, a gradual failure of the soil element (cyclic failure) arises (Figure 4.4-b). In the cyclic triaxial test, this condition means that, in a short time or after a small number of loading cycles, failure of the soil element occurs. A local violation to the yield surface after a certain number of loading cycles (N) in addition to the accumulated cyclic deformation (ε_{cp}^{N}) leads to further plastification and produces visco-plastic strains ($\varepsilon_{vp}^{N,t}$) in the material. Visco-plastic deformation increments arise in the case that, and as long as, the limit value criterion is exceeded. This corresponds to the visco-plastic model conception after Zienkiewicz and Cormeau [75], which permits, contrary to the classical theory of plasticity, the material to have stress states for a finite time outside the failure criterion.

For the numerical implementation, this means that, the entire load shall be applied in one step and on the basis of the elastic solution of the problem, shall be approved if the stresses are within the flow surface; plastic strains shall be gradually computed. Otherwise, the stresses shall be relocated and visco-plastic strain increments shall accumulate over the total time, i.e. up to the keeping of failure criterion (F ≈ 0), whereby all strain rates are equal to zero.

In the context of the quasi-static material statements, the terms of pseudo time and time increment (Δt) are often mentioned. Since, for the considered method, only the final result of the visco-plastic strain, and not the physical temporal process is important, Cormeau [12] has derived an upper limit for time increment (Δt) in numerical analysis with explicit statement in soil-mechanics with an associated flow rule (visco-plasticity, $\theta = 0$). This time increment limit used in the quasi-static Mohr Coulomb failure criterion is therefore to be set:

$$\Delta t \leq \frac{4\ (1+v).(1-2v).\eta}{(1-2v+\sin^2\varphi').E} \tag{4.23}$$

where:

Δt : time increment

E : modulus of elasticity

v : Poisson's ratio

η : viscosity

φ' : angle of internal friction

4.2 Definition of material parameters for the developed material statements

The material parameters required to define the permanent deformation behavior are essentially determined from static and cyclic triaxial tests.

In Table 4.2, the necessary empirical parameters for a soil element are arranged along with the dependant input data for material model statements (see section 4.1.4). Altogether 14 parameters are necessary for the description of the material behavior of granular soils under cyclic load effect with the developed statements. Six of these parameters fall in the region of the well-known material law of Mohr Coulomb as static parameters.

Table 4.2: Necessary input parameters for the selected material equations for granular soils

Material behavior			Required parameters	
			Static	Cyclic
Elastic	Deformability	Isotropy	E, v	-
Plastic		$\varepsilon_{1,cp}^{N}$	-	α, β, χ
		$\varepsilon_{2,cp}^{N}$, $\varepsilon_{3,cp}^{N}$	-	λ_1, λ_2, ω_0, $\sigma_{3,0}$
	Exceeding of stiffness		C_0', φ_0', ξ	K
	Dilatation		Ψ'	-

For the description of the cyclic-plastic deformation behavior, eight parameters are needed; three of them (α, β, and χ) are required for the description of the cyclic-plastic strain ($\varepsilon_{1,cp}^{N}$) in the direction of the maximum principle stress (σ_1). Of the remaining five parameters, four are required to define the other strain components ($\varepsilon_{2,cp}^{N}$) and ($\varepsilon_{3,cp}^{N}$) in the directions of the other two principle stress components (σ_2) and (σ_3).

The fifth parameter is the quantity (K), which is required for the definition of the reduced Mohr Coulomb failure criterion. For simplicity, the strains in the two other principle directions can also be assessed, whereby the number of the required four parameters, after the falling of λ_1, ω_0, and $\sigma_{3,0}$ is reduced to one. In this case five cyclic parameters remain (α, β, χ, λ_2 and K) for the practical applications of the suggested material statement.

4.2.1 Stiffness beyond flow surface and reduced Mohr Coulomb criterion

The friction angle (φ') and the cohesion (c') are determined from conventional tests, e.g. from static triaxial tests (see section 4.1.4). For fine grained soils, the value of φ' depends primarily on the mineral structure of the soil, and for coarse-grained soils it depends on the particle size distribution, the particle shape, and the roughness of the grain surface. Therefore, for coarse grained soil, φ' is a function of the maximum dry density and for crushed stone material, it is observed that with increasing lateral stresses, the effective friction shear strength decreases as follows [22]:

$$\varphi' = \varphi'_0 - \xi \sigma_3 \tag{4.24}$$

These observations can generally also be applied, with restriction, to granular soils. The regression constant ξ in equation 4.24 can be set for practical applications to $\xi = 0.0$ for simplicity. In this case the internal friction is treated independently to the lateral stress.

For quasi-static computations with the developed material statements for granular soils and crushed stones under cyclic loads, reduced shear parameters are needed. Figure 4.8 shows monographs of the cyclic shear parameters φ_c' as well as c_c' as a function of the deviator failure stress parameter (K) and the friction angle (φ').

The relationship of the cyclic to the static deviator failure stress, needed for the material statements (K), depends on the dynamic load boundary conditions, such as, amongst others, frequency and saturation.

$$K = \frac{(\sigma_{1,c} - \sigma_{3,c})_f}{(\sigma_{1,s} - \sigma_{3,s})_f} \leq 1.0 \tag{4.25}$$

At present K is determined, however, from cyclic triaxial tests independent of frequency, and is simply assumed in the range of $0.60 < K < 0.90$. Independent of the load frequency, K must be ≤ 1.0, since under dynamic effects the friction between the grains decreases.

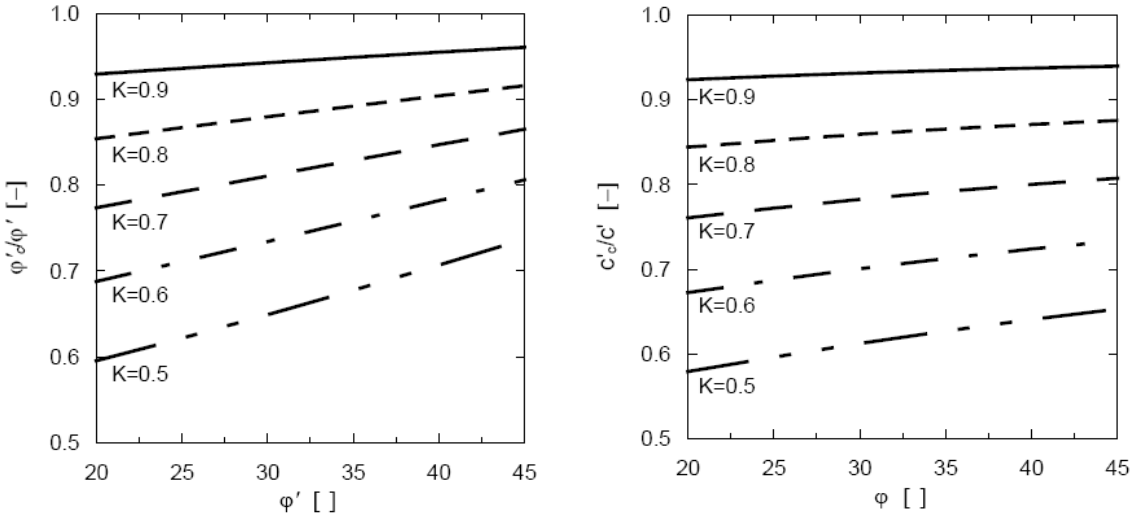

a) Cyclic angle of friction (φ'_c) b) Cyclic cohesion (c'_c)

Fig. 4.8: Derived monographs of cyclic shear parameters as a function of the static friction angle and the parameter K [54]

4.2.2 Dilatation

For the description of material laws for numerical computations, the variation in volume becomes important through the dilatation angle (ψ') (see details in Gudehus [20]). For volumetric strain of cohesionless soil, e.g. sand, a rectangular element of a Mohr Coulomb material with a thickness *h* shall be considered (Figure 4.9).

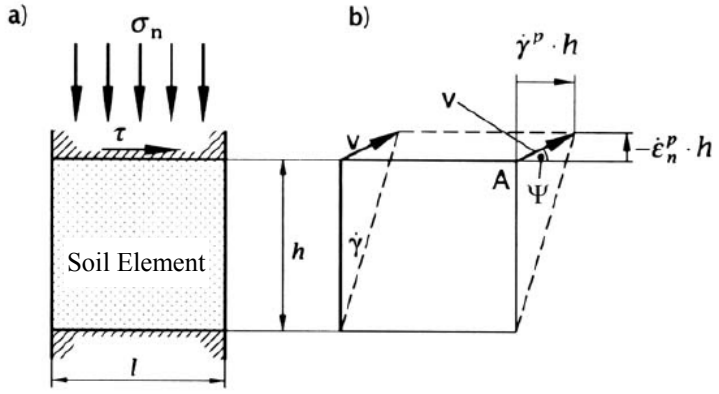

a) Soil with shear stress b) Associated strain rates

Fig. 4.9: Volume strain and strain rates [51]

The volumetric strain is only possible in the vertical direction and the relevant stresses are τ and σ_n. If the material possesses an associated flow rule, the horizontal strain rate $\dot{\gamma}^p . h$ at the point A must accompany a vertical strain rate [51]. From Figure 4.9, it can be concluded that:

$$-\dot{\varepsilon}_n^p \,.h = \dot{\gamma}^p \,.\, h \,.\, \tan\, \psi' = \dot{\gamma}^p \,.h \,.\tan\, \varphi' \tag{4.26}$$

This leads to volumetric strain, which increases proportionally to the shear strength.

$$-\dot{\varepsilon}_n^p = \dot{\gamma}^p \,.\tan\varphi' \tag{4.27}$$

These rate vectors at the upper boundary surface of the element are not movable with reference to the lower boundary surface, so:

$$\arctan\left(-\frac{\dot{\varepsilon}_n^p}{\dot{\gamma}^p}\right) = \psi' = \varphi' \tag{4.28}$$

The angle ψ', called the dilatation angle for the boundary condition, defines the plastic potential within the range of the cyclic failure and can be selected as:

$\psi' = 0$: for volume-constant flow

$\psi' = \varphi'$: for associated flow rule

In order to obtain an applicable value for the dilatation angle, appropriate perfect drained tests are to be evaluated, within which purely deviator stresses are applied and the relevant volumetric strains are measured. However this procedure is considered quite complex. Therefore, it is frequently sufficient to set a rough estimation for the dilatation angle for problems of small volumetric deformation by kinematics boundary conditions [50]. As an approximation for the implemented material statements, ψ' shall be equal to 1/3 φ'.

4.3 Implementation of material statements in ABAQUS

According to the material statements and the procedure mentioned in the last sections, a user material subroutine UMAT was written in 2002 by Stöcker [54] and used with ABAQUS to simulate the behavior of ballast materials in railway structures. This subroutine has been based on 4 steps for the calculation of different deformations under cyclic load conditions.

Therefore, the load history shall be defined in four steps for any problem intending to use the UMAT subroutine for the definition of the behavior of unbound granular materials. These four steps are described as following:

1- The 1st step is to calculate the elastic deformation in the primary stress state due to the own weight of the material itself and any pre-loading history (for example own weight of the superstructure). An equilibrium condition between the applied stresses and the initial stresses has to be achieved (called Geostatic step).

2- The 2nd step is to calculate the plastic deformation, if found, due to the resulting stresses at the end of the 1st step. The total deformation at the end of this step consists of the sum of elastic deformation in the last step and the found plastic deformation in this step.

3- The 3rd step is a quasi-static stress state. The elastic deformation due to the application of the foreseen (cyclic) load, which is considered in this step as a simple monotonous static load shall be computed and added to both of the deformation arts calculated in the last two steps. No consideration for cyclic behavior is included in this step.

4- The 4th step is a quasi-static stress state. The calculation of the cyclic permanent deformation in the procedure takes place during this step. The calculation depends on the variation in principle stresses, due to applying the cyclic load in the 3rd step. Calculation is made with an explicit procedure, according to the empirical equations as mentioned in previous sections. The computation is continued until the required number of loading cycles (N) is reached. The final resulting deformation is the sum of the elastic deformations plus cyclic permanent deformation.

The permanent deformation at different numbers of loading cycles for a certain element can be determined through the deduction of the elastic deformation from the total deformation at the given number of loading cycles.

Figure 4.10 shows a schema for the mentioned four steps of loading history with the resulting deformations.

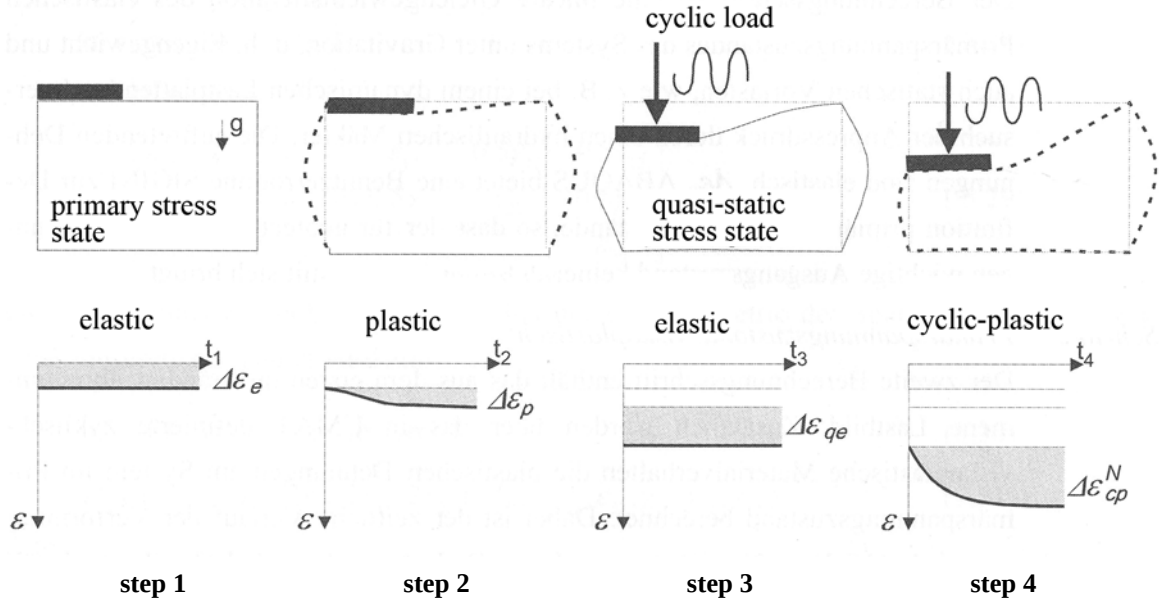

Fig. 4.10: Description of calculation phases used by the UMAT in ABAQUS [54]

Figure 4.11 presents a flowchart for the description of the UMAT subroutine and the different routines which it comprises. For more details, please refer to Stöcker [54].

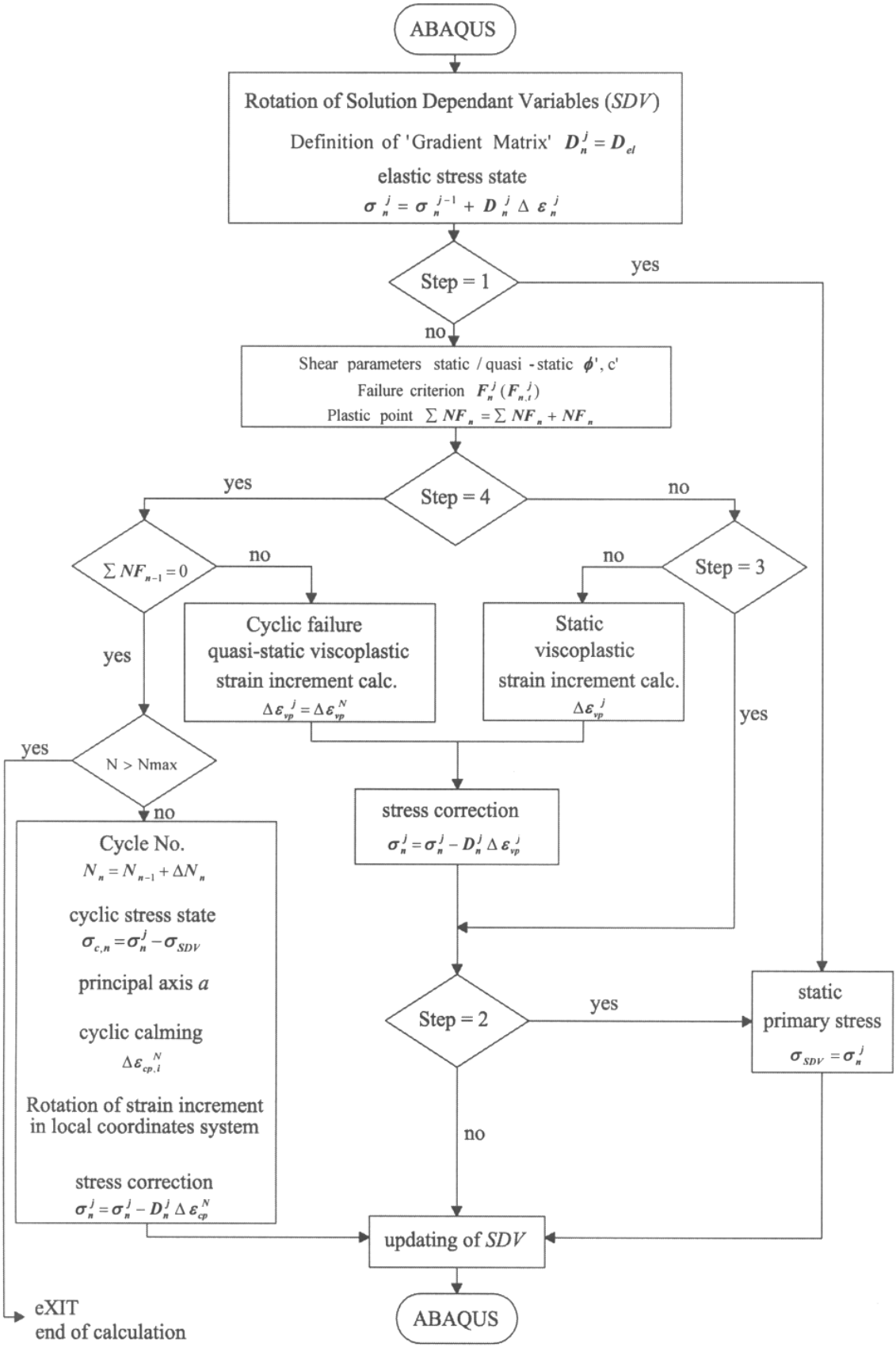

Fig. 4.11: Flow chart of the UMAT subroutine used in ABAQUS

5 MODELING OF RIGID PAVEMENT SYSTEM IN ABAQUS

5.1 Introduction

One of the salient features of ABAQUS is its use of the library concept to create different models by combining different solution procedures, element types, and material models. The analysis module consists of an element library, a material library, a procedure library, and a loading library. Selections from each of these libraries can be mixed and matched in any reasonable way to create a finite element model. Chen et al [10] have made a comprehensive study of various FEM pavement analysis programs and have shown that the results from ABAQUS were comparable to those from other programs. Zaghlol et al [74] simulated the pavement response under FWD loading for flexible pavements and Uddin et al [63] investigated the effects of pavement discontinuities on the surface deflections of rigid pavements using 3-D dynamic analysis throughout, showing very good results. The main capabilities of ABAQUS in solving pavement engineering problems include:

1- Linear and non-linear elastic, visco-elastic, and elasto-plastic material modeling. Additionally, user defined material can be implemented through a user material subroutine (UMAT).

2- Two-dimensional and three-dimensional calculation.

3- Static, harmonic dynamic, and transient dynamic loading simulation.

4- Cracking propagation modeling.

5- Thermal gradient analysis.

Among the element families in the element library are the following, which are of specific interest for this research:

1- First- and second-order continuum elements in one, two, and three dimensions.

2- Hydrostatic-fluid elements, which are used to simulate a fluid structure interaction.

3- Fluid-link element, to simulate the transfer of fluid between two fluid-filled cavities.

4- Special purpose stress elements such as springs, dashpots, and flexible joints.

One can use different types of elements to simulate a given problem with regard to the nature of loading, boundary conditions and any desired analysis procedure.

5.2 Development of a user material subroutine (UMAT)

5.2.1 General assumptions

For ideal simulation in numerical methods, some conditions and assumptions have to be fulfilled for the used material model. These assumptions help achieve a better understanding of material properties and deformation behavior. They also define the limits and the area of application of the used material. The following general assumptions are made:

1- From the macroscopic point of view, the principles of continuum mechanics are based on material laws. With the assumption that, the particles are so small in relation to the total system, the soil shall be considered as a homogenous continuum.

2- The unbound granular material and soil are considered as a one-phase system. This means that pore and pore water pressure shall be excluded.

3- The stress-strain relationship shall be considered as a pure mechanical process. This means that; thermal, chemical, and electrical properties have no effect.

4- The system is subjected to static loads only, the loads and predefined strains are applied incrementally (independently of time). This means that only quasi-static deformation is considered and mass-inertia effects are neglected.

5- Phenomena like softening because of non-homogenous deformations shall not be considered.

5.2.2 Development of a new version of UMAT subroutine

The UMAT subroutine written by Stöcker [54] was modified to describe the behavior of unbound granular materials according to the Dresden model mentioned in Chapter 3. These modifications were verified and approved through many steps and now the new version is available working perfectly with ABAQUS. This new version shall be used in the following analyses.

The modification was not only made for the definition of permanent deformation behavior but also for the elastic behavior of UGMs. Validation of the new version shall be discussed in the next sections.

5.2.2.1 Elastic deformation behavior

The material statements for the elastic deformation behavior are based on the well-known Hooke's law, with a material modulus of elasticity E and Poisson's ratio v. The stiffness relationship between the individual soil layers is of great importance to stress re-allocation. For simplicity, it is accepted that the quasi-elastic modulus E can be determined depending only on the stress-level.

The UMAT written by Stöcker [54] considers the unbound material to be a linear elastic material. This does not reflect the real behavior of such a material, as described in section 3.1. The UMAT was then modified in this area to take into account the material non-linearity through a resilient modulus of elasticity E_r (see eqn 3.13) and a resilient Poisson's ratio v_r (see eqn 3.14), which are stress-dependent and will be automatically updated after each iteration for all integration points in the material group.

According to the Dresden model for resilient behavior, the modulus of elasticity E increases with growing principle stresses, which means decreasing the elastic strains and enhancing the performance of the unbound base layer, especially in the regions of high stresses under traffic loads.

5.2.2.2 Permanent deformation behavior

A re-formulation to the UMAT subroutine written by Stöcker [54], regarding the permanent deformation calculation, was necessary for two reasons: firstly, the old version is developed for ballast materials used in the construction of railways, and secondly, the permanent deformation calculation in the old version of UMAT depends on three parameters (α, β, and χ) which are only available for some materials used as ballast in railways construction. The new version is intended to use a permanent deformation model suitable for unbound granular materials used as base layers in pavement construction. The chosen model was the Dresden model (refer to section 3.3.2) and accordingly the UMAT was modified.

In general, the ballast materials hove a similar behavior to the unbound granular materials in permanent deformation under cyclic loads, with the exception of different material models and related parameters. This conclusion leads to the fact that, the old version of the UMAT can be used with its basic assumptions, as discussed in Chapter 4, to simulate the behavior of UGMs with another material model whose parameters are available through RLT tests.

The parameters for three different UGMs frequently used in road construction are available for the Dresden model. These parameters are stress-dependent and have no constant values; contrary to the parameters in the UMAT written by Stöcker (α, β, and χ), which are determined as average values from many RLT tests conducted under different stress conditions (stress paths) for each given material. Therefore the modifications were necessary to allow for updating the values of the parameters involved in permanent deformation calculation, after each increment, according to the actual stress-levels in all elements of UGMs.

5.3 Validation of the new version of the UMAT

In order to validate the new version of the UMAT subroutine and to approve its correctness, it was important to make some analyses with the FEM program ABAQUS using the new version as a material model for the UGMs. The results of the analyses

shall be compared with existing field and laboratory results for the same material under the same conditions. The validation was made in two levels:

1- for the resilient deformation behavior

2- for the permanent deformation behavior

5.3.1 Validation for resilient deformation behavior

Wellner [67] conducted plate-bearing tests to investigate the resilient behavior of unbound granular materials. From the test results, he developed the Dresden model as a model for resilient behavior (see section 3.3). Wellner used the developed model with two FEM programs: FENLAP and FEEREPGT, to simulate the resilient behavior of UGMs. He simulated the plate bearing tests through these two programs and then compared the results with the actual measurements.

In the current research, a simple subroutine was written to simulate the resilient behavior of UGMs in order to use it with ABAQUS. The plate-bearing test conducted by Wellner was modeled again with ABAQUS and the results of the analysis are compared with the previous study of Wellner [67].

5.3.1.1 Plate bearing test model in ABAQUS

An axisymmetry 2-D model was chosen to simulate the plate-bearing test in ABAQUS. The model has a 1.50 m radius and a 1.50 m depth. The model dimensions, loads, boundary conditions, and finite element mesh were constructed exactly as the model used by Wellner in his study (Figure 5.1).

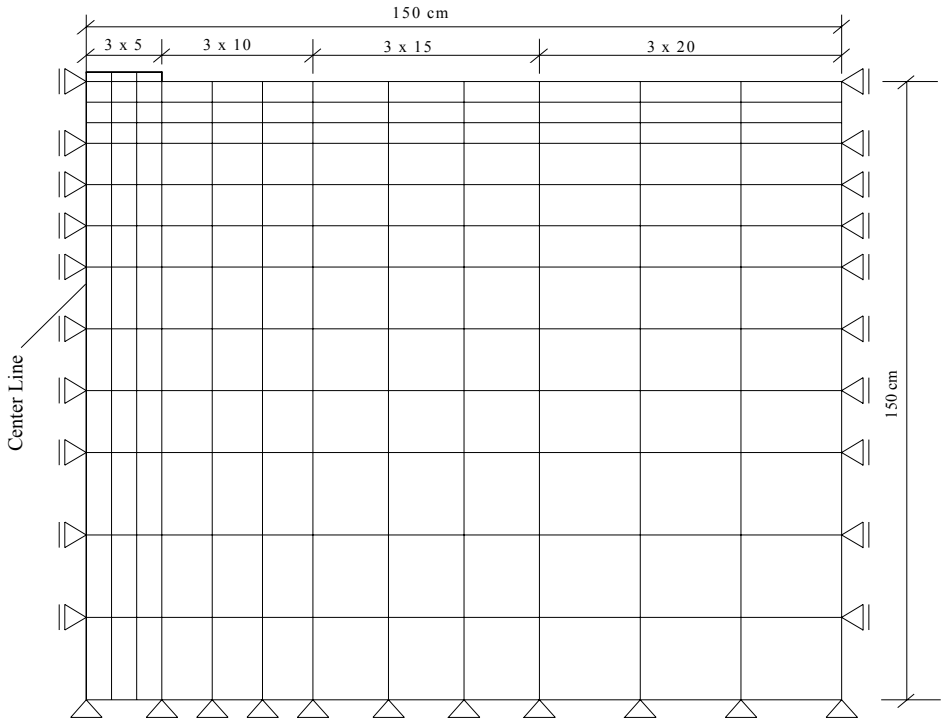

Fig. 5.1: Plate bearing test model, geometry and FEM mesh

The vertical load was applied using a uniformly distributed pressure on the top face of a rigid circular steel plate with a radius of 0.15 m. Two analyses were made for Gravel-Sand material with two different loads; firstly, with a pressure of 0.30 MPa, and secondly, with a pressure of 0.70 MPa.

The material parameters used in the analyses for Gravel-Sand are the same used by Wellner [67] in his study and are as listed in Table 5.1.

Table 5.1: Parameters for resilient modulus calculation

Parameters for elastic Dresden model		Material (Gravel-Sand)
Q	$[kPa]^{1-Q2}$	8617.7
C	$[kPa]^{1-Q1-Q2}$	3064.0
Q1	[-]	0.421
Q2	[-]	0.33
D	[kPa]	30000
R	[-]	0.075
A	$[kPa]^{-1}$	-0.0012
B	[-]	0.458

Vertical strains were obtained beneath the center of the bearing plate in addition to many other points in the radial direction on the top surface of the model.

The results of FEM analysis with ABAQUS were compared against the previous results in the study of Wellner. These comparisons are shown in the next Figures: Figure 5.2 for a vertical pressure of 0.30 MPa, and Figure 5.3 for a vertical pressure of 0.70 MPa.

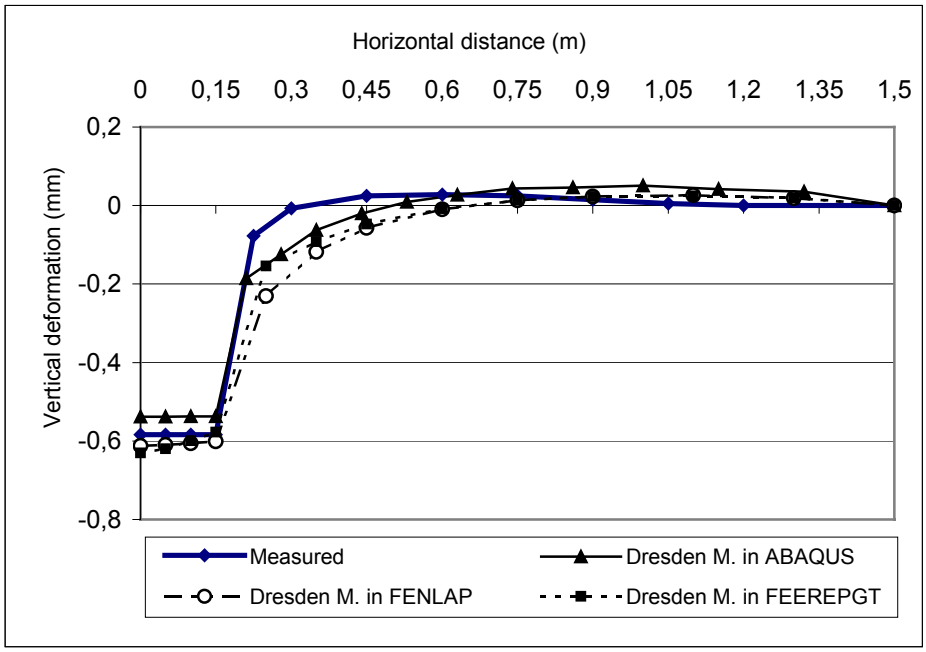

Fig. 5.2: Surface deformation in plate bearing test, Gravel-Sand, pressure 0.3 MPa

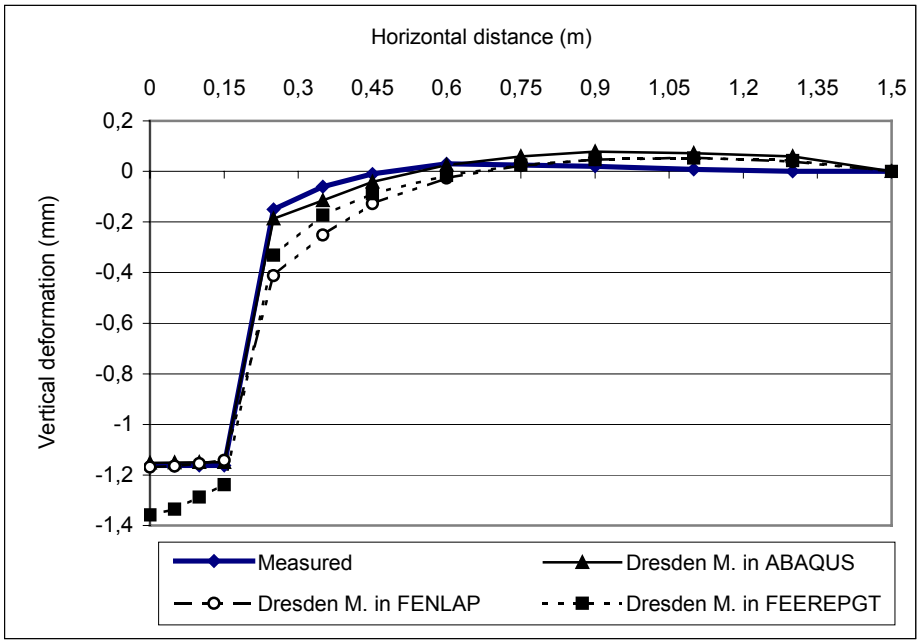

Fig. 5.3: Surface deformation in plate bearing test, Gravel-Sand, pressure 0.7 MPa

From the previous Figures, it can be concluded that, the Dresden model for the description of resilient behavior of UGMs (Gravel-Sand) gives a good prediction for strains when used in FEM programs (please refer to section 3.3). Moreover, the shape of the vertical strain bowl from ABAQUS analysis is the nearest one to the measured values. This indicates the correct implementation of material statements for the description of resilient behavior in the user material subroutine with the Dresden model.

5.3.2 Validation for permanent deformation behavior

Having modified the UMAT subroutine of Stöcker [54], to include the Dresden model for both resilient and permanent deformation behavior of UGMs, it was necessary to validate the new version before using it in advanced analysis for permanent deformation behavior in pavement systems.

In order to make the validation, a triaxial test was simulated in ABAQUS and the results were compared with those calculated using the Dresden model. Moreover, as the triaxial test simulation in FEM is not enough to judge the correctness of a material model implementation, the new version was used in the analysis of a simple 3-D model to assess the sound function of it. This analysis of the 3-D model shall be discussed in the following sections.

5.3.2.1 Triaxial test model in ABAQUS

Werkmeister [68] conducted repeated load triaxial tests for three different unbound granular materials at Nottingham University. Each material was tested at different stress paths and at different water content ratios. The relevant material parameters were then obtained for the Dresden model.

For triaxial test simulation, an axisymmetry 2-D model with eight-node quadratic elements was chosen in ABAQUS. The dimensions of the model are chosen to be the same as the actual triaxial test dimensions. The dimensions are 0.25 m for radius and 1.00 m for height. The geometry, finite element mesh, and boundary conditions are shown in Figure 5.4.

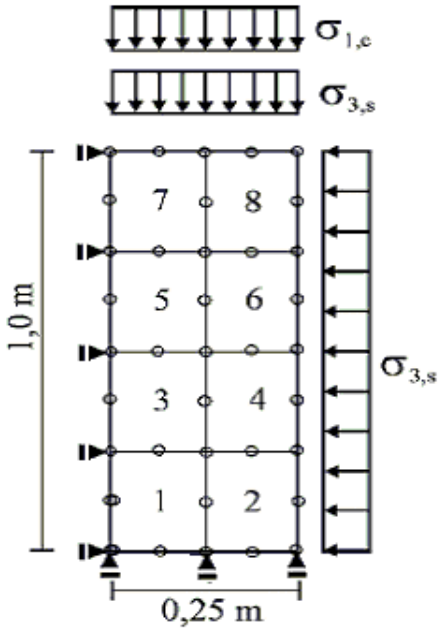

Fig. 5.4: Model of triaxial test in FEM analysis

The loads were applied in two steps:

1- Application of the confining pressure ($\sigma_{3,s}$) in vertical and radial directions.

2- Application of the vertical cyclic deviator pressure ($\sigma_{1,c}$) which equals the difference between the maximum and minimum principle stresses.

The simulation was made for three different materials, namely: Granodiorite, Sandy-Gravel, and Diabase. Each material was subjected to different stress levels ($\sigma_{max} - \sigma_{min}$) as described in Table 5.2.

Table 5.2: Stress paths used in triaxial analyses

Stress path	σ_{max} (kPa)	$\sigma_{min}=\sigma_{3,s}$ (kPa)	$\sigma_{1,c}$ (kPa)
1	60	20	40
2	100	20	80
3	100	40	60
4	150	70	80

The material parameters used in the analyses for the three different materials are mentioned in Table 5.3.

Table 5.3: Parameters for granular materials [68]

Parameters for Dresden model			Material		
			Diabase w/c = 4%	Granodiorite w/c = 4%	Gravel-Sand w/c = 3.4%
Resilient Deformation	Q	$[kPa]^{1-Q2}$	8617.7	5,386.1	16158.3
	C	$[kPa]^{1-Q1-Q2}$	3064.0	2315.6	3862
	Q1	[-]	0.421	0.593	0.561
	Q2	[-]	0.333	0.333	0.333
	D	[kPa]	30,000	38,000	30,000
	R	[-]	0.075	0.017	0.015
	A	$[kPa]^{-1}$	-0.0012	-0.0024	-0.0018
	B	[-]	0.458	0.352	0.285
Permanent Deformation	a_1	[-]	0.00003	0.00001	0.00004
	a_2	$[kPa]^{-1}$	-0.0129	-0.0097	-0.0247
	a_3	$[kPa]^{-1}$	0.0003	0.00001	0.00005
	a_4	[-]	0.0584	0.4134	0.4257
	b_1	[-]	0.0009	0.0009	0.0009
	b_2	$[kPa]^{-1}$	-0.0107	-0.0107	-0.0107
	b_3	$[kPa]^{-1}$	0.0067	0.0067	0.0067
	b_4	[-]	0.5579	0.5579	0.5579

For each system, the vertical permanent strain were obtained under different load paths and compared against the calculated ones through the Dresden model. These comparisons are shown in Figures 5.5, 5.6, and 5.7.

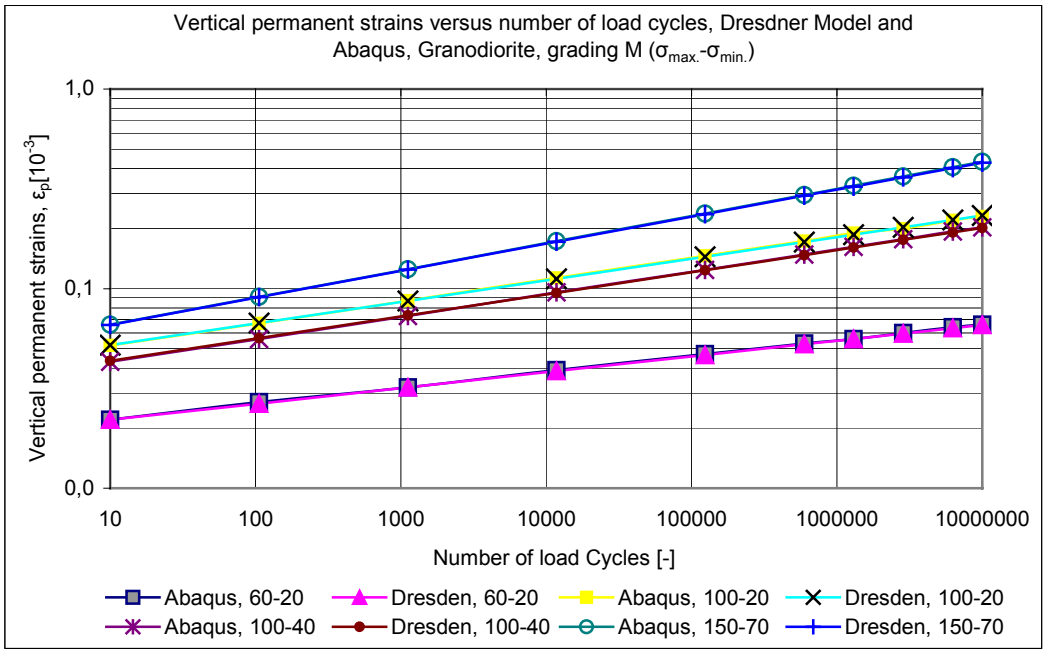

Fig. 5.5: Results of permanent strains in RLT test, ABAQUS and Dresden model (Granodiorite)

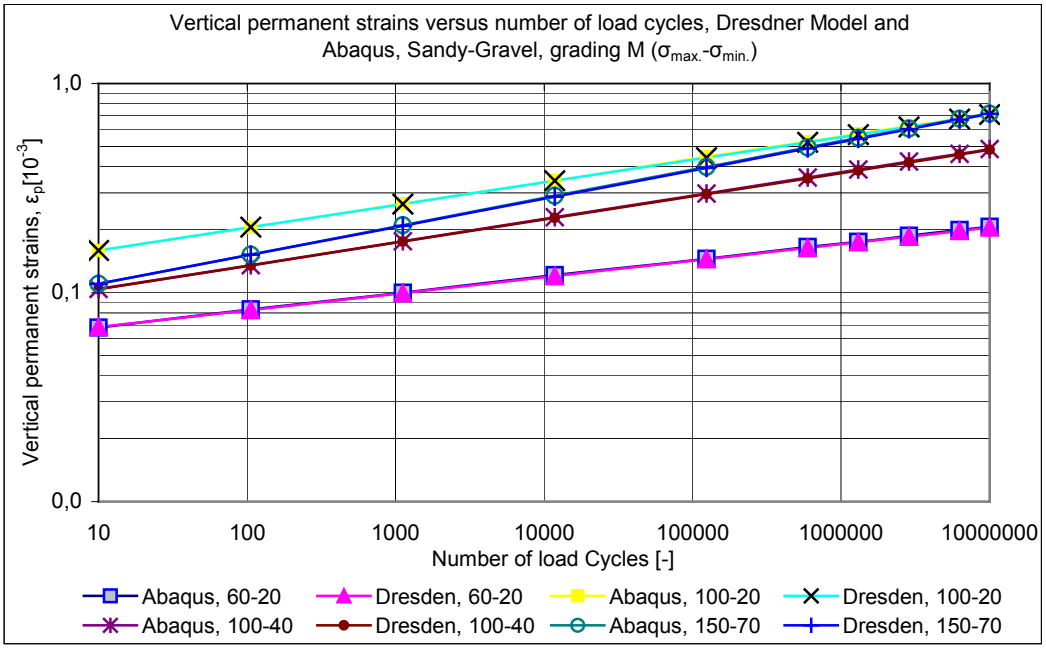

Fig. 5.6: Results of permanent strains in RLT test, ABAQUS and Dresden model (Sandy-Gravel)

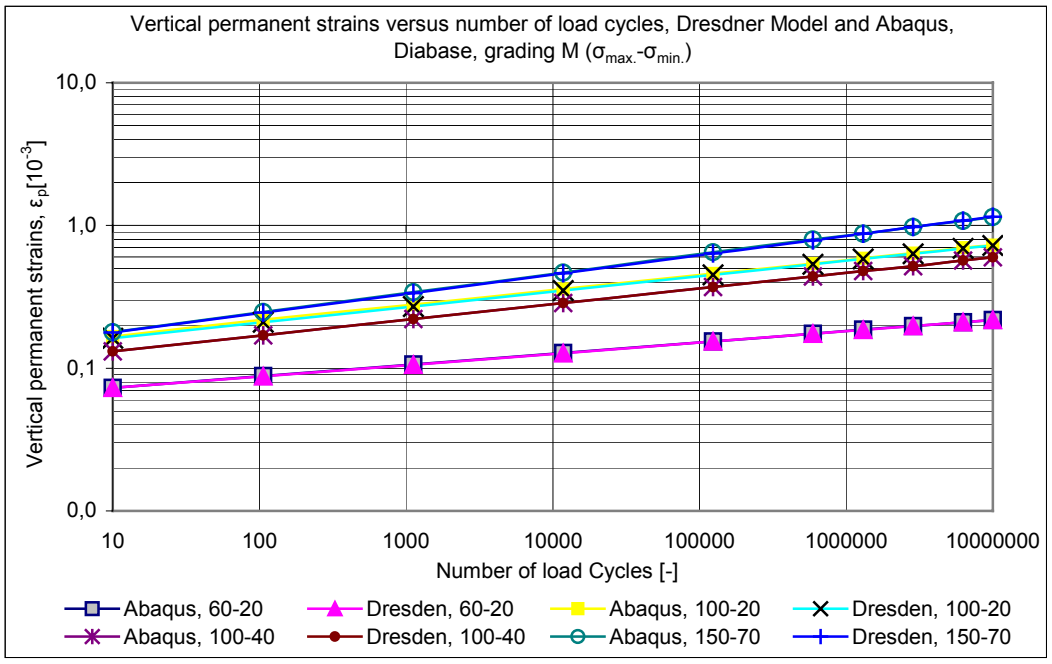

Fig. 5.7: Results of permanent strains in RLT test, ABAQUS and Dresden model (Diabase)

The comparison shows that the results of the triaxial tests in ABAQUS match the results after calculation with the Dresden model for the three considered materials at different stress paths. This assures us that the implementation of the Dresden model in the new version of the UMAT subroutine is correct and is reliable within ABAQUS to describe the behavior of the unbound granular materials in pavement systems subjected to cyclic loading.

It is noted that, the matching of results between FEM and the Dresden model is almost 100%. This may refer to the fact that the triaxial test is an idealization of the stress strain relationship upon which the material model for permanent deformation is based.

It is also noted that, for all materials, the permanent deformation at the first 100 cycles has high values when compared to the total values after a million cycles. This happens usually with the cyclic triaxial tests because of the lack of good compaction and consequently lack of development of residual lateral stresses (see section 3.1.1 for the effect of residual lateral stresses on strains). Therefore, many researchers [14, 27, 45] have neglected the permanent deformation values for the first 100 and sometimes 1000 cycles in their developed models.

5.3.3 Conclusion

The new version of the UMAT subroutine has shown good results when used with ABAQUS to simulate both resilient and permanent deformation behavior of UGMs. The new version can be used now for the analysis of pavement systems, as a material model for the unbound granular materials subjected to cyclic loads. An assessment for using the new subroutine with a 3-D model shall be discussed in the following section.

5.4 3-D modeling of rigid pavement

A simple 3-D model for rigid pavement analysis was considered in this research for the following reasons:

1- To ensure that the newly developed UMAT subroutine functions properly with 3-D problems and will properly simulate the behavior of UGMs for both resilient and permanent deformations (as discussed in section 5.3).

2- To get an equivalent traffic load for the simulation of rigid pavement system in the 2-D analysis for the purpose of faulting computation.

3- To predict the required time and computing cost for the analysis of rigid pavement subjected to cyclic loading.

5.4.1 Description of the system

The 3-D model for rigid pavement system in this analysis comprises of two slabs (two halves for reasons of symmetry) with a transversal joint between them. This way enables us to simulate both edge and corner load cases. The system is composed of three layers. As a first layer come the concrete slab which is supported on a base layer consisting of unbound granular materials. The pavement construction is consequently supported by the subgrade soil (Figure 5.8).

5.4.2 Geometry of the system

A 3-D model is chosen to simulate the rigid pavement problem at the joint location. The model consists of two adjacent slabs each 2.50 m long, 3.50 m wide, 0.26 m thick, resting on an unbound granular base layer with a thickness of 0.60 m. The pavement structure is supported by a 3.00 m depth subgrade soil. Therefore, we have a 3-D model with the dimensions of 5.00 m length, 5.00 m width, and 3.86 m depth.

The discretisation of FEM mesh is chosen to be uniform on the horizontal plan to enable the application of wheel load at any location on the top surface of the concrete slab. As the depth of both the concrete slab and base layer is small compared with the subgrade soil, it was better to have uniform element lengths in the vertical direction for both layers. The discretisation of the subgrade layer in the vertical direction is generated in a biased manner to minimize the total number of elements in the system. Figure 5.8 shows the geometrical model with the generated finite element mesh.

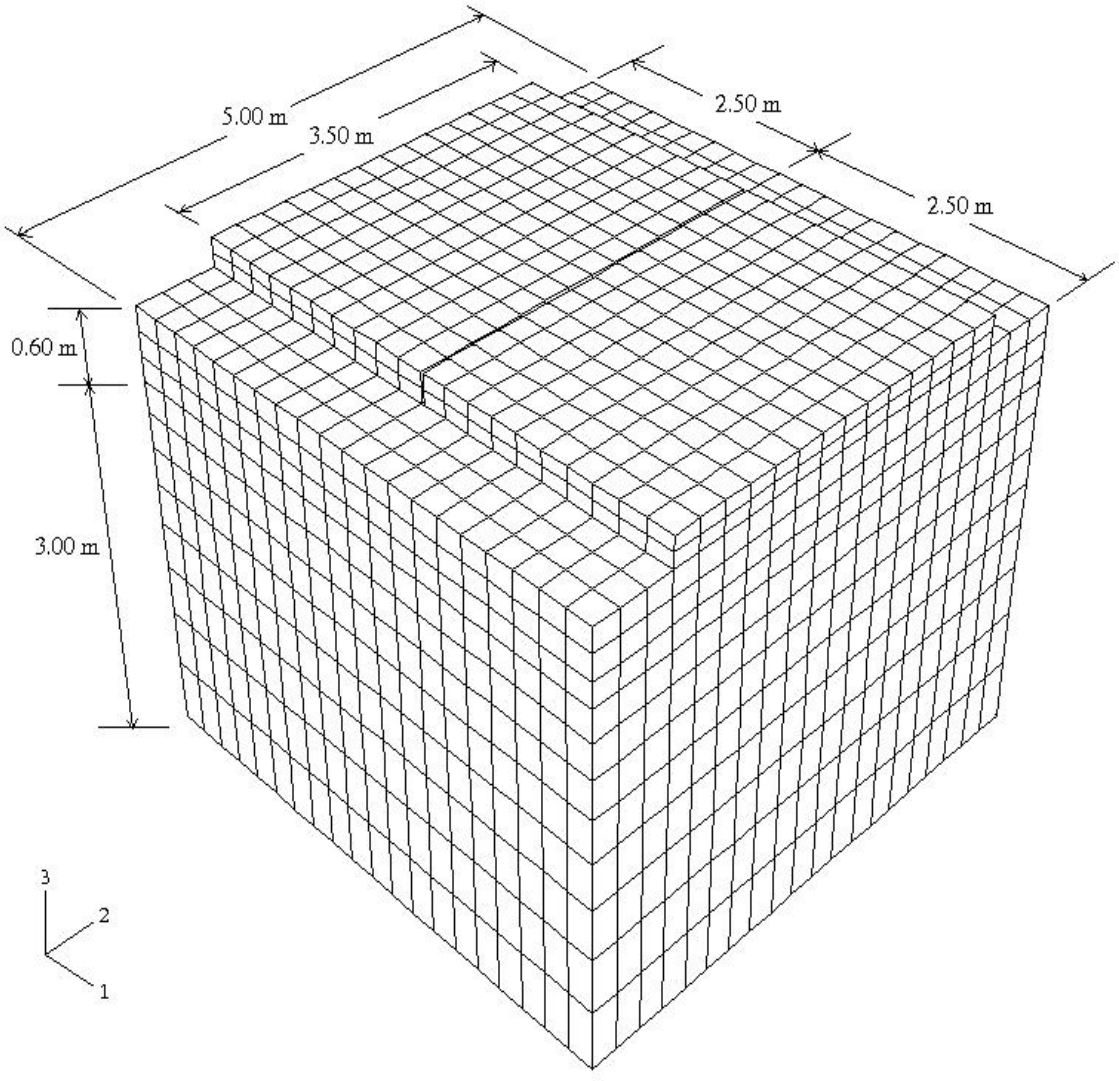

Fig. 5.8: 3-D model, geometry and FEM mesh

5.4.3 Elements

The elements for the concrete slab, base layer, and subgrade soil are chosen to be common ‘first-order 8-node 3-D’ continuum elements with eight integration points for each element.

5.4.4 Materials

After defining the geometry of a model and discretisation of all entities to finite elements, the second procedure is to assign a material for each element or element group. Following this, properties for each material should be defined.

For the rigid pavement system, there are different materials with different mechanical behaviors. For accurate modeling, and for the achievement of reasonable results, the following materials properties for different layers shall be assumed:

5.4.4.1 Material properties of plain concrete

The material library in ABAQUS includes, in addition to the common elastic model of plain concrete, another two models for plastic behavior. For the current model, in order to enhance the convergence, especially when using the UMAT subroutine for the cyclic behavior of UGMs, it was better to model the concrete slab as an elastic material. The elastic properties for the concrete material are assumed to be as following: Young’s modulus of 30,000 MPa and Poisson’s ratio of 0.20. The density of plain concrete is assumed to be 25.0 kN/m^3.

5.4.4.2 Material properties of the base layer

The main subject in the current analysis is the behavior of unbound granular material under cyclic loading and investigation into certain related problems (faulting) in rigid pavement structures. Then, the material model for this layer was chosen according to the Dresden model for unbound granular materials, as discussed before in Chapter 3, and shall be defined in ABAQUS through the new version of the UMAT subroutine.

Through the implementation of the user material subroutine UMAT in ABAQUS to define the behavior of UGMs, it is possible to run the analysis up to any defined number of loading cycles (e.g. one million cycles). The different parameters for the definition of the Dresden model are taken from Numrich [42], Wellner [67], and Werkmeister [68].

After running some analyses with the three different materials mentioned in the previous section (section 5.3.2), it was found that, there is no great difference in the behavior of those materials when used in rigid pavement, regarding permanent deformation behavior. Therefore, only one material shall be considered in the following analyses. This material is Gravel-Sand and the material parameters are the same as previously mentioned in Table 5.3. The density of Gravel-Sand is assumed to be 20.0 kN/m^3.

5.4.4.3 Material model of subgrade soil

For the description of subgrade soil, many material models were suggested by different researchers for the definition of both resilient and permanent deformation behavior in this layer under repeated loads. These models are similar to those of UGMs. In rigid pavement systems, because of the high stiffness of pavement structure, it is supposed that, the induced stresses due to traffic loads in the subgrade layer are so minute that the predicted permanent deformations are too small and do not greatly affect the permanent deformation behavior of the whole system. On the other hand, there is not available enough data to simulate the behavior of subgrade soil under cyclic loads as in the case of unbound granular base layer.

Therefore the material of subgrade soil was considered to be a linear elastic material with Young's modulus of 45.0 MPa and Poisson's ratio of 0.30. The density of subgrade soil is assumed to be 17.0 kN/m^3.

5.4.5 Boundary conditions and interaction formulation

The next step in the definition of a finite element model is assigning the boundary conditions for free edges and defining of interaction behavior between different layers.

5.4.5.1 Boundary conditions

The whole system is allowed to deform in the vertical direction except the bottom surface of the subgrade layer, which is prevented from moving either in the horizontal or vertical direction.

All vertical planes of base layer and subgrade layer are prevented from deformation in the horizontal direction (due to symmetry and infinite domain). The two concrete slabs are prevented from deformation in the horizontal direction only at the plane of symmetry (plane of cut). These boundary conditions are shown in Figure 5.9.

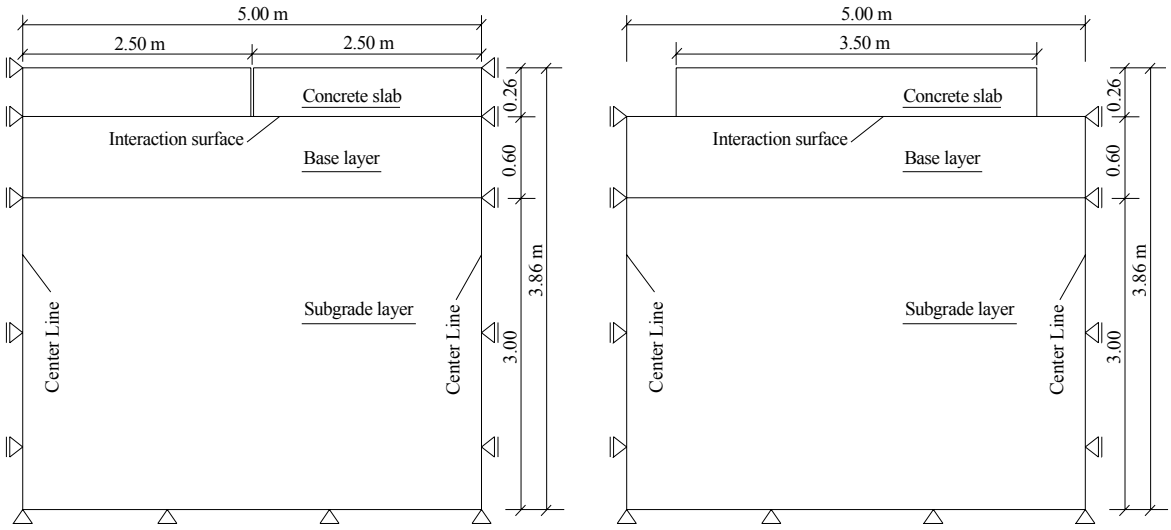

a) Longitudinal section *b) Transversal section*

Fig. 5.9: Boundary conditions for 3-D model

The two concrete segments are neither connected together through dowels nor other interaction devices. For numerical simplicity, a gap of 2.0 mm is assumed between the two slabs along the transversal joint to allow for the free displacement and rotation of the slab edges against each other.

5.4.5.2 Interaction between layers

Interaction conditions between layers could affect the behavior of multi-layered pavement systems. The most important interaction is the one between the concrete slab and the unbound base layer. This allows discontinuous deformation across the interface surface. According to the preliminary numerical evaluation, the existence of an interaction made a large impact on the numerical results, but variation in the interface conditions (changing the friction coefficient between the slab and base layer) only produced minor changes in the global response of pavement system.

The interaction between the concrete slab and base layer is defined through frictional contact option, which can be defined for two surfaces in contact. The angle of friction (δ) between the concrete slab and base layer depends on the internal angle of friction (φ) of the base layer material and the nature of the concrete surface in contact (smooth or rough). For a rough surface, it is assumed that $\delta = \varphi$ and for a smooth surface $\delta = 2/3\ \varphi$. The coefficient of friction is defined as $f = \tan \delta$.

The option of contact interaction in ABAQUS [2] can be used to model the interaction between two deformable bodies or between a deformable body and a rigid body in two- and three-dimensions. With this approach, one surface definition provides the **master** surface and the other surface definition provides the **slave** surface. In this case, a kinematic constraint that the slave surface nodes do not penetrate the master surface is assumed. The two surfaces in contact need not have matching meshes. However, the highest accuracy is obtained when the meshes are initially matching. For initially non-matching meshes, accuracy can be improved by judiciously specifying initial adjustments to ensure that all slave nodes that should initially be in contact are located on the master surface.

There are two types of interaction:

1- Small-sliding formulation

2- Finite-sliding formulation

Generally small-sliding contact is computationally less expensive than finite-sliding contact and was therefore used in the current analysis.

5.4.6 Loading

The external loads applied to the system should be defined according to the loading history. These loads are defined through the areas of application, magnitude, variation, and nature of the load (static or dynamic). In the current model, the traffic cyclic loads are defined as static loads and no consideration to dynamic effects are included. The

magnitude of a load is usually defined by the data lines of the loading option, and the variation of the load during a step can be defined by the default amplitude variation for the step or by a user-defined amplitude curve. Two cases of loading shall be considered in the current 3-D model, as described below:

1- Case 1: a wheel load of 53.0 kN shall be applied in the middle area of the edge parallel to the transversal joint. The wheel load is distributed over a contact area of 0.25 x 0.25 m^2 with a contact pressure of 850.0 kPa (Figure 5.10).

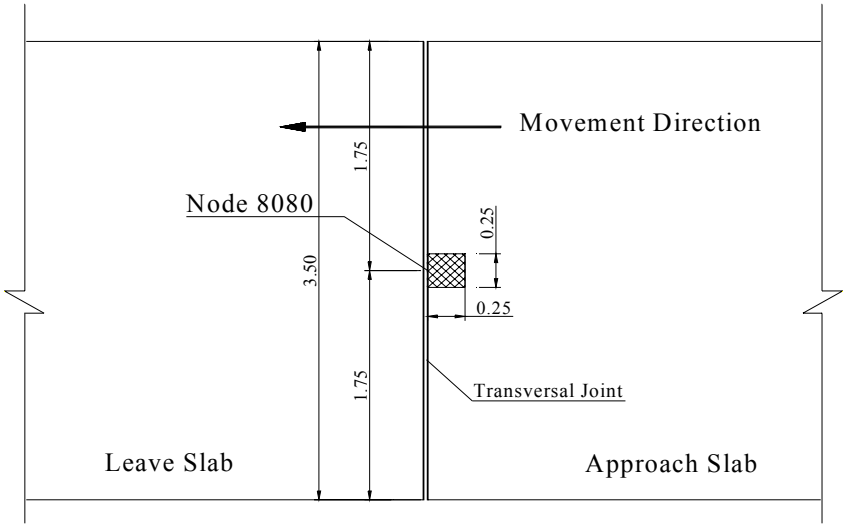

Fig. 5.10: Applied load to 3-D model, tire pressure q = 850.0 kPa, case 1

2- Case 2: two wheel loads each of 53.0 kN (simulating an axle load) shall be applied near the corners of the edge parallel to the transversal joint. The wheel loads are distributed over two contact areas each 0.25 x 0.25 m^2 with a contact pressure of 850.0 kPa (Figure 5.11).

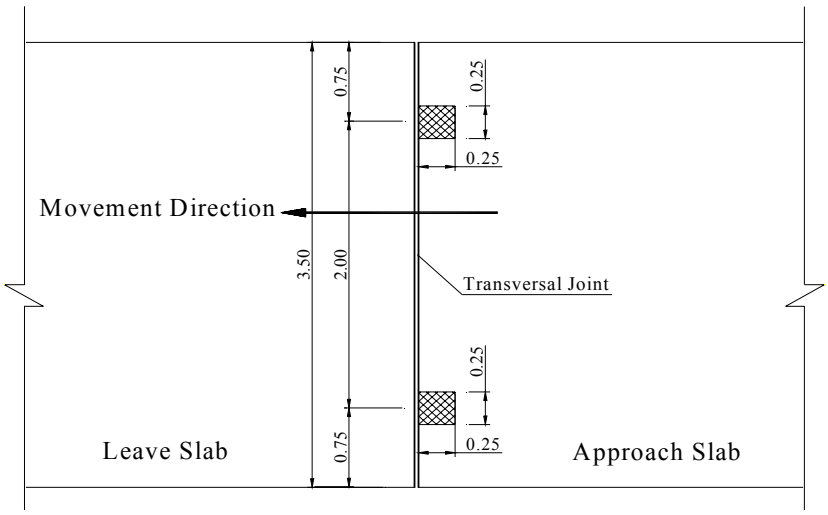

Fig. 5.11: Applied loads to 3-D model, tire pressure q = 850.0 kPa, case 2

The number of loading cycles is defined as an input data to the UMAT constants in the ABAQUS input file. In this analysis the number of cycles shall be set as one million cycles (can be also set up to any greater number).

The 3-D model shall be analyzed for each case of loading and the corresponding results shall be obtained regarding elastic and plastic deformations in addition to stresses and contact pressure between the concrete slab and the base layer. The results are presented in the next section.

5.5 Results of the 3-D model

5.5.1 Load case 1, one central wheel on edge

Both elastic stresses and displacements can be obtained for all layers at the end of step 3 in the analysis (applying of wheel load). Total deformation (elastic + permanent) can be obtained at the end of step 4.

5.5.1.1 Elastic stress in the concrete slab

For the concrete slab, the tensile elastic stress (maximum principle stress) is presented as contour lines in Figure 5.12. Section A-A shows the stress distribution along the edge of the concrete slab in the area directly under the applied load.

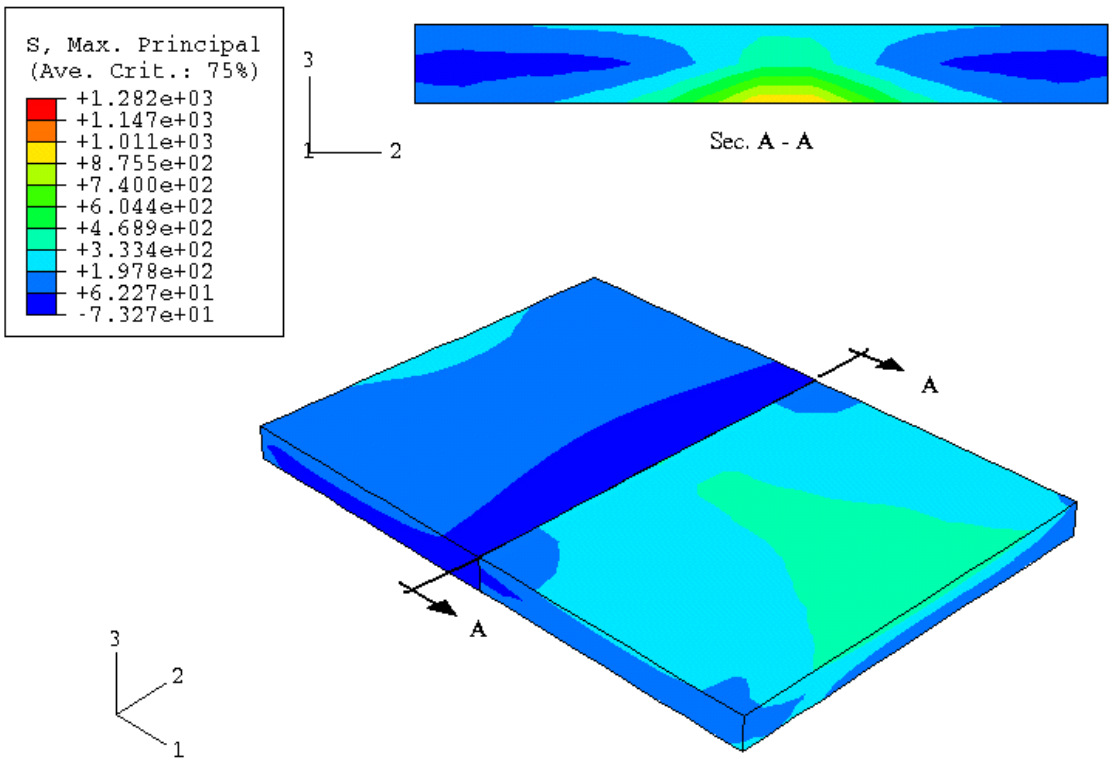

Fig. 5.12: Maximum principle stress in concrete slab [kPa], load case 1

5.5.1.2 Elastic displacement in base and concrete layers

Figure 5.13 presents a contour plot for the elastic vertical displacement in the base layer at the end of step 3. It is clear that the maximum elastic displacement occurs directly beneath the wheel load.

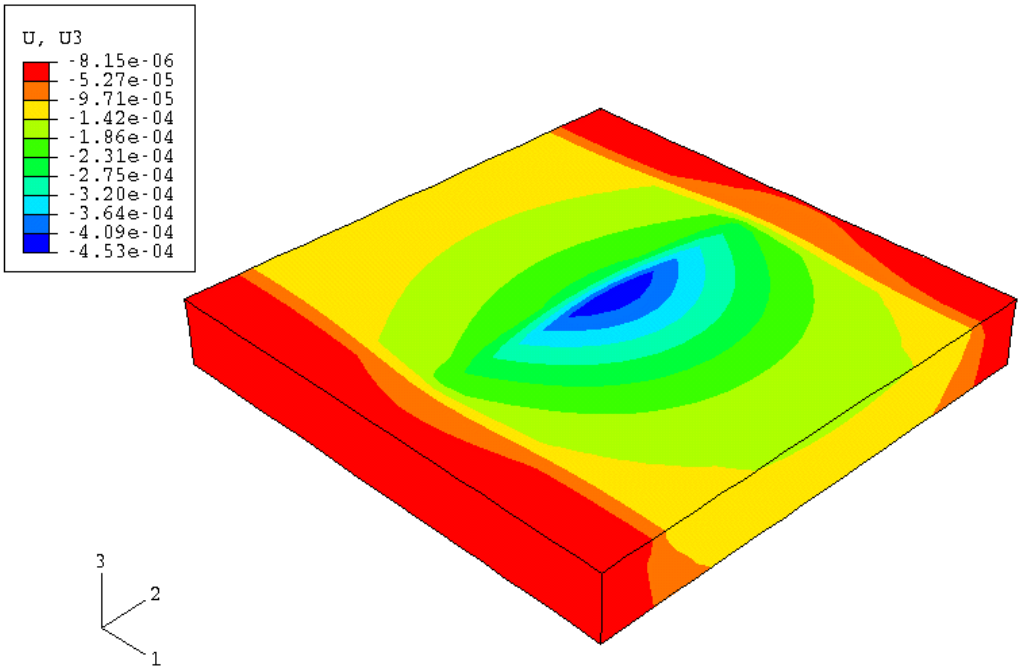

Fig. 5.13: Vertical elastic displacement in base layer [m], load case 1

The maximum elastic displacement in the concrete slab at a node directly beneath the wheel load is nearly equal to that in the base layer. Figure 5.14 presents the maximum vertical elastic displacement against a vertical load ratio in step 3. The given values of displacement are positive for convenient simulation in the following figures. The linear relationship in Fig 5.14 is similar to the experimental results in the work of Gleitz [18].

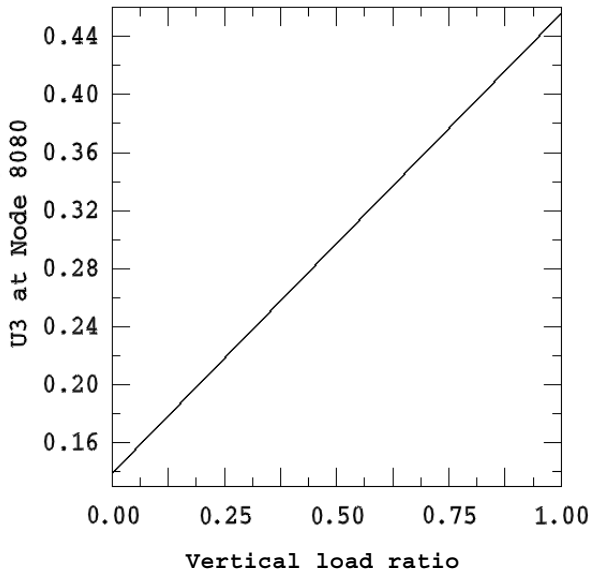

Fig. 5.14: Maximum vertical elastic displacement [mm] in concrete and base layer, load case 1

5.5.1.3 Comparison of FEM results with Westergaard theory

For the previous 3-D pavement system with load case number one, calculation of maximum tensile stress and maximum deflection according to Westergaard is accomplished as following:

1- First, the modulus of subgrade reaction (k) can be calculated from the plate bearing tests conducted by Wellner [67] for the used material (Gravel-Sand). In section 5.3.1.1, the results of plate bearing tests showed that an applied pressure of 300.0 kPa produced a vertical deflection of 0.58 mm and an applied pressure of 700.0 kPa produced a vertical deflection of 1.18 mm in Gravel-Sand material. So (k) can be calculated by dividing the applied pressure by the resulted deflection, then we get two values for (k) which are 5170.0 and 5930.0 kPa/cm respectively. For the calculation with Westergaard, (k) shall be assumed to have a value of 5000.00 kPa/cm.

2- The radius of the tire print can be calculated from an equivalent circular area to the real area in FEM (square with 0.25 m edge). The input data for calculation with Westergaard theory is presented in Table 5.4.

Table 5.4: Parameters for Westergaard calculation

Parameter	(k), UGMs (kPa/cm)	E,concrete (kPa)	a (cm)	h (cm)	P (kN)	b (cm)	l (cm)
Value	5000.00	$3x10^7$	14.07	26.00	53.00	13.96	55.00

3- Using equations 2.7 and 2.9 to calculate the maximum tensile stress and the maximum vertical deflection of the concrete slab according to Westergaard, the following results are obtained and compared to those of FEM in Table 5.5.

Table 5.5: Comparison of FEM and Westergaard results, edge loading

Calculation method	Westergaard	FEM Load case 1
Max. tensile stress (kPa)	1593.50	1282.00
Max. vertical deflection (mm)	0.121	0.310

The maximum tensile stress calculated with Westergaard's theory is about 24% more than that calculated through FEM, which may refer to the under-estimation of the subgrade reaction (k) used in Westergaard's theory. However, the prediction of vertical deflection with Westergaard is about 40% of the value predicted with FEM analysis. This may refer to the modeling of the base layer as elastic springs in Westergaard's theory, these springs have only one degree of freedom in the vertical direction. On the other hand the simulation of base and subgrade layers in FEM as continuum elements allows them to deform in all directions, thus increasing the deformation in the direction of maximum principle stress.

5.5.1.4 Maximum vertical stress in the base layer

Figure 5.15 presents the maximum vertical stress against vertical displacement in step 3 for an element lying directly beneath the wheel load area in the base layer. The linear relationship in Fig 5.15 is similar to the experimental results in the work of Gleitz [18].

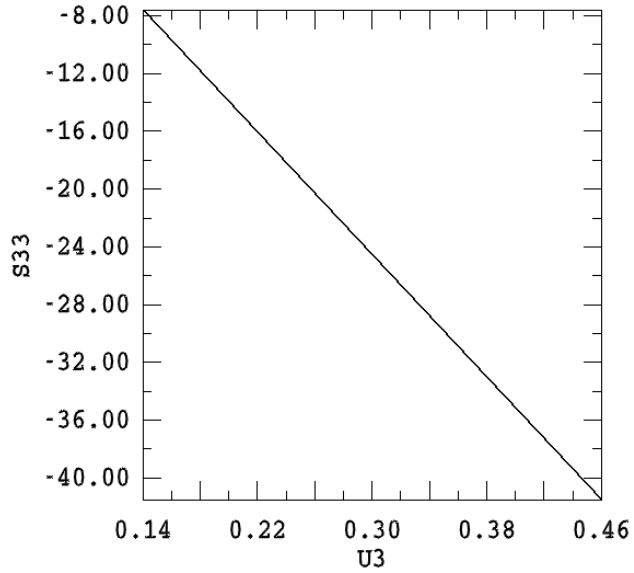

Fig. 5.15: Maximum vertical stress [kPa] against disp [mm] in base layer, load case 1

5.5.1.5 Variation of E-Modulus and Poisson's ratio with stresses

The following figures present the variation of the resilient modulus of elasticity and Poisson's ratio depending on the stress-level in base layer elements, for example, E-Modulus and Poisson's ratio for the element whose maximum vertical stress shown in Figure 5.15 are presented against displacement in Figures 5.16 and 5.17 respectively. Contour plots for E-Modulus and Poisson's ratio are presented in Appendix B.

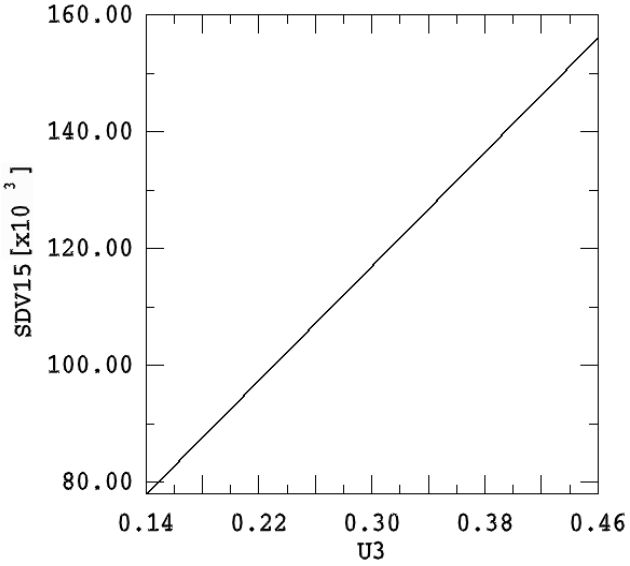

Fig. 5.16: Maximum resilient modulus [kPa] against disp [mm] in base layer, load case 1

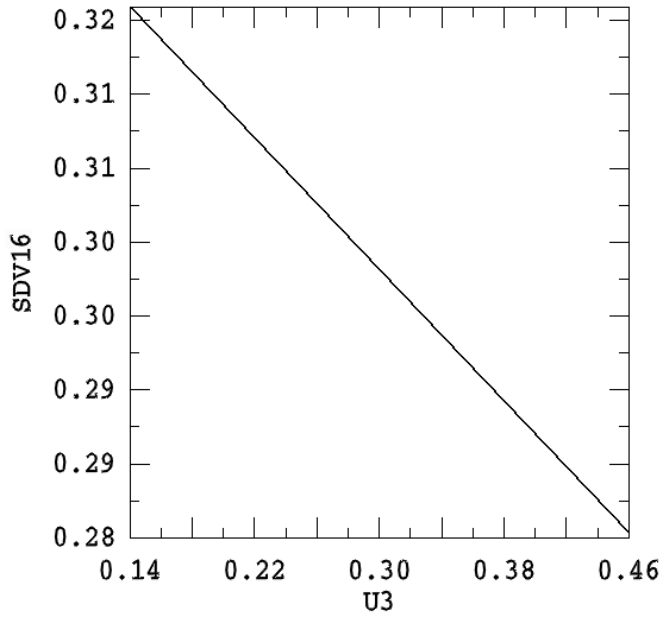

Fig. 5.17: Poisson's ratio [-] against disp [mm] in base layer, load case 1

5.5.1.6 Total displacement in the base layer

Figure 5.18 presents the development of the maximum total vertical displacement in the base layer during step 4 (application of one million cycles). The permanent displacement can be calculated after the deduction of the elastic displacement from the total displacement.

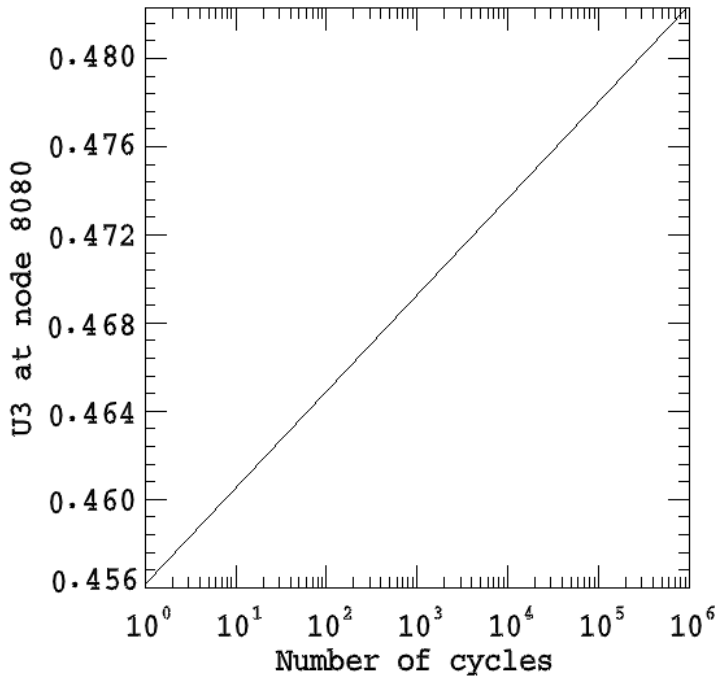

Fig. 5.18: Total vertical displacement in base layer [mm] after 10^6 cycles, load case 1

5.5.1.7 Variation of parameters *A* and *B* of the Dresden model with stresses

The following figures present the variation of the *A* and *B* parameters during step 4 (calculation of cyclic permanent deformation) depending on the stress-level in the base layer elements. For example, *A* and *B* for an element whose maximum vertical stress shown in figure 5.15 are presented against number of cycles (N) in Figures 5.19 and 5.20 respectively. Contour plots for *A* and *B* parameters are presented in Appendix B.

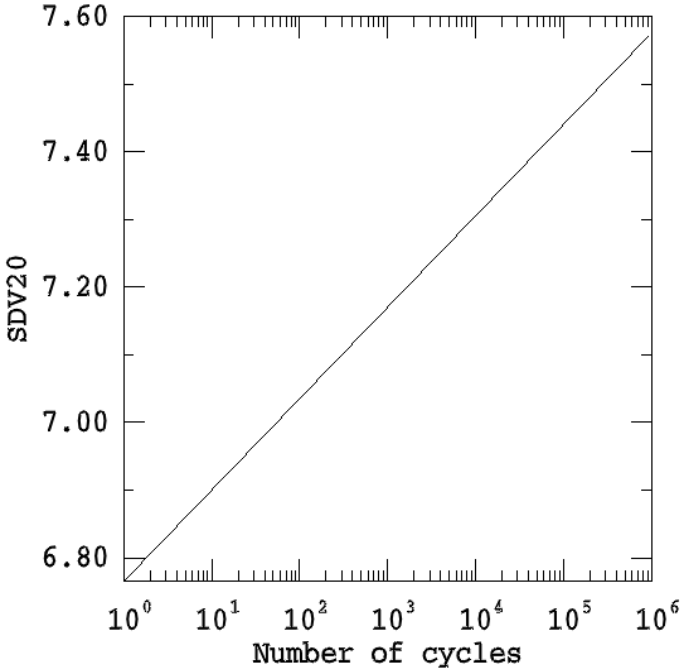

Fig. 5.19: Parameter (A) of Dresden model against N in base layer, load case 1

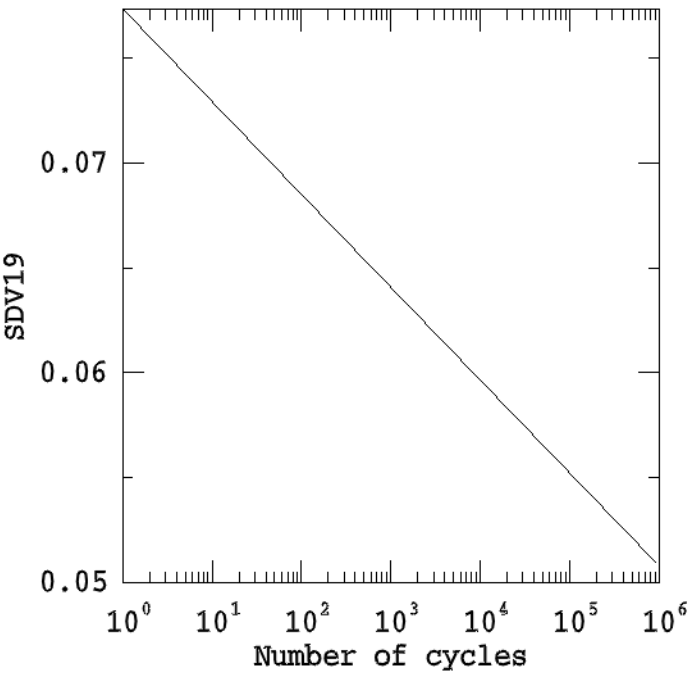

Fig. 5.20: Parameter (B) of Dresden model against N in base layer, load case 1

5.5.1.8 Contact pressure on the top surface of the base layer

Figure 5.21 presents the contact pressure between the concrete slab and the base layer at interface surface at the end of step 3.

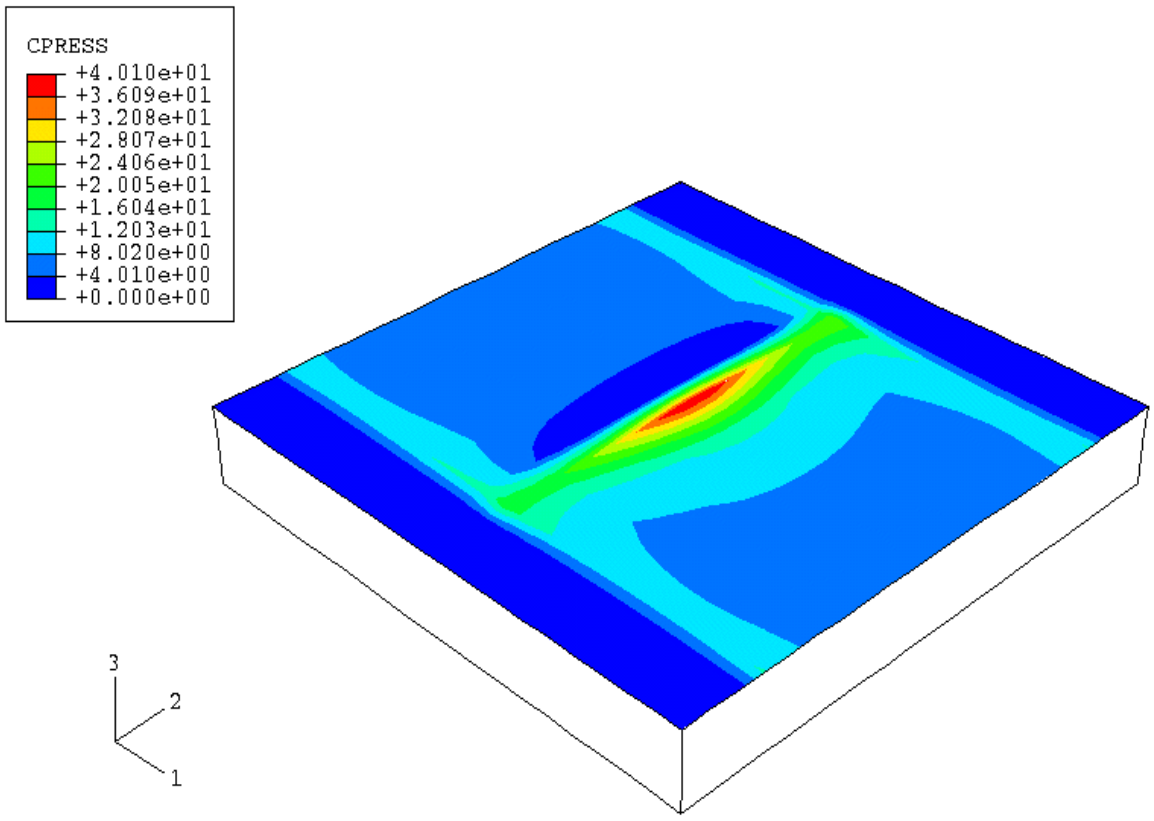

Fig. 5.21: Contact pressure between concrete slab and base layer [kPa], load case 1

The contact pressure has its maximum value directly beneath the wheel load's application area and has a value of 40.10 kPa for this loading case.

5.5.2 Load case 2, two wheels near the corners

The results for the second case of loading (two wheel loads on the edge) can be presented in the same way as for load case number 1 (one central wheel on the edge). But only those results needed for comparison with load case 1 are presented here in this section. The comparison between the two cases of loading defines which case has the maximum influence on the base layer regarding maximum elastic stresses and deformations. Then, an equivalent 2-D system with an equivalent load can be developed from the 3-D system.

Other results regarding the maximum stresses in the concrete slab and a comparison with the Westergaard's theory are found in Appendix A.

5.5.2.1 Maximum elastic stress in the base layer

Figure 5.22 presents the maximum vertical stress against the displacement in step 3 for an element lying directly beneath the wheel load area in the base layer. The linear relationship in Figure 5.22 is similar to the experimental results in the work of Gleitz [18].

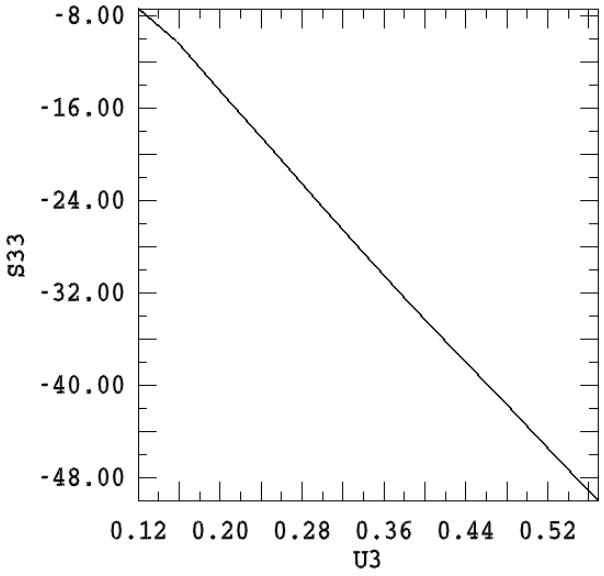

Fig. 5.22: Maximum vertical elastic stress [kPa] against disp [mm] in base layer, load case 2

5.5.2.2 Maximum elastic displacement in the base layer

The maximum elastic displacements in the concrete slab for the nodes directly beneath the both wheel loads are nearly equal to those in the base layer. Figure 5.23 presents the maximum vertical elastic displacement against the vertical load (wheel load) ratio in step 3.

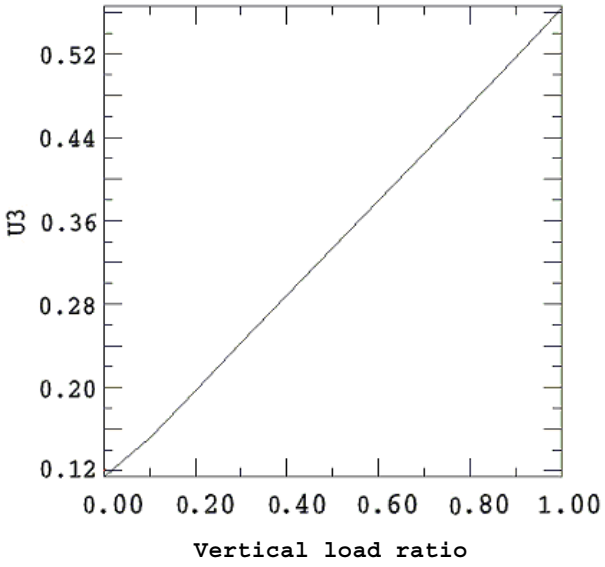

Fig. 5.23: Maximum vertical elastic displacement [mm] in concrete and base layer, load case 2

5.5.2.3 Contact pressure on the top surface of the base layer

Figure 5.24 presents the contact pressure between the concrete slab and the base layer at the interaction surface at the end of step 3.

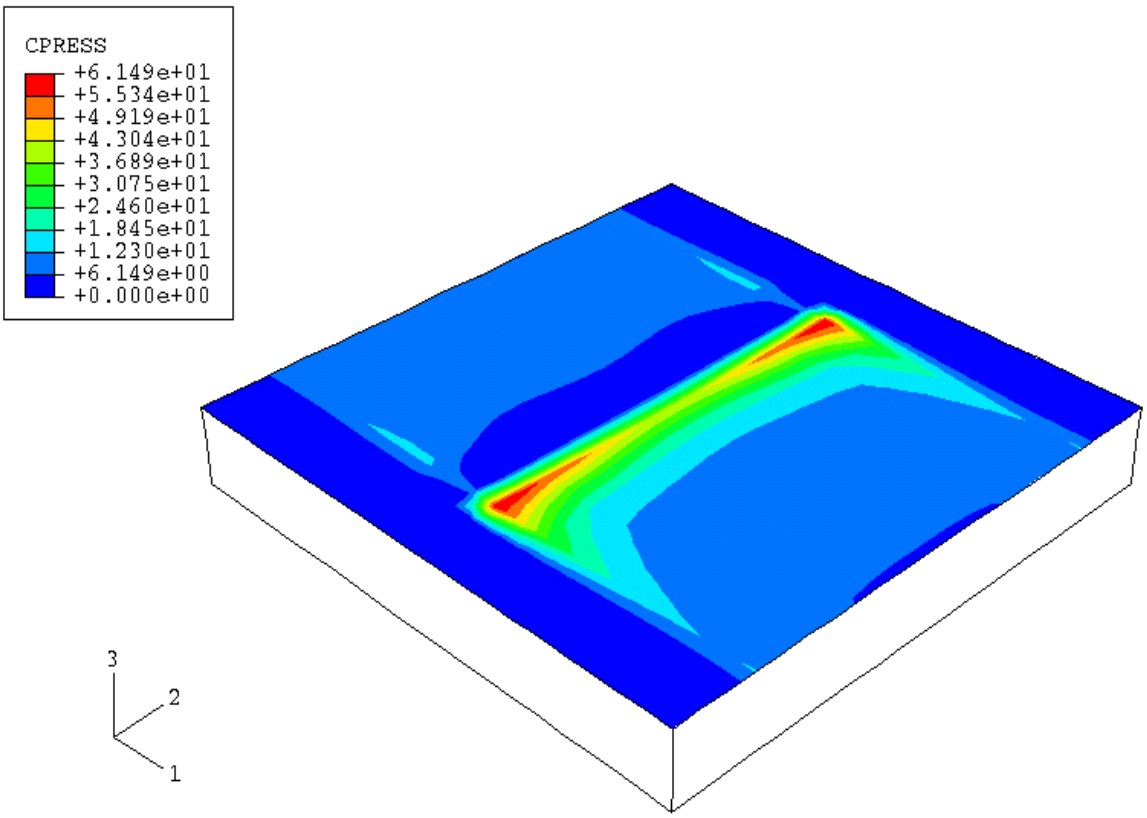

Fig. 5.24: Contact pressure between concrete slab and base layer [kPa], load case 2

From both Figures 5.21 and 5.24 showing contact pressure between the concrete slab and the base layer, it can be noted that, at the interface surface, high concentration in contact pressure exists under the loaded edge of the concrete slab. Therefore, the faulting problem arises.

5.5.3 2-D model selection

The analysis platform for ABAQUS in this research is a UNIX based workstation composed of 32 hyper nodes (*IBM* p Series 690); each node is equipped with 32 processors Power 4 (1,30 GHz). The whole memory of the machine is divided into: two nodes with 256 GB RAM, two nodes with 128 GB RAM, and 28 nodes with 64 GB RAM (the whole machine contains 1024 processors and 2560 GB RAM) [41].

Large-scale 3-D finite element problems often provide good approximate solutions. But in our case of cyclic load calculation (up to one million cycles) with a non-linear material model to compute the permanent deformation in the unbound granular base layer, the analysis requires a very long computing time and too much data storage space. The previous 3-D model as described in section 5.4 contains 6282 nodes and

4960 elements, in addition there is only one contact interface pairs between the concrete slab and the base layer.

The analysis for the model with one million loading cycles required about 70089 seconds for completion with one processor. In order to minimize the computing time, parallel computation was put into practice. With 2 processors, the time was reduced to 43090 seconds. Trying again with 4 processors, the analysis was not completed due to time spent waiting for the allocation of free processors to the problem. Anyhow, using two processors reduced the computing time to 62.5% of the time required by one processor. In an ideal situation, the reduction of the time should be 50%. The volume of the output data bank file (*.odb) for the results is about 3.864 GB.

It means that for such a simple 3-D model, the required time and storage capacity is very high. If we imagine a 3-D model, for faulting simulation, with the following dimensions: about 15.00 m length, 7.00 m width, and 7.00 m depth in addition to having fine mesh in stress concentration regions, then the supposed model may be 8 to 10 times greater than this simple one. The use of a 2-D model for the simulation of faulting problem was advised but such 2-D finite element problem still creates a demand for rapid processors and large amount of memory space.

5.6 Equivalent 2-D system

For the study of rigid pavement system under heavy cyclic loads with regard to the faulting problem, it is important to know the distribution and frequency of wheel loads over the cross-sectional area of a traffic lane.

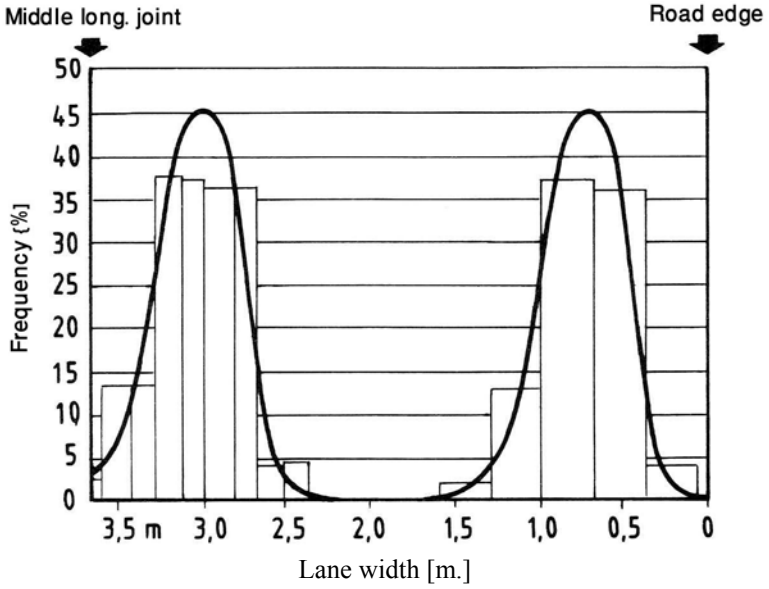

Fig. 5.25: Frequency of wheel load positions for 3.60 m lane width [47]

An earlier study showed that, the frequencies of wheel loading positions over a 3.60 m wide lane have their maximum values at a distance of about 0.60 m from both the road edge and the middle longitudinal joint. Figure 5.25 presents the distribution and frequency of wheel positions over a cross-section in rigid pavement [47]. From Figure 5.25, one can conclude that, the load case number 2 in the 3-D model for rigid pavement system presented in section 5.5 represents more than 75% of rolling-axles over the cross-section of a 3.60 m wide lane.

5.6.1 Equivalent loads for 2-D model

From the results of the 3-D model analysis, it is noted that the loading case number 2 (two wheels near the corners) caused more stress and deflection in the base layer than load case number 1. If an assumption shall be considered for redistribution of the two wheel loads over the whole edge length (3.50 m) of the concrete slab, then the resulting maximum stresses and displacement in the base layer should be equivalent to those in a real situation. This assumption needs verification through FEM calculation. For this reason, a 2-D model is chosen to simulate the rigid pavement in the 2-D plane for the verification of wheel loads redistribution. The results of the 2-D model shall be compared with those of the 3-D model.

5.6.1.1 2-D model analysis

The 2-D model is chosen in such a way that it represent a longitudinal section through the 3-D model. The dimensions, FEM mesh, material properties, and boundary conditions shall be maintained from the 3-D model to the 2-D model. Figure 5.26 shows the equivalent 2-D system.

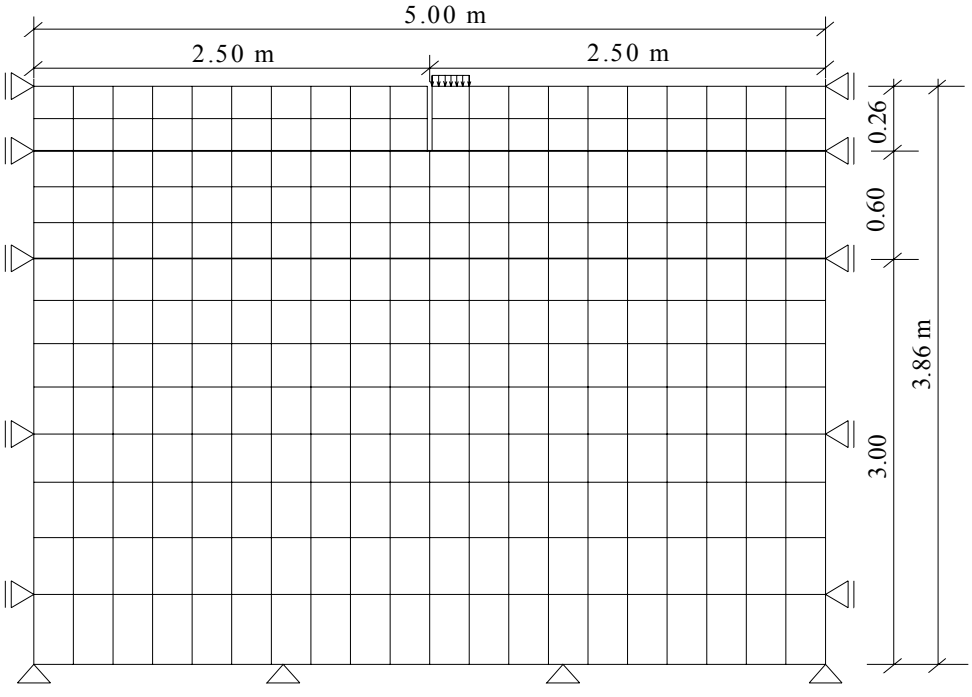

Fig. 5.26: Chosen system of the 2-D model

After some trials with the 2-D analysis assuming different values for the equivalent pressure of wheel load, it was determined that, an equivalent pressure of 125.00 kPa with a width of 0.25 m acting on the edge of the concrete slab gives approximate prediction of the results to those obtained with the 3-D model. This is discussed in the following section.

5.6.1.2 Results of the 2-D analysis

The results of the 2-D model can be presented in the same way as of those of the 3-D model. Only these results required for the comparison with the 3-D model shall be presented her.

Figure 5.27 presents the elastic vertical displacement in the base and subgrade layers at the end of step 3.

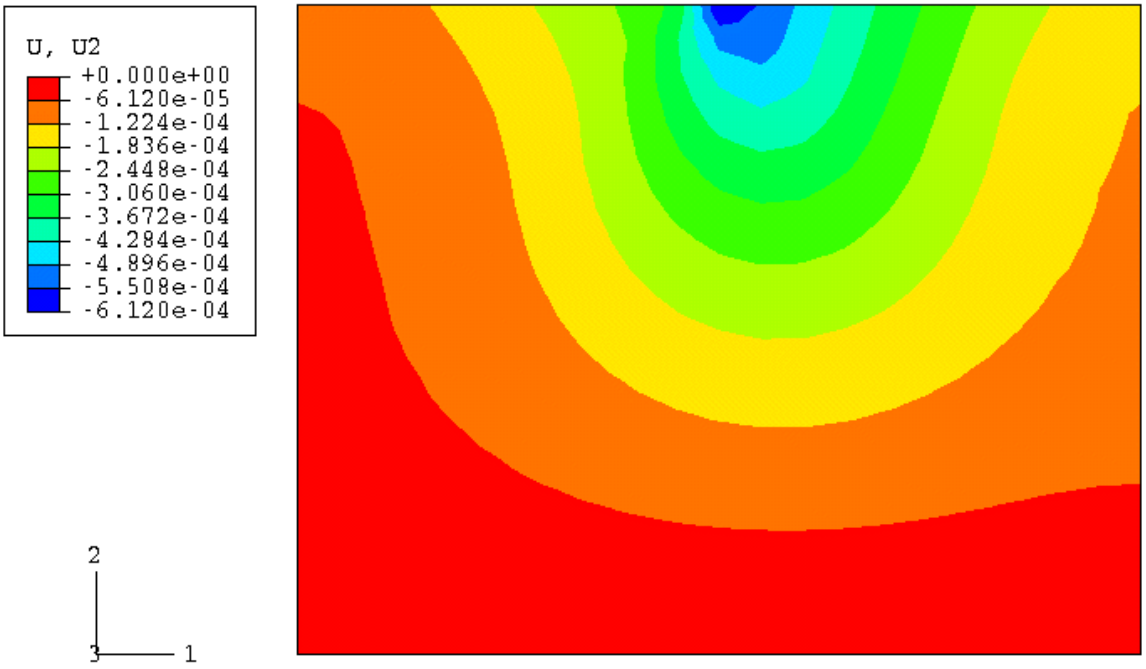

Fig. 5.27: Vertical elastic displacement in base & subgrade layers [m], 2-D model

From Figure 5.27, the maximum elastic displacement in the unbound base layer is found under the edge of the concrete slab directly beneath the application area of the equivalent pressure (equivalent to wheel load).

For better comparison, x-y plots are presented for both maximum elastic displacement and stress of an element lying directly beneath the loaded edge of the concrete slab. Figure 5.28 presents the maximum vertical elastic displacement against the vertical load (equivalent pressure) ratio in step 3.

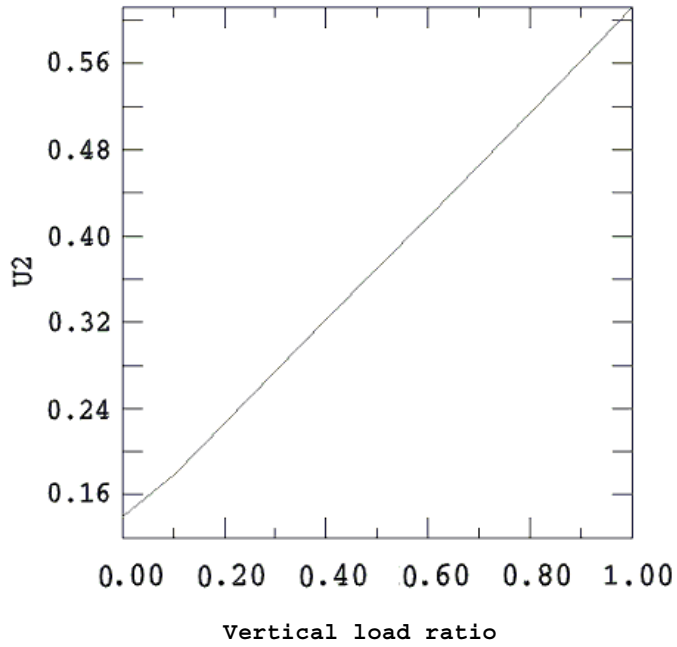

Fig. 5.28: Maximum vertical elastic displacement [mm] in concrete and base layer, 2-D model

Figure 5.29 presents the development of maximum vertical stress against the displacement in step 3 for an element in the base layer lying directly beneath the wheel load area. The nearly linear relationship in Figure 5.29 is similar to the experimental results in the work of Gleitz [18].

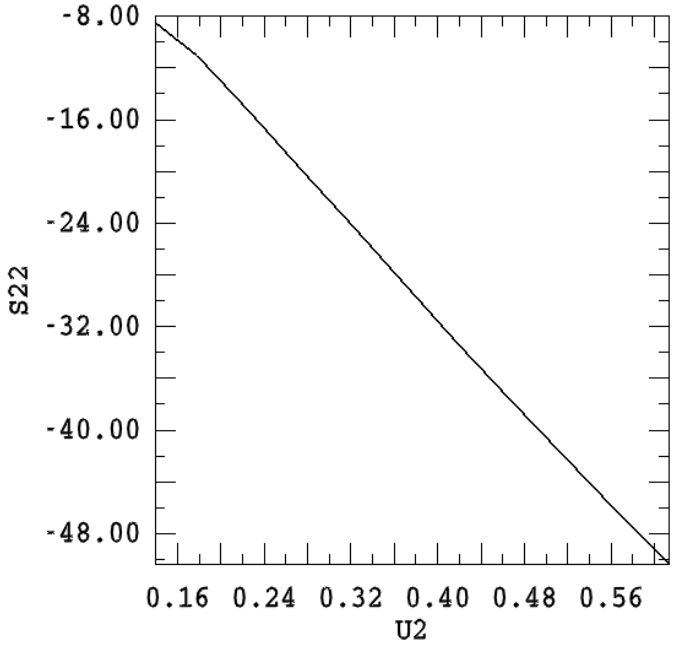

Fig. 5.29: Maximum vertical elastic stress [kPa] against disp [mm] in base layer, 2-D model

5.6.2 Comparison between 2-D and 3-D results

The following table shows a comparison between the 2-D and 3-D results regarding maximum elastic vertical stress and displacement values in the base layer material for an element lying directly beneath the applied loads.

Table 5.6: Comparison between 2-D and 3-D results

Result variable of base layer	2-D model (Equiv. pressure)	3-D model (Load case 2)
Max. vertical elastic deformation (mm)	0.47	0.44
Max. vertical stress (kPa)	50.37	49.95
Max. contact pressure on base layer surface (kPa)	77.40	61.50
Relative displacement of concrete slab edges (mm)	0.282	0.29

From the above results in Table 5.6, it can be concluded that the maximum vertical elastic deformation and stresses of the 2-D model are very close to the same results of the 3-D model with load case number 2.

For more assessment, the distribution of vertical stress (σ_{33}) in the base layer for a section beneath the centerline of the applied loads is plotted for both the 2-D model and the 3-D model with load case number 2 (Figure 5.30).

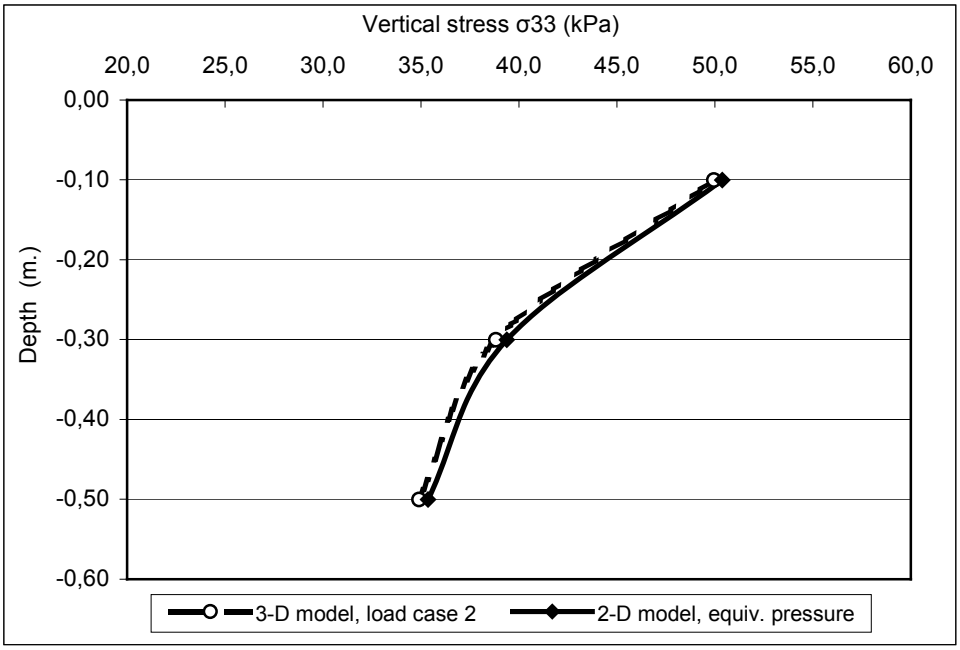

Fig. 5.30: Comparison of vertical stress (σ_{33}) between 2-D and 3-D models, R^2= 0.96

It is to be noted that, the shown vertical stresses are plotted for the centroid points of the elements in the chosen element set (section). Therefore, the stresses on the top and bottom surfaces of the base layer; at depth equal 0.0 and 0.60 m respectively cannot be presented in the shown figure.

5.6.3 Conclusion

From the above results and comparisons, it can be concluded that, an equivalent pressure of 125.00 kPa in the 2-D model can give the same influence as real pressure of 850.00 kPa due to the wheel load in the 3-D model for the load case number 2 (an axle load of 2 wheels, each being 53.00 kN). This conclusion is only valid for the current model with the given materials and load configuration. It cannot be generalized for other models with another materials or another load configurations. The analysis for a faulting prediction with a 2-D model can now use this equivalent pressure for the simulation of applied wheel loads. The analyses of faulting problem are presented in the following chapter.

6 PREDICTION OF FAULTING

6.1 Introduction

The main objective of the current research is the development of a model with FEM aiming to study the faulting problem at the joint location between two adjacent concrete slabs. Also important is the attempt to simulate the physical concept of the faulting process numerically in order to find a tool, which would help in the understanding of the problem.

A model was built to simulate, to an extent, the real conditions, with the consideration of a moving cyclic load crossing the joint from the approach slab towards the leave slab.

The model is chosen in a 2-D system because of many factors:

1- To have a reasonable model, which can achieve good convergence.

2- To minimize the computation time and cost.

3- As the faulting occurs in the longitudinal direction of a road, the maximum vertical deformation and relative displacement between the transversal concrete slab edges are the dominating factors.

Firstly, the faulting shall be computed according to the empirical formula of Khazanovich et al [31].

Secondly, through a new developed procedure, using the fluid structure interaction capability in ABAQUS, the faulting shall be computed through FEM analysis under cyclic loading. In order to assess the correctness of the developed procedure, firstly, the unbound granular base material shall be considered as an elastic material with Mohr Coulomb hardening. The moving load across the joint is applied firstly on the edge of the approach slab then moved across the joint to the edge of the adjacent leave slab. The analysis shows good results indicating that the forming of a fault is a result of applying a load which moves from the approach slab towards the leave slab across a joint with no or a very low load transfer efficiency device.

Following that, the model shall be analyzed again using the UMAT subroutine to account for the behavior of the unbound granular base materials under cyclic loading in relation to the computation of faulting. The unbound granular base material shall be assumed having two cases regarding moisture content; (1) a uniform constant moisture content, and (2) a non-constant moisture content. For the suggested procedure some factors need calibration. Unfortunately, neither field nor experimental data are available for the calibration purpose, therefore, these factors shall be assumed in a reasonable way.

6.2 2-D model for the simulation of faulting

6.2.1 Description of the system

The 2-D model for rigid pavement system in this analysis comprises of three slabs (two complete slabs + two halves), in order to have three joints, which are symmetrical with reference to the middle joint under study.

The choice of such a system was to have all possible contributions to the calculation of faulting, as a load crossing a joint causes not only faulting to this joint but to the preceding joint and to the proceeding joint as well.

The system is composed of three layers: the first one is the surface layer made up of the concrete slabs which are supported on the second layer (base layer) of an unbound granular material, the whole structure being supported by the subgrade soil layer (Figures 6.1 and 6.2). The traffic loads shall only be applied to the intermediate joint, as described in detail in the following sections.

The chosen 2-D system will be used in two analyses: firstly as it is described below to calculate the elastic displacement of concrete slabs' edges under wheel load, and secondly, it will be used with the new developed procedure to calculate the faulting using the fluid structure interaction through the addition of two fluid-filled cavities under the edges of concrete slabs (as described in Section 6.4).

6.2.2 Geometry and mesh generation

The 2-D model chosen to simulate the rigid pavement for prediction of faulting at the joint location consists of two adjacent slabs, each 5.00 m long, bounded by two half slabs, each 2.50 m long. The thickness of the concrete layer is chosen to be 0.26 m (after RStO, Road Class I). The thickness of the unbound granular base layer is chosen to be 0.60 m. The pavement structure is supported by a 6.00 m depth subgrade soil. It means that the 2-D model has total dimensions of 15.00 m long x 6.86 m deep.

Because the loads are localized near the joints, the FEM mesh is generated in the horizontal direction, so that it is very fine in the regions of the transversal joints and coarser towards the outside.

As the depth of both the concrete slabs and base layers is very small compared with that of the subgrade soil, it was better to have uniform element lengths in the vertical direction for both layers. This method provides a better aspect ratio (from 1.3 to 2.0) for elements under high stresses due to wheel loads and also a good ratio (up to 5.0) for elements in the regions of small stress gradients.

The discretisation of the subgrade layer in the vertical direction is generated in a biased manner to minimize the total number of elements in the system. Figure 6.1 shows the geometrical model with the generated finite element mesh.

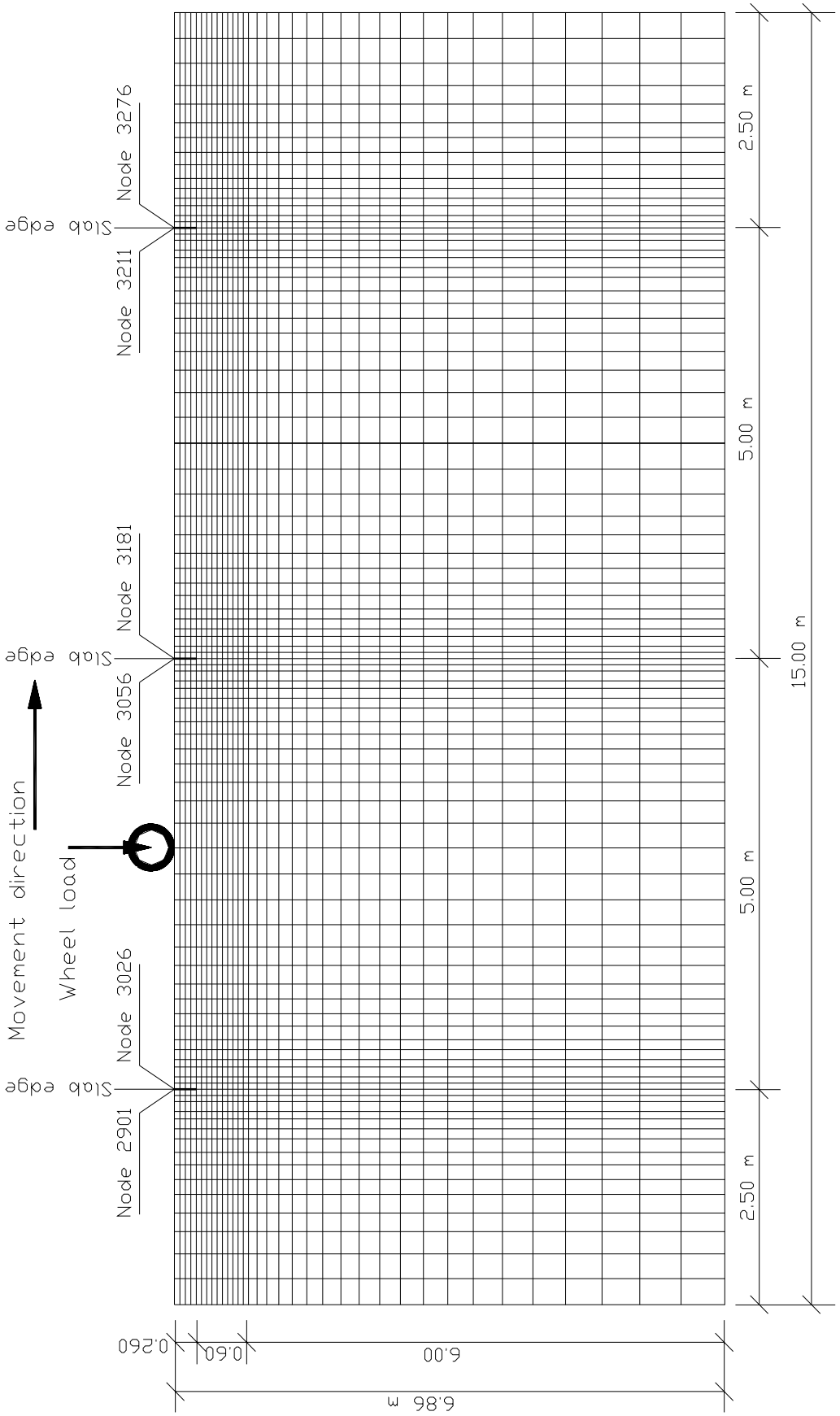

Fig. 6.1: FEM model and mesh generation

6.2.3 Elements

The elements for the concrete slab, the base layer, and the subgrade soil are chosen to be a common first-order 4-nodes 2-D continuum elements with four integration points for each element.

6.2.4 Materials

The definition of the materials is the same as that of the 3-D model in Chapter 5. Here again is a brief definition of the different materials used in the analysis.

6.2.4.1 Material properties of plain concrete

The concrete slab was modeled as an elastic material with Young's Modulus of 30,000.00 MPa and Poisson's ratio of 0.20. The density of plain concrete is considered to be 25.00 kN/m^3.

6.2.4.2 Material properties of base layer

The analysis of the 2-D model for the prediction of faulting shall be conducted using four material models for the unbound base layer:

1- Firstly, with an elastic material model to calculate the elastic displacement of concrete slabs under wheel load, from which, the faulting shall be computed according to the empirical formula of Khazanovich et al [31].

2- Secondly, with a classical Mohr Coulomb plasticity model in order to verify the proposed procedure with fluid structure interaction capability in ABAQUS when applying the wheel load for only one cycle.

3- Thirdly, after verifying the procedure with the Mohr Coulomb plasticity model, the analysis shall be performed again using the Dresden model for the unbound granular base layer assuming a constant low relative moisture content (RMC) over the whole base layer, using the UMAT subroutine.

4- Fourthly, assuming that regions of the base layer beneath the transversal joints have higher relative moisture content than those beneath the middle of the concrete slabs, a new analysis shall be conducted to study the influence of a high RMC of the base layer on the faulting process.

Detailed description of material models for the base layer shall be discussed in respective sections.

6.2.4.3 Material model of subgrade soil

The material model of subgrade soil is defined as a linear elastic material with Young's Modulus of 45.00 MPa and Poisson's ratio of 0.30. The density of subgrade soil is assumed to be 17.00 kN/m^3.

6.2.5 Boundary conditions and interaction formulation

Assigning correct boundary conditions for the free edges in the current model is of great importance, because the model is not symmetric in loading history.

6.2.5.1 Boundary conditions

The whole system is allowed to deform in the vertical direction except the bottom surface of the subgrade layer, which is prevented from moving in either the horizontal or vertical direction. All vertical edges of the base and subgrade layers are prevented from deformation in the horizontal direction (due to infinite domain). The concrete slab layer is free to move in both horizontal and vertical directions. In order to keep the stability of the concrete slabs, the two bounding half slabs are connected to artificial ground springs with a very low spring stiffness (10.0 kPa/m). These boundary conditions are shown in Figure 6.2. The adjacent concrete slabs are neither connected together through dowels nor other interaction devices. There is a gap of 2.00 mm between adjacent edges of the slabs at the joint location to allow for free translation in both horizontal and vertical directions.

6.2.5.2 Interaction between layers

The same conditions of the 3-D model in Chapter 5 apply here. The only interaction between the concrete slab and the base layer is defined by the frictional contact option. The angle of friction between the concrete slab and the base layer is defined as (δ). The coefficient of friction is defined as f = tan δ, and is assumed to be 0.50.

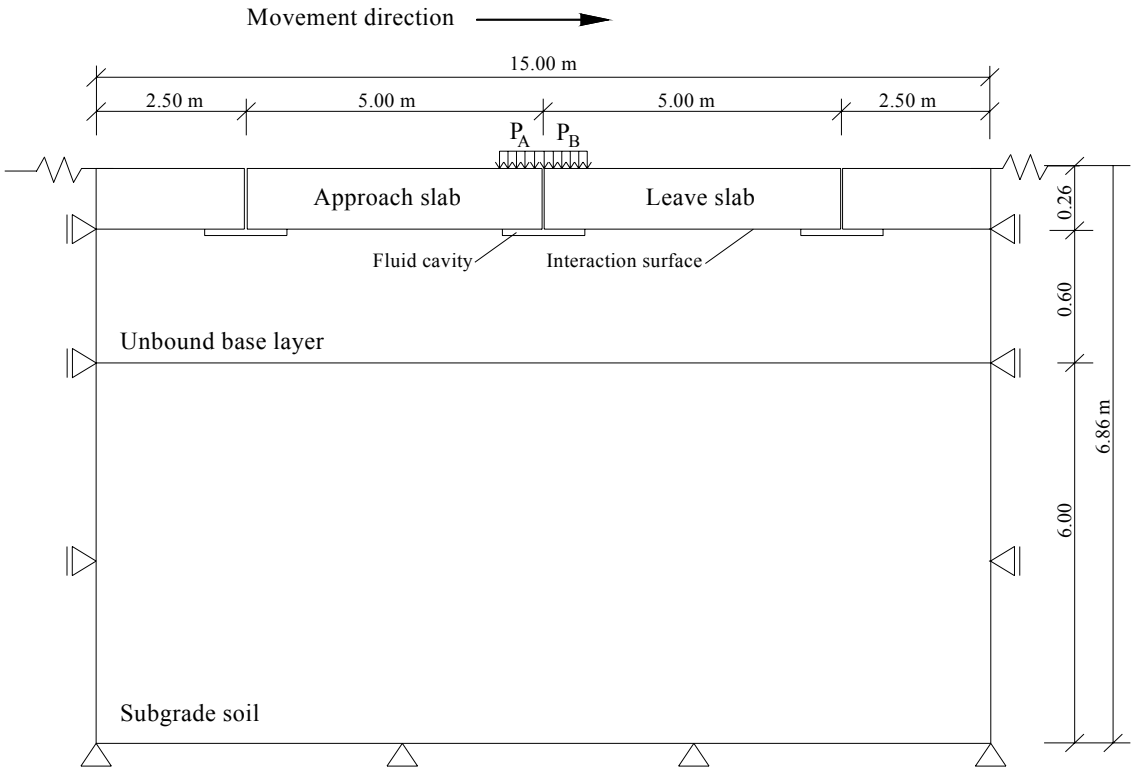

Fig. 6.2: Chosen system for faulting calculation, loads & boundary conditions

6.2.6 Loading

The external loads applied to the system should be defined exactly according to the real loading history. Three methods for applying the external traffic loads are considered:

1- Applying the wheel load on one edge of the concrete slab to get the elastic displacement under the load for the purpose of empirical calculation of faulting.
2- Applying only one loading cycle to solve the model with Mohr Coulomb material definition for UGMs within the proposed FEM procedure for prediction of faulting.
3- Applying the load as a cyclic load with a defined number of loading cycles using the UMAT subroutine for the definition of the behavior of UGMs.

Each model has its own loading history which shall be discussed in detail in respective sections.

6.2.6.1 Equivalent traffic load for a 2-D model

In the real conditions of traffic loads, the wheel load acts randomly at different points on the concrete slab. It means that all points on the transversal edge of concrete slabs could be subjected to the same loading at different times. As more than 75% of rolling-axles are found to act like the load case 2 in the previous analysis of the 3-D model in Chapter 5. The analysis for equivalent pressure for 2-D modeling in Section 5.6 indicated that, a uniform pressure of 125.0 kPa is equivalent to the real loads of case 2 in the 3-D model (axle load of 106 kN).

6.3 Prediction of faulting with empirical method

6.3.1 An example of Khazanovich et al [31]

Khazanovich et al [31] developed an empirical formula for the calculation of faulting (described in Section 2.4). They gave an example for the calculation of faulting in a rigid pavement system with the following configuration: 0.26 m concrete slab thickness, 4.50 m distance between joints, an unbound granular base layer of 0.40 m thickness, and a lane width of 3.70 m. They considered an equivalent axle load of about 80.0 kN (i.e. wheel load 40.0 kN) for a design period of 20 years.

The analysis of joint faulting damage involves the calculation of differential elastic deformation energy (*DE*), which is a function of slab corner deflections obtained from FEM analysis with loading at the transverse joint (Figure 6.3). (*DE*) is defined as:

$$DE = \tfrac{1}{2} \times k \times (W_L + W_{UL}) \times (W_L - W_{UL}) \quad \text{[kPa.mm]} \qquad (6.1)$$

Where:

W_L = deflection of loaded slab [mm]

W_{UL} = deflection of unloaded slab [mm]

k = modulus of subgrade reaction [kPa/mm]

Using ILLI-SLAB for the FEM analysis of the given model, and assuming a modulus of subgrade reaction (k) = 27.15 kPa/mm, the results of the slab deflections on both loaded and unloaded sides at the corners of the slabs were obtained as follows:

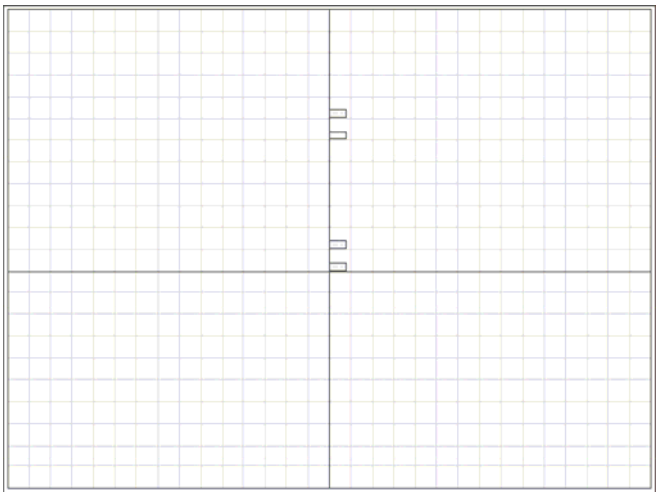

Fig. 6.3: Overview of analysis of joint faulting, Khazanovich et al [31]

Unloaded deflection, W_{UL} = 0.35044 mm

Loaded deflection, W_L = 0.44773 mm

For the given modulus of subgrade reaction (k) = 27.15 kPa/mm and using equation (6.1), the differential elastic deformation energy could be calculated as follows:

DE = ½ x 27.15 x (0.44773 + 0.35044) x (0.44773 - 0.35044)

= 1.053871 kPa.mm

A typical load spectrum and a typical climatic condition for Michigan State are assumed for this example, the faulting calculation could be conducted using equations (2.12) through (2.15). It should be noted that an erodibility index of 3 (erosion resistant) is assumed for the calculation of faulting. The predicted faulting at the end of the design period (20 years) is found to be about 4.24 mm.

Referring to the used equations in the calculation of faulting, one can see that there are many factors which need calibration. Anyhow, it is clear that the faulting magnitude is directly proportional to the differential elastic deformation energy (DE), if the other factors remain constant.

For the current research, the same procedure of Khazanovich et al [31] shall be used to calculate the faulting, assuming the same conditions and factors of the previous example. The only difference shall be the configuration of the chosen system and the software used for the FEM analysis. Hence from the results of FEM, the differential elastic deformation energy (DE) shall be calculated, and with the assumption that, faulting is linearly proportional to the differential elastic deformation energy, the related faulting magnitude can be concluded.

6.3.2 Analysis of chosen model with 40.00 kN wheel load

Following the same procedure of Khazanovich et al [31] to predict faulting in the chosen system, an analysis with FEM shall be conducted to get the elastic displacement of concrete edges under the given wheel load. The properties for the unbound granular materials in this analysis shall be assumed to be elastic material with Young's Modulus of 120.00 MPa and Poisson's ratio of 0.40. The density of this material is considered to be 20.00 kN/m^3. The material properties for plain concrete and subgrade soil layers are the same as defined in Section 6.2.4.

The wheel load shall be assumed 40.00 kN, applied on the edge of concrete slab to the left side in middle joint (as P_A in Figure 6.2). The contour plot of the vertical elastic displacement (U2) is shown in figure 6.4 below.

From the analysis results, the following values are found:

Unloaded deflection, W_{UL} = 0.47111 mm

Loaded deflection, W_L = 0.57559 mm

For the given modulus of subgrade reaction (k) = 27.15 kPa/mm and using equation (6.1), the differential elastic deformation energy could be calculated as follows:

DE = ½ x 27.15 x (0.57559 + 0.47111) x (0.57559 - 0.47111)

= 1.48455 kPa.mm

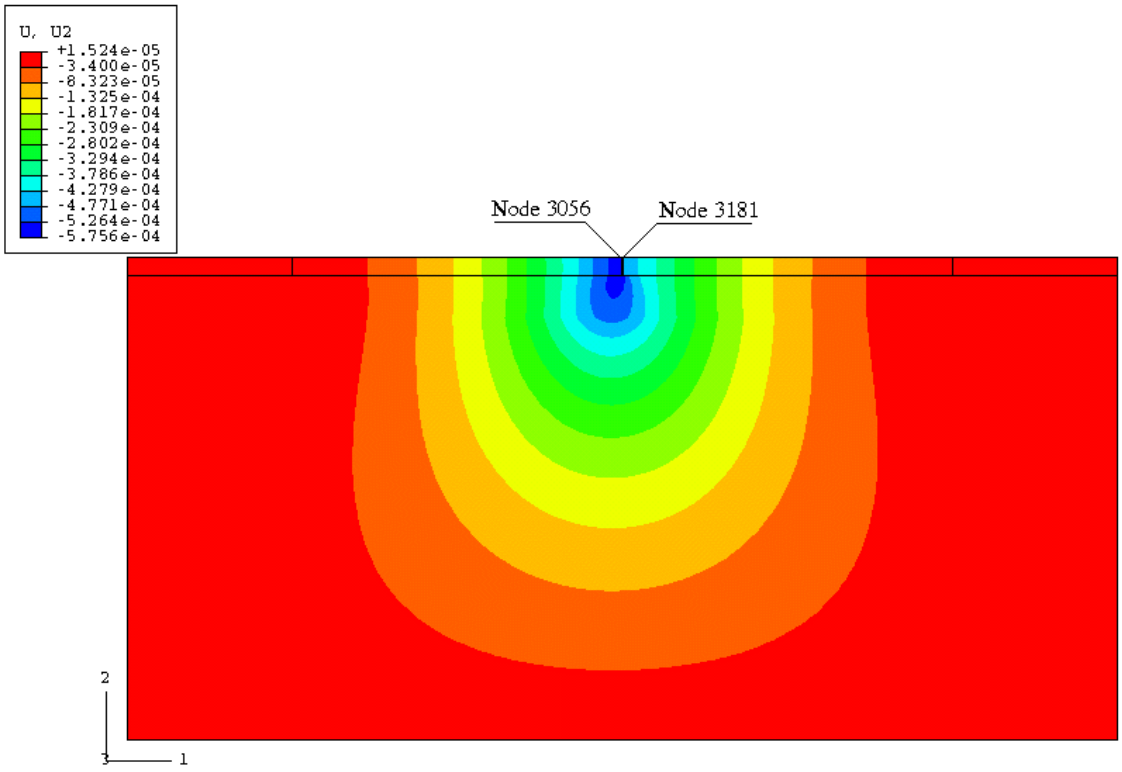

Fig. 6.4: Vertical elastic displacement [m], wheel load 40.00 kN

6.3.2.1 Calculation of faulting after Khazanovich et al [31]

If we consider the ratio of the differential elastic deformation energy in this analysis to that in the example of Khazanovich, the ratio shall be found of about 1.408665, then the faulting can be predicted at the end of the design period (20 years) to be about 1.408665 x 4.24 = 5.97 mm.

6.3.2.2 Comparison with Khazanovich et al [31]

Comparing the results of the current model to that of Khazanovich, one can find that the differential elastic deformation energy of the current model is greater than that of Khazanovich of about 40%. This can refer to the use of different FEM analysis programs with different assumptions in both systems. Khazanovich used ILLI-SLAB assuming finite size Kirchhoff plate bending elements for the concrete slab supported by Winkler/elastic foundation (refer to Section 2.1.3.3 for the description of ILLI-SLAB), whereas, the current model is analyzed with ABAQUS using continuum elements for the whole layers with different material properties. Hence the faulting of the current system is greater than that of Khazanovich with the same ratio (40%).

6.3.3 Analysis of chosen model with 53.00 kN wheel load

The analysis will be conducted again for the same system of Section 6.3.2 above, assuming a wheel load of 53.00 kN, applied on the edge of concrete slab to the left side in middle joint. The contour plot of the vertical elastic displacement (U2) is shown in figure 6.5 below.

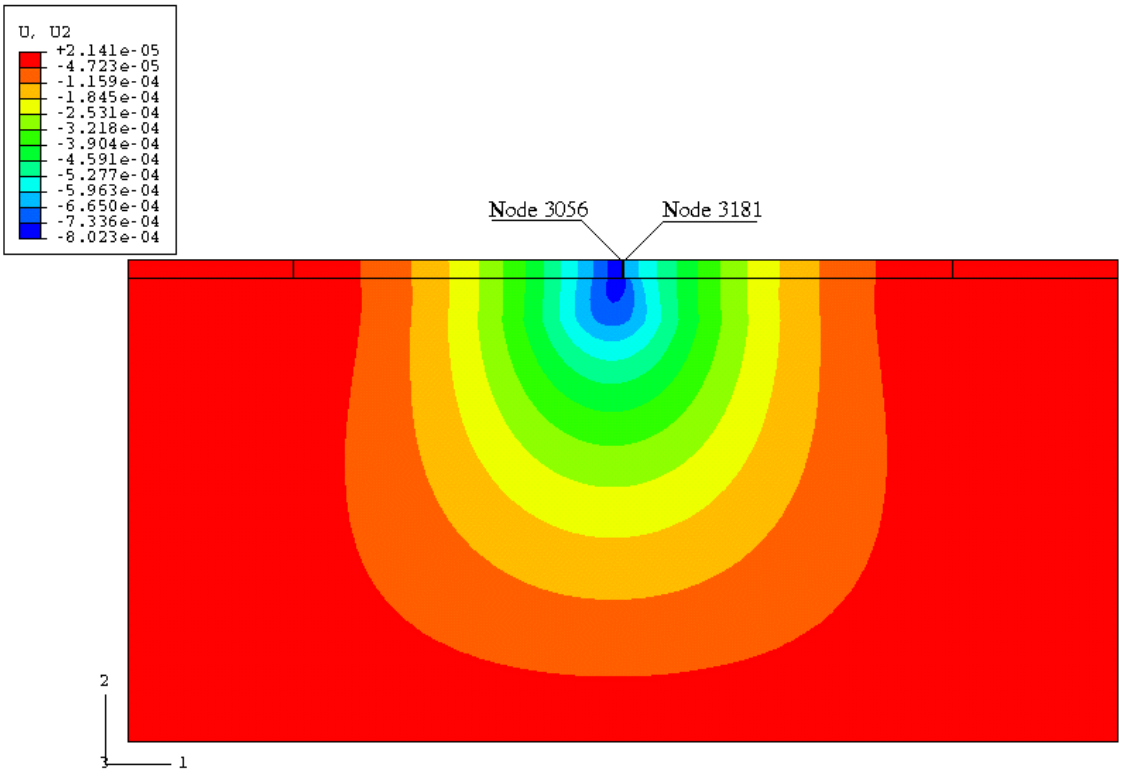

Fig. 6.5: Vertical elastic displacement [m], wheel load 53.00 kN

From the analysis results, the following values are found:

Unloaded deflection, W_{UL} = 0.65128 mm

Loaded deflection, W_L = 0.80226 mm

For the given modulus of subgrade reaction (k) = 27.15 kPa/mm and using equation (6.1), the differential elastic deformation energy could be calculated as follows:

DE = ½ x 27.15 x (0.80226 + 0.65128) x (0.80226 - 0.65128)

= 2.9791 kPa.mm

6.3.3.1 Calculation of faulting after Khazanovich et al [31]

If we consider the ratio of the differential elastic deformation energy in this analysis to that in the example of Khazanovich, the ratio shall be found of about 2.979108, then the faulting can be predicted at the end of the design period (20 years) to be about 2.979108 x 4.24 = 12.63 mm.

6.3.4 Assessment of results

It is noted that, through increasing the applied wheel load from 40.00 kN to 53.00 kN with all other factors remaining constant, the faulting is increased from 5.97 mm to 12.63 mm, i.e. more than the double. One can not assess the correctness of this conclusion as there are no relevant data to compare with. The prediction of faulting depends not only on the differential elastic deformation energy (DE) obtained from FEM analysis but also on many other factors which must be calibrated according to field or experimental tests.

Increasing the applied wheel load may affect the values of some input parameters used in the calculation, for example; modulus of subgrade reaction (k), erodibility factor ($EROD$), etc. (refer to Section 2.4 for more details). Hence, one cannot generalize this procedure without having good reliable calibrated parameters taking into consideration all factors affecting the faulting process.

6.4 Prediction of faulting with FEM simulation

6.4.1 Fluid structure interaction in ABAQUS

In certain applications it may be necessary to predict the mechanical response of a structure coupled with a fluid-filled cavity. A primary difficulty in addressing such applications is the coupling between the deformation of the structure and the pressure exerted by the contained fluid in the cavity. The response of the structure depends not only on the external loads but also on the pressure exerted by the fluid, which, in turn, is affected by the deformation of the structure. The hydrostatic fluid elements provide the coupling needed to analyze such situations. The cavity is assumed to be completely filled with fluid. Structures with fluid-filled cavities are modeled by using standard

elements to model the main structure and hydrostatic fluid elements to provide the coupling between the deformation of the structure and the pressure exerted by the contained fluid (Figure 6.6).

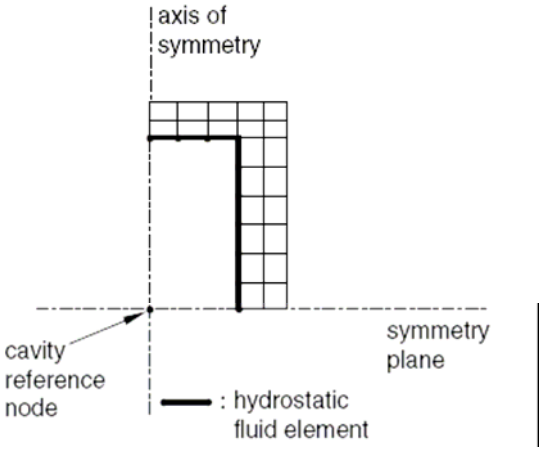

Fig. 6.6: Model for a fluid-filled cavity [2]

Hydrostatic fluid elements appear as surface elements that cover the boundary of the fluid cavity but they are actually volume elements when the cavity reference node is accounted for. All hydrostatic fluid elements associated with a given cavity share a common node known as the cavity reference node. This cavity reference node has a single degree of freedom representing the pressure inside the fluid cavity and is also used in calculating the cavity volume.

The hydrostatic fluid elements share the nodes at the cavity boundary with the standard elements which used to model the boundary of the cavity. These fluid elements are needed to define the cavity completely and to ensure proper calculation of its volume. The fluid within a fluid-filled cavity must be modeled by using one of the available hydrostatic fluid models. In these models, the following properties can be defined for a fluid: bulk modulus, density, and coefficient of thermal expansion.

6.4.2 Fluid link element

In addition to the fluid cavity elements, ABAQUS also offers a 2-node fluid link element that can be used to model fluid flow between two cavities or between a cavity and the environment. This is typically used when the fluid has to flow through a narrow orifice. Fluid properties of the nodes of the link element are assumed to be the same as in their respective cavities. The program will not check whether a fluid link element has been defined between two cavities that are filled with dissimilar fluids; e.g., a fluid link element between two cavities filled with two fluids of different densities. If this situation exists, the mass transferred from one cavity needs to be converted to a volume change in the second cavity.

The mass flow rate through the link element is defined as a function of the pressure differential, and may also depend on the average pressure and temperature. The fluid

link element will account for differences in fluid density between the cavities. The conversion of mass flow rate into volume flow rates at the two ends of the link element is based on the fluid properties given for both cavities. Hence, the volume flow rates at the two ends may not balance.

The fluid transfer between the two fluid-filled cavities depends on many factors. Among these factors are the induced pressure on the fluid cavities, the fluid properties (density and bulk modulus), the resistance of the hydraulic link element connecting both cavities, and any other field variables defined by the user. An implicit functional relationship between the mass flow rate (q) and the pressure difference (Δp) between the two nodes of a fluid link element can be defined through a viscous resistance coefficient (C_v) and a hydrodynamic resistance coefficient (C_h). This can be defined as:

$$\Delta p = C_v\, q + C_h\, q\, |q| \qquad (6.2)$$

6.4.3 Proposed model with fluid cavities

The problem of faulting is caused mainly through the transfer of fine materials through water in the base layer at joint locations and cracks. In the current 2-D model for the computation of faulting, two cavities under the edges of the concrete slabs are assumed (Figure 6.7). The cavity dimensions are assumed to be about 0.06 x 0.50 m (depth x width). In order to simulate the material transfer between the two cavities, a fluid-link element between the two cavities is needed.

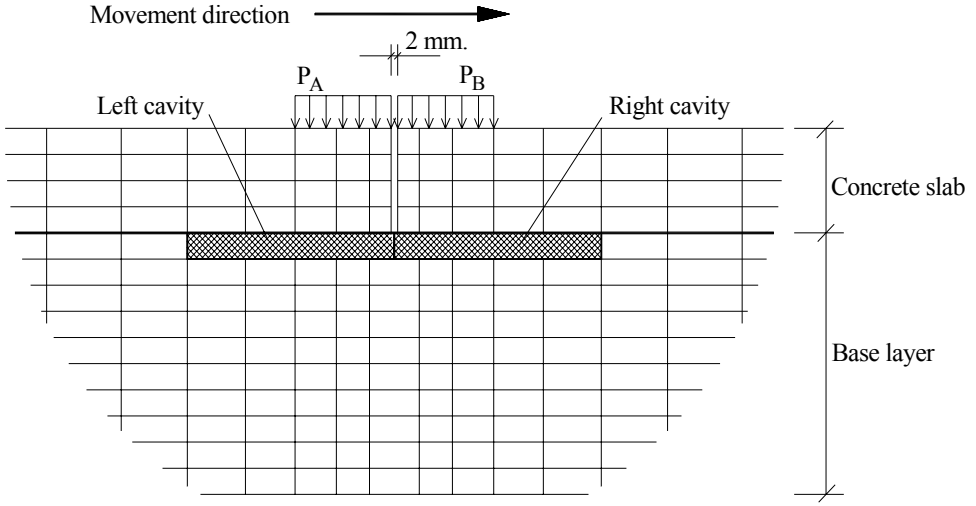

Fig. 6.7: Simulation of fluid-filled cavities under concrete slab edges

In the faulting process, the fines are supposed to be transferred through water from the right cavity to the left one, as the moving load is crossing the joint from the left to the right side. Therefore a higher density shall be assigned for the fluid in the right cavity more than the fluid in the left cavity. This assumption refers to the fact that, the transfer happens for fines in real conditions, which have a higher density, and not for a fluid as assumed in the current model.

6.4.4 Material properties for fluid elements

The properties of hydrostatic fluid elements are defined through the bulk modulus (K) and density. In the current analysis a value of 20,000.00 MPa was assumed for the bulk modulus (an incompressible fluid) in both cavities. The density of the fluid in left cavity is assumed to be 10.00 kN/m^3 and that for the fluid in right cavity (equivalent to density of fines) is assumed to be 20.00 kN/m^3. The fluid link element is mainly supposed to be used in dynamic loading applications of fluid flow in a form of steady-state vibration. Here in the current analysis, the procedure is static and there is no pressure difference between the two cavities (i.e. $\Delta p = 0.0$), in this case, the mass flow rate does not depend on the two resistance values (C_h) and (C_v) of the fluid link element. Hence they are not needed for the analysis.

6.5 2-D model with Mohr Coulomb for prediction of faulting

6.5.1 Material definition for the base layer

The first model to predict the faulting due to traffic moving load will be analyzed using the Mohr Coulomb plasticity model for the unbound granular base layer. This model helps to verify the proposed procedure when applying the loads for only one cycle at the intermediate joint. The material parameters of UGMs are presented in Table 6.1. Other properties of concrete and subgrade soil materials are mentioned in section 6.2.4.

Table 6.1: Material properties with Mohr Coulomb model of base layer

E (MPa)	*v* (-)	*φ´* (deg.)	*ψ´* (deg.)	*c´* (kPa)	*Density* (kN/m^3)
120.00	0.40	45°	15°	5.00	20.00

6.5.2 Loading

The loading procedure for the model using the Mohr Coulomb material definition for UGMs takes the following sequences (Figure 6.8):

1- Step 1 (timing from 0.0 to 1.0) is for the equilibrium condition for the system under initial stresses and own weights of different materials.

2- Step 2 (timing from 1.0 to 2.0), the wheel load (P_A) is applied on the left side to the intermediate joint (on the edge of the approach slab).

3- Step 3 (timing from 2.0 to 3.0), the wheel load (P_B) is applied on the right side to the intermediate joint (on the edge of the leave slab), at the same time, unloading the left side. In this step, (P_B) goes up from 0.0 to 1.0 and (P_A) goes down from 1.0 to 0.0, which means that the load moves from the left to the right side.

4- Step 4 (timing from 3.0 to 4.0), the wheel load (P_B) is removed from the right side of the intermediate joint. At the end of this step there are no more external loads and the system returns to its initial conditions (only its own weights).

Time scale has no physical meaning here and is only used for the definition of the load amplitudes' sequences.

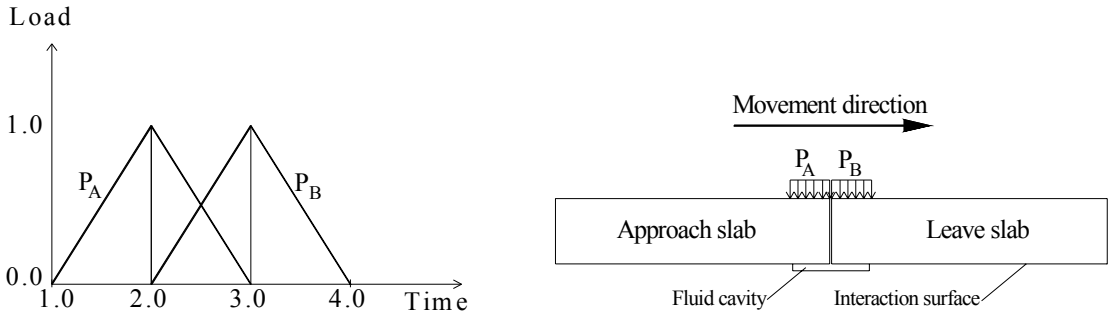

Fig. 6.8: Load amplitudes for model with Mohr Coulomb material definition

6.5.3 Results

In the following figures, the results of the analysis with the Mohr Coulomb material model are presented in two ways: Figure 6.9 presents a contour plot of vertical displacement (U2) at the end of the last step of loading (removing the applied loads from the system), and Figures 6.10 to 6.12 present x-y plots for vertical displacement of transversal edges of the concrete slabs during the whole loading history.

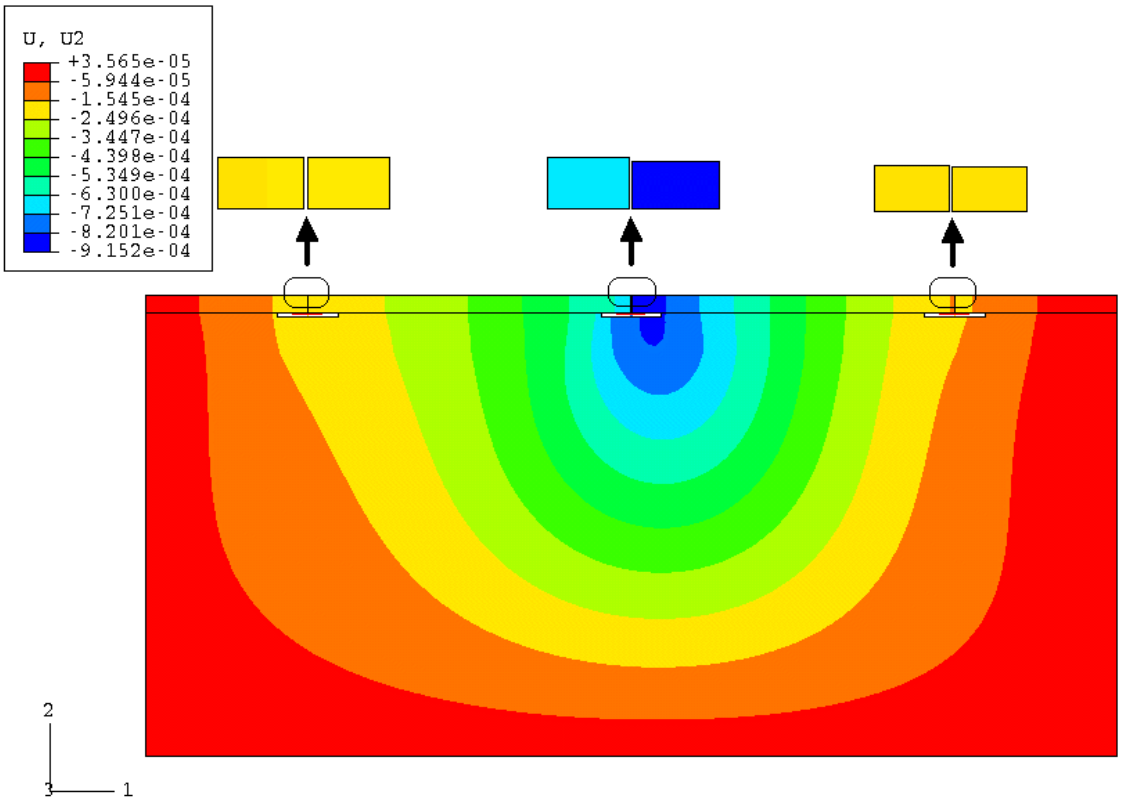

Fig. 6.9: Permanent vertical displacement [m], Mohr Coulomb model; step 4 (no loads)
Scale factor for magnified views is 5.0 in the vertical direction

The following x-y plots, present the results for the development of vertical displacement (U2) against loading time with Mohr Coulomb material's assumption. As the procedure is static analysis, time here has no physical meaning and therefore has no unit.

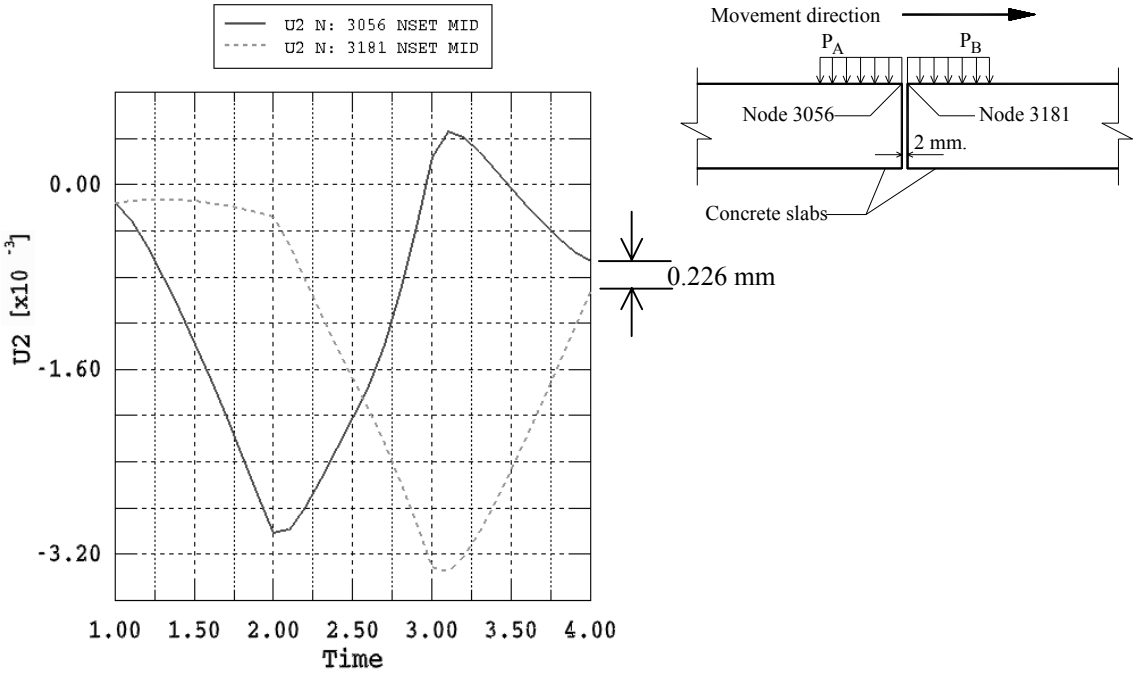

Fig. 6.10: Vertical displacement [m] at joint under load; Faulting = 0.226 mm

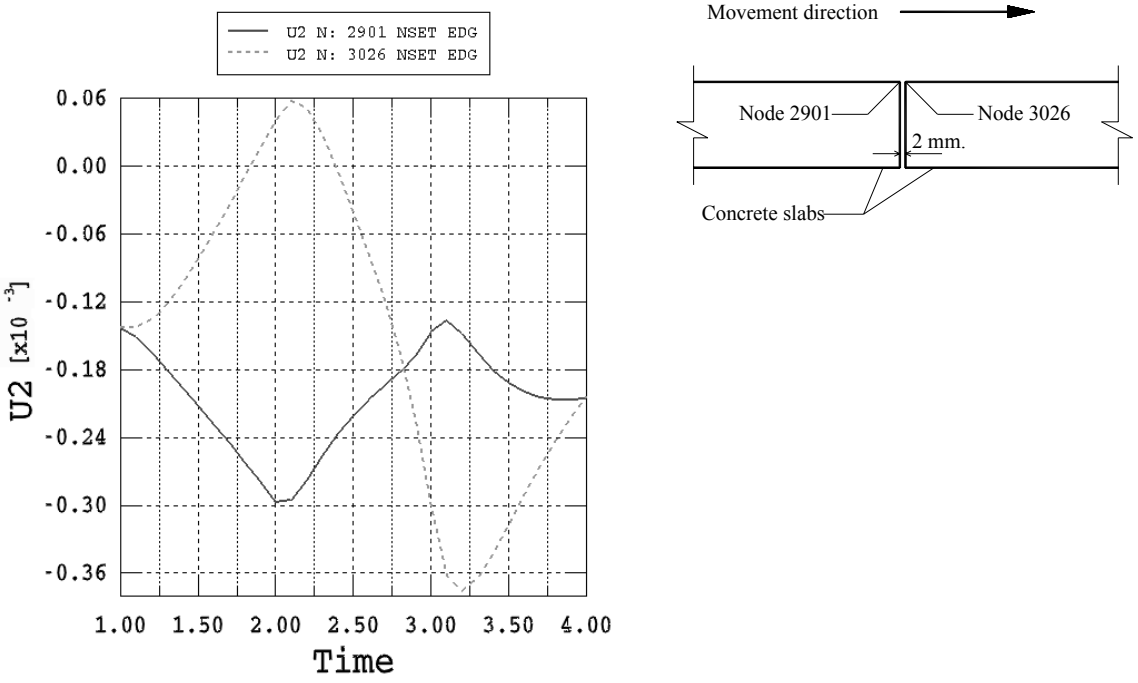

Fig. 6.11: Vertical displacement [m] at joint preceding to load; Faulting =0.0

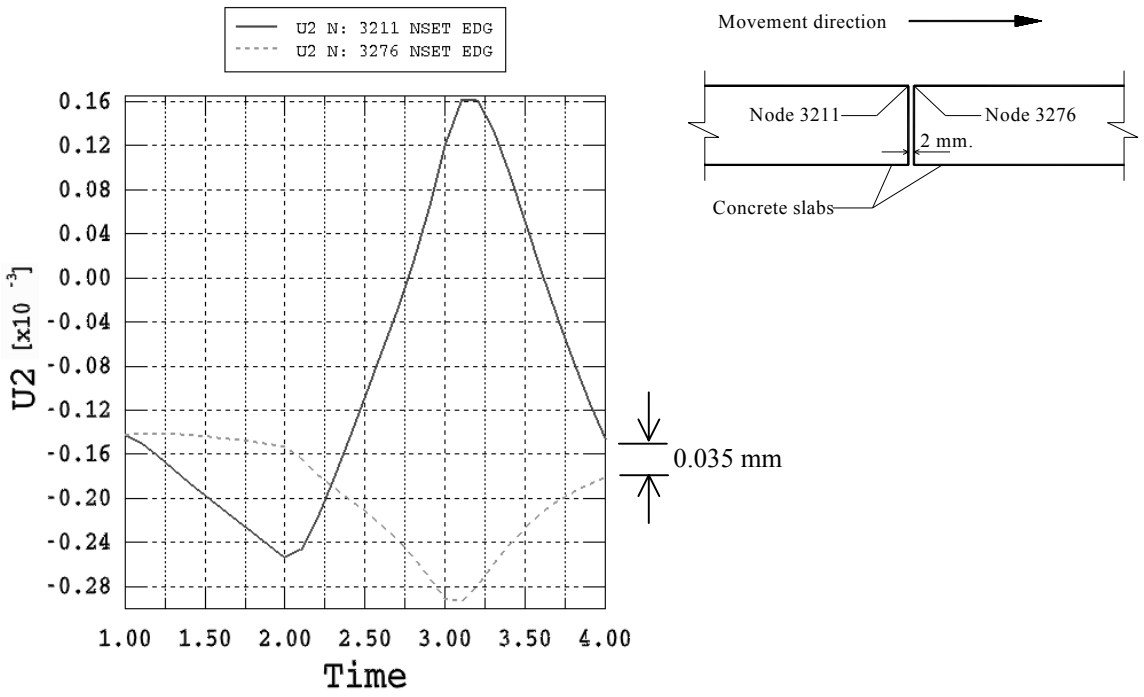

Fig. 6.12: Vertical displacement [m] at joint proceeding to load; Faulting = 0.035mm

6.5.4 Assessment of results

The results of the analysis with the Mohr Coulomb material assumption yield the following conclusions:

1- From Figure 6.10, at time (t) = 4.0, the fault in the joint under load is about 0.226 mm and shall be defined as the main fault.

2- From Figure 6.11, at time (t) = 4.0, the fault in the preceding joint to the joint under load is about 0.00 mm (i.e. about 0.0% of the main fault).

3- From Figure 6.12, at time (t) = 4.0, the fault in the proceeding joint to the joint under load is about 0.035 mm (i.e. about 15.5% of the main fault).

4- In real conditions, the fault in both joints (those preceding and proceeding to the joint under load) may be equal, but in the analysis they are not equal. This may refer to the unsymmetrical boundary and load conditions. Anyhow, the contribution of an applied load to cause a fault in the both joints can be calculated from both values. This means that this contribution is about 15.50% of the value of the main fault at the joint under load.

5- From Figure 6.10, when loading the left side of the joint (time, t = 1.0 → 2.0), both slab edges deform downwards. However, the left edge deforms greater than the right edge, because it is the edge under loading. On moving the load to the right side of the joint (time, t = 2.0 → 3.0), the right edge deforms downwards and the left edge deforms upwards. Anyhow, the relative displacement between

both edges is greater than that in the left side loading. Moreover, it is noted also that at the end of loading on the right side and starting to remove the load (time, $t \approx 3.0$), the left edge heaves up above its original position. This refers to the fact that the fluid in the right cavity has a higher density than that in the left one. Therefore, when fluid flows from the left cavity to the right one, the transferred fluid volume shall become smaller than its original volume. To the contrary, when fluid flows from the right cavity to the left one, the transferred fluid volume shall become greater than its original volume (refer to Section 6.4.2). These conversions of the transferred fluid masses into equivalent volumes of respective cavities resulted in a greater increase of the left cavity's volume more than the right cavity's volume which in return cause the left slab edge to heave up above the original position.

6.6 2-D model using UMAT for UGMs with constant low RMC

6.6.1 Material definition for the base layer

After verifying the procedure with the Mohr Coulomb plasticity model, the analysis can be conducted again using the UMAT subroutine for the definition of the unbound granular base layer according to the Dresden model. Therefore, computation of faulting under any defined number of loading cycles can be made possible. The chosen material for the UGMs in the current model is Gravel Sand with a relatively constant low water content of 3.40%. Different material parameters have been presented in Table 5.3. Other properties for concrete and subgrade soil materials are as defined in section 6.2.4.

6.6.2 Loading

Running the analysis under a very high number of loading cycles (for example one million cycles), with the Dresden material model for UGMs, can only be possible using the UMAT subroutine, as previously discussed in Chapter 5.

The UMAT subroutine is based on 4 steps of loading history (refer to Section 4.3). According to those steps, it is impossible to take into consideration the movement (as in the previous model with the Mohr Coulomb material) of the applied cyclic loads (traffic loads) that is the main cause of the occurrence of faulting in rigid pavement. To overcome this problem, the superposition of loading history shall be used. Figure 6.13 presents the load amplitudes acting on the two edges of the concrete slabs in transversal joints. Time scale here has no physical meaning, consequently no unit and is only used to define the sequence of loading amplitudes.

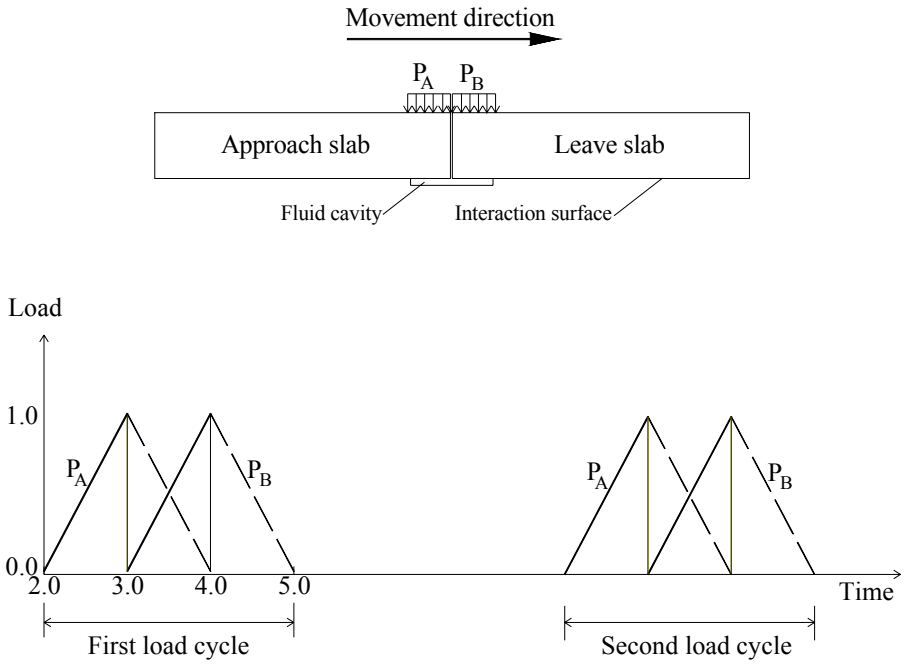

Fig. 6.13: Cyclic load amplitudes in joint area

The idea of superposition assumes that the loads are applied as two successive amplitudes: (P_A) for the left side and (P_B) for the right side. Therefore, two analyses have to be run, firstly for the left side load amplitude (P_A) and secondly for the right side load amplitude (P_B). By adding the results of both analyses, the faulting values can be obtained at different times (cycle numbers).

The loading history in the two models shall follow the same procedure. For the first model, the following four steps are considered:

1- The first step (timing from 0.0 to 1.0) is a geostatic step to achieve equilibrium conditions between the initial stress in the supporting layers and the own weight of the structure itself.

2- The second step (timing from 1.0 to 2.0) is for the calculation of plastic deformation due to the previous stresses in step no 1 if found.

3- The third step (timing from 2.0 to 3.0) is for the application of the supposed cyclic load (P_A) on the left side, on the intermediate joint only (refer to Figure 6.13).

4- The fourth step (timing from 3.0 to '3.0+Δt') is for the computing of the permanent deformation due to the applied load in step no 3 up to reaching the given number of loading cycles.

For the second model, the first and second steps are the same as for the first model. Only the third and fourth steps are different as following:

- The third step (timing from 2.0 to 4.0) is for the application of the supposed moving cyclic load onto the right side, which moves from the left side ('P_A'

for timing from 2.0 to 3.0) to the right side ('P_B' for timing from 3.0 to 4.0). This way the movement of the load across the joint is considered and this movement should affect the resulting stresses at the end of the step.

- Fourth step (timing from 4.0 to '4.0+Δt') is for the computing of the permanent deformation up to reaching the same given number of cycles.

Note: the (Δt) variable, defined in the step no 4 mentioned above, depends on the given number of loading cycles in addition to the convergence criterion controlled by ABAQUS and is not an input data.

Following the above procedure and analyzing both systems, the prediction of faulting magnitude in the intermediate joint at different cycle numbers can be obtained.

6.6.3 Results

6.6.3.1 Left side loading

The following are the results of the analysis with UMAT subroutine as a material model for the unbound granular base layer. The load is applied only to the intermediate joint.

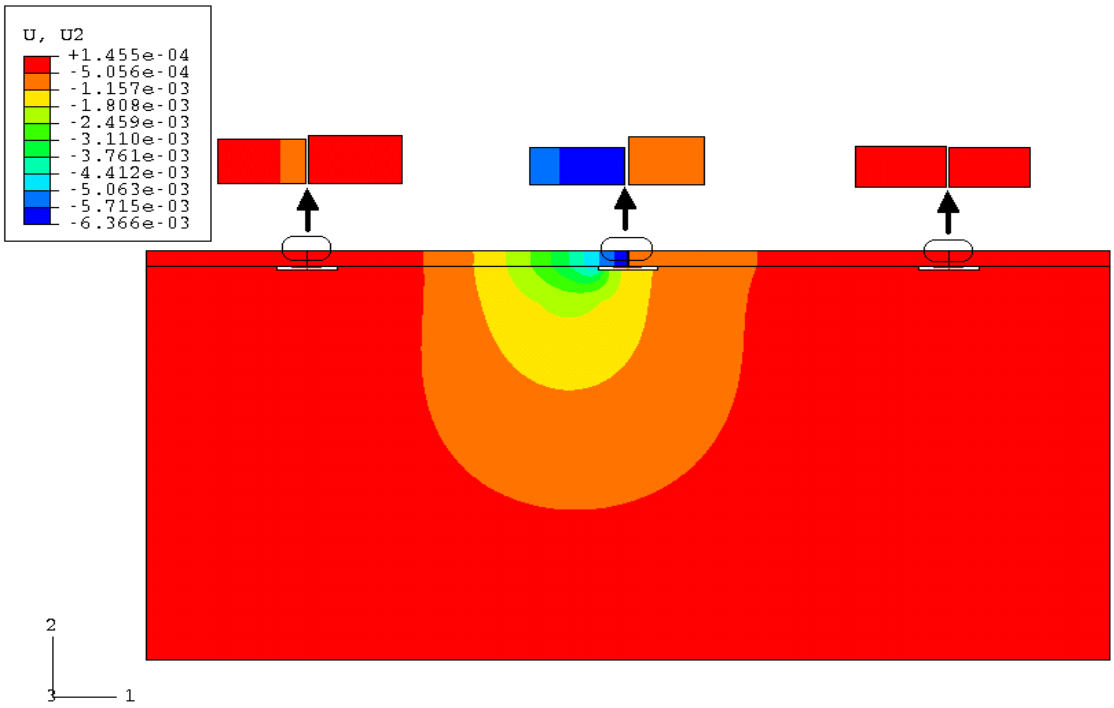

Fig. 6.14: Total vertical displacement [m] for left side loading (P_A) after 10^6 cycles
Scale factor for magnified views is 5.0 in the vertical direction

The following x-y plots present the results for the development of total vertical displacement against loading time/number of loading cycles for the left side loading at the intermediate joint.

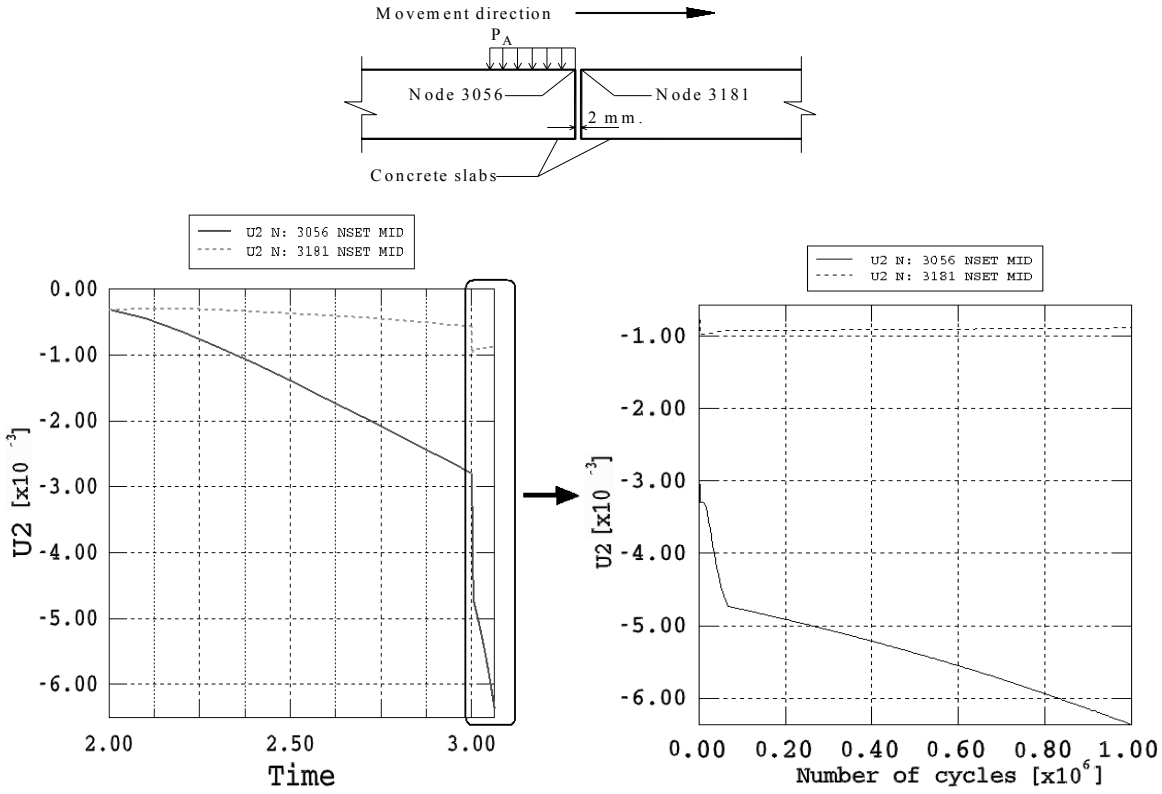

Fig. 6.15: Vertical displacement [m] at joint under load, left side amplitude (P_A)

6.6.3.2 Right side loading

The results for the right side loading are presented in the same way as those for the left side loading.

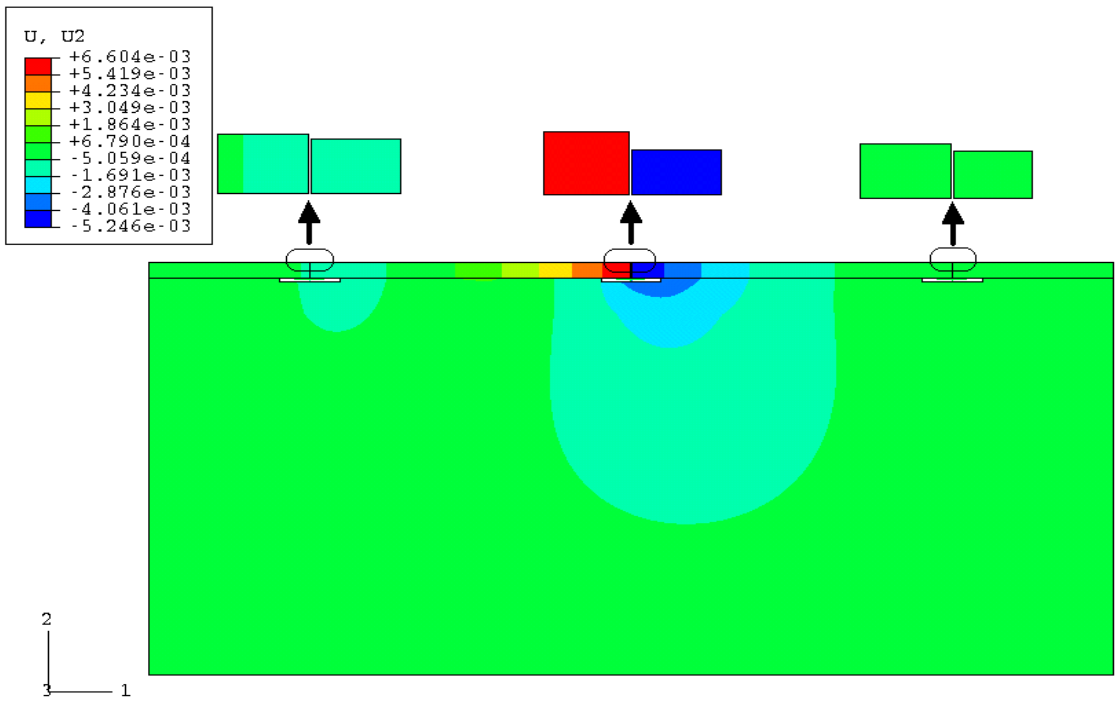

Fig. 6.16: Total vertical displacement [m] for right side loading (P_B) after 10^6 cycles

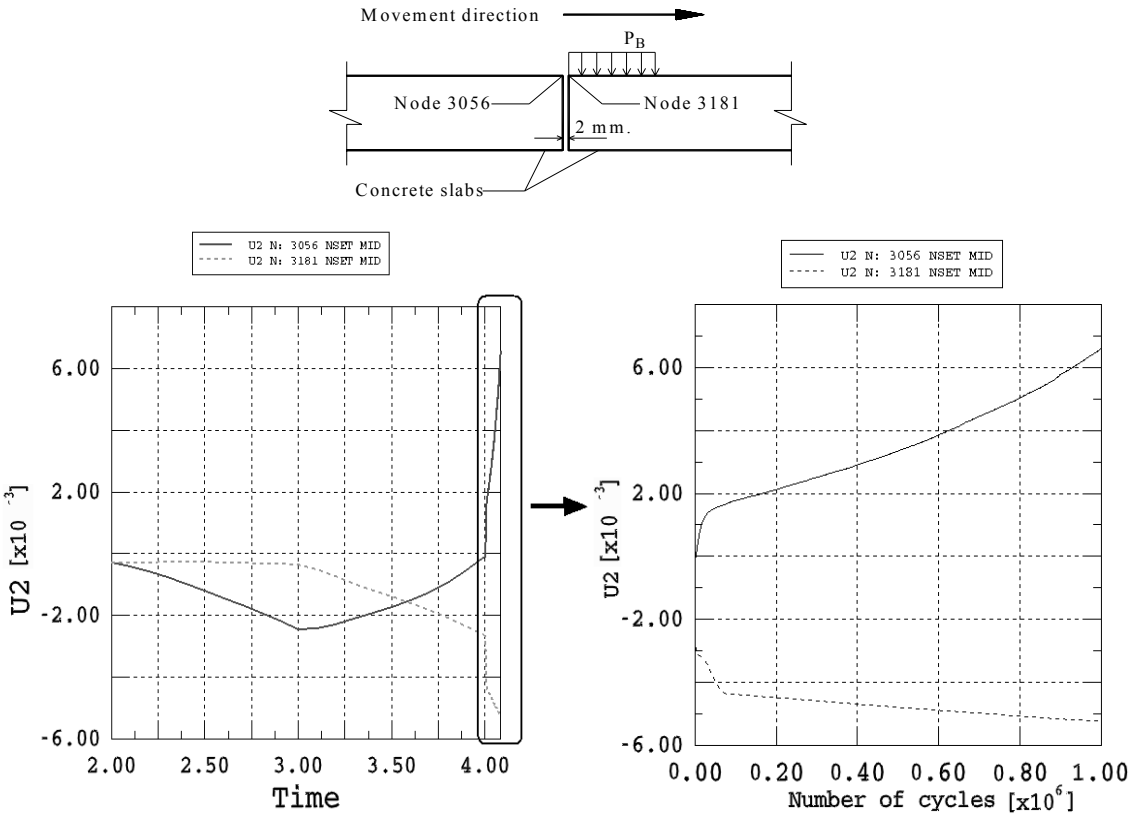

Fig. 6.17: Vertical displacement [m] at joint under load, right side amplitude (P_B)

6.6.4 Conclusion of the 2-D model using UMAT with low RMC

The results of the analysis with the UMAT subroutine yield the following: from the x-y plots for the development of vertical displacement against loading time, it can be noted that:

1- In loading case 2, when loading on the left side (on the edge of the approach slab) the elastic displacement between the two edges is found to be about 2.45 mm (Figure 6.17, time=3.0). When the load was being moved to the right side (on the edge of the leave slab) the elastic displacement increased to about 2.65 mm (time=4.0), which is similar to what happened to the Mohr Coulomb model.

2- In Figure 6.17, the heave up of the left slab's edge during the right side loading was explained in Section 6.5.4.

3- In step no 4 one can determine the total displacement for the both loading cases (models) at different number of cycles up to 10^6 cycles (Figures 6.15 and 6.17).

4- The permanent displacement can be calculated at different numbers of cycles throughout the deduction of the elastic displacement resulting at the end of step no 3 from the total displacement developed during step no 4.

The results of the x-y plots of displacement in the other two joints (preceding and proceeding the joint under load) are presented in Appendix C.

6.6.5 Calculation of faulting

By adding the results of the permanent displacement at different numbers of cycles (N), for the above two loading cases (models), the relevant difference in elevation between each two adjacent edges of the concrete slabs can be determined in the three joint positions. These elevation differences present the faulting at the three joint positions and can be presented against the number of loading cycles (Figure 6.18 in normal-log scale) and (Figure 6.19 in log-log scale).

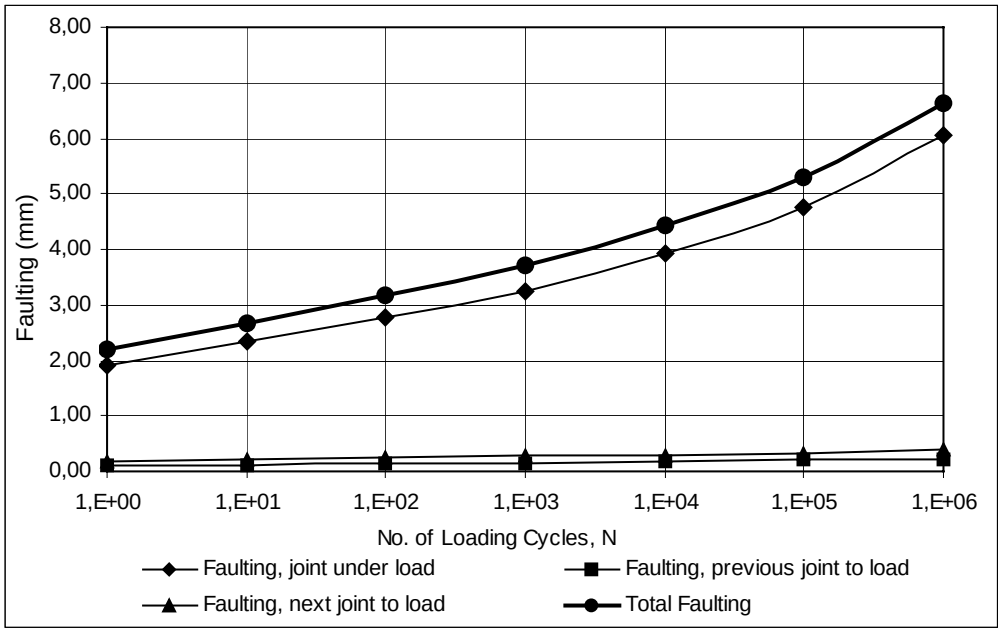

Fig. 6.18: Faulting against number of loading cycles (N): (normal-log scale)

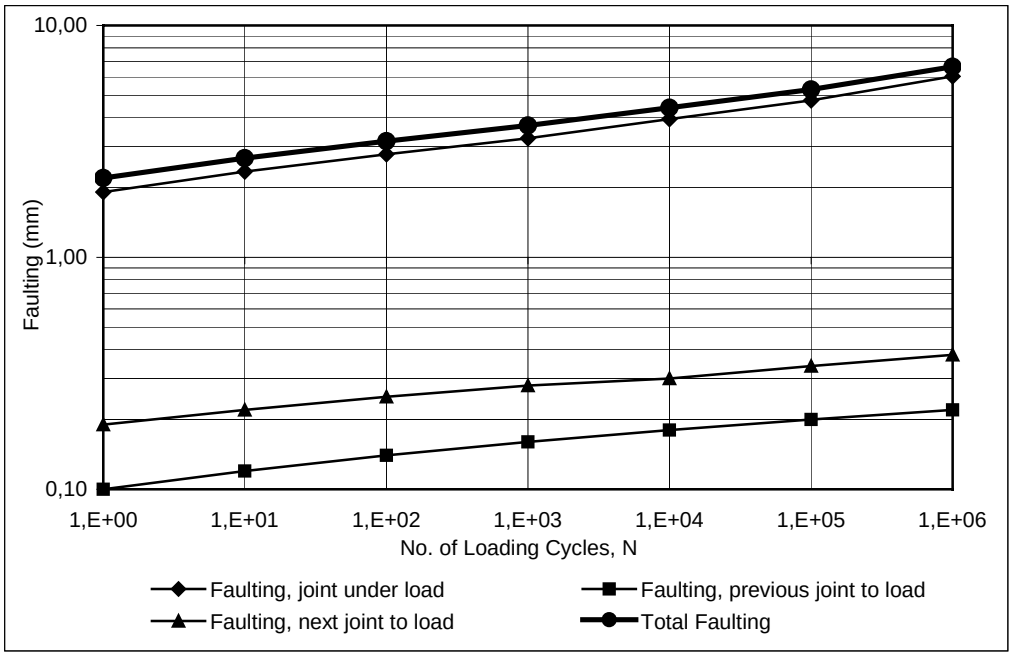

Fig. 6.19: Faulting against number of loading cycles (N): (log-log scale)

The magnitude of faulting in the first loading cycle is not realistic, but that may be a result of using a permanent deformation model which assumes also unrealistic values for the first loading cycle (refer to Section 5.3.2). However, in order to obtain realistic values, this magnitude can be ignored from the total faulting.

The results of the elastic and total vertical displacements for the three joints in the 2-D model are found in Appendix C. The calculation of faulting is based on these results.

6.6.6 Assessment of faulting results

For the assessment of the obtained results, the following remarks should be made:

1- The development of the faulting matches the development of the permanent deformation behavior of the unbound granular materials, in both the linear growth in a log-log relationship against the number of loading cycles, and the magnitude of faulting in the first loading cycle. It means that faulting is going to be stabilized as the number of loading cycles grows. To get representative values of faulting against the number of loading cycles, the magnitude at the first loading cycle (2.20 mm) is to be ignored.

2- On calculation with the Mohr Coulomb material model for UGMs, it was found that the ratio of faulting at the preceding joint is 0.0% and that at the proceeding joint is 15.50%. The relevant two ratios are found to be 5.25% and 10.00% respectively for the first loading cycle when using the UMAT Subroutine. One can conclude that the difference is very small, and the sum of both values is nearly equal.

3- The total faulting in the presented 2-D model, after the removal of the fault at the first cycle, is about 4.45 mm after one million cycles. By extrapolation, one can predict that, the total faulting after 20 million cycles is about 5.93 mm. The faulting magnitude obtained from the calculation after Khazanovich is 12.63 mm (see Section 6.3.3), which is more than twice the resulting value with FEM model using fluid cavities. A modification has to be made in the proposed model to enhance the results and make it reasonable as described in the next section.

6.7 2-D model using UMAT for UGMs with higher RMC

6.7.1 Material definition for the base layer

In order to study the influence of higher moisture content in the regions in the base layer under transversal joints on faulting, a new analysis shall be performed using a Grnodiorite material as the base layer material with non-constant water content. It shall be assumed that only regions under transversal joints as shown in Figure 6.20 have higher moisture content than other regions.

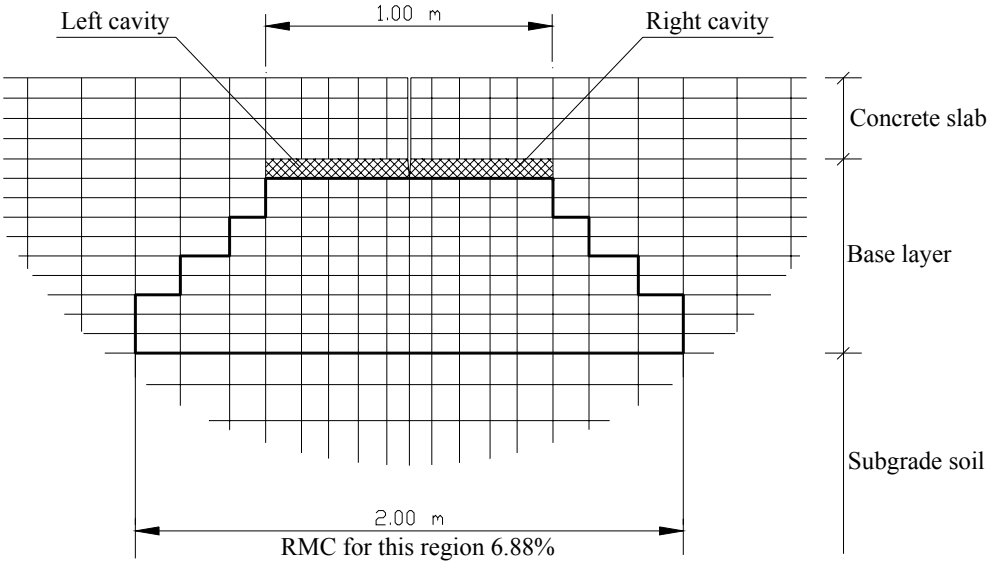

Fig. 6.20: Regions with high water content under transversal joints

The chosen material for the UGMs in the current model is Grnodiorite. A relatively low water content of 4.0% for regions away from joints and a higher water content of 6.88% for regions under joints are assumed. Different material parameters have already been presented in Table 5.3 for the material with a w/c ratio of 4.0%. With the same material parameters and using equation 3.21, the behavior of the material with a higher w/c ratio can also be defined (refer to Section 3.4.3). Other properties for concrete and subgrade soil materials are previously defined in Section 6.2.4.

6.7.2 Loading

The loading history of the previous model shall be applied here (refer to Section 6.6.2).

6.7.3 Results

The results of the analysis can be presented in the same way as those of the last model in Section 6.6. Only the x-y plots for the development of total vertical displacement against loading time/number of loading cycles are presented here for the calculation of faulting at the intermediate joint.

Figure 6.21 presents the x-y plot for the left side loading (P_A) and Figure 6.22 presents the x-y plot for the right side loading (P_B).

The results of x-y plots for the displacement in the other two joints (preceding and proceeding the joint under load) are presented in Appendix D.

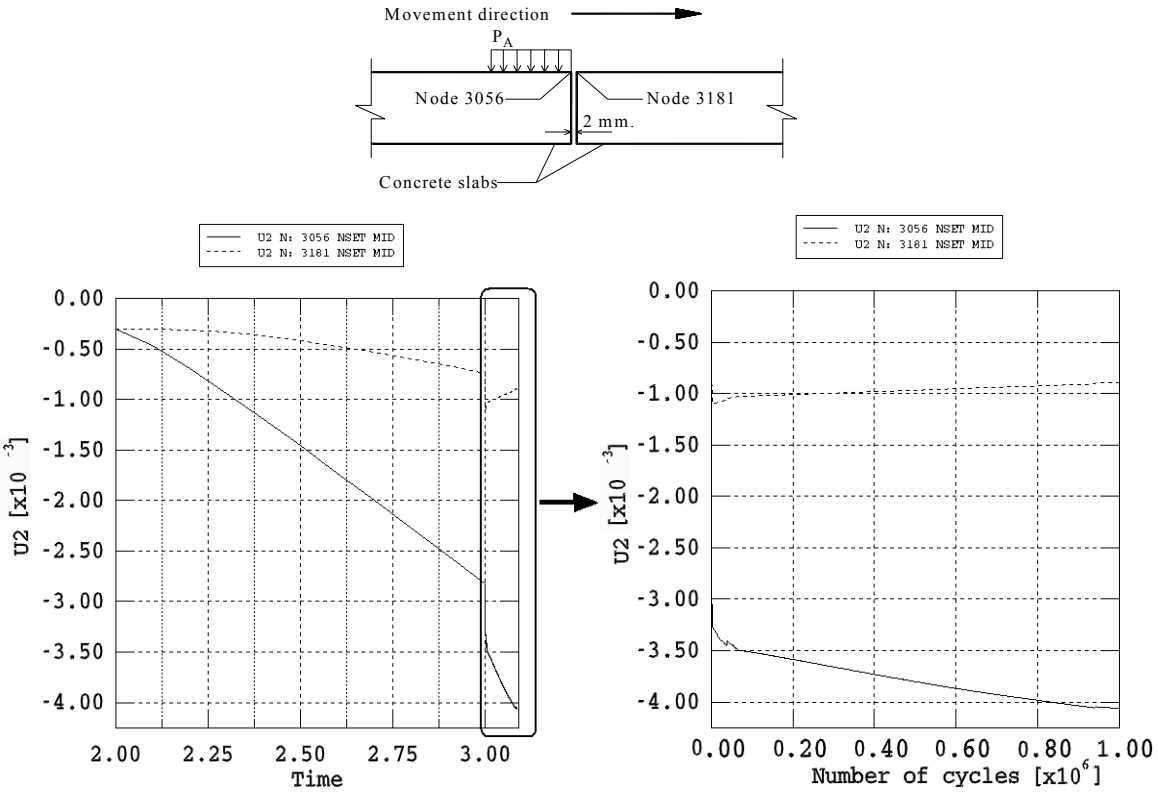

Fig. 6.21: Vertical displacement [m] at joint under load with higher w/c; left side amplitude (P_A)

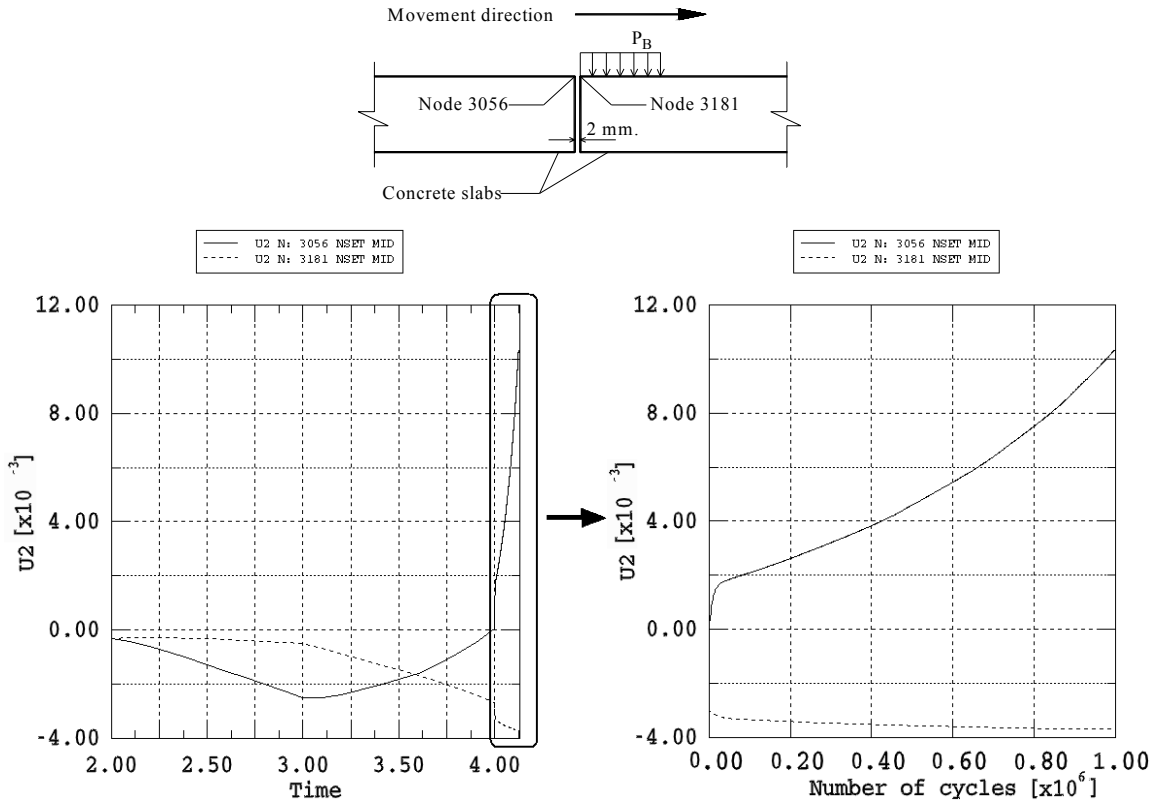

Fig. 6.22: Vertical displacement [m] at joint under load with higher w/c; right side amplitude (P_B)

6.7.4 Conclusion of the 2-D model using UMAT with higher RMC

The same conclusions of the model with constant low RMC are applied here. Moreover, comparing Figures 6.15 and 6.17 of the previous model (base layer is Gravel Sand material with constant low RMC) to Figures 6.21 and 6.22 of the current model (base layer is Granodiorite material with higher RMC) we can conclude that, the shape of relative deformation between the two slab edges is nearly the same, except that the deformation rate in step 4 (cyclic behavior) is more greater in the model with Granodiorite material than that of the model with Gravel Sand material. This can due to the assumption of a higher w/c ratio of the regions under joints.

6.7.5 Calculation of faulting

By adding the results of the permanent displacements at different numbers of cycles (N) for the above two loading cases (models), the relative difference in elevation between each two adjacent edges of the concrete slabs can be determined in the three joint positions. These elevation differences present the faulting at the three joint positions and can be presented against the number of loading cycles (Figure 6.23 in normal-log scale) and (Figure 6.24 in log-log scale).

The magnitude of faulting in the first loading cycle is not realistic, but that may be a result of using a permanent deformation model. This also assumes unrealistic values for the first loading cycle. However, in order to obtain realistic values of faulting, this magnitude can be ignored from the total faulting.

The results of the elastic and total vertical displacements for the three joints in the 2-D model are found in Appendix D. The calculation of faulting is based on these results.

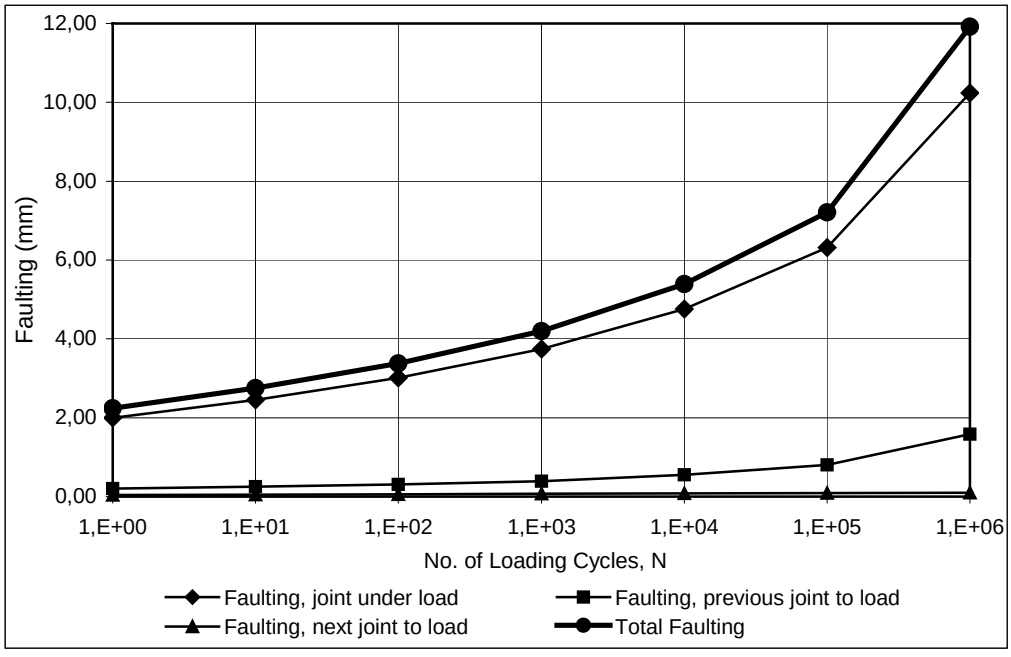

Fig. 6.23: Faulting due to high w/c against number of loading cycles (N): (normal-log scale)

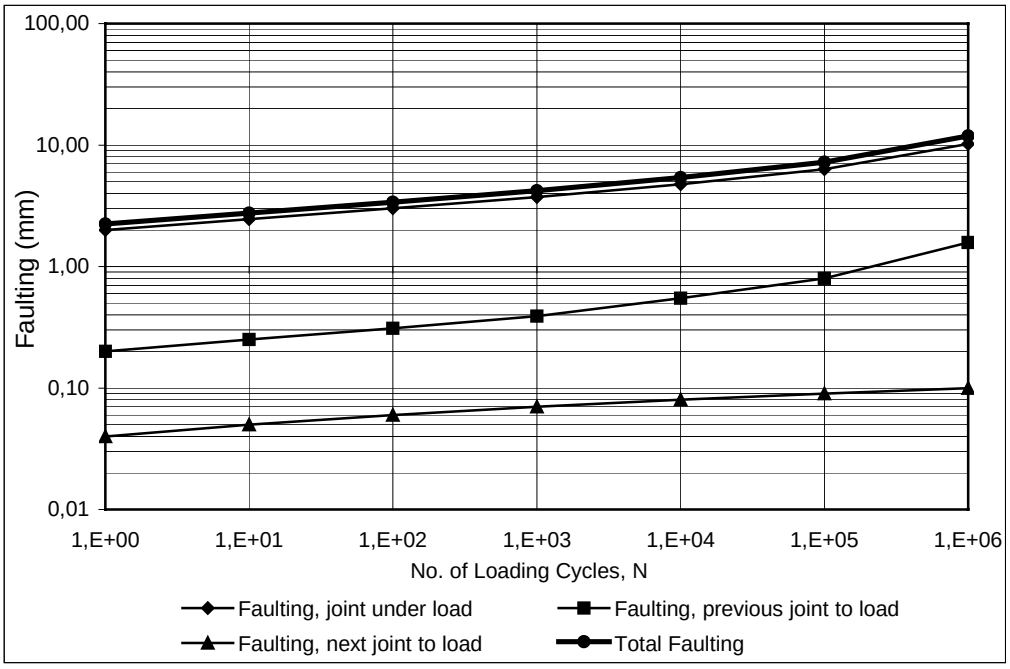

Fig. 6.24: Faulting due to high w/c against number of loading cycles (N): (log-log scale)

6.7.5.1 Prediction of faulting at a higher number of loading cycles

Figure 6.25 presents the total faulting for the first million cycles after the deduction of faulting at the first cycle. In order to predict the faulting at a higher number of loading cycles, the faulting data of the first million cycles are fitted to an exponential function whose equation is presented below. The faulting after 10.0 million cycles can be expected to be 18.7 mm.

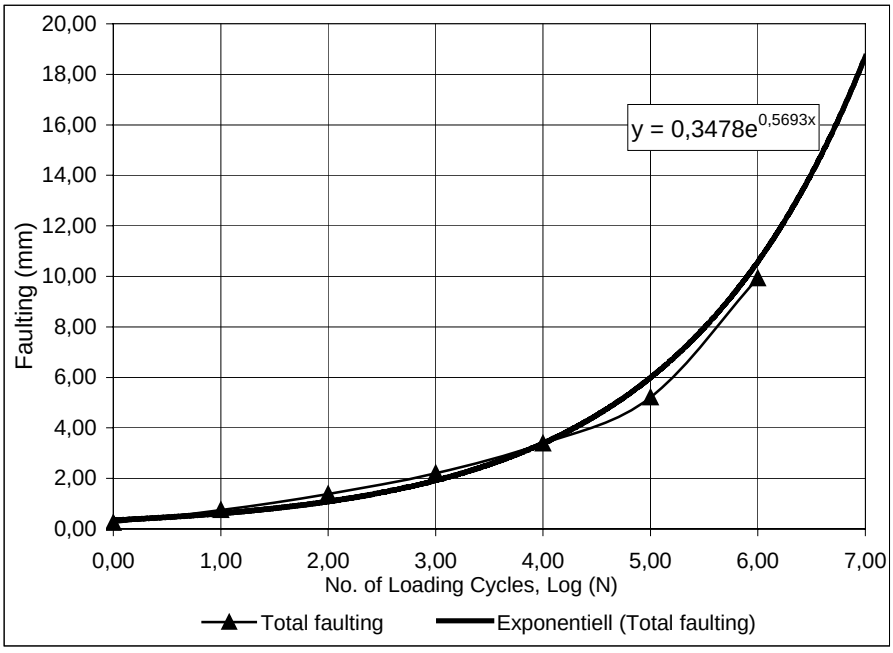

Fig. 6.25: Prediction of faulting due to higher w/c at increased number of loading cycles

6.7.6 Assessment of faulting results

For the assessment of the obtained results, the following remarks should be made:

1- The development of the faulting matches the development of the permanent deformation behavior in the unbound granular materials with higher RMC, in both the exponential growth in a normal-log relationship against the number of loading cycles, and the magnitude of faulting in the first loading cycle (compare Figure 6.23 to Figure 3.11). To get representative values of faulting against the number of loading cycles, the magnitude of faulting at first loading cycle (2.24 mm) should be ignored.

2- By extrapolation, one can predict that, the total faulting after 20 million cycles is about 22.2 mm. The faulting magnitude obtained from the calculation after Khazanovich is 12.63 mm (see Section 6.3.3), which is less than the resulting value with FEM model using fluid cavities with higher RMC.

3- Comparing the faulting results obtained from both analyses in Sections 6.6 and 6.7, one can see that faulting magnitude depend strongly on the properties of unbound granular materials, especially the RMC.

6.8 Conclusion

Comparing the resulted value of faulting after Khazanovich (12.63 mm) for a design period of 20 years with both values of the 2-D FEM model with cavities which are 5.93 mm for model with constant low RMC and 22.20 mm for model with relative high RMC, one can see that the value after Khazanovich exists between the two values of FEM models. Therefore it can be concluded that, there are some input data which must be calibrated before using the proposed procedure with FEM analysis. The most important factors are:

1- The value of w/c and region of application in base layer under transverse joints.

2- Densities of both fluids in cavities.

3- Volume of fluid-filled cavities.

These can be calibrated through experimental and/or field tests.

Comparing both models of faulting simulation which are the model for a base material with a constant low RMC (Section 6.6) and the model for a base material with a relative higher RMC in regions under joints (Section 6.7), it can be concluded that the faulting rate in the second model rapidly increases with the growing number of loading cycles which refers to the decrease of the stiffness of the UGMs with higher RMC levels (refer to Section 3.4). This can lead to quick failure of a pavement system in a short time or before reaching a considerable number of loading cycles (compare Figures 6.18 and 6.23).

7 CONCLUSIONS AND RECOMMENDATIONS

7.1 Conclusions

For many years, structural analysis of pavement systems was based on the two classical solution methods developed by Westergaard and Burmister. In the last few decades many computer programs have been developed according to these classical methods, for example, BISAR, ILLI-PAVE, FENLAP, WESLEA, amongst others. The assumptions of solutions with these two historical methods are no longer accepted, especially since the development of finite element method for analysis not only in engineering but also in many other applications, for example medicine.

The FEM gives us the opportunity to simulate a given problem to a greater extent as in real conditions. The choice of the appropriate element type is available (i.e. shell element, beam element, axisymmetric 2-D or 3-D continuum elements, etc.). It also better defines the boundary conditions and applied loads. This enables the simulating recent complex and different load types. The interaction between different materials and element types is also available. The most effective tool in FEM analysis is the possibility of defining new material constitutive laws to model the engineering characteristics of the behavior of different materials according to experimental and field test results.

For the problems in geotechnical engineering, much effort is being made to better model the behavior of different soil types and granular materials in order to obtain reasonable solutions and design methods. The unbound granular material used in base layer construction of pavement systems is one of the geo-materials, which according to its nature, has a complex behavior. In the past and according to the classical methods of Westergaard and Burmister, this material was assumed to be elastic, which does not reflect its real nature. Consequently, results of design are not accurate. Hence many efforts are still being made to better model these materials in pavement analysis and design.

These materials are found to have a resilient behavior, with stress-dependent Young's modulus and Poisson's ratio; referred to as resilient Young's modulus and resilient Poisson's ratio. On the other hand, the accumulation of permanent deformation increments was observed during the repeated load triaxial test. This explains the rutting problem in flexible pavements, which is first initiated in the unbound base layer. Many researchers have been trying to model the permanent deformation behavior of the unbound granular materials and many models are being developed. It is concluded that many of these models have a common point of view, that the permanent deformation behavior depends on many factors, i.e. stress history, number of loading cycles, stress-level, water content, grading, degree of compaction, maximum dry density, and

mineralogical composition. Many factors were considered in wide research, but the water content influence was not closely studied in spite of its great influence on the permanent deformation behavior which may lead to the failure of the material before reaching a high considerable number of loading cycles.

Having all this research for the modeling of the behavior of UGMs in both elastic and plastic states, it was an urgent requirement to use such new models for modeling such materials in FEM analysis. Some programs have used the non-linear elasticity model for the modeling of UGMs in the analysis and design of flexible pavement. Until now, no program has counted for the permanent deformation behavior. The first trial to use the permanent deformation models for the description of the behavior of the UGMs in FEM analysis for ballast materials subjected to cyclic loads was performed by Stöcker [54] in the GH University of Kassel. Stöcker implemented the material model in a user material subroutine (UMAT) which can be used with the FEM program ABAQUS. He used the reduced Mohr Coulomb failure criterion to model the material in an explicit procedure (independent of loading path), assuming the system is in equilibrium in the initial conditions. Then the additional cyclic loads, which are considered as quasi-static loads, do not endanger the stability of the system. The accumulating strain increments are computed with an approximation method.

Stöcker [54] considered the material behavior as linear elastic and implemented the calculation of permanent deformation increments with three different empirical models (see equations 4.11 to 4.18). The material parameters (for example α und β) in these empirical equations are obtained from the average values after evaluating many results of repeated load triaxial tests, conducted at different stress-levels. According to the work of Werkmeister [68], a similar empirical equation was concluded (see equation 4.19) with stress dependant parameters (A and B). The parameters can be calculated for any stress-level using the maximum and minimum principle stress values. It was therefore important to modify the UMAT subroutine developed by Stöcker to take into account; firstly, the resilient behavior of the UGMs and, secondly, the stress-dependent parameters (A and B) for the calculation of permanent deformation increments of these materials under cyclic loads.

One of the most important problems in rigid pavements is stepping or faulting, which is defined by the difference in elevation of adjacent concrete slabs across transversal joints. This problem affects the riding quality and causes a big impact on the life-cycle cost of the rigid pavement in terms of rehabilitation and vehicle operating costs. The faulting occurs as a result of erosion in the UGMs in the presence of water under unsealed or damaged joints between concrete slabs. The fine materials are transferred through water from underneath the edge of the leave slab to underneath the edge of the approach slab because of the sudden pressure on the UGMs beneath the edge of the leave slab as the wheel crosses the joint.

In order to study this problem closely, the transfer of fines through water in FEM analysis is nearly impossible. So it is assumed that the transfer of a hydrostatic fluid will

simulate the transfer of these fines instead. This transfer is simulated through a fluid link element, which connects between two cavities filled with fluids; underneath the edges of both the leave and approach slabs. This link element has a viscous and hydrodynamic resistance that allows a specific volume of fluid to cross the link under a specific pressure deferential in steady state dynamic analysis. In static analysis, the resistance of the fluid link element is not active, hence, has no influence on the results.

Through this assumption and with the help of the UMAT subroutine for the description of the permanent deformation of UGMs, it is possible to calculate the faulting with FEM analysis but only in a qualitative way. A 2-D model was developed and the load was applied as a moving load crossing the joint. In order to verify the proposed procedure, the model was analyzed firstly with a Mohr Coulomb material definition for the unbound material of base layer. From the results, it was found that the movement of the load is the main cause of faulting.

After that, the analysis was performed again with two materials using the UMAT subroutine. The first material is Gravel Sand with a relatively low water content which is assumed to be constant over the whole base layer, and the second material is Granodiorite with an assumption that, regions of base layer under transversal joints have a higher water content than those under the middle of concrete slabs. The results showed that, the faulting rates increase rapidly in the model with assumptions of higher water content than the model with a low water content ratio. Assessment of results showed that the employed procedure is reliable and can be used after calibration of some input data, i.e. fluid densities, volume of cavities, and w/c values. This calibration can be made through experimental or field tests under application of cyclic loads.

7.2 Recommendations

In the recent research into the behavior of unbound granular materials, the radial permanent deformation has received little recognition. Some extra research is required in the future to relate the radial permanent strain to the axial one, as this may have an impact on the implemented material models in FEM analysis.

Another very important issue to be addressed is the effect of water content on the behavior of UGMs. Consideration of this variable in the developed formulae for both resilient and permanent deformation behavior, which currently only concentrate on the stress-level and number of loading cycles, is very important. In this research a suggested formula was concluded according to the observations from the COURAGE project. This suggested formula still needs some verification through research based on repeated load triaxial tests.

Regarding faulting problem, some field measurement and monitoring is required to study the problem and to define the factors, which are affecting this phenomenon. Among these factors are, the situation of load transfer devices in transversal joints, the nature of UGMs, the thickness of the concrete slab, the thickness of the unbound

granular base layer, the level of stress, consideration of thermal stresses, and any other effects of boundary conditions. From these previous studies, the most dominating factors for the occurrence of faulting can be determined and the most suitable solution to overcome such problem can be suggested.

As the joints present the weakest points in rigid pavement systems and are responsible for many distress problems in those systems, new research considering the mode of interaction between adjacent slabs in the joint area is urgent and necessary. New methods for a durable load transfer mechanism across joints to overcome the problem of faulting also need more research. On the other hand, one of the reasons for faulting is the erosion in base layer materials. Preventing this erosion would greatly help prevent the faulting problem, and can be achieved by using strips of geosynthetic materials (for example geonets or geogrids) under the edges of the concrete slabs along the transversal joints. This method will help reinforce the base layer in these areas in addition to controlling the erosion process. Some research in this subject is needed to assess the suggested method.

The UMAT subroutine, used in the current research for the definition of permanent deformation behavior of unbound granular materials under cyclic loads will greatly aid the analysis of rigid pavement systems. On the other hand, it is recommended to use the new version of the subroutine in the future research of flexible pavement systems to analyze some problems due to cyclic loading, for example, fatigue and rutting in Asphalt layer.

References

[1] AASHTO, 1986, *'Guide for the design of pavement structures'*, American Association of State Highways and Transportation Officials, Washington D.C.

[2] ABAQUS, 2005, '*Theory and Users Manual'*, Version 6.4, Hibbit, Karlsson & Sorenson, Inc., Pawtucket, Rhode Island.

[3] Allen, J.J., and Thompson, M.R., 1974, *'Resilient response of granular materials subjected to time dependant lateral stresses'*, Transportation Research Record 510, Transportation Research Board, National Research Council, Washington D.C., pp. 1-13.

[4] Barksdale, R.D., 1972, *'Laboratory evaluation of rutting in base course materials'*, Proceedings, 3rd international conference on the structural design of asphalt pavements, London, Vol. 1, pp. 161-174.

[5] Barret, J.R., and Smith, D.M., 1976, *'Stress history effects in base course materials'*, Proceedings, 8th Australian road research board conference, Perth, Vol. 8, pp. 30-39.

[6] Boreci, A.P., Schmidt, R.J., and Sidebottom, O.M., 1993, *'Advanced mechanics of materials'*, 5th ed., John Wiley & Sons, New York, pp. 732-779.

[7] Boyce, H.R., 1980, *'A non linear model for the elastic behavior of granular materials under repeated loading'*, Proceedings of the international symposium on soils under cyclic and transient loading, Swansea.

[8] Burland, J.B., Potts, D.M., and Walsh, N.M., 1981, *'The overall stability of free and propped embedded retaining walls'*, Ground Engineering, 14:6, pp. 28-38.

[9] Burmister, D.M., 1943, *'The theory of stresses and displacements in layered systems and applications to the design of airport'*, Proceedings, Highway Research Board, Vo1. 23, pp. 126-144.

[10] Chen, D.H., Zaman, M., Laguros, J., and Soltani, A., 1995, *'Assessment of computer programs for analysis of flexible pavement structure'*, Transportation Research Record 1482, Transportation Research Board, National Research Council, Washington D.C., pp. 123-133.

[11] Cook, R.D., Malkus, D.S., and Plesha, M.E., 1989, *'Concepts and applications of finite element analysis'*, 3rd ed., John Wiley & Sons, New York, pp. 118-124, 196-199, 252-256, 278-280, 314-328, 558-565, 578-582.

[12] Cormeau, I.C., 1975, *'Numerical Stability in Quasi-static Elasto Visco-plasticity'*, Int. Journal for Numerical Methods in Eng., Vol. 9, pp. 109-127.

[13] COST 337- Task 2b, June 2002, *'Review of Models and Modeling Requirements of Unbound Granular Materials for Road Pavements'*.

[14] COURAGE, European Commission, 1999, *'Construction with Unbound Road Aggregates in Europe'*, Final report of European Commission prepared by University of Nottingham.

[15] Duncan, J.M., and Seed, R.B., 1986, *'Compaction induced earth pressures under k_o conditions'*, ASCE, Vol. 112, No. 1, pp. 1-23.

[16] Förster, W., 1996: *Mechanische Eigenschaften der Lockergesteine*, B. G. Teubner Verlagsgesellschaft, Leipzig, Germany.

[17] Garg, N., Tutumluer, E., and Thompson, M.R., 1998, 'S*tructural modeling concepts for the design of airport pavements for heavy aircraft'*, Proceedings, 5th international conference on the bearing capacity of roads and airfields, Trondheim, Norway, pp. 115-124.

[18] Gleitz, T., 1996: *Beitrag zur rechnerischen Erfassung des nichtlinearen Spannungs-Verformungsverhaltens ungebundener Tragschichtmaterialien in flexiblen Straßenkonstruktionen*, PhD Thesis, Dresden University of Technology.

[19] Gotschol, A., 2002: *Veränderlich elastisches und plastisches Verhalten nichtbindiger Böden und Schotter unter zyklisch-dynamischer Beanspruchung*, Fachgebiet Geotechnik, Universität GH Kassel.

[20] Gudehus, G., 1996: *Stoffgesetze der Bodenmechanik*, Grundbautaschenbuch, Teil 1, 5. Auflage, Verlag Ernst & Sohn.

[21] Harichandran, R.S., Baladi, G.Y., and Yeh, M., 1989, *'Development of a computer program for design of pavement systems consisting of bound and unbound materials'*, Department of Civil and Environmental Engineering, Michigan State University, Lancing, Michigan.

[22] Hettler, A., 1987: *Schottertriaxialversuche mit statischem und zyklischem Belastungs-Verlauf*, Eisenbahn Technische Rundschau 36, Heft 6, S 399-405, Hesta- Verlag, Darmstadt.

[23] Hicks, R.G., and Monismith, C.L., 1971, *'Factors influencing the resilient properties of granular materials'*, Transportation Research Record 345, Transportation Research Board, National Research Council, Washington D.C., pp. 15-31.

[24] Hu, Y., 2000: *Zum Verformungsverhalten von wassergesättigten bindigen Böden unter zyklischer Belastung*, Schriftenreihe Geotechnik, Universität GH Kassel, Heft 8.

[25] Huang, Y.H., 1985, *'A Computer package for structural analysis of concrete pavements'*, Proceedings, 3rd international conference on concrete pavement design and rehabilitation, Purdue University, West Lafayette, Indiana, pp. 295-307.

[26] Huang, Y.H., 1993, *'Pavement analysis and design'*, Prentice Hall, Eaglewood Cliffs, New Jersey, pp. 63-82, 106-121, 173-186, 197-202, 364-367.

[27] Huurman, M., 1997, *'Permanent deformation in concrete block pavements'*, PhD Thesis, Delft University of Technology, pp. 119 –125.

[28] Ioannides, A.M., and Korovesis, G.T., 1990, *'Aggregate interlock: A pure-shear load transfer mechanism'*, Transportation Research Record 1286, Transportation Research Board, National Research Council, Washington D.C., pp. 14-24.

[29] Ioannides, A.M., 1984, *'Analysis of slab-on-grade for a variety of loading and support conditions'*, PhD Thesis, Department of Civil and Environmental Engineering, University of Illinois at Urbana-Champaign, Illinois.

[30] Jeuffrey, G., and Sauterey, R., 1996, *'Cement Concrete Pavements'*, A.A. Balkema, Rotterdam, Brookfield.

[31] Khazanovich, L., Darter, M.I., and Yu, T., 2004, *'Mechanistic-empirical for transverse joint faulting prediction'*, Presented at the 83rd Annual Meeting of the TRB, Washington D.C., USA.

[32] Kim, J., and Hjelmstad, K., 2000, *'Three-dimensional finite element analysis of multi-layered systems'*, Center of Excellence for Airport Pavement Research, University of Illinois, USA.

[33] Lang, H-J., and Huder, J., 1990: *Bodenmechanik und Grundbau*, 4. Auflage, Springer-Verlag, Berlin.

[34] Lashine, A.K., Brown, S.F., and Pell, P.S., 1971, *'Dynamic properties of soils'*, Report No. 2, Submitted to Shell Laboratories, Dept. of Civil Engineering, University of Nottingham, Nottingham, England.

[35] Logan, D.L., 1992, *'A first course in the finite element method'*, 2nd ed., PWS-KENT, Boston, Massachusetts, pp. 169-172, 312-319.

[36] Mehta, M.R., 1959, *'Stresses and displacements in layered systems'*, PhD Thesis, Department of Civil and Environmental Engineering, University of Illinois at Urbana-Champaign, Illinois.

[37] Michelow, J., 1963, *'CHEVRONELP: Analysis of stresses and displacements in an n-layered elastic system under a load uniformly distributed on a circular area'*, California Research Corporation, Richmond, California.

[38] Morgan, J.R., 1966, *'The response of granular materials to repeated loading'*, Proceedings Australian Road Research Board, Vol.3, Part 2, pp. 1178-1191.

[39] Nazarian, S., and Boddspati, K.M., 1995, *'Pavement-Falling Weight Deflection Interaction Using Dynamic Finite Element Analysis'*, In Transportation Research Record 1449, TRB, National Research Council, Washington D.C., pp. 123-133.

[40] Niemunis, A., 2000: *Akkumulation der Verformung infolge zyklischer Belastung des Bodens – numerische Strategien*, Workshop: *Boden unter fast zyklischer Belastung: Erfahrungen und Forschungsergebnisse*, Schriftenreihe des Institutes für Grundbau und Bodenmechanik der Ruhr-Universität Bochum, Heft 32, S 1-20.

[41] North Germany Organization For Highest Computation Performance (in German: Norddeutschen Verbundes für Hoch- und Höchstleistungsrechnen ‚HLRN', http://www.hlrn.de/), Berlin, Germany.

[42] Numrich, R., 2003: *Untersuchung zum nichtlinear-elastischen Spannungs-Verformungsverhalten von Tragschichten ohne Bindemittel*, PhD Thesis, Dresden University of Technology.

[43] O'Reilly, M.P., and Brown, S.F., 1991, *'Cyclic Loading of Soils: from theory to design'*, Department of Civil Engineering, University of Nottingham, Nottingham, England.

[44] Pappin, J.W., 1979, *'Characteristics of granular material for pavement analysis'*, PhD Thesis, Dept. of Civil Engineering, University of Nottingham, Nottingham, England.

[45] Paute, J.L., Hornych, P., and Benaben, J.P., 1996, *'Repeated load triaxial testing of granular materials'*, in the French network of Laboratories des Ponts et Chaussées, Flexible Pavements, Proceedings, Eur. Symp. Euroflex 1993, A.G. Correia, ed., Balkema, Rotterdam, The Netherlands, pp. 53–64.

[46] Raad, L.A.M., and Figueroa, J.L., 1980, *'Load response of transportation support systems'*, Transportation Engineering Journal, ASCE, Vol. 106, pp. 111-128.

[47] Ray, G.K., and Fordyce, P., 1966, *'New procedure for the design of pavements'*, Proceedings, 5th World Meeting, International Road Federation, London.

[48] Raymond, G.P., and Williams, D.R., 1978, *'Repeated Load Triaxial Tests on Dolomite Ballast'*, Journal of Geotechnical Engineering, ASCE, 104 (7), pp. 1013-1029.

[49] Sawicki, A., Swidzinski, W., 1995, *'Cyclic compaction of soils'*, grains and powders, Powder Technology 85, pp. 97-104

[50] Schad, H., 1979: *Nichtlineare Stoffgleichungen für Böden und ihre Verwendung bei der numerischen Analyse von Grundbauaufgaben*, Institut für Geotechnik, Universität Stuttgart, Mitteilung 10.

[51] Schmidt, H.-H., 1996: *Grundlagen der Geotechnik: Bodenmechanik - Grundbau - Erdbau*, B.G. Teubner, Stuttgart.

[52] Selig, E.T., 1987, *'Tensile zone effects on performance of layered systems'*, Geotechnique, Vol. 37, No. 3, pp. 247-254.

[53] Shell Research, 1978, *'BISAR Users manual'*, Koninklijke/Shell-Laboratorium, Amsterdam, The Netherlands.

[54] Stöcker, T., 2002: *Zur Modellierung von granularen Materialien bei nichtruhenden Lasteinwirkungen*, Fachgebiet Geotechnik, Universität GH Kassel, Heft 13.

[55] Suiker, A.S.G., 1999, *'Static and cyclic loading experiments on non-cohesive granular materials'*, Technical Report 1-99-DUT-1, Delft University of Technology, Faculty of Civil Engineering.

[56] Sweere, G.T.H., 1990, *'Unbound granular bases layer for roads'*, PhD Thesis, University of Delft, Delft, The Netherlands.

[57] Tabatabaie-Raissi, A.M., 1978, *'Structural analysis of concrete pavement joints'*, PhD Thesis, Department of Civil and Environmental Engineering, University of Illinois at Urbana-Champaign, Illinois.

[58] Taciroglu, E., 1998, *'Constitutive modeling of the resilient response of granular solids'*, PhD Thesis, Department of Civil and Environmental Engineering, University of Illinois at Urbana-Champaign, Illinois.

[59] Tayabji, S.D., and Colley, B.E., 1986, *'Analysis of Jointed Concrete Pavements'*, FHWARD-86-041, Turner-Fairbanks Highway Research Center, McLean, Virginia.

[60] Thom, N.H., 1988, *'Design of road foundation'*, PhD Thesis, Department of Civil Engineering, University of Nottingham.

[61] Thompson, M.R., and Elliot, R.P., 1985, *'ILLI-PAVE Based response algorithms for design of conventional flexible pavements'*, Transportation Research Record 1043, Transportation Research Board, National Research Council, Washington D.C., pp. 50-57.

[62] Thompson, M.R., Dempsey, B.J., Hill, H., and Vogel, L., 1987, *'Characterizing temperature effects for pavement analysis and design'*, Transportation Research Record 1121, Transportation Research Board, National Research Council, Washington D.C., pp. 14-22.

[63] Uddin, W., Noppakunwijai, T., and Chung, T., 1997, *'Performance evaluation of jointed concrete pavement using 3-D finite element dynamic analysis'*, Transportation Research Board, 76th Annual meeting, Washington D.C.

[64] Uzan, J., 1985, *'Characterization of granular materials'*, Transportation Research Record 1022, Transportation Research Board, National Research Council, Washington D.C., pp. 52-59.

[65] Van Cauwelaert, F.J., 1987, *'Stress and displacement in two-, three-, and four-layered structure submitted to flexible or rigid loads'*, Final Report, WES Research Contract DAJA45-86-M-0483, U. S. Army Waterways Experiment Station, Vicksburg, Michigan.

[66] Wang, Z., 2000 *'Behavior of Soils and Foundation Structures under Cyclic Loads'*, Mitteilungen aus dem Fachgebiet Grundbau und Bodenmechanik, Universität GH Kassel, Heft 25, Verlag Glückauf GmbH.

[67] Wellner, F., 1994: *Grundlagen zur Bemessung flexibler Straßenbefestigungen mit Tragschichten ohne Bindemittel*, Professorial Dissertation, Dresden University of Technology.

[68] Werkmeister, S., 2002, *'Permanent deformation behavior of unbound granular materials in pavement construction'*, PhD Thesis, Faculty of Civil Engineering, Technical University of Dresden, Dresden, Germany.

[69] Westergaard, H.M., 1926, *'Computations of stresses in concrete roads'*, Proceedings, 5th Annual meeting, Highway Research Board, pp. 90-112.

[70] Westergaard, H.M., 1926, *'Stresses in concrete pavements computed by theoretical analysis'*, Public Roads, Vol. 7, pp. 25-35.

[71] Westergaard, H.M., 1939, *'Stresses in concrete runways in airports'*, Proceedings, Highway Research Board, Vol. 19, pp. 192-202.

[72] Westergaard, H.M., 1948, *'New formulas for stress in concrete pavement of airfields'*, Transactions, ASCE, Vol. 113, pp. 425-444.

[73] Wolff, H., and Visser, A.T., 1994, *'Incorporating elasto-plasticity in granular layer pavement design'*, Proceedings, Institution of Civil Engineers, Transp., 105, pp. 259–272.

[74] Zaghloul, S.M., and White, T.D., 1993, *'Use of a Three-Dimensional, Dynamic Finite Element Program for Analysis of Flexible Pavement'*, Transportation Research Record 1388, TRB, National Research Council, Washington D.C., pp. 60-69.

[75] Zienkiewicz, O.C., and Cormeau, I.C., 1974, *'Visco Plasticity - Plasticity and Creep in Elastic Solids - a Unified Numerical Solution Approach'*, International Journal for Numerical Methods in Engineering, 8, pp. 821-845.

[76] Zienkiewicz, O.C., and Taylor, R.L., 1991, *'The Finite Element Method, Basic Foundation and Linear Problems'*, 4th Ed., Vol. 1, McGraw-Hill International, United Kingdom.

[77] Zienkiewicz, O.C., and Taylor, R.L., 1991, *'The Finite Element Method, Soil and Fluid Mechanics Dynamics and Non-Linearity'*, 4th Ed., Vol. 2, McGraw-Hill International, United Kingdom.

Appendices: Results

Appendix A

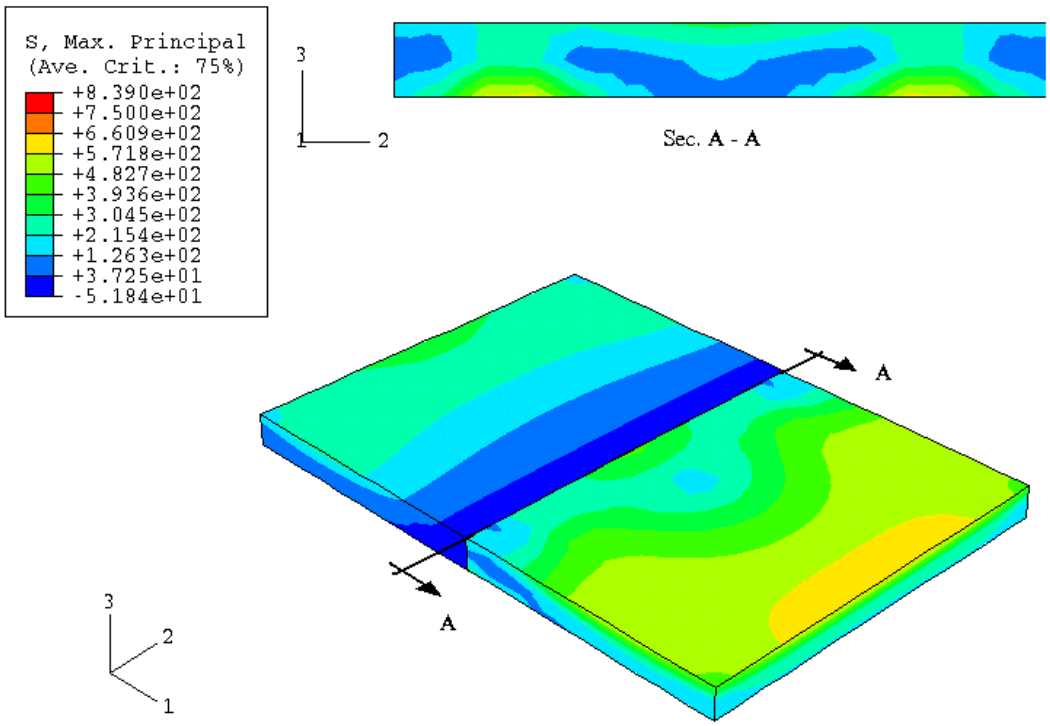

Fig. A.1: Maximum principle stress in concrete slab [kPa], load case 2

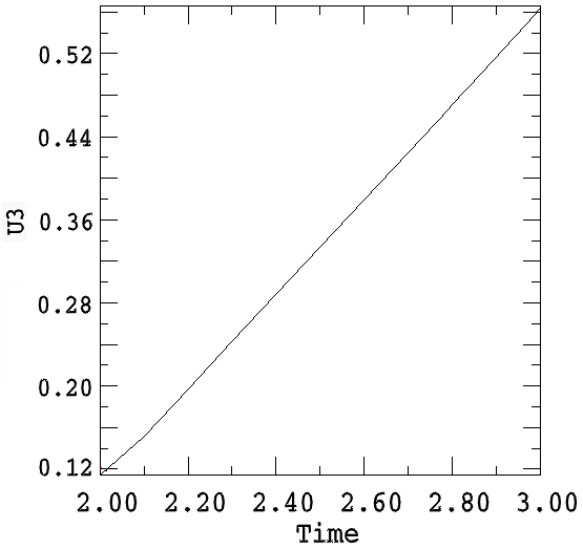

Fig. A.2: Maximum vertical elastic displacement [mm] in concrete slab, load case 2

Table A.1: Comparison of FEM and Westergaard results; load case 2 (corner loading)

Calculation method	Westergaard	FEM, Load case 2
Max. tension stress (kPa)	1075.00	839.00
Max. vertical deflection (mm)	0.274	0.440

Appendix B

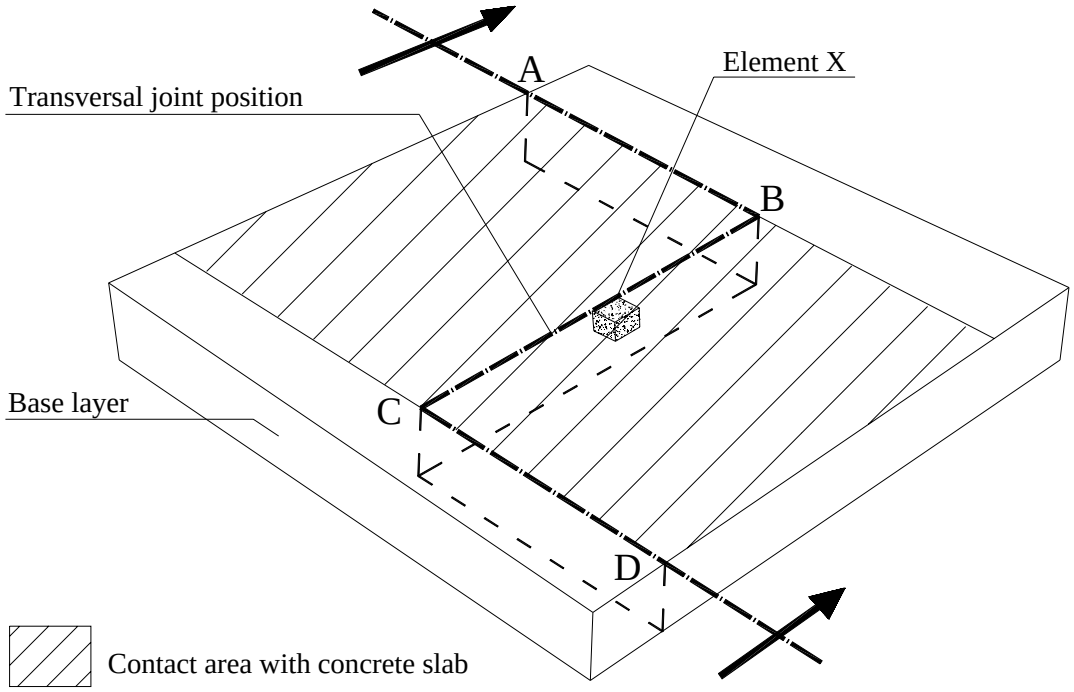

Fig. B.1: Plan view for base layer in 3-D model with section A-B-C-D

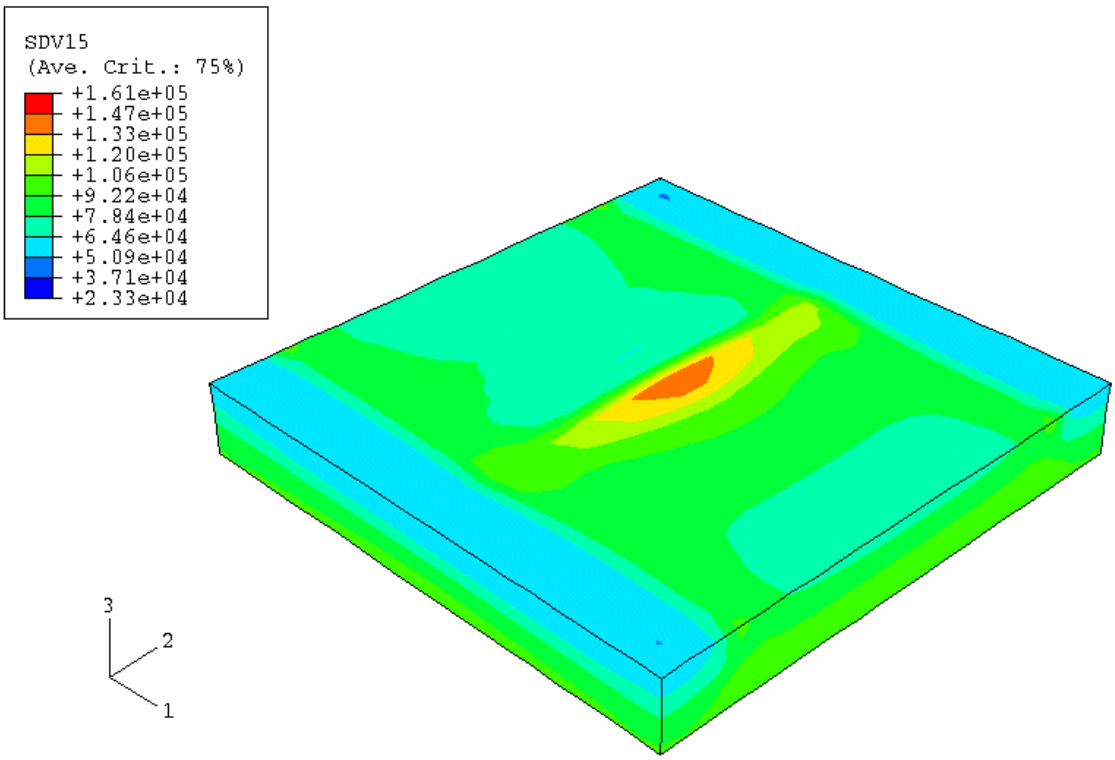

Fig. B.2: Resilient E-Modulus in base layer [kPa] at end of step 3, load case 1

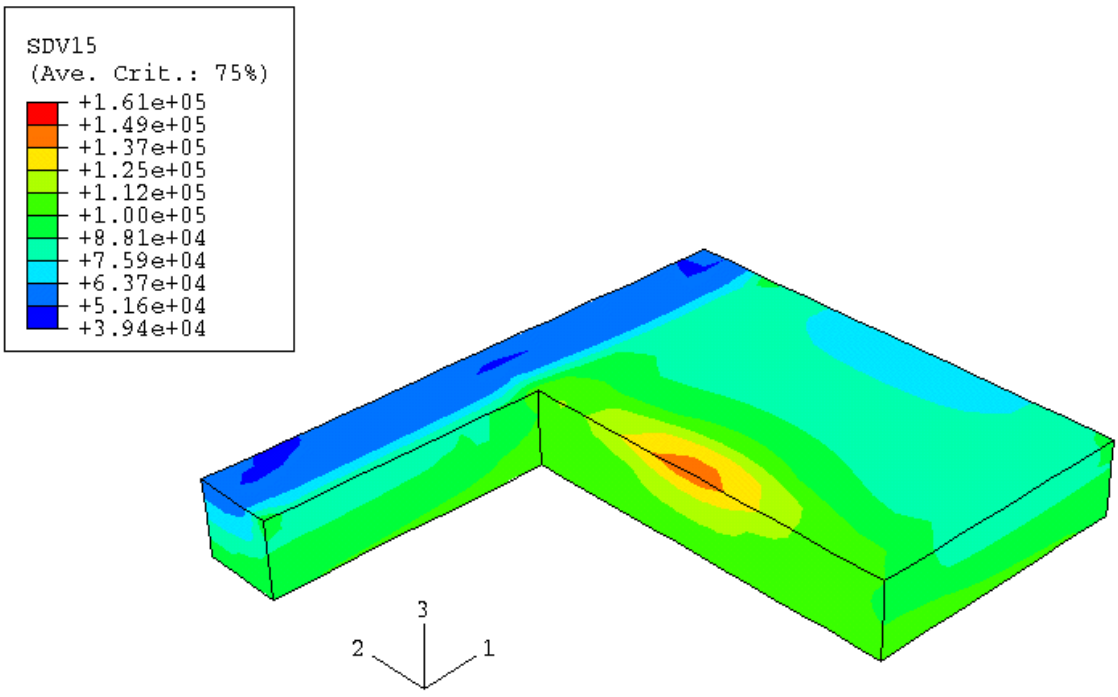

Fig. B.3: Section A-B-C-D for Figure B.2 (E-Modulus)

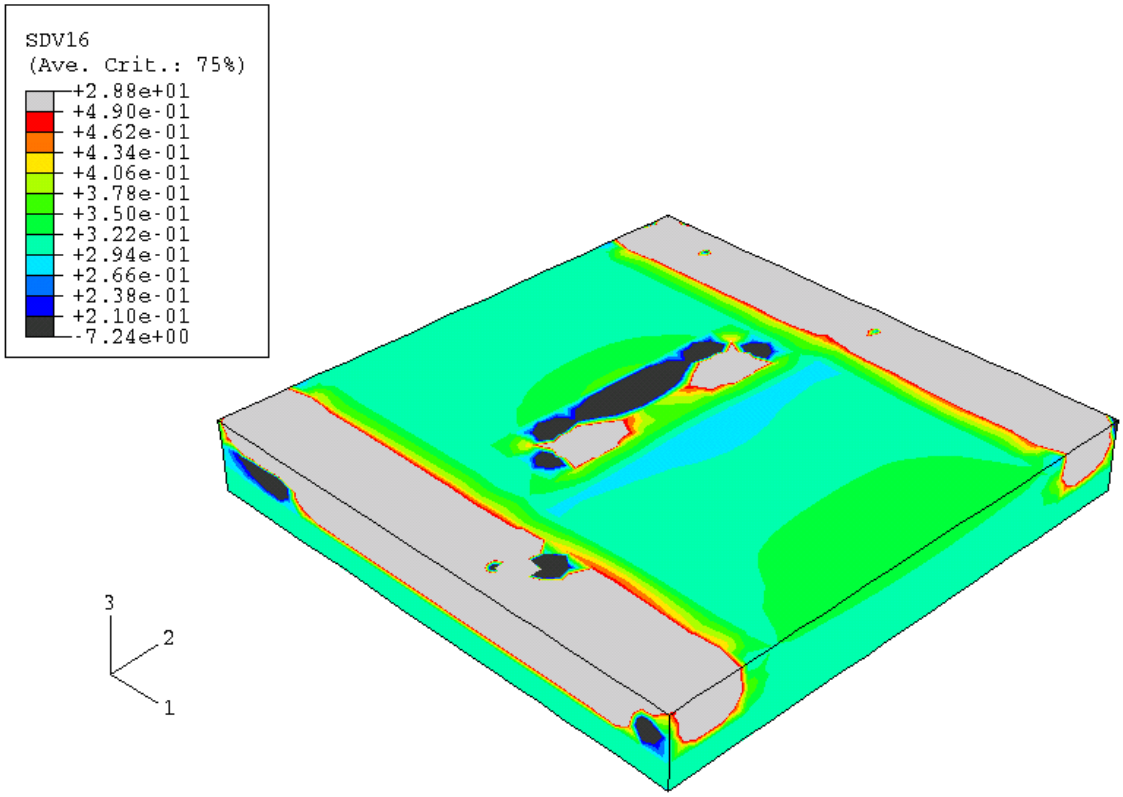

Fig. B.4: Resilient Poisson's ratio in base layer [-] at end of step 3, load case 1

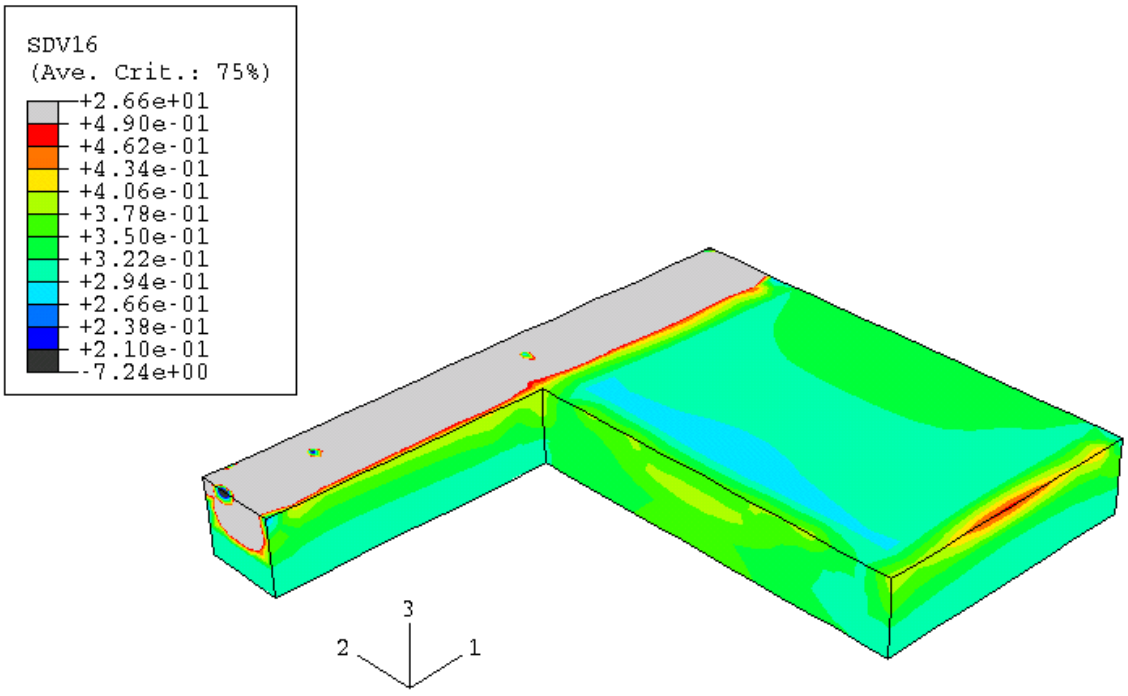

Fig. B.5: Section A-B-C-D for Figure B.4 (Poisson's ratio)

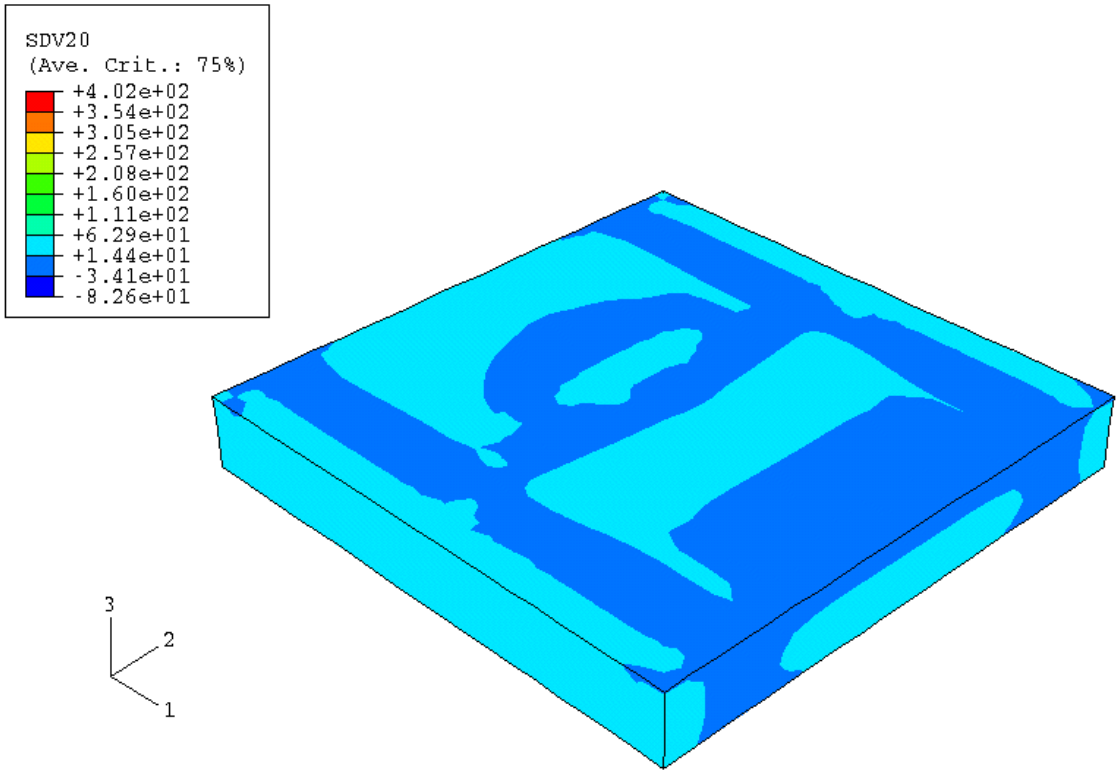

Fig. B.6: Parameter (A) for permanent deformation in base layer at end of step 4, load case 1

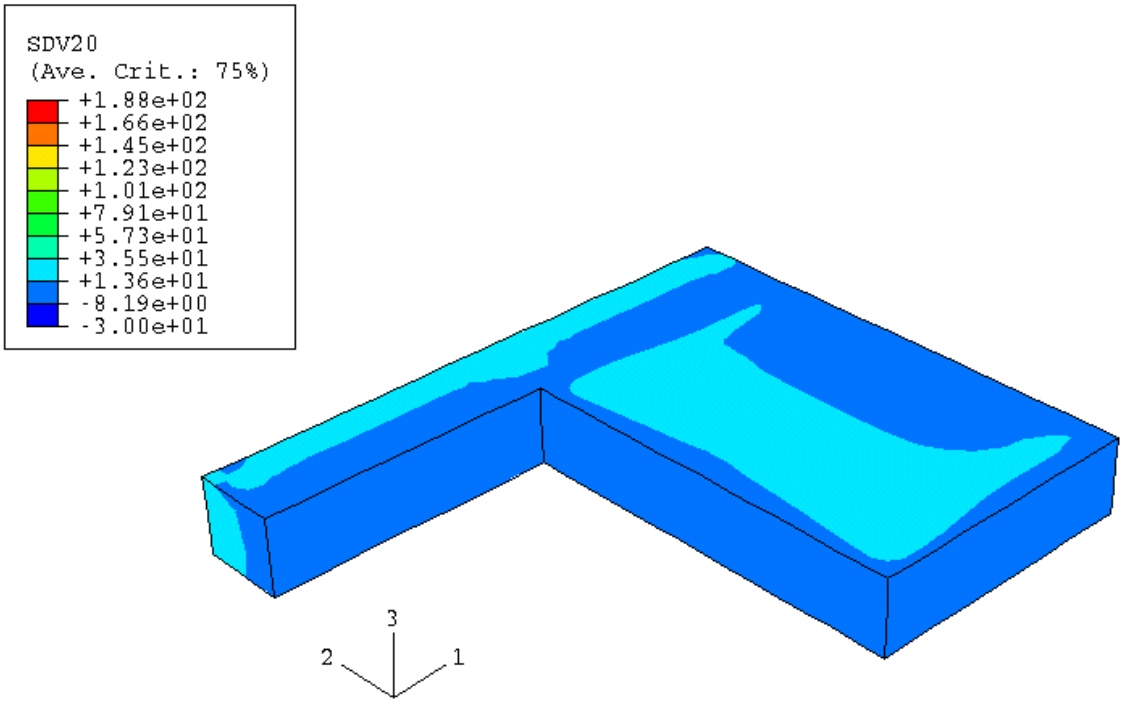

Fig. B.7: Section A-B-C-D for Figure B.6 (Parameter 'A')

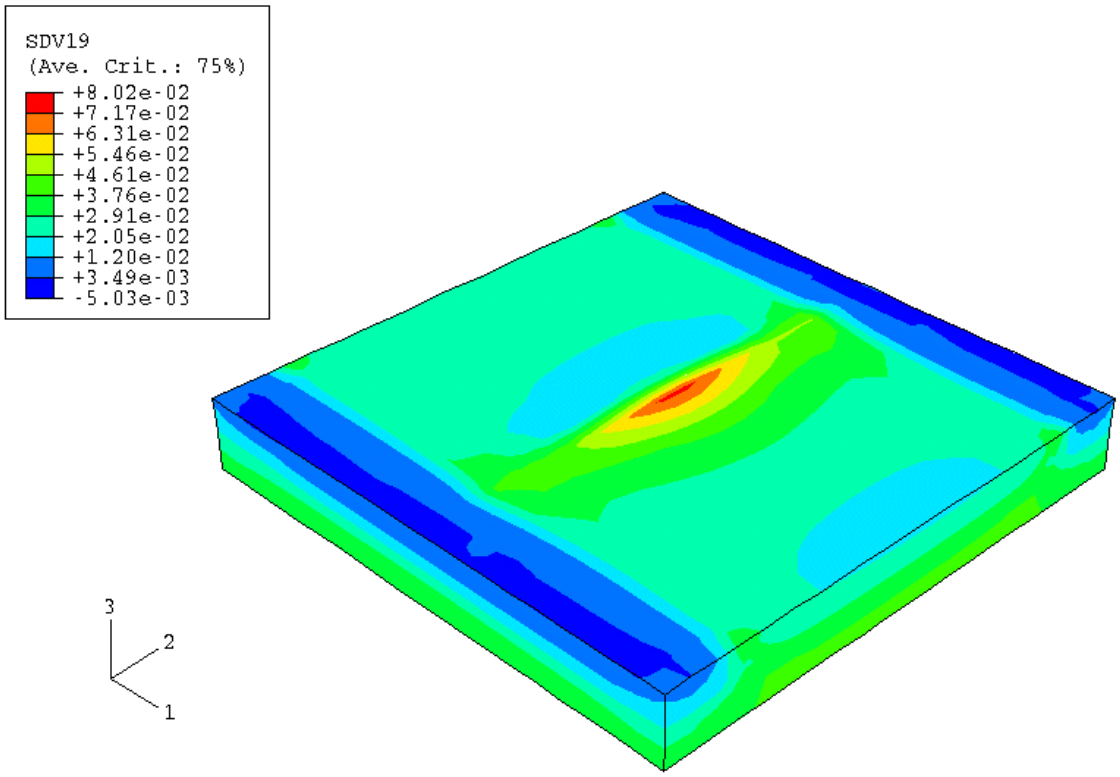

Fig. B.8: Parameter (B) for permanent deformation in base layer at end of step 4, load case 1

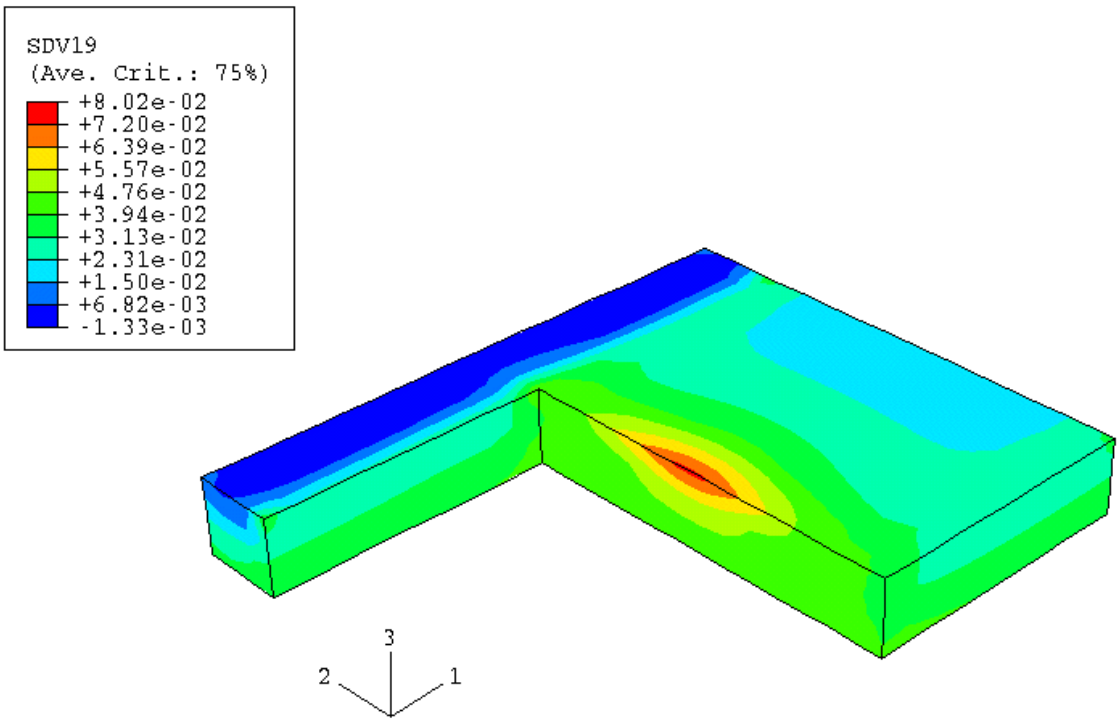

Fig. B.9: Section A-B-C-D for Figure B.8 (Parameter 'B')

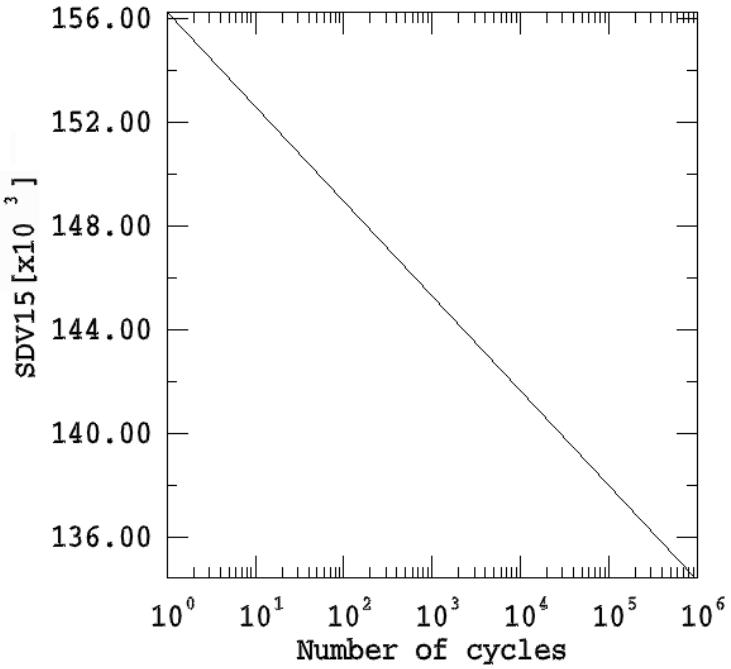

Fig. B.10: Resilient modulus [kPa] against (N) for element X in base layer; step 4, load case 1

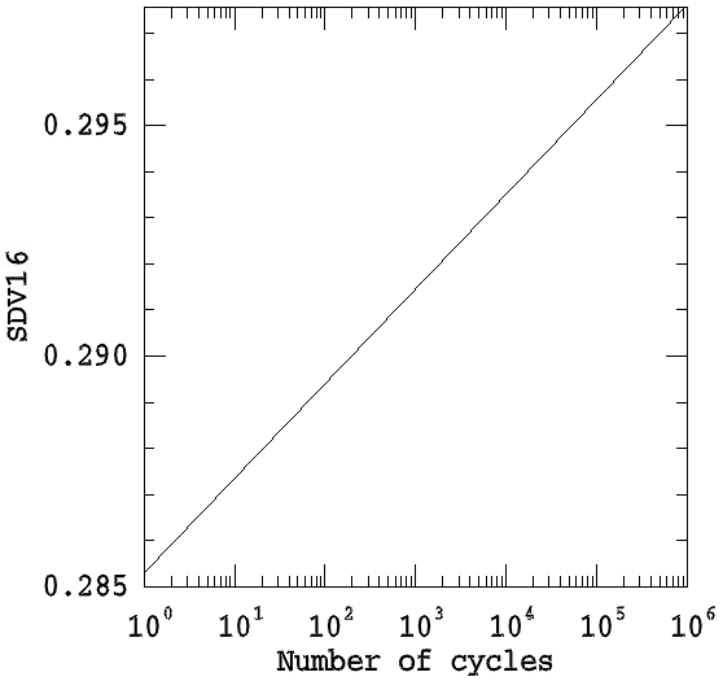

Fig. B.11: Poisson's ratio [-] against (N) for element X in base layer; step 4, load case 1

Appendix C

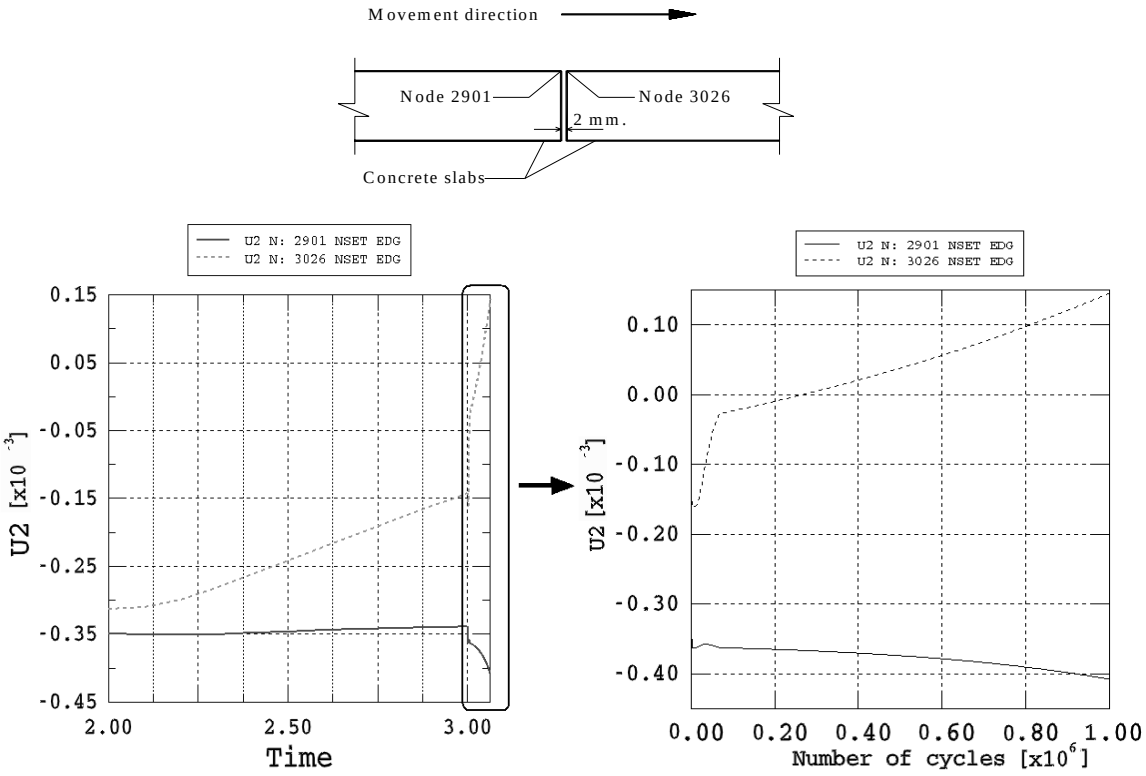

Fig. C.1: Vertical displacement [m] at joint preceding to load; left side amplitude (P_A)

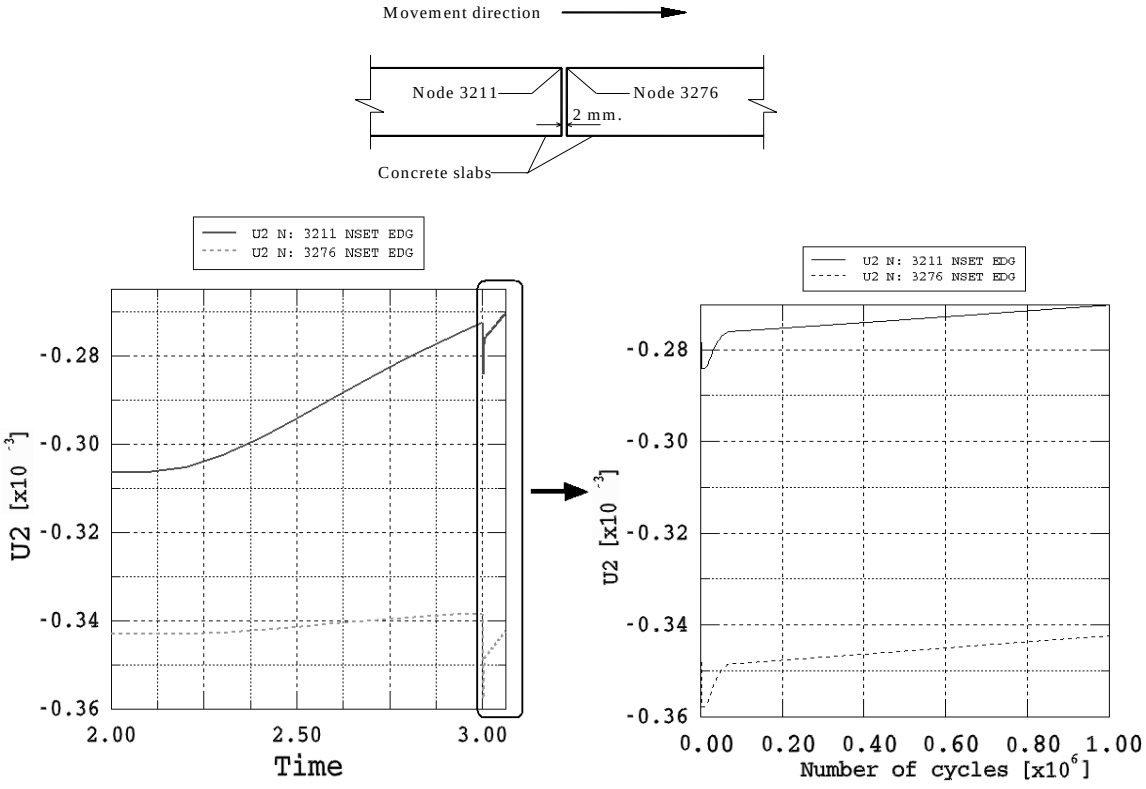

Fig. C.2: Vertical displacement [m] at joint proceeding to load; left side amplitude (P_A)

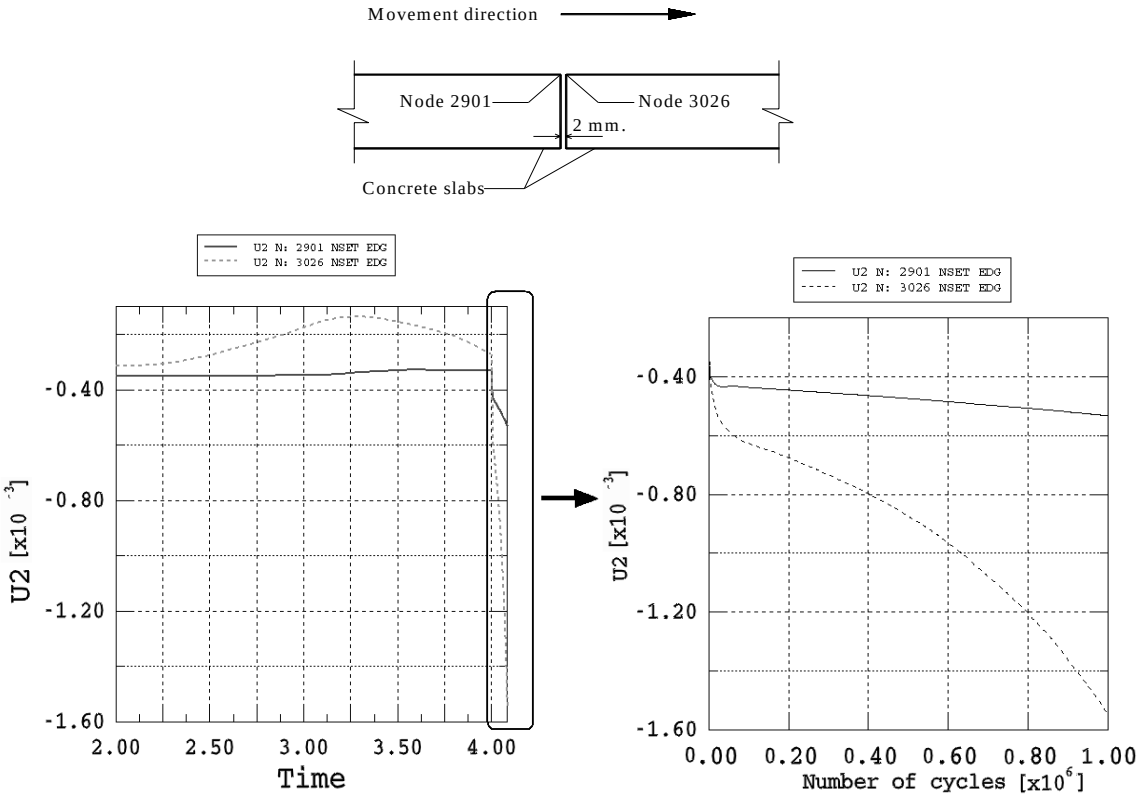

Fig. C.3: Vertical displacement [m] at joint preceding to load; right side amplitude (P_B)

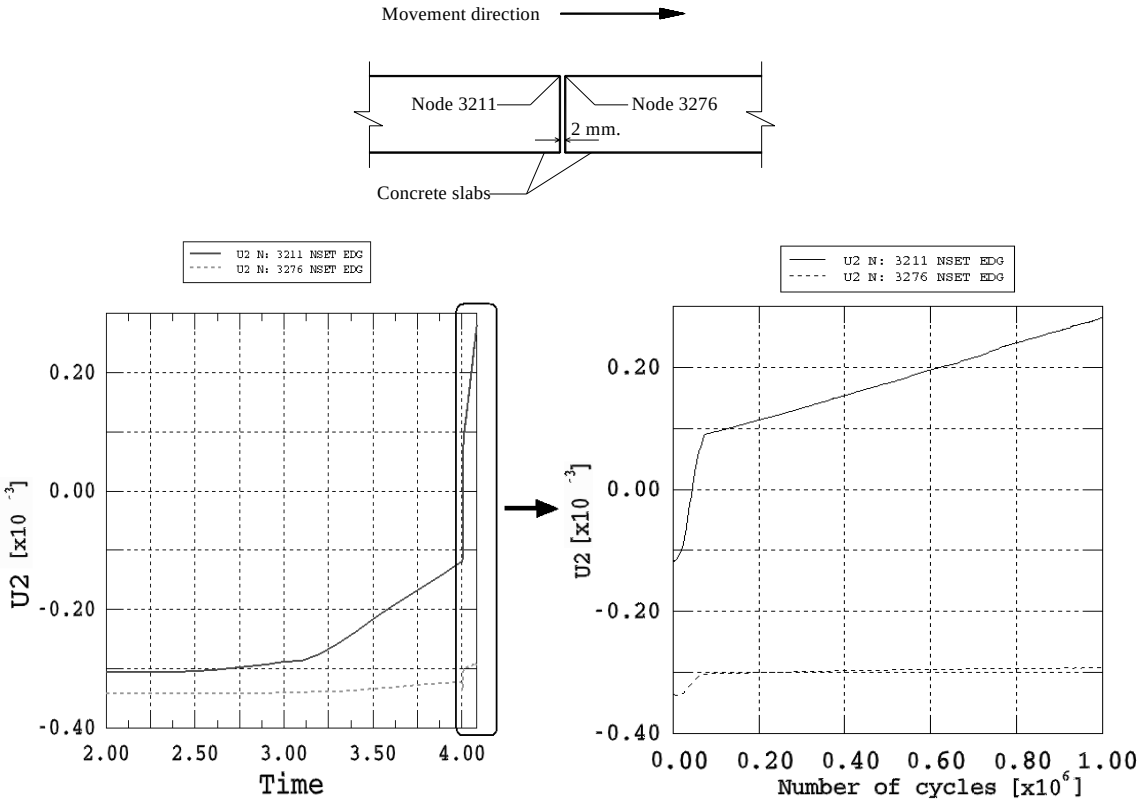

Fig. C.4: Vertical displacement [m] at joint proceeding to load; right side amplitude (P_B)

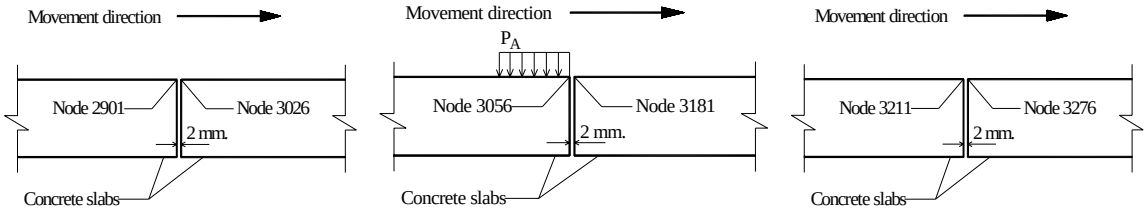

Joint (1) Joint (2) Joint (3)

Table C.1: Vertical displacement [mm] at three joint positions; left side amplitude (P_A)

		Joint (1) Previous to load		Joint (2) Under load		Joint (3) Next to load	
Node No.		**2901**	**3026**	**3056**	**3181**	**3211**	**3276**
Elastic deformation		-0.34	-0.14	-2.80	-0.57	-0.27	-0.34
Total deformation at cycle No.	1	-0.36	-0.03	-4.73	-0.92	-0.28	-0.35
	10	-0.37	-0.01	-4.93	-0.92	-0.28	-0.35
	100	-0.37	0.02	-5.17	-0.91	-0.27	-0.35
	1000	-0.38	0.04	-5.42	-0.90	-0.27	-0.35
	10,000	-0.38	0.07	-5.71	-0.90	-0.27	-0.34
	100,000	-0.39	0.11	-6.03	-0.89	-0.27	-0.34
	1000,000	-0.41	0.15	-6.37	-0.88	-0.27	-0.34

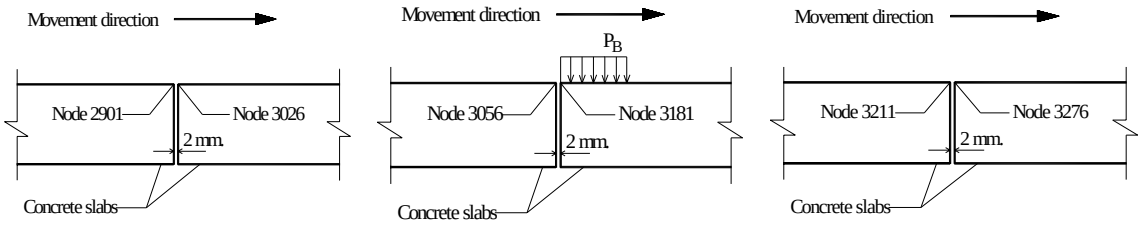

Joint (1) Joint (2) Joint (3)

Table C.2: Vertical displacement [mm] at three joint positions; right side amplitude (P_B)

		Joint (1) Previous to load		Joint (2) Under load		Joint (3) Next to load	
Node No.		**2901**	**3026**	**3056**	**3181**	**3211**	**3276**
Elastic deformation		-0.33	-0.28	-0.12	-2.65	-0.12	-0.32
Total deformation at cycle No.	1	-0.43	-0.61	1.66	-4.36	0.09	-0.30
	10	-0.45	-0.68	2.15	-4.50	0.12	-0.30
	100	-0.46	-0.76	2.70	-4.64	0.14	-0.30
	1000	-0.47	-0.86	3.30	-4.78	0.17	-0.30
	10,000	-0.49	-1.01	4.12	-4.93	0.20	-0.30
	100,000	-0.51	-1.22	5.11	-5.09	0.24	-0.30
	1000,000	-0.53	-1.54	6.58	-5.25	0.28	-0.30

Appendix D

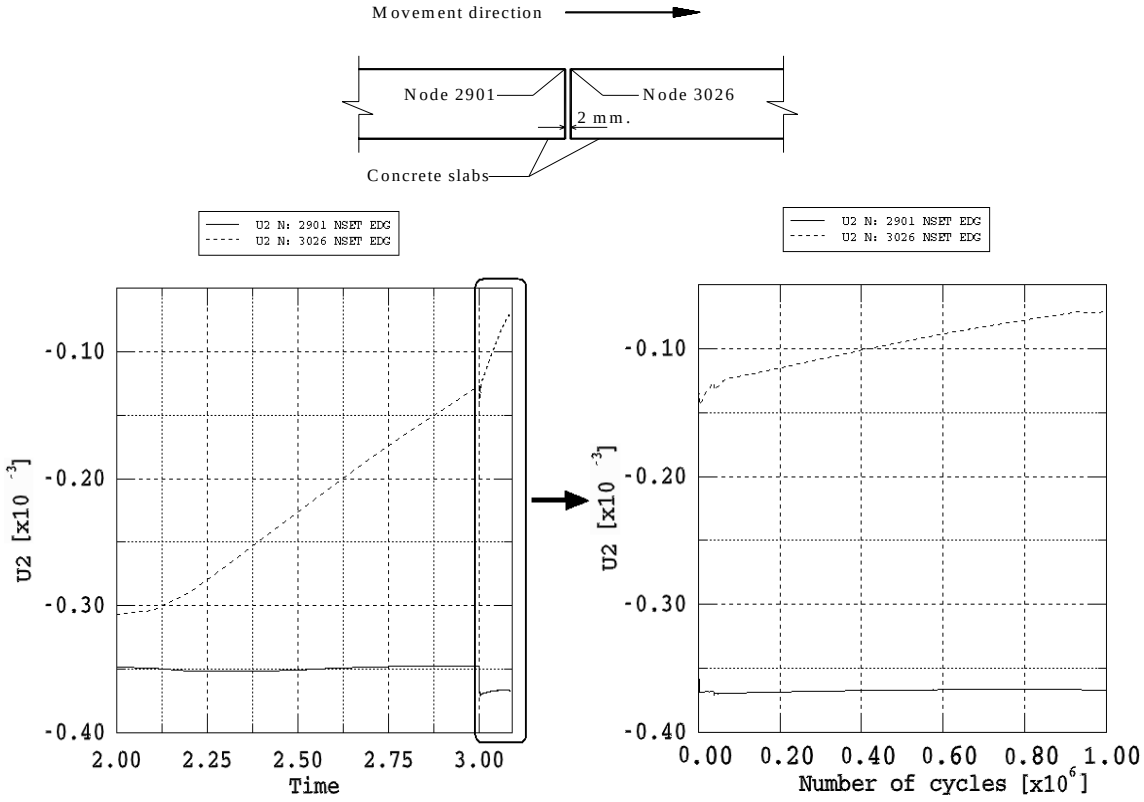

Fig. D.1: Vertical displacement [m] at joint (with high w/c) preceding to load; left side amplitude (P_A)

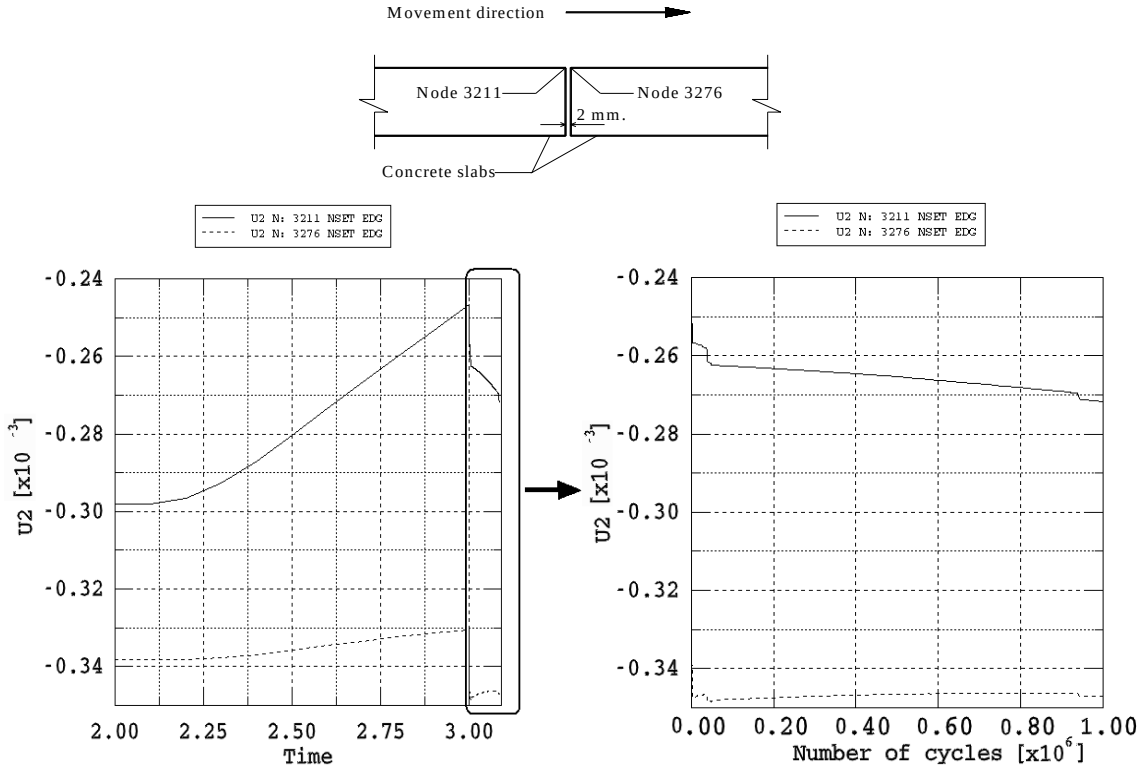

Fig. D.2: Vertical displacement [m] at joint (with high w/c) proceeding to load; left side amplitude (P_A)

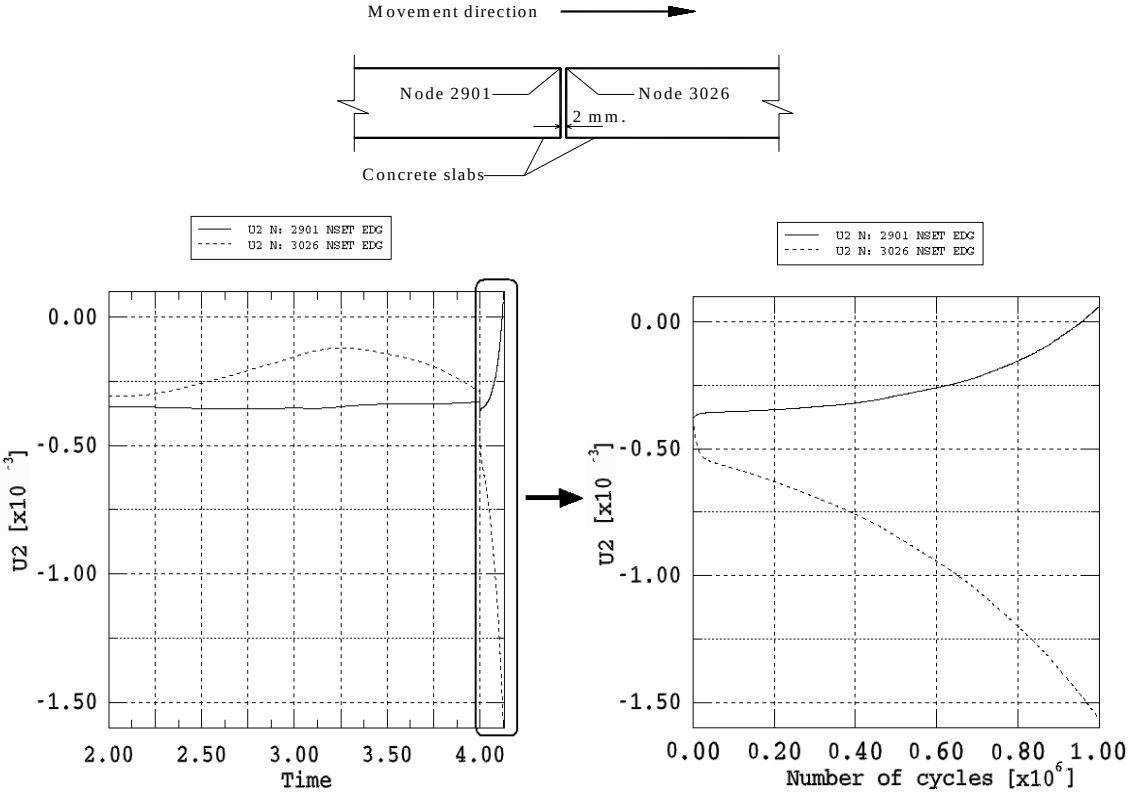

Fig. D.3: Vertical displacement [m] at joint (with high w/c) preceding to load; right side amplitude (P_B)

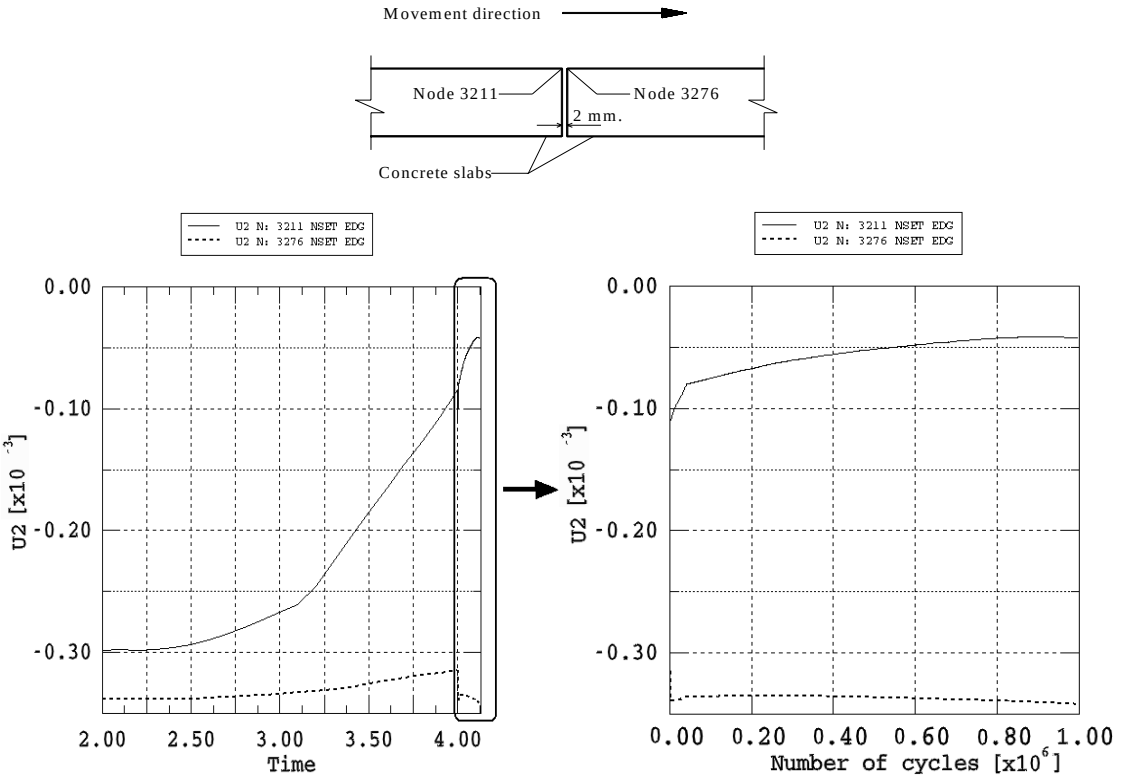

Fig. D.4: Vertical displacement [m] at joint (with high w/c) proceeding to load; right side amplitude (P_B)

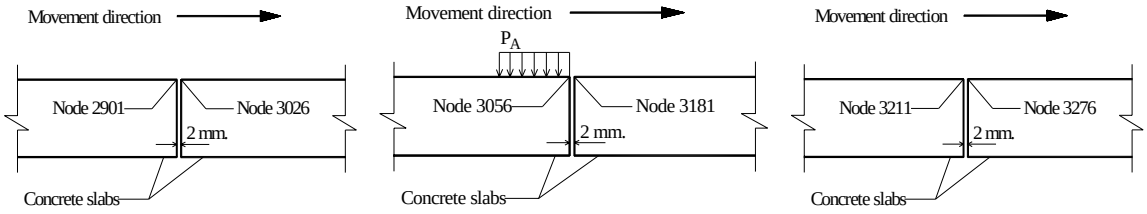

Joint (1) Joint (2) Joint (3)

Table D.1: Vertical displacement [mm] at three joints with high w/c; left side amplitude (P_A)

		Joint (1) Previous to load		Joint (2) Under load		Joint (3) Next to load	
Node No.		**2901**	**3026**	**3056**	**3181**	**3211**	**3276**
Elastic deformation		-0.35	-0.13	-2.83	-0.74	-0.25	-0.33
Total deformation at cycle No.	1	-0.37	-0.12	-3.50	-1.03	-0.26	-0.35
	10	-0.37	-0.12	-3.57	-1.01	-0.26	-0.35
	100	-0.37	-0.11	-3.66	-0.99	-0.26	-0.35
	1000	-0.37	-0.10	-3.76	-0.98	-0.26	-0.35
	10,000	-0.37	-0.09	-3.85	-0.95	-0.27	-0.35
	100,000	-0.37	-0.08	-3.97	-0.93	-0.27	-0.34
	1000,000	-0.37	-0.07	-4.06	-0.89	-0.27	-0.34

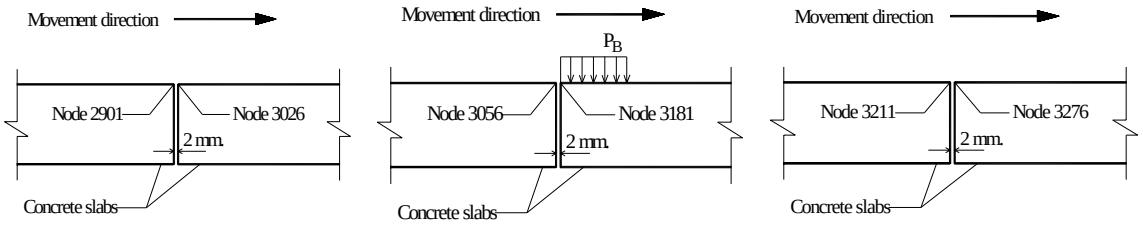

Joint (1) Joint (2) Joint (3)

Table D.2: Vertical displacement [mm] at three joints with high w/c; right side amplitude (P_B)

		Joint (1) Previous to load		Joint (2) Under load		Joint (3) Next to load	
Node No.		**2901**	**3026**	**3056**	**3181**	**3211**	**3276**
Elastic deformation		-0.33	-0.29	0.03	-2.67	-0.08	-0.31
Total deformation at cycle No.	1	-0.36	-0.55	1.79	-3.29	-0.08	-0.34
	10	-0.35	-0.59	2.25	-3.37	-0.07	-0.34
	100	-0.34	-0.65	2.85	-3.44	-0.06	-0.34
	1000	-0.33	-0.73	3.62	-3.51	-0.06	-0.34
	10,000	-0.29	-0.86	4.70	-3.57	-0.05	-0.34
	100,000	-0.22	-1.05	6.33	-3.64	-0.04	-0.34
	1000,000	0.06	-1.56	10.33	-3.69	-0.04	-0.34